Development of 'Smart' Biomaterials for Tissue Repair

Thesis submitted in fulfilment of the requirements of the degree of Philosophiae Doctor, University of Wales, Cardiff

Kate Silverthorne BSc. (Hons)

September, 2004

UMI Number: U583951

All rights reserved

INFORMATION TO ALL USERS
The quality of this reproduction is dependent upon the quality of the copy submitted.

In the unlikely event that the author did not send a complete manuscript
and there are missing pages, these will be noted. Also, if material had to be removed,
a note will indicate the deletion.

UMI U583951
Published by ProQuest LLC 2013. Copyright in the Dissertation held by the Author.
Microform Edition © ProQuest LLC.
All rights reserved. This work is protected against
unauthorized copying under Title 17, United States Code.

ProQuest LLC
789 East Eisenhower Parkway
P.O. Box 1346
Ann Arbor, MI 48106-1346

In memory of Laurie Williams

1972-1997

Development of 'Smart' Biomaterials for Tissue Repair

Overall Contents

Detailed Contents of Chapters

Acknowledgements

Firstly, I should acknowledge my supervisor, Prof. D.P. Aeschlimann, for his contribution to this work. I would like to thank the EPSRC and Smith & Nephew for funding this PhD.

At the College of Medicine, I would like to thank Dr Phil Stephens, Dr Ryan Moseley and Dr Stuart Jones for checking this thesis and invaluable advice throughout the PhD. I would also like to thank Dr Elke Schoenherr for her advice and reagents for the immunohistochemistry work. I am grateful to Ms Kath Allsop for preparing sections for histological analysis of tissues, and to Dr Chris Pepper for his assistance with the flow cytometry. I would like to extend my thanks to Dr David Williams for his help in the surface plasmon resonance work, and to Dr Rachel Waddington for the use of equipment to carry out the protein purification. I am also very grateful to Helen Thomas, Sally Rosser-Davies and Martin Langley for their support, assistance and patience.

From the School of Biosciences, I would like to thank Dr Pascale Grenard for her help with the molecular biology work. I am grateful to Prof. Bruce Caterson and Dr Claire Curtis for the porcine chondrocytes. I would like to extend my thanks to Dr Gary Dowthwaite for his guidance with the CAM assay.

From Smith & Nephew, I am very grateful to my supervisors Dr Julian Adams and Dr Caroline Mayne for their support and ideas. I would like to especially thank Dr Mayne for her advice regarding the thesis. I am grateful to Ms Elizabeth Turp for organising the rat metatarsal assay, and to Ms Hannah Bowring for her assistance with the FT-IR. My thanks also to Dr Robin Chivers for his help with the rheology. I would like to thank Dr Hanne Bentz at Orthogene (USA) for carrying out the animal work for the ectopic bone formation assay, and Dr Neil Smythe at University of Cologne for the gift of 293 EBNA cells and vectors.

Finally, I am extremely grateful to my family and friends for their unending patience and support, and to Neil taking care of me.

Summary

Cartilage has only a limited capacity for self-regeneration following injury, leading to experimental and clinical attempts to induce healing of lesions. The use of biodegradable biomaterials for the delivery of bioactive agents or cells is key to facilitating tissue repair. This study focused on the regeneration of cartilage, with the hypothesis that a matrix that supports angiogenesis will, in the presence of, for example, bone morphogenetic protein-2 (BMP-2), stimulate rapid bone formation, while a matrix that inhibits angiogenesis will only undergo chondrogenesis. To provide a suitable matrix, this project characterised a hydrogel previously developed in this laboratory[1], formed by chemical crosslinking of an ethylenediamine derivative of hyaluronan. The crosslinking reaction could be carried out under physiological conditions, indicating that the hydrogel could be injected and crosslinked *in situ*. However, potentially toxic effects require further investigation. The hydrogel successfully delivered active BMP-2, to induce ectopic bone formation in a rat model. To inhibit angiogenesis, this project described the production of a truncated form of the vascular endothelial growth factor (VEGF) receptor, fms-like tyrosine kinase-1 (flt-1), consisting of the 3 N-terminal extracellular domains responsible for binding VEGF. This decoy receptor was demonstrated to bind VEGF. Preliminary angiogenesis and ossification assays revealed that higher levels of purity of the decoy receptor are required than achieved in this work, to determine if it can block VEGF-mediated angiogenesis and prevent progression of cartilage to bone. Nonetheless, this project demonstrated the suitability of the hyaluronan-based hydrogel, for the delivery of growth factors in regards to cartilage repair.

1. Bulpitt, P. and Aeschlimann, D. New strategy for chemical modification of hyaluronic acid: preparation of functionalized derivatives and their use in the formation of novel biocompatible hydrogels. J. Biomed. Mater. Res. **47**, 152-169 (1999).

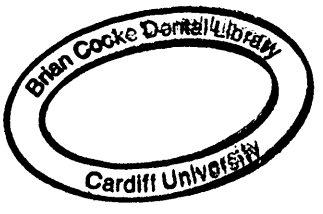

Abbreviations

BMP	Bone morphogenetic protein
CAM	Chick chorioallantoic membrane
cDNA	Complementary deoxyribonucleic acid
ECM	Extracellular matrix
ELISA	Enzyme-linked immunosorbant assay
ES	Embryonic stem cell
FBS	Foetal bovine serum
Flt-1	Fms-like tyrosine kinase-1
FT-IR	Fourier-transform infrared spectroscopy
GAG	Glycosaminoglycan
HA	Hyaluronan, hyaluronic acid
HAED	Hyaluronan, ethylene diamine derivative
KDR	Kinase domain receptor
MMP	Matrix metalloproteinase
MSC	Mesenchymal stem cell
OA	Osteoarthritis
PCR	Polymerase chain reaction
RA	Rheumatoid arthritis
ROS	Reactive oxygen species
SC_4-PEG	Succinimide ester of carboxymethylated 4 - arm polyethylene glycol
SDS/PAGE	Sodium dodecyl sulphate/polyacrylamide gel electrophoresis
Sflt-1	Soluble fms-like tyrosine kinase-1
SPA_2-PEG	2 - arm polyethylene glycol - succinimidyl propionate
SPA_4-PEG	4 - arm polyethylene glycol - succinimidyl propionate
TGF-β	Transforming growth factor β
TNF-α	Tumour necrosis factor-α
VEGF	Vascular endothelial growth factor
vWF	von Willebrand factor
WT	Wild-type

Introduction

Osteoarthritis (OA) and rheumatoid arthritis (RA) are debilitating diseases that affect millions of people worldwide, at a considerable cost to the Health services. Important developments have led to a surge of interest in the field, but cartilage still remains an elusive tissue to repair[1].

This project describes a strategy to regenerate cartilage by a) using certain signalling molecules that stimulate cartilage synthesis during development, b) via the application of a biomaterial that is based on cartilage components and is known to benefit the tissue and c) a control mechanism to ensure that only cartilage is synthesised.

This introduction provides the background to cartilage and how it develops naturally. The osteoarthritic and rheumatoid arthritic pathologies are discussed, as are the mechanisms that lead to joint destruction. The report focuses on a particular agent, vascular endothelial growth factor, known to be centrally involved in cartilage degradation and considers its role in health and disease. The treatment approaches for RA and OA will be discussed, including the application of biomaterials, perceived as being fundamental to many repair attempts.

1.1 Cartilage

Cartilage is a remarkable tissue. It functions for the lifetime of the organism in one of the physically toughest environments - provided it is disease free[2].

1.1.1 Cartilage organisation

Cartilage is an atypical tissue, as it is avascular and aneural, as blood vessels and nerves would compromise the compression properties of the structure. Three types of cartilage have been described – hyaline cartilage, fibrocartilage and elastic cartilage. The first type provides flexibility and support; it is responsible for reducing friction in joints and can resist compression. Hyaline cartilage is the most abundant form of cartilage in the body and is located at the ends of long bones, the anterior ends of ribs,

nose, and bronchi and constitutes part of the larynx[3]. Fibrocartilage is located in the menisci of the knee joint and intervertebral discs of the spine[3]. As its name suggests, elastic cartilage provides strength and elasticity, giving shape to structures such as the external ear and epiglottis[3].

Articular cartilage at the ends of long bones is classified as hyaline. The cartilage at the medial femoral condoyle (i.e., the bottom of the thigh bone) is only 2-3mm thick in humans, but nonetheless allows virtually frictionless movement[4]. The part of the joint conferring these properties can be divided into three groups – the articular hyaline cartilage, the synovial membrane and excreted fluid, and the underlying subchondral bone. The strength of the cartilage is conferred by collagen fibrils, with proteoglycans offering resistance to compression.

The predominant cell in articular cartilage is the chondrocyte, which is responsible for maintenance and homeostasis of the tissue. Surrounding each chondrocyte is a pericellular region that contains few collagen fibrils, but does contain type VI collagen and the proteoglycans, decorin and aggrecan. The territorial region surrounds this, and the extracellular matrix (ECM) most remote from the cells is termed the interterritorial region[4,5]. The ECM of cartilage is responsible for the strength and compressive properties of the tissue. It is primarily composed of collagens, proteoglycans and hyaluronan, but also contains other proteins important for the homeostasis. The components are described below. Figure 1.2 outlines the basic ECM structure. Table 1.1 summarises the components of cartilage responsible for homeostasis of the tissue.

Articular cartilage is organised into distinct zones that run parallel to the surface (Figure 1.1). The superficial zone at the cartilage surface contains isolated chondrocytes with a flat, spindle-like or ellipsoidal morphology, surrounded by a fine network of collagen fibrils (20nm diameter) orientated parallel to the surface. There are low levels of the proteoglycan aggrecan, although other proteins such as decorin, biglycan, and cartilage oligomeric matrix protein/thrombospondin-5 are more

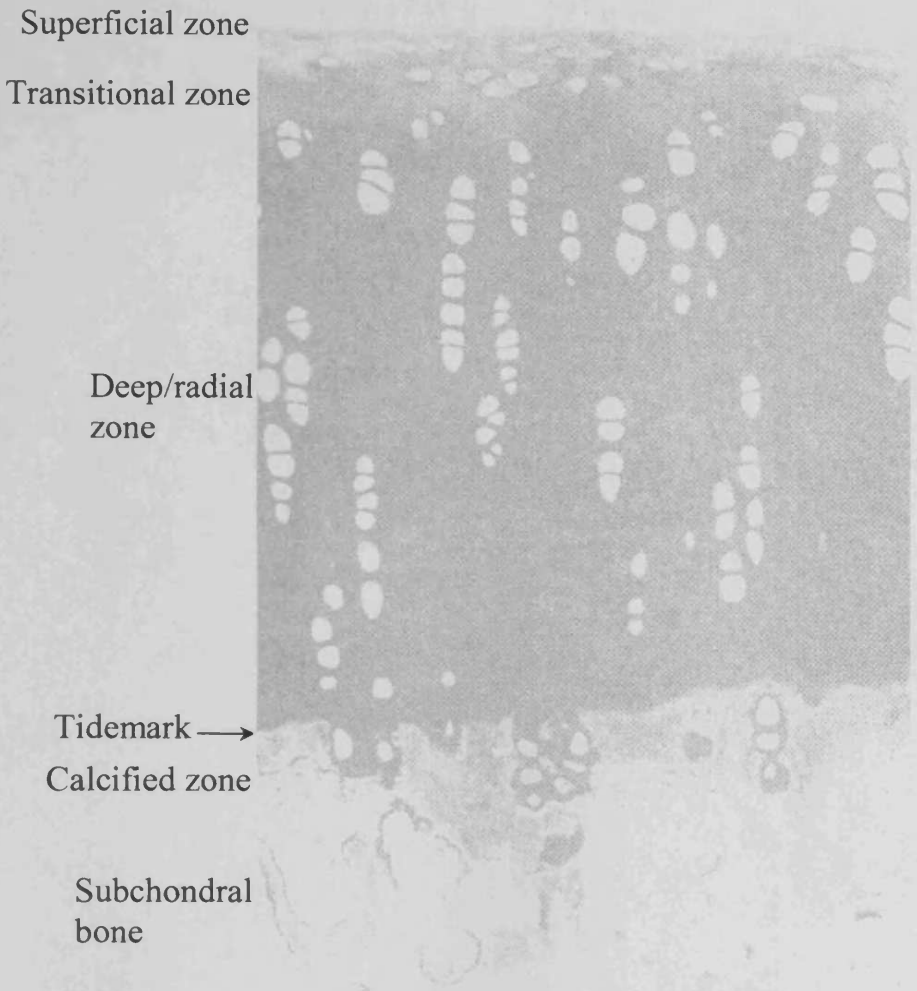

Figure 1.1: Light micrograph of mature rabbit cartilage from the femoral condoyle, stained with toluidine blue. Arrowheads indicate chondrocytes in the calcified zone. Original magnification: 300x. Adapted from Hunziker[4].

abundant in this zone[5], along with the zone-specific proteoglycan, surface zone protein[6]. High levels of collagen are necessary in this zone to resist high shear stresses, by imparting tensile strength on the tissue[7].

The transitional, or mid zone, underneath the superficial zone, occupies a greater volume of the tissue than the superficial zone. The chondrocytes assume a more spherical morphology and the collagen fibrils in this zone appear more disorganised compared to those in other zones, with some aligned in a more oblique manner[4]. Once again, each chondrocyte exists in isolation from its neighbour[4,7]. Cartilage intermediate layer protein (CILP) has been identified in this zone and although its role is not fully known, workers have speculated that it may be involved in maintaining ECM structure[8].

The radial, or deep zone, contains chondrocytes of a much larger size that are organised into distinctive stacks, or chondrons, each consisting of three or four cells[4]. These structures appear perpendicular to the surface, and form vertical columns of cells. The chondrocytes in this region are the most metabolically active and are rich in cytoplasmic organelles, such as endoplasmic reticulum and Golgi apparatus[7]. In the pericellular region surrounding each chondrocyte, increased levels of proteoglycans have been observed, and although collagen fibrils are less numerous compared to the zones above, the fibril diameter is increased (70-120nm diameter). These fibrils are also aligned perpendicular to the articular surface. The radial zone comprises the largest proportion of the cartilage volume and the high content of proteoglycans indicates that this layer may be primarily responsible for the dispersal of applied force[4,5,7].

The deepest zone of cartilage adjacent to the subchondral bone is the calcified zone. A tidemark exists between this region and the rest of the cartilage, which represents the front of mineralisation. During development, this front advances into proliferating cartilage with subsequent bone formation and lengthening. In the adult, the progression of the mineralization front is suppressed, otherwise the cartilage would become mineralised with loss of function. This suppression may be mediated by chondrocytes in the lower radial zone above the tidemark[4]. Early observations led to the conclusion that the chondrocytes in the calcified zone were metabolically inactive,

necrotic or dead, however, this may have been a consequence of the routine fixation process used and more subtle techniques have since revealed that these chondrocytes are in fact metabolically active[4]. These are encased in a non-mineralised pericellular and interterritorial matrix but are otherwise enclosed in calcified matrix, remaining organised in chondrons. Remodelling of this zone may be undertaken by osteoclasts[4]. As the calcified zone provides the interface between cartilage and bone, it is subject to considerable shear stresses and contains large collagen fibrils that are aligned perpendicular to the surface. The tidemark between the radial and calcified zones is observed to be gently undulating, but the cement line between the calcified zone and subchondral bone is much more convoluted and this inter-digitation provides the anchorage to the bone. This is the only region of cartilage where blood vessels exist, but no capillary loops are formed[9].

1.1.2 Collagens

Collagens confer tensile strength to the tissue. The fibrillar type II collagen accounts for 95% of the overall collagen composition in cartilage and is composed of three identical α_1 chains that form a triple helix[7,10]. Type II collagen is for the most part responsible for the basic network of cartilage[10]. The collagen network also entraps and provides binding sites for proteoglycans such as decorin and fibromodulin[10]. In addition, type II collagen contains a large number of carbohydrate groups, allowing more interaction with water than other collagen types[7].

Other collagens in cartilage include types VI, IX, X and XI. Types IX and XI are involved in the regulation of collagen fibril formation and crosslinking of fibrils[10]. Type X collagen is located in the hypertrophic and calcified zones of cartilage[10], although it has been identified at the cartilage surface[11]. Although the exact function of type X collagen is unclear, it may stimulate vascularisation[12]. Alternatively it may stabilise the matrix through interactions with chondrocytes and proteoglycans[14].

Table 1.1: A summary of the components of the adult cartilage ECM responsible for homeostasis of the tissue. (Continued on the next page.)

Component	Function	Interacts with	Ref.
Collagen type II	Provides structure. Confers tensile strength.	Types IX, XI collagens	7, 10
type VI	Attaches to chondrocytes. Forms microfibrils.	Chondrocytes	10, 15
type IX	Crosslinks type II collagen fibrils.	Type II collagen, itself	10
type X	Unclear, may stabilise proteoglycans or act as point for mineralisation.	Chondrocytes	13, 14
type XI	Regulates fibril formation.	Types II, IX collagens	10
Hyaluronan (HA)	Protective. Anchors aggrecan. Contributes to compressive properties. Induces cell proliferation and migration.	Chondrocytes, aggrecan	38, 43, 40, 47
Aggrecan	Confers shock-absorbing properties and resistance to compression.	HA, link protein	19, 22
Link protein	Stabilises interaction between aggrecan and HA.	HA, aggrecan	22
Fibronectin	Organises matrix.	Chondrocytes, proteoglycans	48, 27
Decorin	Regulates fibril formation. Inhibits cell migration.	Collagens, chondrocytes	25, 27, 28
Biglycan	Regulates fibril formation.	Collagens	15
Lumican	Mediates fibril formation by fibromodulin.	Collagens	29
Fibromodulin	Regulates fibril formation.	Collagens	29

(Table 1.1 continued from previous page)

Component	Function	Interacts with	Ref.
Superficial zone protein	Lubricates cartilage surface. Prevents adherence of cells to surface.	Heparan sulphate	6, 49
Cartilage intermediate layer protein (CILP)	Maintains ECM structure.	Matrix components	8
Thrombospondin-2 (TSP-2)	Anti-angiogenic.	Chondrocytes	50
Thrombospondin-5 (TSP-5)/cartilage oligomeric matrix protein (COMP)	Stabilises the ECM.	Collagens, matrilins	51, 52
Chondroadherin	Enhances chondrocyte adherence to ECM.	Chondrocytes	53
Matrilins	Involved in microfibril formation. Forms a link with larger fibrils.	Thrombospondin-5, aggrecan, collagens, itself	54, 28
Troponin I	Anti-angiogenic.	Chondrocytes	55
Tissue inhibitors of matrix metalloproteinases (TIMPS)	Anti-angiogenic. Inhibits matrix metalloproteinase (MMP) and aggrecanase activity.	Collagens	56, 57, 58
Chondrocyte-derived inhibitor of angiogenesis and metalloproteinase activity (CHIAMP)	Anti-angiogenic.	Collagens	59
Fibrillin-1	Forms fibrils. Inhibits chondrocyte proliferation/differentiation.	Chondrocytes, TGF-β, itself	60
Transforming growth factor-β (TGF-β)	Chondrogenic. Increases cell proliferation and differentiation.	Chondrocytes, collagens	61
Bone morphogenetic protein-2 (BMP-2)	Chondrogenic. Osteogenic.	Collagens, chondrocytes	62, 63, 64
BMP-7	Chondrogenic. Osteogenic. Maintains homeostasis.	Chondrocytes	65, 66, 62
Cartilage-derived morphogenetic proteins (CDMPs)	Upregulates aggrecan GAG synthesis.	Chondrocytes	67, 68

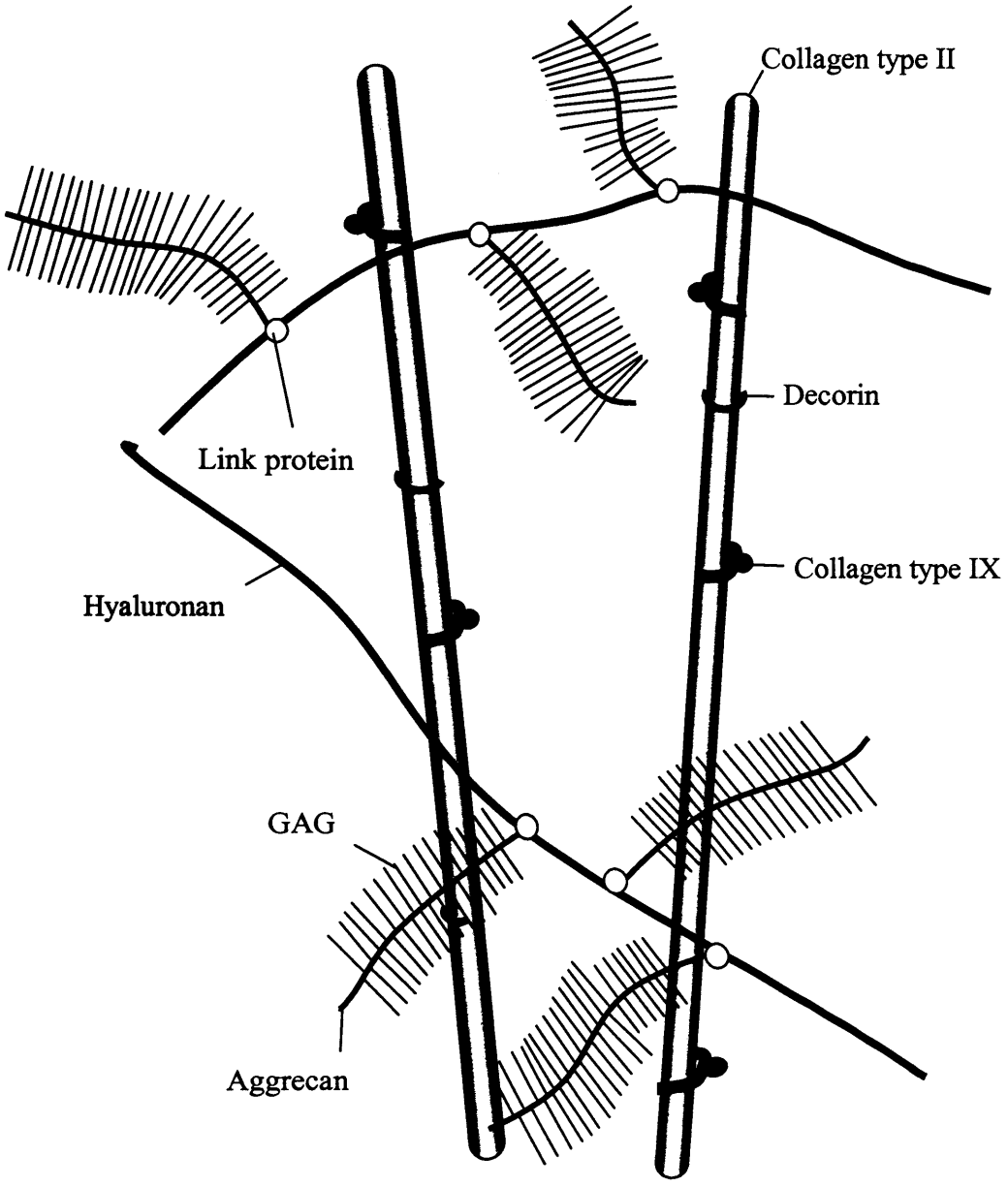

Figure 1.2: A schematic representation of the main components of cartilage and their inter-relationships. Adapted from Poole *et al.*[5].

1.1.3 Proteoglycans

Proteoglycans enable the tissue to resist compression. The prominent proteoglycan species is aggrecan (large aggregating protein) which has a mass of about three million Daltons. This is anchored to hyaluronan (HA) and the interaction is stabilised by link protein[22]. Over 100 glycosaminoglycan (GAG) chains are attached to the core protein and are comprised of chondroitin sulphate and keratan sulphate (Figure 1.3), which confer an overall negative charge on the whole structure and form nearly 90% of the total aggrecan mass[19,20]. These polyanions attract water to become highly, but not completely hydrated as the restrictive collagen network limits the degree of swelling. Cations in the surrounding fluid, such as Na^+ and H^+, are attracted to the GAGs[5]. The high ionic concentration increases the external osmotic pressure and therefore draws water into the cartilage. This swelling pressure contributes to the compression-resistant properties of cartilage[5,19].

Other proteoglycans include the small leucine rich proteoglycans (SLRPs), such as decorin, biglycan, fibromodulin and lumican[23]. They are involved in matrix organisation, indirectly influencing cell metabolism through the binding and requisition of growth factors[23], and modulate cell migration[27]. They also regulate collagen fibril formation[15,23,25,28,29]. Perlecan is a proteoglycan that contains heparan sulphate chains and acts as a cell-attachment protein[31]. In addition, heparan sulphate groups on the cell surface can sequester heparin-binding proteins, to provide a reservoir or facilitate ligand interaction with receptors[33-36].

1.1.4 Hyaluronan

HA can be utilised to form biomaterials in tissue repair (Section 1.6), and as such is of relevance to the present study (Section 1.7). Therefore, the role of endogenous HA in cartilage needs to be considered.

Meyer and Palmer first isolated HA in 1934 from the vitreous body in the eye[37]. Although HA is a GAG, it is not covalently attached to a protein and is not sulphated, unlike other GAGs (Figure 1.3). It is ubiquitously expressed throughout the body, usually associated with connective tissues[39]. The chain length of HA can vary, but is frequently found to be over a million Daltons, with an extended length of 2-25μm[38]. The anionic charges on the molecule form hydrogen bonds with water, while the

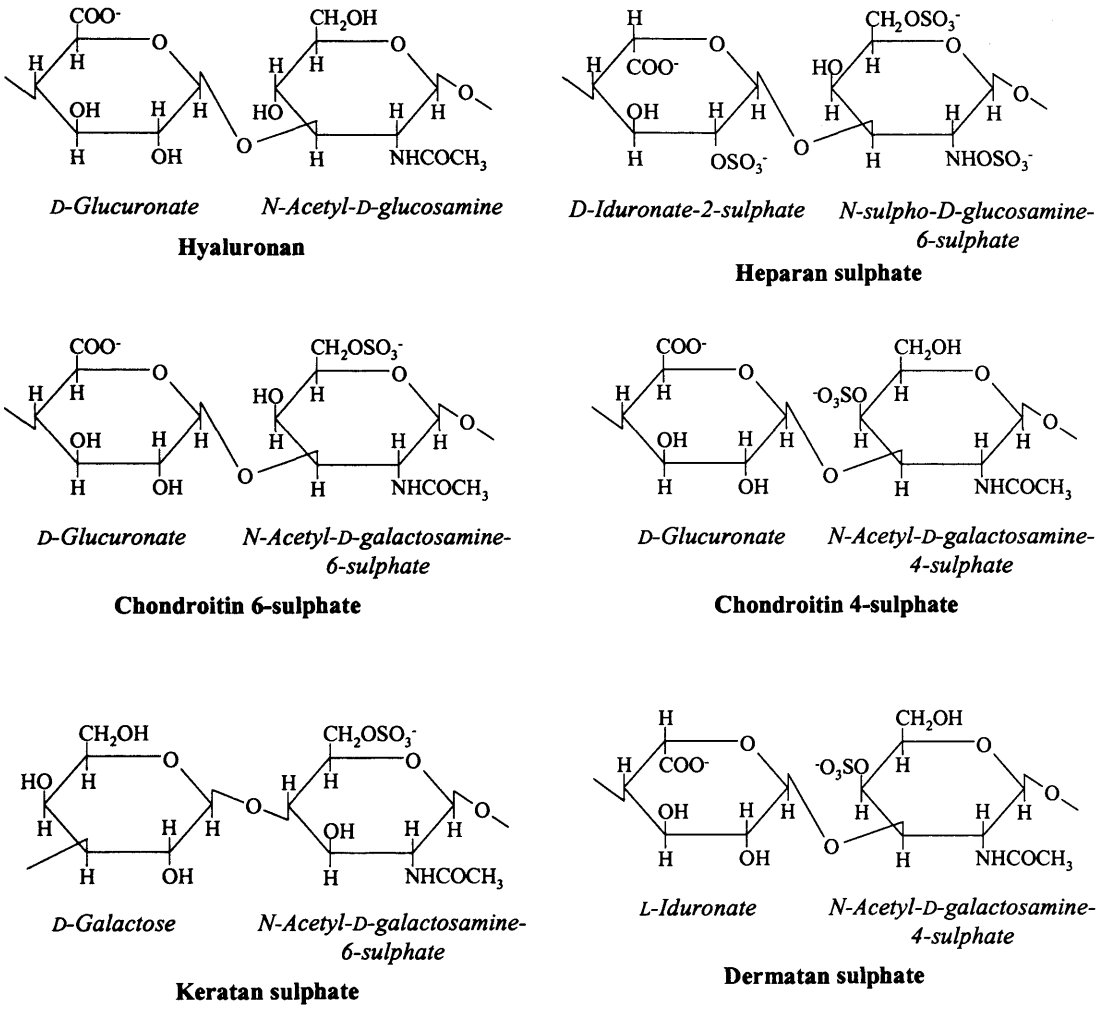

Figure 1.3: The disaccharide units of the GAGs commonly found in cartilage. Adapted from Voet and Voet[21].

backbone forms a loose coil structure in solution. This results in a very viscous fluid, containing HA coiled into a sphere with approximately 1000-fold water molecules associated with it[39].

Its hydration properties make HA a good space filler, where it can provide a protective pericellular coat around cells[40], regulate hydration in a tissue, and act as a lubricant on fibrils in skeletal muscle[38,39]. Furthermore, HA may ensure that chondrocytes do not aggregate together in the cartilage matrix[41]. During embryonic development, the high levels of HA found in the mesenchyme may be required to target cartilage formation and HA receptors have been implicated in the mediation of matrix assembly[40,42].

HA also forms a link between the chondrocyte and aggrecan chains to prevent dispersal and diffusion of aggrecan out of the tissue. The N-terminal G1 domain of the aggrecan core protein noncovalently binds to HA, stabilised by the link protein to create a very strong interaction[21]. HA attaches to chondrocytes via the cell surface CD44 receptor[43], which anchors the aggrecan/HA aggregate to the ECM. This immobilisation of aggrecan is of critical importance to the integrity of cartilage and its ability to withstand compression. HA also binds to the receptor for HA-mediated cell motility (RHAMM)[44].

The CD44 receptor activates a number of signalling pathways, including nuclear factor κB (NFκB), erB2 tyrosine kinase, the Rho and Rac1 GTPases, and src-related kinases[43]. This led to the recognition of HA as a signalling molecule. It can induce cell migration and proliferation through re-organisation of the actin cytoskeleton of the cell, as well as providing an ECM environment which promotes migration[43]. Furthermore, HA appears to have a function in the intracellular environment, but the exact roles are unclear[43]. HA has also been identified in the synovial fluid and contributes to the control of other macromolecule concentrations, via its space-filling capacity[45].

The physical properties of the HA molecule can be described in terms of viscoelasticity. During slow movement, the mechanical energy applied to HA is slow enough to allow the molecules to line up parallel with the direction of the force and

act as a viscous material. During more vigorous movement (running, jumping), there is insufficient time to allow re-orientation of the HA molecules and they act in a more elastic manner[46]. HA concentration and chain length is depleted with increasing age and arthritis, both in cartilage and the synovial fluid[45,69]. The shortening of the HA chain, combined with loss of the HA/aggrecan aggregate formation, means that the joint can no longer withstand loading as efficiently[46].

The protective role of HA around cells is observed in arthritic conditions. During inflammation such as RA, there is a risk of reactive oxygen species (ROS) arising from inflammatory cells destroying cartilage. These include hydrogen peroxide (H_2O_2), the superoxide radical species ($O_2^{\bullet-}$), and the hydroxyl radical ($^{\bullet}OH$), the latter being the most reactive but short-lived[70]. Although chondrocytes produce catalase and peroxidases to neutralise these agents, cell damage is still evident[71,47]. Furthermore, ROS can damage collagen, proteoglycans, glycoproteins and GAG components of the ECM, as well as de-polymerising HA[71]. However, HA absorbs ROS before cell damage can occur[47]. This protective role of HA has led workers to develop HA-based treatments for OA, by firstly replacing some of the destroyed HA, and secondly by enhancing the defence of the joint (Section 1.6.4).

However, there is a detrimental aspect to the de-polymerisation of HA, in the context of cartilage. West *et al.*[72] demonstrated pro-angiogenic activity of HA chains of between 3 and 45 disaccharides in length (1.1-17.0kDa). This has since been narrowed to 3 to 10 disaccharides, which have also been shown to increase cell proliferation and migration[73]. Furthermore, these HA oligosaccharides act in synergy with vascular endothelial growth factor (VEGF), an angiogenic growth factor with a pathological function in cartilage (Section 1.4.5)[74]. It appears that HA fragments elicit the angiogenic effect at least in part through the stimulation of matrix metalloproteinase (MMP)-9 and MMP-13 expression[75]. Although these properties are beneficial in events such as wound healing, they are of particular concern regarding cartilage, as these proteinases degrade collagen fibrils, aggrecan core protein and fibronectin[75].

1.1.5 Other cartilage matrix proteins

There are a number of other proteins present in cartilage that contribute to the properties and homeostasis of the tissue, summarised in Table 1.1. These include endogenous angiogenesis inhibitors, which prevent invasion of the subchondral bone into cartilage. These are of relevance to the present study, which aims to block angiogenesis to facilitate cartilage repair (Section 1.7). Angiogenesis inhibitors include Thrombospondin (TSP)-1 and TSP-2[76]. These proteins also regulate bone growth during development[50,76]. Another anti-angiogenic agent isolated from cartilage is troponin I, which is located in the chondrocytes[55]. This increases cell adhesion to the surrounding matrix, thus not allowing chondrocytes to detach and divide[55].

Tissue inhibitors of matrix metalloproteinases (TIMPs) are a family of proteins of which four members have been identified to date[77]. These elicit an anti-angiogenic effect by inhibiting the MMPs required for blood vessel formation. TIMP-3 can also inhibit an aggrecanase, ADAMTS-4 (a disintegrin and metalloproteinase with thrombospondin motif-4) in cartilage[57] and inhibit binding of VEGF to its kinase-domain receptor (KDR)[58].

In 1995, Ohba *et al.*[59] described the isolation of an anti-angiogenic agent from a chondrosarcoma line, identified by its inhibition of MMP-2 activity. This protein, chondrocyte-derived inhibitor of angiogenesis and metalloproteinase activity (CHIAMP), was found to be very similar to TIMP-2, so was speculated to be a member of the TIMP family.

1.1.6 The bone morphogenetic proteins

Bone morphogenetic proteins (BMPs) were originally identified as cartilage and bone formation-inducing proteins in ectopic bone formation assays[78] and thus are good candidates, BMP-2 in particular, to stimulate cartilage growth in the present study. They constitute a family of over 47 members identified so far, which exist in an inactive precursor form requiring proteolytic cleavage to an active form[62]. These are involved in the development of cartilage and bone, with several of the family being expressed in growing bone. BMPs 1-7 have been identified in chondrocytes associated with the human growth plate during development (Section 1.1.8)[79].

When applied to isolated chondrocytes, BMP-3 and BMP-4 induce some cell proliferation and matrix synthesis, and chondrogenic effects have also been shown in response to BMP-2 and BMP-7 *in vivo*[62,80]. BMP-2 also stimulates long bone growth during development by increasing not only chondrocyte proliferation, but also hypertrophy and alkaline phosphatase expression, a marker of ossification[63,64]. Interestingly, BMP-2 has been shown to retain the chondrocyte phenotype *in vitro* over 28 days[81], but this environment does not contain all the elements and signals found in a cartilage lesion.

Endogenous BMP-7 (osteogenic protein-1, OP-1) has been located in adult cartilage and exhibits higher expression of the mature protein in the superficial zone, while the deeper zones contain more of the precursor form[65].

1.1.7 Chondrocytes

Articular chondrocytes are derived from the mesoderm during embryogenesis[82] and although these only comprise 1% of cartilage, chondrocytes are responsible for the homeostasis of the tissue through anabolic and catabolic mechanisms[83]. Cartilage represents a relatively harsh environment for cells. The lack of blood vessels make diffusion of nutrients and cytokines difficult and there are considerable forces applied to the tissue. The accompanying osmolarity changes, combined with a high number of cations associated with the GAGs, further increase overall osmolarity[84]. Despite these challenges, chondrocytes synthesise the collagens, GAGs, glycoproteins and proteoglycans required for cartilage maintenance[83].

Generally, chondrocytes have a rounded morphology, except in the superficial zone where they are more flattened[4]. In the deeper zones, chondrocytes become hypertrophic, as identified by enlargement of the cells and the expression of type X collagen. The chondrocytes are responsible for the formation of zones throughout cartilage, through the varying degrees of expression of matrix components[8,85].

Chondrocytes can respond to mechanical or physical changes in the tissue in response to loading. Dynamic loading effects such as fluid flow, hydrostatic pressure and matrix deformation lead to increased synthesis of ECM[84]. However, continued, static

loading, such as a prolonged increase in osmolarity, can downregulate matrix synthesis[84]. The effects of dynamic loading explain why active exercise can promote cartilage integrity, while immobilisation of the joint lead to degeneration[86].

At least some of the stimuli to the chondrocytes are transmitted from ECM components through cell surface receptors, such as the integrin family, CD44 and annexin V[43,83,87]. It appears that adhesion to the surrounding matrix negatively regulates chondrocyte death. This is of particular relevance to OA, where progressive loss of the ECM components may result in reduced adhesion and cell death[88].

1.1.8 Endochondral ossification during development

The process of endochondral ossification described herein applies to the long bones, rather than intramembranous ossification that is involved in the formation of flatter bones, such as the skull and lower mandible.

During embryogenesis, limb development starts as an ectodermal bud that contains mesenchyme, at the tip of which forms the apical ectodermal ridge[117, 89]. Mesenchyme that is designated for chondrogenesis aggregates into condensations[117]. The cells become rounded and switch from the production of a mesenchymal matrix (types I and III collagens) to a cartilaginous matrix (types II, IX, and XI collagens)[118,90]. An isoform of type II collagen specific to the embryo is produced and termed type IIA collagen[119]. The pre-chondrocytes that are located towards the midregion of the condensed region become flattened and their axes lie perpendicular to the direction of the bone growth. Meanwhile, the cells in the epiphysis (towards the end of the forming bone) remain rounded. The flattened cells located in the mid-region of the forming bone undergo hypertrophy, when they exit the cell cycle, increase in size, synthesise type X collagen, chondrocalcin and accumulate glycogen[3,120,474]. This region now represents the mid-diaphysis, the centre of the bone shaft. In parallel, the rounded, epiphyseal chondrocytes continue to divide[117,118]. A membrane, the perichondrium, develops around the forming bone[121]. Some of the hypertrophic cells undergo apoptosis[3] and the lacunae left behind provide tunnels into which blood vessels can invade. These come from the perichondrium, accompanied by osteoblasts, osteoclasts, chondroclasts and haematopoietic cells. Matrix vesicles extrude from the hypertrophic chondrocytes and contain ATPase, to pump calcium

Figure 1.4: Haematoxylin & eosin stain of half of a foetal rat metatarsal, removed from the foetus at developmental day 19, and grown in organ culture for 7 days. The diaphysis is at the bottom of the image. Scale bar = 300μm.

and phosphorus ions into the vesicles against a concentration gradient[474]. This gives rise to mineralisation as calcium-phosphorus aggregates form and spread beyond the vesicle wall. These integrate with type I collagen synthesised by osteoblasts and water is displaced[474]. The resultant hydroxyapatite ($Ca_{10}(PO_4)_6(OH)_2$ forms rods or plates with hexagonal symmetry and confer compressive strength with rigidity, while the collagen provides flexibility and tensile strength[474]. As the trabeculae (calcified cartilage structures) surrounding the tunnels are resorbed by chondroclasts, osteoblasts begin laying down bone matrix[474]. This forms a collar of compact bone around the diaphysis of the cartilage, forming the primary ossification centre[3,120]. The blood vessels invade the epiphysis, to form the secondary ossification centre. The layer of cartilage sandwiched between the forming bone shaft and the secondary ossification centre is termed the epiphyseal growth plate[3]. As the chondrocytes proliferate and produce cartilage matrix, the growth plate moves away from the centre of the long bone. The accompanying mineralisation of the lower hypertrophic zone ensures long bone growth, while the growth plate width remains relatively constant[474]. Figure 1.4 illustrates the organisation of chondrocytes during endochondral ossification.

Several factors are involved in chondrogenesis, chondrocyte proliferation and matrix secretion. These allow longitudinal bone growth by ensuring cartilage is not totally replaced by bone and are summarised in Table 1.2. Table 1.3 summarises factors that are required for bone formation from the cartilaginous tissue.

The articular cartilage at the surface undergoes appositional growth, whereby new matrix is deposited on the surface and recently discovered progenitor cells in the surface zone are likely to synthesise this[122].

Table 1.2: A summary of the chondrogenic factors involved in endochondral ossification.

Factor	Function	Ref
Sonic Hedgehog (Shh)	Mediates limb patterning. Induces expression of BMPs.	89
Fibroblast growth factor-4	Interacts with Shh to mediate limb patterning.	89
BMPs (BMP-2, -4, -7)	Chondrogenic and osteogenic.	90, 62
Fibrillin-2	Interacts with BMP-7 to create a BMP-7 gradient through the tissue for chondrocyte differentiation.	91
Fibronectin	Mediates condensation of mesenchyme.	92
Syndecan-3	Organises cytoskeleton of cells during condensation.	93
Perlecan	Guides ECM structure. Involved in cell adhesion.	95
Sox9	Enhances expression of collagens and aggrecan.	95, 96, 97
Indian hedgehog (Ihh)	Involved in perichondrium formation and maturation of cells to osteoblasts. Inhibits chondrocyte progression to hypertrophy. Maintains proliferating chondrocytes.	98
Parathyroid hormone-related protein (PTHrP)	Stimulates proliferation of chondrocytes. Downregulates hypertrophy. Anti-angiogenic.	99, 100, 101
Chondromodulins	Anti-angiogenic. Stimulates proteoglycan synthesis.	102, 103
TGF-β1	Anti-angiogenic.	104
bFGF	Enhances matrix synthesis at low concentration. Decreases matrix synthesis at high concentrations. May decrease chondrocyte proliferation.	105
Insulin-like growth factor-1 (IGF-1)	Stimulates proteoglycan synthesis. Induces chondrocyte proliferation.	103,106
Matrix Gla Protein (MGP)	Inhibits mineralisation. Promotes chondrocyte survival.	107

Table 1.3: A summary of factors required for angiogenesis and bone growth during endochondral ossification.

Factor	Function	Ref.
Membrane type-1 MMP (MT1-MMP)	Involved in cartilage resorption. May create vascularisation canals to form secondary ossification centre. Stimulates VEGF expression.	108, 109
MMP-9	Pro-angiogenic. Degrades cartilage matrix. Induces apoptosis of terminally hypertrophic chondrocytes.	110, 111
VEGF	Pro-angiogenic. Involved in mineralisation. A chemoattractant for osteoblasts and osteoclasts. May provide directional cues for angiogenesis.	112, 113, 114
Vitamin D3	Stimulates VEGF expression in osteoblasts.	115
Transferrin	Chemoattractant to endothelial cells, to promote blood vessel invasion	116

1.2. Osteoarthritis and rheumatoid arthritis

The inability of cartilage to spontaneously repair major damage has been recognised for hundreds of years and led Hunter to state in 1743 that "ulcerated cartilage is a troublesome thing in that when once destroyed it is not repaired"[123]. Although there are several diseases associated with cartilage and bone, this report focuses on cartilage damage that can lead to the arthritic conditions that afflict millions of people each year. It is estimated that 350,000 people in the UK currently suffer RA and that eight million suffer from OA (ARC, www.arc.org.uk).

Both OA and RA increasingly occur with age, as a possible consequence of changes in the structure of cartilage. During ageing, the HA polymers decrease in length and partially lose their viscoelastic properties[69]. The proportion of type II collagen increases, rendering the tissue more brittle[124]. Aggrecan core protein length decreases, with the free G1 domain accumulating in the matrix[125]. The SLRPs also exhibit shortening of their GAG chains[126]. Some of these changes may be attributed to ROS damage throughout the lifetime of the cartilage, although the true effects on tissue function are not completely understood[127]. These changes can exacerbate the progression of arthritic diseases.

RA is an autoimmune disorder[128,129]. It is characterised by inflamed synovial membranes that contain antibodies against type II collagen, derived from synovial T-cell stimulation[128,129]. An increase in angiogenesis causes more inflammatory cells to target the synovial membrane, with proteinases and inflammatory cytokines being secreted from the inflamed synovial membrane[129]. Furthermore, a pannus forms, which is a synovial tissue that overlays and invades the articular cartilage, through the activity of proteinases produced by the mononuclear cells and fibroblasts within the pannus[129] (Figure 1.6B).

OA can result from injury, genetic disposition or wear and tear on the joint. Historically, degradation of cartilage was seen as a passive process, but in the last few decades, activity within the tissue and surrounding synovium has led to the recognition of a disease state[130]. An overview of the progression to OA is shown in Figure 1.5. The condition is characterised by the loss of cartilage accompanied by

invasion of subchondral bone. Osteophytes form, which are spurs that start as chondrophytes, extending from the synovium at the joint margins. These reduce the joint space and restrict movement. They may protect articular cartilage by re-distributing forces and represent attempts at repair by the tissue. However, they have also been associated with joint deformity and severe pain[131]. The synovium becomes inflamed as the disease progresses[3,132]. As in RA, a pannus-like material develops over the cartilage, which synthesises catabolic enzymes[133] (Figure 1.6A). The surface of the joint becomes fibrillated as the matrix is degraded, causing a rough surface with fissures that eventually reach the underlying bone[134] (Figure 1.6C and D).

Injury to cartilage can be classified into three types. The first is matrix disruption from blunt trauma, which chondrocytes compensate for by synthesising new ECM[7]. The second is a partial defect resulting from disruption of the surface of cartilage, but does not extend to the subchondral bone[7]. The third is the full thickness defect that penetrates the subchondral bone[7]. The last two types do not repair successfully and in the long term can lead to OA. Penetration of the subchondral bone allows progenitor cells and blood vessels to enter the injured site, leading to clot formation and regeneration of a cartilage matrix[135,2]. However, this new matrix is more fibrous than hyaline cartilage and cannot withstand the demands placed upon it, leading to progressive degeneration[7,136]. Partial defects exhibit little repair, as chondrocytes initially do respond by increased proliferation and matrix synthesis, but these have a low mitotic and proliferative activity and are embedded in a fairly rigid ECM, making relocation to the site of injury difficult[7,137]. Such problems are increased with age, as the number of progenitor cells in bone marrow are decreased[136].

A genetic factor was first identified from studying occurrences of OA between monozygotic and dizygotic twins, although environmental factors also influence predisposition[138]. However, the role of genetics is very complex, as variables such as weight, muscle mass and predisposition to injury may arise from a genetic or an environmental origin[138].

The healthy joint

Mild osteoarthritis

Severe osteoarthritis

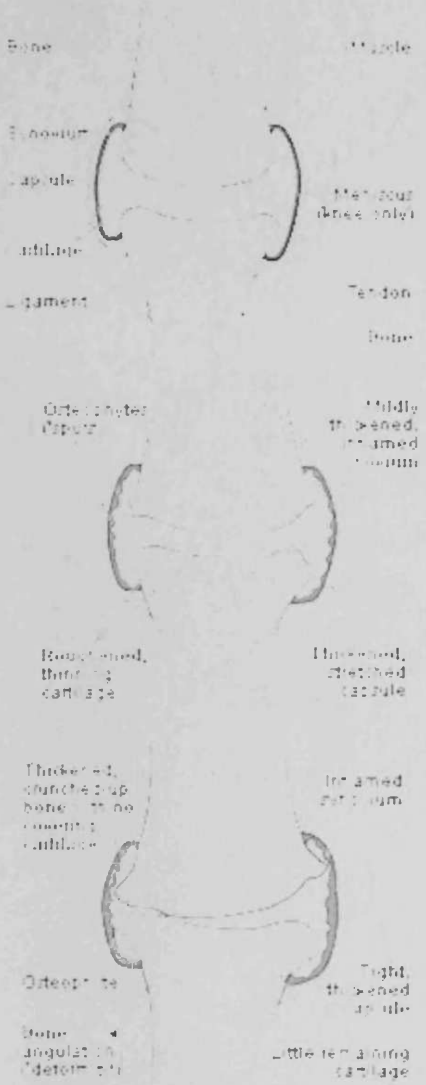

Figure 1.5: A representation of the degradation of the joint with progressive OA. Adapted from ARC (www.arc.org.uk).

1.2.1 Biological factors in osteoarthritis

The present study describes the development of a biomaterial for the treatment of cartilage damage leading to OA (Section 1.7), so this form of arthritis is focussed on. OA generally develops from the surface of cartilage, with the initial changes observed by fibrillation of the superficial zone (Figure 1.6C and D)[137,140]. In normal cartilage, there is a fine balance between anabolic and catabolic matrix turnover that becomes disrupted in OA[137].

Chondrocyte death following mechanical trauma has been reported[141], which, in the absence of a phagocytosis mechanism in cartilage, leads to release of calcium ions and cytokines that may further enhance degradation[137]. Chondrocyte apoptosis may be a consequence of matrix degradation during OA, as cell adherence via integrins to the ECM has been recognised as a key element in chondrocyte survival[88]. However, sufficient chondrocytes may remain metabolically active to synthesise new matrix[137].

Chronic inflammation of the joint is accompanied by the expression of inflammatory cytokines by both inflammatory cells in the synovium and chondrocytes[142,143]. The effects of these cytokines are summarised in Table 1.4. The degradation of cartilage generates ECM fragments, some of which can further exacerbate the destruction of the tissue. Furthermore, proteinases and other enzymes, induced by inflammatory cytokines, are responsible for the degradation of the cartilage matrix.

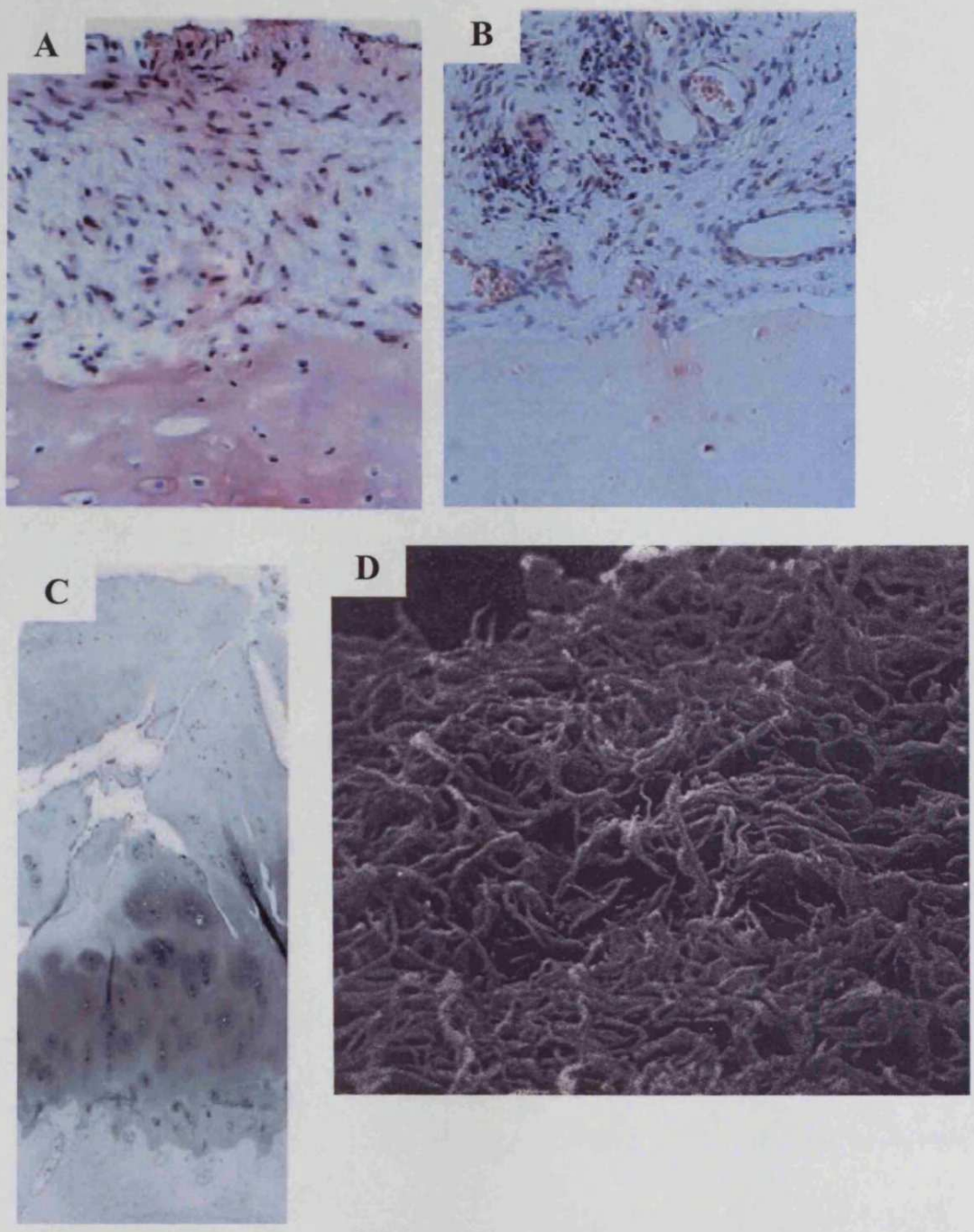

Figure 1.6: Light micrographs of histological sections of pathologies observed in arthritic diseases. A: haematoxylin & eosin stain of a pannus (top) overlaying cartilage in OA. B: haematoxylin & eosin stain of a pannus (top) covering cartilage in RA. C: safrinin O/fast green stain of a cartilage section in severe OA, loss of the dark staining towards the surface (top) indicating loss of proteoglycans. Original magnification: x40. D: scanning electron micrograph of the surface of OA cartilage, showing the exposed collagen fibrils. Original magnification: x100. A and B adapted from Yuan *et al.*[133], C adapted from Nakase *et al.*[139], D adapted from Minns *et al.* [134].

Table 1.4: Factors involved in the degradation of cartilage associated with OA. (Continued on the next page.)

Factor	Effects in OA	Ref.
ECM fragments:		
Fibronectin	Induces production of TNF-α, IL-1β, MMP-1, MMP-2, MMP-3, MMP-9.	144, 145
Type II collagen	Inhibits type II collagen expression.	146
HA	Pro-angiogenic. Decreases aggregation of aggrecans.	72, 147
Link protein	Induces collagen synthesis.	148
Inflammatory cytokines:		
Interleukin-1 (IL-1) (α and β forms)	Stimulates the production of IL-6 and IL-18. Inhibits prostaglandin synthesis. Inhibits chondrocyte proliferation. Induces NO and COX-2 synthesis. Downregulates *Sox9* expression. Induces MMP-1, MMP-3, ADAMTS-4 synthesis. Upregulates VEGF expression.	49, 142, 149, 150, 151, 152,153, 154, 155, 156
IL-6	Stimulates production of TIMPs.	158, 159
IL-8	Chemoattractant to neutrophils.	160
IL-17	Stimulates IL-1 and TNFα production. Induces activity of aggrecanases.	161, 162
IL-18	Inhibits chondrocyte proliferation. Increases NO and COX-2 synthesis. Induces IL-1 and TNF-α expression.	149
Tumour necrosis factor-α (TNF-α)	Induces ROS expression. Pro-angiogenic, through the upregulation of VEGF.	163, 164, 165, 166, 167
Reactive oxygen species (ROS), including nitric oxide (NO)	May induce chondrocyte apoptosis. Decreases matrix synthesis. Induces MMP-3 and MMP-13 expression. Stimulates inflammatory cytokine synthesis. Induces NO synthesis. Degrades collagen and HA. Can inhibit inflammatory cytokine synthesis. Involved in production of TIMP-3.	165, 168, 169, 170, 171

(Table 1.4 continued from the previous page)

Factor	Effects in OA	Ref.
Proteinases:		
MMP-1	Degrades type II collagen in RA.	157
MMP-3	Activates other members of MMP family. Cleaves types II, IX, X, XI collagens. Stimulates TGF-β expression.	172,173, 174
MMP-9	Digests denatured collagens.	175
MMP-13	Degrades type II collagen in OA.	176
MT1-MMP	Can promote angiogenesis, through inducing VEGF.	177, 178
Aggrecanases: A disintegrin and metalloproteinase domain with thrombospondin motif (ADAMTS)-4, -11	Degrades core protein of aggrecan. ADAMTS-4 may digest decorin and fibromodulin. ADAMTS-4 (with MMPs) degrades TSP-5.	179, 180, 181, 153
Cathepsin-B	Activates MMPs. Degrades aggrecan, TIMPs and type X collagen.	182, 183, 184, 185
Cyclooxygenase-2 (COX-2)	Stimulates prostaglandin E_2 production.	186, 187
Prostaglandins	Upregulate COX-2, IL-6 expression. Promote inflammation. Osteogenic. Upregulate VEGF.	186,188, 189, 190

Table 1.5: Growth factors upregulated in OA

Factor	Effects	Ref.
TGF-β	Upregulates aggrecan, HA synthesis. Antagonises IL-1. Downregulates MMP-1,-8,-2. Upregulates MMP-9,-13. Induces TIMP expression.	191, 62, 192, 193, 194, 195, 171
IGF-1	Antagonises IL-1, TNF-α. Inhibits chondrocyte apoptosis.	191, 196
BMP-2	Induces type X collagen synthesis. Stimulates proteoglycan synthesis.	197, 139
BMP-7	Upregulates aggrecan, HA synthesis. (Levels of BMP-7 decrease with age.)	147, 198
TNF-stimulated gene-6 (TSG-6)	Competes with HA for aggrecan binding, potentially disrupting matrix. Blocks activation of MMPs.	201, 202
TIMPs	Inactivates MMPs, ADAMTS-4,-5. Blocks VEGF activity.	57, 58
Growth factors with deleterious effects		
bFGF	Involved in bone resorption and joint destruction. Pro-angiogenic.	199, 200
VEGF	Pro-angiogenic, pro-inflammatory. Stimulates MMP expression.	224, 225, 318

Several anabolic factors are initially upregulated in response to damage, indicating a repair response by chondrocytes[137]. Some growth factors may be sequestered on the ECM and released, thus activated, upon degradation of the ECM[61]. These are summarised in Table 1.5. The regulation of cartilage degradation or regeneration is not easily divided into solely anabolic or catabolic factors. For example, while reactive oxygen species (ROS) can induce MMP synthesis[165], they also play roles in the synthesis of tissue inhibitors of MMPs (TIMPs), thus protecting cartilage[171]. Moreover, the administration of TGF-β into murine knees resulted in an OA phenotype[203], in contrast to the anabolic activities listed in Table 1.5.

Parallels can be drawn between endochondral ossification during development and OA. Chondrocytes re-express pro-type IIA collagen, expressed in chondroprogenitor cells during development[137]. Markers of hypertrophic chondrocytes[204] and ossification reappear in cartilage[205-207]. Furthermore, the pattern of GAG synthesis during development is replicated in OA[208]. The higher rate of proliferation during endochondral ossification returns in OA[117]. However, without the directional and proliferative controls present in the growth plate, densely packed clonal clusters of over 100 cells have been observed[209,117]. These large groups of cells may result in areas of structural weakness.

1.3. Angiogenesis

This process has been implicated in OA and the present study focuses on the inhibition of the angiogenic factor VEGF as part of a cartilage repair strategy (Section 1.7). Therefore, the roles of angiogenic agents such as VEGF need to be understood.

Angiogenesis describes the formation of new capillaries from pre-existing blood vessels[210,211]. In the adult, angiogenesis is usually restricted to processes, such as wound healing, the female reproductive cycle, placenta function during pregnancy and in bone remodelling[210,474]. Deregulated angiogenesis can contribute to a substantial number of diseases, including cancer, choroidal neovascularisation in the

eye, asthma, psoriasis, allergic dermatitis and arthritis[211]. Angiogenesis responds to hypoxia and various angiogenic factors, such as VEGF (Section 1.4)[212].

1.3.1 The process of angiogenesis

Existing blood vessels dilate and release MMPs to degrade the basement membrane, mediated by VEGF and Angiopoietin-1 (Ang-1)[212,213,211]. This allows the migration of cells[214] and the release of factors sequestered in the ECM of the basement membrane, such as TGF-β, bFGF, TSP-1 and TIMPs, required for controlled degradation and matrix regeneration[211,58,76]. A bud forms, a lumen develops within it and the structure advances to form loops with other buds[215]. A new basement membrane surrounds the new capillary and platelet-derived growth factor-BB (PDGF-BB), TGF-β and Ang-1 stabilise the capillary[215]. They promote junction formation between endothelial cells and recruit pericytes and smooth muscle cells, to stabilise the capillary and regulate endothelial cell proliferation[215].

1.3.2 Angiogenesis in arthritis

During the progression of arthritic diseases, pathological angiogenesis occurs in the synovial membrane and from the subchondral bone[200]. The synovial membrane is vascular under normal conditions and can meet the metabolic demands of the nearby avascular cartilage. Synovitis (synovial inflammation) exhibits changes in the pattern of blood vessels within the synovial membrane[216,217]. This results in less regulated blood vessel growth[218,219] and VEGF, Ang-1, bFGF and TNF-α are upregulated in the synovial membrane[166,220]. Resultant synovial proliferation leads to pannus formation, especially in RA[221] VEGF is discussed in more detail in Section 1.4).

Angiogenesis also contributes to osteophyte growth and maintains an inflamed synovium[222]. Moreover, sensory innervation can follow angiogenesis resulting in neurogenesis in the joint, with subsequent pain[222].

Invasion of blood vessels from the subchondral bone also contributes to cartilage destruction. In OA, capillaries encroach above the calcification tidemark, with subsequent calcification and mineralisation of the tissue, mirroring endochondral ossification. This causes structural weakening and as the tidemark rises and cartilage is replaced by bone[9,223].

Enomoto *et al.*[224] revealed that hypertrophic chondrocytes from both OA and healthy patients express VEGF, but its receptors (fms-like tyrosine kinase-1 (flt-1) and kinase domain receptor (KDR) (Section 1.4.6), were only expressed in OA cartilage. Furthermore, this study demonstrated that VEGF stimulated MMP-1 and MMP-3 expression in OA chondrocytes. Other MMPs, including MMP-8 and MMP-13, have been discovered to be upregulated by VEGF in cartilage[225]. While only the $VEGF_{121}$ and $VEGF_{189}$ isoforms have been detected in osteoarthritic cartilage, isoforms $VEGF_{121}$ and $VEGF_{165}$ have been identified in synovial fluid of rheumatoid arthritis patients[226]. The isoforms are discussed in more detail in Section 1.4.2.

VEGF associated with the chondrocytes may also stimulate blood vessel invasion from the pannus into cartilage[227]. The VEGF in normal cartilage may be sequestered and neutralised by connective tissue growth factor (CTGF), which is produced by the chondrocytes in normal tissue[227]. MMPs can release VEGF from its complex with CTGF, thus activating it[227]. Furthermore, HA fragments have been found to act in synergy with VEGF, which would further stimulate blood vessel invasion[74].

Normal articular cartilage contains anti-angiogenic agents that prevent blood vessel invasion in healthy tissue[200]. For angiogenesis to occur, either the increase in active VEGF overrides the inhibitory effects, or the anti-angiogenic factors are decreased. The latter possibility was demonstrated by the loss of the anti-angiogenic agent, chondromodulin-1, from the superficial zone in early OA, followed by a reduction throughout the tissue in more advanced OA[228].

4. Vascular Endothelial Growth Factor

The existence of a factor inducing the growth of blood vessels was first proposed in 1948, following studies of vascularisation of foetal and neo-natal retinas[229]. In 1989, two groups described a novel growth factor, expressed by pituitary cells, capable of stimulating endothelial cells, but not affecting other cell types[230,231]. This was identified as vascular permeability factor (VPF), discovered earlier in the decade[232] and was subsequently named vasculotropin[230], or vascular endothelial growth factor

(VEGF). VEGF was later discovered to have a physiological role in angiogenesis and has since been implicated in numerous physiological and pathological processes[233].

1.4.1 The structure of VEGF

The human VEGF gene is organised into eight exons, separated by seven introns[234]. Studies on the crystal structure of this molecule have shown that VEGF exists as a homodimer, covalently linked by two disulphide bridges, in an anti-parallel orientation[235]. VEGF is typically secreted as a 46kDa homodimer, which upon glycosidase digestion is reduced to 42kDa[236]. The N-terminus contains a hydrophobic signal peptide targeting the growth factor for secretion[234].

1.4.2 Splice variants

Alternative exon splicing gives rise to a number of isoforms, five of which have been identified[234,237,238] and are named according the number of amino acids (Figure 1.7). The variants $VEGF_{121, 165}$ and $_{189}$ are more prolifically expressed, with $VEGF_{165}$ being the most abundant form in the majority of tissues and is responsible for the 46kDa product most commonly found[239]. The $VEGF_{145}$ and $VEGF_{183}$ variants are less abundant[238,240]. Exons 6 and 7 are basic heparin-binding sequences, so the isoforms $VEGF_{165}$ and $VEGF_{145}$ bind heparin weakly, while $VEGF_{189}$ and $VEGF_{206}$ bind heparin with a greater affinity, for immobilisation on cell surfaces or in the ECM[239]. $VEGF_{121}$, an acidic variant that lacks the heparin-binding domains, remains soluble in the ECM[239]. Digestion of $VEGF_{165}$ by plasmin removes the heparin-binding domain and gives rise to another isoform of VEGF, $VEGF_{110}$[239,241]. Although there is some evidence that removal of the C-terminal heparin-binding domain does not inactivate the growth factor[239], the ability of cleaved VEGF to stimulate mitogenesis and cell proliferation appears to be reduced[242].

It has been suggested that the spatial arrangement of bound VEGF on the cell surface provides directional stimulatory cues to the orientation of vessel formation[239]. Alternatively, the binding of VEGF to heparan sulphate may facilitate binding to VEGF receptors. This was supported by Gitay-Goren *et al.*[33], who determined that the addition of heparin to cultures of endothelial cells enhanced interactions between VEGF and its receptors.

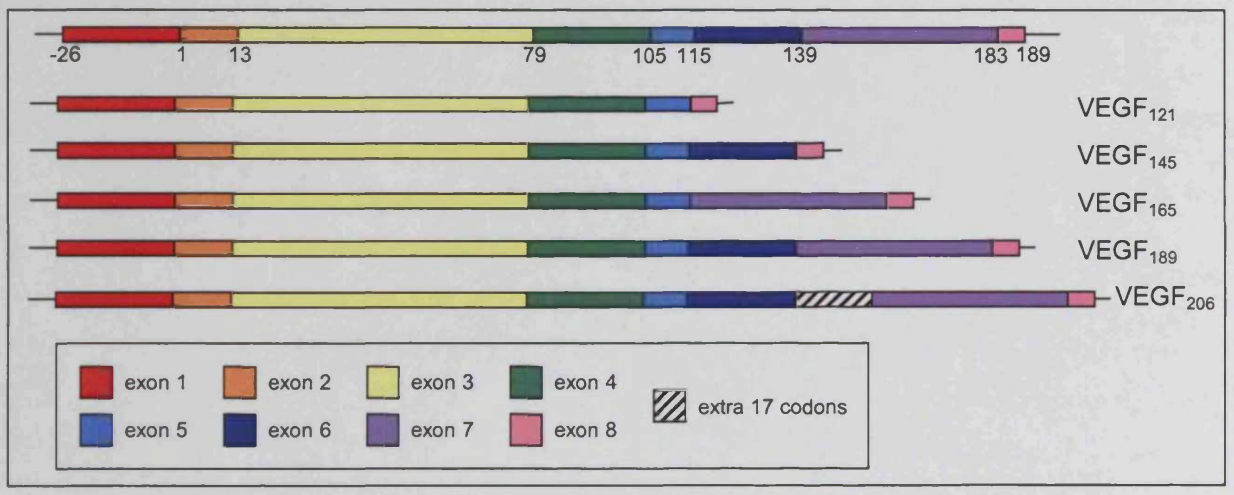

Figure 1.7: Top, the 8 exons of the VEGF gene. Numbers refer to the amino acids. The 5 splice variants of VEGF are represented below. Exon 1 is mainly the signal peptide, exons 6 and 7 confer heparin-binding ability.

Keyt *et al.*[241] postulated that the distribution of the various VEGF isoforms created an activity gradient away from the trigger site. They suggested that upon stimulation, a number of isoforms are secreted, $VEGF_{165}$ probably being the most abundant. The smaller isoforms ($VEGF_{110}$ and $VEGF_{121}$) can diffuse the furthest to stimulate proliferation and migration. As they have a weaker signalling ability, intensity of the angiogenic signal would therefore be decreased. At the trigger site, sequestered $VEGF_{189}$ and $VEGF_{165}$ can more strongly stimulate angiogenesis, to generate a strong signal at the trigger site which decreases with distance.

1.4.3 Related growth factors

VEGF (also known as VEGF-A) has been shown to have structural and sequence similarities with other cysteine-knot growth factors, such as PDGF, TGF-β2 and placenta growth factor (PlGF)[235,243]. PlGF exists as a homodimer, but has been found to form heterodimers with VEGF and as such, can elicit an angiogenic response[244].

Other members of the VEGF family have been identified. VEGF-B has approximately 43% homology with $VEGF_{165}$ in the mouse equivalents, and has been located primarily to the muscle, heart and pancreas[245]. VEGF-C has approximately 32% homology to $VEGF_{121}$ and it guides the angiogenesis of the lymphatic system[246]. VEGF-D is more closely related to VEGF-C than to other family members[247]. VEGF-D is most abundant in the lung and heart, but due to its similarity in binding specificities to VEGF-C, it has been implicated in the development of the lymphatic system[247]. VEGF-E is a virally encoded protein and stimulates angiogenesis in the host, following infection[248]. An interesting feature of VEGF-E is that it lacks the heparin-binding domain, yet is still highly active and can bind to the KDR receptor[248].

1.4.4 Biological functions of VEGF

VEGF expression is induced by low oxygen and nutrient levels (hypoxia and hypoglycaemia, respectively) through the transcription factor HIF-1[249]. Reducing excess capillary formation from an initial hypoxic signal is controlled by a reduction in the concentration of VEGF[249].

Its importance was indicated by embryonic lethality caused by deletion of only one of the VEGF alleles, accompanied by reduced vascularisation in the embryos[250,251]. It

has been shown to be a potent angiogenic agent both *in vitro* and *in vivo* assays[230]. VEGF induces vascular permeability[252] and acts as a chemotactic agent[253], attracting endothelial cells to the site of new vessel formation. Furthermore, VEGF stimulates the expression of plasminogen activators[254] and MMPs[225], to digest the basement membrane around pre-existing blood vessels. VEGF also has a vaso-protective role in promoting endothelial cell survival, as it can act as an anti-apoptotic agent[255,250] and increase focal adhesions[256].

VEGF can promote haematopoietic stem cell survival[257] and has a role in endochondral ossification (Table 1.3). Identification of VEGF receptors on non-endothelial cells has led to the proposal of an autocrine loop in VEGF signalling[258,259,260,114]. This mechanism was deduced when small intracellularly acting inhibitors of VEGF blocked haematopoietic stem cell colony formation, while extracellularly acting ligand/receptor inhibitors failed to have any effect[257].

VEGF retains a physiological role in the adult, even though flt-1 and KDR receptors are down-regulated in the adult endothelium[261]. Inhibition of VEGF in the adult has led to defects in wound healing[244], infertility through disruption of the female reproductive cycle, teratogenicity, a halt in ulcer healing in the gastrointestinal tract[200], and amyotrophic lateral asclerosis[262].

1.4.5 The pathological role of VEGF

As VEGF is stimulated in response to hypoxia, expression of VEGF is elevated in tumours, especially in regions close to avascular necrotic patches[263,264,265]. The role of VEGF in tumour formation has been well documented[265,266]. Therefore, the inhibition of VEGF has gained considerable merit as an anti-cancer therapy[267-272]. Mechanisms of VEGF inhibition are discussed in Section 4.1.

One of the leading causes of age-related blindness is due to VEGF-induced vascular invasion into the retina, leading to conditions such as retinopathy, sometimes as a result of diabetes mellitus[273]. Atherosclerosis is accompanied by inflammation, resulting in accumulation of macrophages at the site of injury[3]. VEGF has been found to stimulate vascularisation of the atherosclerotic plaque that destabilises it, increasing the risk of potential rupture with haemorrhaging[274]. Moreover, inappropriate VEGF

expression can lead to skin conditions, such as psoriasis and dermatitis[275,276]. Section 1.3.2 discusses the role of VEGF in RA and OA.

1.4.6 Receptors of VEGF

The present study aims to inhibit angiogenesis through a decoy receptor of VEGF (Section 1.7), which requires an appreciation of the structures and roles of the endogenous receptors. The two cell-surface VEGF receptors are fms-like tyrosine kinase-1, (flt-1, VEGF receptor-1) and kinase domain receptor (KDR, VEGF receptor-2, flk-1 in mice)[277]. Both are glycosylated and produce mature proteins of 180-185kDa (flt-1)[278], and 200kDa (KDR)[279]. Flt-1 exhibits a higher affinity for VEGF than KDR, with a dissociation constant (K_d) of 10-20pM[280], compared to a K_d of 75-125pM for KDR[281]. The extracellular region of each receptor contains seven Ig-like domains and the VEGF-binding site. After a short membrane-spanning sequence, the intracellular region contains tyrosine kinase domains[280,281]. The receptors belong to the immunoglobulin superfamily, which include receptors for FGF, stem cell factor and PDGF[282-284].

The first three extracellular domains of both flt-1 and KDR contain the VEGF binding site[285,286], illustrated in Figure 1.8. Residues on each monomer of VEGF contribute to receptor binding, via a groove between the monomers[287,235]. It has been proposed that the linker between the second and third domains of flt-1 fits into this groove[287]. In contrast, residues on KDR that fit into the VEGF groove are located in the third domain[235,288,289].

The first extracellular domain of flt-1 and KDR is required for high affinity binding[288] and may shield the hydrophobic binding interface of domain 2, to be displaced by VEGF binding[287]. The fourth domain on both receptors is responsible for dimerisation, lacking the disulphide bridges present in the other domains, which allows greater flexibility[289,290]. VEGF binding may result in a conformational change in the fourth domain to activate the receptors[290]. This prevents a signal arising from spontaneous dimerisation of receptors in the absence of VEGF, although *in vitro* studies have found that receptors dimerise and weakly signal without VEGF[286].

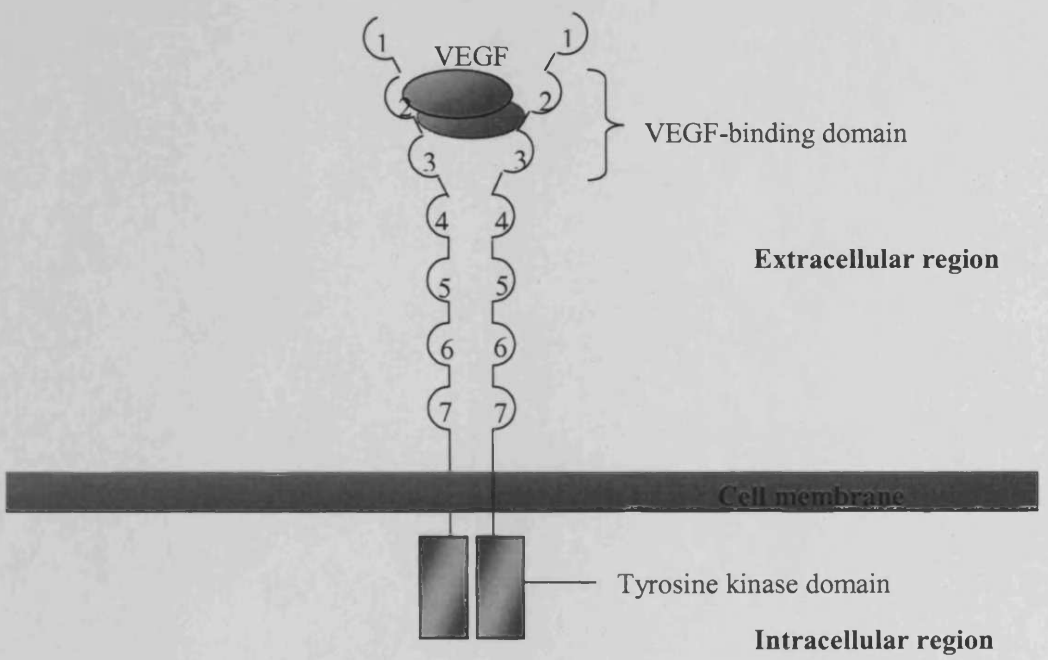

Figure 1.8: A schematic representation of the VEGF dimer bound to a dimer of flt-1.

Neuropilin-1, a receptor that binds semaphorins, is located in the nervous system[300] but has also been implicated in arterial growth[301]. It binds $VEGF_{165}$[302], and may act as a co-receptor, to facilitate VEGF binding to KDR[301]. Indeed, a neuropilin-1/KDR/$VEGF_{165}$ complex is involved in continued arterial growth during angiogenesis[215].

1.4.7 Intracellular signalling

The intracellular regions of flt-1 and KDR contain split tyrosine kinase domains and a kinase insert[240]. The receptors undergo autophosphorylation upon VEGF-induced dimerisation, though there is stronger signal transduction with KDR[291-294]. Phospho-tyrosines on KDR and flt-1 associate with Phospholipase Cγ (PLCγ)[295,296], leading to activation of the protein kinase C pathway, with subsequent stimulation of the MAP kinase pathway[296,297]. The receptors also act through the Src family signalling pathway[298]. Earlier studies described activation of the Ras pathway by the receptors to activate protein kinase C[292,293,299], but subsequent research discovered that VEGF activated a Ras-independent pathway in endothelial cells[297].

1.4.8 Biological effects of receptor activation

KDR is required for blood vessel formation and organisation[303] and is generally perceived as the more mitogenic receptor[233,240]. There has been some debate, however, over the role of flt-1. Flt-1 may influence the organisation of the vasculature[304,305]. Interestingly, removal of the intracellular tyrosine kinase domain of flt-1 resulted in normal development of the vasculature through to the adult and no change in VEGF-induced vascular permeability, although macrophage migration was decreased[306]. Moreover, an *in vitro* chimeric study found that stimulation of flt-1 did not induce proliferation of endothelial cells, whereas KDR stimulation did[294]. Flt-1 has been suggested to function as a negative mediator of KDR-induced cell growth[294]. It was proposed that the purpose of flt-1 was to maintain critical concentrations of VEGF in developing tissues by sequestering any excess[278].

In contrast, PlGF binds flt-1 but not KDR, yet PlGF/VEGF heterodimers have been reported to stimulate angiogenesis, suggesting that flt-1 does possess angiogenic action[307]. Flt-1 is expressed in inflammatory cells, whereas KDR is not. Inhibition of

flt-1 in RA reduced the infiltration of inflammatory cells, accompanied by reduced proteoglycan degradation and an overall reduction in swelling[308]. VEGF is also chemotactic for monocytes, mediated through the flt-1 receptor on the cells[309]. These studies suggest that flt-1 stimulation of inflammatory cells gives rise to angiogenesis, rather than direct stimulation of endothelial cells[308]. Cells such as monocytes, macrophages and haematopoietic stem cells can differentiate into a variety of cell types including osteoclasts, explaining how VEGF can activate these differentiated cells[278,310,311].

1.4.9 The soluble flt-1 receptor

A number of cytokine receptors are also synthesised in truncated, soluble forms, which may function in the regulation of signalling, including soluble receptors for IL-1, FGF and colony stimulating factor[312-314]. An endogenous 687-amino acid truncated form of flt-1 (soluble flt-1, or sflt-1) arising from alternative splicing has been identified. It consists of the first six domains of the extracellular region, with a unique 31 residue C-terminus[315]. Its mass is between 85kDa and 90kDa, which upon removal of the signal peptide is reduced to 75kDa. SFlt-1 has a similar affinity to VEGF as that of the full-length flt-1 and it inhibits VEGF-induced mitogenesis *in vitro*[315]. It was proposed that sflt-1 acts as a dominant negative inhibitor of angiogenesis, as it can form heterodimers with KDR or flt-1 with or without VEGF, and through binding VEGF, prevents VEGF interacting with the full-length receptors[316]. The heparin-binding domain on sflt-1 may allow it to accumulate in the vicinity of the receptors, thus promoting dimerisation[315,317]. Of importance to this study is evidence that sflt-1 reduces the severity of induced arthritis[318]. As sflt-1 is endogenously expressed, it appears to be a natural regulator of angiogenesis and tumourigenesis and provides a useful candidate for inhibition of VEGF activation.

Recently, an endogenous soluble form of KDR has been identified from human plasma and is larger that sflt-1 (160kDa). It is believed that sKDR acts in a similar manner to sflt-1, as constructed soluble forms of KDR have exhibited inhibitory properties[319,320].

In summary, VEGF is a potent angiogenic cytokine in health and disease, mediated through its two receptors flt-1 and KDR. A naturally occurring control mechanism

exists, as the concentration of VEGF appears essential in guiding the development of the vasculature and in response to ischaemia. The high levels observed in the adult during disease make VEGF an attractive target for inhibition studies.

1.5. Cartilage Repair Strategies

It must be noted that regeneration and repair represent two separate processes of restoration[1]. Repair involves the use of cells to proliferate and synthesise new matrix. Regeneration describes the formation of a completely new joint surface, identical to the original tissue. Although some progress has been made in terms of repair, regeneration has not yet been achieved[1].

1.5.1 Initial approaches

An early attempt at cartilage repair was based on the observation that a full-thickness defect (extending to the subchondral bone) fills with a hyaline or fibrocartilage, whereas a partial thickness lesion does not[2]. The technique involved abrasion or drilling through a partial defect into the subchondral bone to stimulate bleeding and a healing response, first described by Pridie[321,135]. However, the new cartilage had a lower proteoglycan density, appeared more fibrous and did not integrate with the surrounding cartilage, with long-term disintegration[135].

Autologous transplantation of a section of cartilage from a non-weight bearing region can decrease pain in the majority of patients, but this technique is limited by the low availability of donor sites[322]. Moreover, the age of the donor cartilage is the same as that of the lesion, and may have undergone similar matrix changes that led to the initial loss of cartilage[2]. Furthermore, cartilage from a non-weight bearing region may have a different composition and be unable to withstand the compressive forces placed upon it[323]. Advanced arthritis can result in transplantation of a prosthetic joint[2]. While prosthetics, such as hip replacements, are a popular clinical approach, there is a limited lifetime of the implant and damage to the bone into which it is implanted may be such that a second implant cannot be used. This limits the use to older patients.

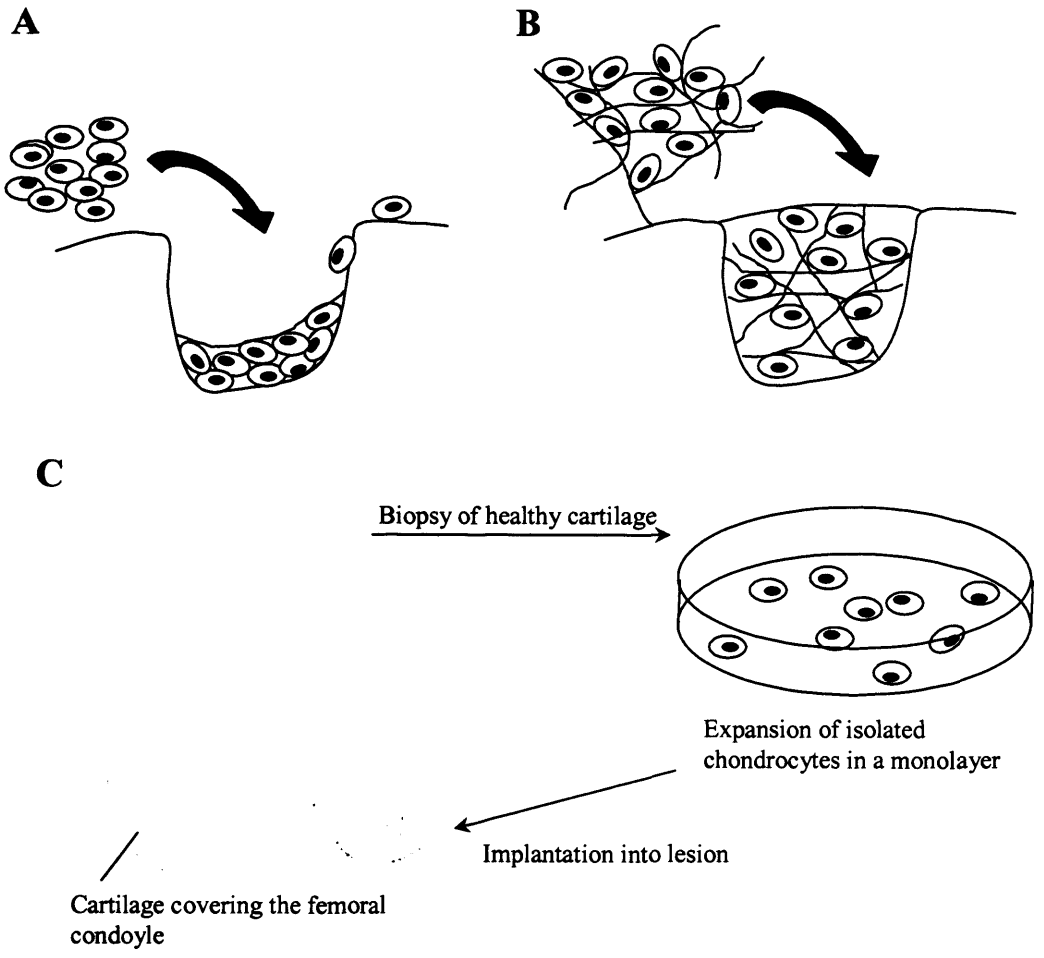

Figure 1.9: Three approaches to cartilage repair. A: Implantation of chondrocytes expanded *in vitro* into a cartilage defect with only partial filling. B: Loading of chondrocytes into a three-dimensional scaffold to promote better defect filling. C: Autologous chondrocyte transplantation as described by Brittberg *et al.*[324], adapted from Ochi *et al.*[322].

partial-thickness cartilage lesion has been shown to stimulate migration of mesenchymal stem cells from the synovial membrane into the scaffold, with differentiation into chondrocytes[340,341].

However, the subchondral bone contains a variety of cell types that respond very differently to growth factors, with the potential for bone growth. Hunziker and Driesang[342] addressed this challenge, by inhibiting angiogenesis with suramin, thus preventing angiogenesis-dependent ossification. Bone invasion into the cartilage compartment was halted, while simultaneous stimulation with TGF-β or IGF-1 and BMP-2 induced the formation of a cartilaginous tissue.

1.5.4 Inhibition of pathological pathways

The inhibition of angiogenesis mentioned above is important when inducing cartilage repair, as the dislocation of implanted cells expressing BMP-2 has led to osteophyte formation[344]. However, broad, systemic inhibition of angiogenesis can have deleterious side-effects, such as impaired wound healing, impaired muscle function, infertility, teratogenicity, and gastrointestinal ulcers[200,222]. Furthermore, some inhibitors may be able to prevent the onset of angiogenesis, but cannot reverse the process. For example, TNP-470 can inhibit endothelial cell proliferation at disease onset, but has little effect after arthritis has developed[345]. Additionally, some endogenous anti-angiogenic agents may actually promote angiogenesis under certain circumstances, such as TGF-β or the N-terminal domain of thrombospondin-1[346,347].

Antagonism of integrins that are required for bFGF or VEGF-induced angiogenesis provides a greater degree of control over the pathway to be blocked[348]. Consequently, a number of integrin antagonists have been patented for clinical trials[222]. Neutralising antibodies also provide a higher degree of specificity[349,350]. Several studies have investigated the inhibition of VEGF-induced angiogenesis as both cancer and arthritis treatments. These are summarised in Section 4.1.

Gene therapy for angiogenesis inhibition has received interest[351]. This has the advantage of continued expression of the anti-angiogenic agent over months or even years without the need for frequent administrations[351]. A DNA vaccine targeting

KDR suppressed tumour growth with minimal side-effects[268]. This approach may hold potential for arthritis treatment.

The inhibition of a pathological pathway, such as that of IL-1, has received interest. Two endogenous IL-1 receptors have been identified that obstruct IL-1 signalling through non-activation of the intracellular pathways upon IL-1 binding, termed IL-1 receptor antagonist (IL-1ra) and IL-1RII[312,352]. Recombinant IL-1RII added to OA cartilage protected the tissue against IL-1-induced degradation[143]. The inhibition of a pathological pathway, in combination with stimulation of chondrogenesis, may provide successful cartilage repair, and the present study aims to use such an approach (Section 1.7).

1.5.5 Mesenchymal stem cells

Mesenchymal stem cells (MSCs) have been identified in adult tissues, such as bone marrow, the periosteum and the synovial membrane[353-356], although the number of cells declines with age[354]. Recently, MSCs have been identified in adult cartilage, and interestingly, the percentage of these progenitor cells, compared to mature chondrocytes, increases with OA. This may be due to chemotactic factors such as TGF-β, being at higher levels in OA, increasing the number of progenitor cells by attracting more from the synovial membrane[357]. In response to IL-1 and TNF-α, these cells may also be stimulated to produce bone or fibrocartilage[357].

Due to their ability to differentiate into several cell types under certain conditions, MSCs have been experimentally applied to cartilage repair. This has resulted in the synthesis of a hyaline-cartilage material[2,358]. The chondrogenic potential of MSCs can be enhanced by treatment with chondrogenic factors prior to implantation[359] or by transfection with chondrogenic factors. These factors could act in a autocrine manner (*Sox9*[360]) or be secreted and act on endogenous cells (BMP-2, IGF-1[361]). MSCs pre-treated with TGF-β1 have been shown to lose their chondrogenic phenotype *in vivo*[362]. A gene therapy approach involving the stable or transient expression of chondrogenic factors by MSCs may avoid dedifferentiation or osteogenic differentiation. Isolated MSCs have been successfully transfected with

genes encoding for IGF-1, BMP-2[344], Shh and BMP-7[363]. Subsequent implantation of the transfected cells into cartilage defects produced hyaline-like cartilage repair[344].

A perceived drawback of the MSC approach is the decreased proliferative capacity of progenitor cells in older patients[364] and Murphy *et al*[365] showed that there was a significant decrease in the proliferative ability of bone-marrow derived cells during advanced OA. However, MSCs are hypoimmunogenic or nonimmunogenic[356], which suggests that allogenic MSCs could be used. Furthermore, dedifferentiated chondrocytes in culture assume a primitive stem cell phenotype and express markers in common with embryonic stem cells (ES) and multipotent adult progenitor cells (MAPCs)[366]. These could potentially used in the same manner as MSCs.

1.6. Biomaterials

Tissue engineering can be defined as "the creation of new tissues for replacement and regeneration of damaged tissue"[367]. To apply this principle to cartilage and bone repair requires a combination of growth factors, cells, an ECM and biomaterials which can provide the matrix[367]. The present study aims to use a HA-based biomaterial for delivery and as a scaffold (Section 1.7).

Biomaterials can provide a three-dimensional culture in which to grow chondrocytes *in vitro*, or alternatively a space-filling scaffold loaded with cells for transplantion or with chemotactic agents, to encourage infiltration of mesenchymal stem cells from the surrounding tissues[2]. However, the choice of biomaterial requires consideration. Is the material required to replace cartilage and therefore, have similar properties? Or is the material a carrier for growth factors or cells into a lesion, providing a three-dimensional scaffold that will be degraded as neocartilage is formed? Perhaps the biomaterial must support *ex vivo* formation of cartilage, so that new tissue can be transferred into a damaged joint. Therefore, the application of the biomaterial dictates the properties required. A cartilage replacement must possess high tensile strength, but low friction at its surface. Alternatively, to completely fill cracks and fissures in degraded cartilage, the biomaterial may exist as a liquid precursor that can be injected with cells and then solidify into a matrix *in situ*. Biomaterials to support cartilage

synthesis *in vitro* need to maintain the chondrocyte phenotype. The biomaterials discussed here can be loosely grouped into synthetic, protein-based and polysaccharide-based materials.

1.6.1 Synthetic biomaterials

Poly(vinyl alcohol) (PVA) hydrogels have been applied to peptide drug delivery[368] and were assessed as load-bearing replacements for cartilage[369]. Observations of PVA hydrogels possessing mechanical properties similar to that of cartilage, led to the consideration of this material as a replacement[368,369]. However, although PVA hydrogels may provide a cartilage-like material, integration into the surrounding cartilage is important for tissue stability. Moreover, the toxic effects of residual monomers and the biomaterial itself, need to be addressed.

Poly(ethylmethacrylate) (PEMA) hydrogels have shown potential for use in cartilage and bone repair and have good biocompatibility[370,371]. However, optimisation of the hydrogels' physical properties reduces their biocompatibility[372]. Although the polymer may be inert, gradual degradation may yield fragments that are biologically active or toxic. The material may not completely integrate and over time, movement may damage the surrounding cartilage.

Polylactic acid (PLA) and polyglycolic acid (PGA) have been used as biodegradable implants and survive between three and six months depending on the preparation[373]. They confer some stiffness, but not to the same mechanical level as cartilage[136,373]. These materials have supported cell viability, proliferation and the production of a cartilaginous ECM in a number of studies[373,374,375].

1.6.2 Protein-based biomaterials

Type II collagen is the most abundant ECM component in articular cartilage, which has led to substantial interest in this protein for the delivery of cells into a cartilage lesion or for the culture of chondrocytes *in vitro* to synthesise a cartilaginous matrix[376]. Moreover, collagen can be supplemented with GAGs to more closely resemble the cartilage ECM, which improves chondrocyte proliferation[330,377].

Chondrocytes cultured in collagen synthesise a cartilaginous material[329] and those cultured on type II collagen are more chondrogenic than those on type I collagen[330]. Furthermore, when loaded with chondrocytes and implanted into cartilage defects, the collagen scaffold demonstrated a marked improvement in tissue repair over the injection of chondrocytes alone and resulted in a space-filling cartilage material with some evidence of integration with the surrounding tissue[329]. Collagen has also been shown to support infiltration of endogenous MSCs following implantation[376]. The potential of collagen immunogenicity has led to the removal of the immunogenic telopeptide. However, this may disrupt collagen fibrillisation and the integrity of the biomaterial[329]. There have been problems with integration of the repair tissue with the surrounding cartilage when using type I collagen gels, resulting in deterioration of the site[338].

Fibrin glue exploits the reaction of fibrinogen and thrombin to produce a fibrin clot[21]. In addition, modification to affix heparin allows the attachment of heparin-binding factors[378]. Hunziker and Driesang demonstrated delivery of TGF-β, IGF-1, BMP-2 and suramin using fibrin to repair a cartilage lesion, although the fibrin had to be further supplemented with gelatine, to eliminate uncontrolled shrinkage during clot formation[342]. Fibrin can be polymerised *in situ* and as such has been used to deliver mesenchymal stem cells into a lesion[344]. Injection of a liquid precursor is a distinct advantage when considering OA cartilage, which contains cracks and fissures[134]. A liquid can carry cells into these fissures, providing a three-dimensional scaffold upon solidification. The preparation can also be injected, avoiding surgical procedures.

However, commercially available fibrin glue kits may contain fibronectin[344]. Fragments of fibronectin are detrimental to cartilage, by enhancing proteinase expression (Table 1.4). Even though these effects can be countered by anabolic factors[379], the degradation of the fibrin/fibronectin clot could increase cartilage damage. Moreover, fibrin is not a natural component of articular cartilage so is unlikely to aid cartilage regeneration *per se*.

Gelatin can be modified to a thermoresponsive gelatin that can be injected in a liquid form with subsequent solidification *in situ*[333]. This form of gelatin has been found to maintain the chondrocytes phenotype *in vitro* over several weeks[333]. However, the

mechanical and signalling properties of collagen that are essential in articular cartilage may be lost during denaturation to form gelatin.

Short peptides of around 12-16 residues have been demonstrated to self-assemble into a hydrogel under particular ionic conditions[380]. The peptide structure is of alternating hydrophilic and hydrophobic residues, with alternating positive and negative charges on the hydrophilic residues. The resulting nanofibres are significantly smaller than many other polymer fibres[381]. These peptide hydrogels have been shown to support chondrocytes and cartilage-specific proteoglycan synthesis[332]. The peptide hydrogel allows the inclusion of specific sites to enable degradation by particular proteases, or to promote interactions with chondrocytes. The assembly of the peptides can be performed at physiological ionic concentrations and pH, without toxic side-effects[332]. Although some peptides have been shown to be non-immunogenic[382], this may not be the case for all peptides.

1.6.3 Polysaccharide-based biomaterials

Polysaccharides can form hydrogels through ionic or hydrogen bonds more readily than proteins. Some of the key constituents of cartilage are polysaccharides, in the form of GAGs. However, the rod-like structure, high charge density and relatively short length of most GAGs, mean that they do not readily form hydrogels in an aqueous solution[380]. However, HA can be used in hydrogels.

Chitosan is a derivative of chitin, found in arthropod exoskeletons. It consists of D-glucosamine with randomly located N-acetyl glucosamine monomers, the amine groups becoming protonated in slightly acidic conditions. This positive charge has enabled the formation of complexes with anionic polymers, such as GAGs and has been used as a delivery vehicle for such compounds[380]. At physiological pH, an associated polyanion can be partially dissociated from chitosan, enhancing the hydrogel as a delivery scaffold. Chondrocytes can be cultured with chitosan *in vitro*, but the cells do not infiltrate into the biomaterial and there is no increase in proteoglycan synthesis[383]. In addition, chitosan stimulates macrophages and angiogenesis, which is undesirable in cartilage repair[380].

Although agarose is not a constituent of cartilage, it supports the chondrocyte phenotype *in vitro*, which allows experimentation on the chondrocytes[384]. Moreover, implantation of chondrocytes grown in agarose gels into full-thickness defects demonstrated cartilage synthesis, formation of subchondral bone and integration with the surrounding tissue[385].

Alginates are seaweed-derived polysaccharides that can be injected into a cartilage lesion with chondrocytes and crosslinked by calcium. Alginate hydrogels promote cartilage formation *in vivo*[386,387] and support chondrocyte phenotype in culture[388]. However, some forms of alginate have been found to be immunogenic following transplantation[7].

1.6.4. Hyaluronan-based biomaterials

HA has been used for some time in eye surgery, the treatment of joint disease and in wound healing[39]. Healon, which consists of 1% HA at a molecular weight of 2.5 million Daltons, has been used in viscosurgery in the eye[46]. Furthermore, administration of HA into osteoarthritic joints protects against proteoglycan degradation[389]. Interestingly, the benefits of HA administration have been seen long after the HA would have cleared from the site[46], suggesting that the administration of high molecular weight HA upregulates HA synthesis and downregulates degradative pathways[46].

In healthy cartilage, HA molecules are approximately 4-5 million Daltons, at a concentration of approximately 3-4mg/ml in the synovial fluid. The length and concentration are significantly reduced in OA to 1-4 million Daltons, with only 1-2mg/ml remaining in the synovial fluid[46]. To maintain viscoelasticity, exogenous HA would therefore have to be at least 4 million Daltons in size.

Hylan is a derivative of HA that developed to provide a material that had a higher molecular weight and increased viscoelastic properties[46,390]. Hylan has been used in a wide range of treatments, such as local thrombin delivery, topical gels and drug delivery[390,391]. In cartilage, it protects explants against proteoglycan degradation and also reduces cell injury[392]. It was proposed that Hylan (and HA) achieved this by

forming a physical barrier against the diffusion of macromolecules or interacting with offending agents and neutralising them[392]. Furthermore, Hylan decreases pain from mechanical and inflammatory stress, as well as remaining in the joint longer than HA[46]. However, inflammation has been associated with Hylan use[393].

The range of semi-synthetic Hyaff family of biomaterials are synthesised by esterification of the carboxyl group on the D-glucuronic acid moiety of HA with alcohols[394]. These include Hyaff-7 (ethyl ester), Hyaff-9 (propyl ester) and Hyaff-11 (benzyl ester). The Hyaffs are non-toxic and biologically inert *in vitro*[395], and can survive up to a month *in vivo*, depending on their composition and location[396]. Hyaffs have been applied to liver regeneration[397], cutaneous wound healing[70], and vascular grafts[398].

Chondrocytes grown in Hyaff-11 proliferate and exhibit re-differentiation to a chondrocyte phenotype[331]. The resulting tissue has cartilage-like characteristics and the Hyaff-11 is stabilised by the matrix synthesised by the chondrocytes[328,331,334]. Hyaff-11 can also support ectopic cartilage and bone growth when seeded with mesenchymal stem cells or chondrocytes[328,399]. Used on its own or with chondrocytes, Hyaff-11 has demonstrated cartilage repair following implantation into osteochondral defects[338,339]. Furthermore, a sulphated Hyaff-11 preparation has been shown to achieve better chondrocyte infiltration than its non-sulphated counterpart[334].

Hyaffs are of a lower molecular weight than HA, at approximately 145,000-300,000 Daltons[70,395]. Therefore Hyaffs may not contribute physical benefits to the damaged tissue as much as the Hylans, although they can be more readily shaped into films, fleeces and meshes.

ROS are mediators of cartilage degradation in OA, where HA acts as an antioxidant to scavenge ROS[70,71]. This is compromised by decreased levels and shorter chains of HA in OA. Although a HA-based biomaterial may compensate for this, Hyaff does not protect against ROS damage as well as HA, although the higher molecular weight Hylan is more resistant to resulting degradation[70]. The ester bonds of Hyaffs appear to be particularly susceptible to ROS attack to expose the HA backbone, although an aromatic ring on the side chain of Hyaff may have a protective effect[70]. This probably

accounts for the increased resistance of HA to ROS when the steroid, α-methyl-prednisolone, has been coupled to the polymer[71].

Babucci *et al.*[400] described a method of crosslinking HA, via the carboxyl groups on D-glucuronic acid with diamine crosslinkers. In addition, the group revealed that incorporation of sulphate groups reduces enzymatic degradation and improves the elasticity of the resultant hydrogel. This confers increased viscoelastic properties over HA and a longer half-life *in vivo*. The HA-based hydrogel has been shown to increase cartilage repair in a defect compared to an empty defect[337]. Shu *et al.*[401] describe the crosslinking of a thiol derivative of HA with modified polyethylene glycol bi-functional crosslinkers. This reaction is non-toxic to cells and provides a method for *in situ* hydrogel formation[401]. Photopolymerisation can also be used to crosslink HA-based materials *in situ,* with modified PEG crosslinkers[402]. However, while this technique may be successfully applied sub-cutaneously, a cartilage defect may be too deep to achieve complete polymerisation. Incorporation of an RGD sequence onto HA substantially increases *in vitro* fibroblast proliferation, probably through integrin stimulation[402]. This presents an opportunity to enhance the interaction of the biomaterial with either cells being delivered or those already present in the joint.

A collagen scaffold supplemented with HA has demonstrated increased cell migration and proliferation than either material on its own[403], as a combination of the two materials provides a matrix closer to that of cartilage[335,404].

1.7. Aims of this project

Although many strategies have been applied to induce cartilage repair, it has proved very difficult to synthesise hyaline cartilage that demonstrates integration with the surrounding tissue and maintains long-term integrity. This project aimed to produce an injectable biomaterial, capable of stimulating chondrogenesis, but inhibiting osteogenesis. The working hypothesis was that a matrix that supports angiogenesis will, in the presence of BMP-2, induce bone formation, while a matrix that inhibits angiogenesis will only support cartilage formation.

The matrix used in this project was a HA-based hydrogel, previously developed in this laboratory[405]. HA-based biomaterials have shown considerable promise as a three-dimensional scaffold for the repair of cartilage tissue. Moreover, high molecular weight HA provides protection to the joint, and loss during OA can be replaced with a HA-based biomaterial (Section 1.6.4). The optimal concentrations of derivatised HA, crosslinker and collagen were determined to achieve the optimal viscoelastic properties. This biomaterial was not designed to replace the compressive properties of cartilage, but to provide a three-dimensional scaffold to support cell infiltration. The crosslinking reaction was revealed to be non-toxic. Moreover, the hydrogel demonstrated delivery of active BMP-2 and supported infiltration of cells following subcutaneous implantation.

This project produced a decoy receptor, based on the VEGF-binding domains of the extracellular portion of the flt-1 receptor, termed flt-1(1-3). Flt-1 was selected over KDR, as it exhibits a higher affinity to VEGF and the flt-1 monomer can bind VEGF more efficiently than the KDR monomer[287]. Furthermore, flt-1(1-3) has an increased *in vivo* half-life, compared to the entire extracellular domain[112] and its smaller size ensures easier incorporation into hydrogels. This protein retained affinity for VEGF, as determined by surface plasmon resonance.

Preliminary *in vivo* studies undertaken in this project incorporated flt-1(1-3) into the hydrogel without chemical coupling. This meant that flt-1(1-3) could diffuse out, which may facilitate inhibition of VEGF. Anti-angiogenic properties of flt-1(1-3) integrated into the hydrogel were assessed by the chick chorioallantoic membrane assay[406,407,408]. However, further work is required to determine if flt-1(1-3) can inhibit angiogenesis. The foetal rat metatarsal assay was used to test for the inhibition of osteogenesis by flt-1(1-3)[409].

We have shown that the HA-based hydrogel described herein is an appropriate delivery vehicle for chondrogenic agents. Furthermore, the decoy receptor of VEGF is capable of binding this cytokine, although its effects on angiogenesis inhibition in the arthritic joint remain to be fully elucidated.

2. Materials and methods

2.1. Hydrogel Characterisation

2.1.1 Synthesis of HA ethylenediamine derivative (HAED)

The side chain of interest, ethylenediamine.hydrochloride (HCl), was added at a 25-fold molar excess (with respect to the glucuronic acid moieties on hyaluronan (HA) (Figure 3.1, Section 3.1) to a 3mg/ml solution of sodium hyaluronate (RW Greeff, Stamford, CT, molecular weight >1x10^{6}Da). Upon dissolving, hydroxybenzotriazole (Sigma, Poole, UK) made up in dimethyl sulphoxide was added at a 5-fold molar excess and the pH immediately adjusted to 6.8 using either 0.1M NaOH/HCl. Carbodiimide (1-[3-(dimethylamino)propyl]-3-ethylcarbodiimide hydrochloride, (Sigma, Poole, UK)) was added at a 4-fold molar excess and the pH was maintained at 6.8 for 2 – 4 hours to allow the reaction to proceed. The mixture was extensively dialysed (Spectra/Por 4, Spectrum Labs, Rancho Dominguez, CA. MW cut off: 12-14kDa) against distilled water. Sodium chloride was added to a final concentration of 5% w/v to form an HAED salt. A 3-volume equivalent of ethanol was carefully added to precipitate the salt. The HAED was collected by centrifugation (1000x g, 20 minutes) and the pellet lyophilised for 16 hours under sterile conditions. The dried derivative was redissolved in sterile phosphate buffered saline (PBS), pH 7.4 to a concentration of 15mg/ml. Typical yield from 360mg of sodium hyaluronate was 334mg.

2.1.2 Modified TNBS assay

The 2,4,6-trinitrobenzenesulfonic acid (TNBS) assay as previously described[416] was utilised to determine the extent of derivatisation of the glucuronic acid moieties to primary amines. Standards of 6-aminohexanoic acid (Sigma, Poole, UK) were prepared (0 – 150μg/ml) in 0.1 M Na_2CO_3. HAED was diluted in the same buffer to 100 and 500μg/ml, and corresponding dilutions made of HA controls. TNBS (Sigma, Poole, Dorset) was added to a final concentration of 0.005% and the reaction

proceeded at 37°C for 2 hours. The reaction was stopped with sodium dodecyl sulphate (Sigma, Poole, UK) and hydrochloric acid (Fisher, Loughborough, UK), at final concentrations of 2.5% and 125mM respectively. The optical density at 335nm was measured (Pharmacia Biotech Ultraspec 2000, Pharmacia Biotech, Little Chalfont, UK) and the percentage derivatisation calculated from the difference in OD_{335} between native and modified HA, based on the 6-aminohexanoic acid standard curve.

2.1.3 Uronic acid assay

The assay was carried out as described by Bitter and Muir[417]. In brief, sodium hyaluronate (RW Greeff), glucuronic acid (Sigma), glucosamine (Sigma) standards and HAED samples were layered onto a sodium tetraborate (Sigma)/sulphuric acid (Fisher) solution. After boiling, carbazole (Sigma) in ethanol was added and the mixture further boiled for 15 minutes until the reaction underwent a colour change. The optical densities were measured at 530nm (Pharmacia Biotech Ultraspec 2000, Pharmacia Biotech, Little Chalfont, UK). Calibration curves for HA and glucuronic acid were constructed and the percentage of uronic acid in HAED was determined, to indicate the extent of derivatisation.

2.1.4 Crosslinking of HAED to produce hydrogels

Crosslinkers were obtained by custom synthesis from Shearwater Polymers Inc. (Huntsville, AL, USA). Four were used: 2-arm polyethylene glycol – succinimidyl propionate (SPA_2-PEG, MW 3.4kDa); 4-arm polyethylene glycol – succinimidyl propionate (SPA_4-PEG, MW 10kDa and 20kDa); succinimide ester of carboxymethylated 4-arm polyethylene glycol (SC_4-PEG, MW 20kDa). Because of the unstable nature of the crosslinker, it was kept under nitrogen until immediately prior to use. HAED with collagen or PBS was transferred to a sterile 1ml syringe. The crosslinker was resuspended in PBS (20μl for a 265μl hydrogel or 50μl for a larger hydrogel) and transferred to another sterile 1ml syringe. Immediately the syringes were linked and the contents mixed rapidly by approximately 20 passes back and forth. The hydrogel typically set within 7 minutes, depending on the crosslinker concentration and type.

2.1.5 Incorporation of collagen and BMP-2 into HAED hydrogels

Two forms of bovine type I collagen were used: salt-extracted telocollagen (Organogenesis, Canton, MA, USA) and pepsinised collagen (Matrix Pharmaceutical, Fremont, CA, USA). Telocollagen was fibrillised by addition of 0.4ml 10X PBS and 3.0ml 1X PBS to 3.6ml of 5mg/ml telocollagen. After 2 hours gentle mixing the collagen fibrils were collected by centrifugation at 5500xg for 20 minutes. Pepsinised collagen was provided at a concentration of 65mg/ml. Immediately prior to use the collagen network was disrupted to obtain a more homogenous mixture with HAED. This was achieved by shearing through a 0.45mm sterile syringe needle three times. Collagen was incorporated into HAED before crosslinking by repeatedly passing the components between 2 linked syringes, until a uniform cloudy or opaque mixture had formed. BMP-2 (human recombinant bone morphogenetic protein – 2, Genetics Institute, Cambridge, MA, USA) was prepared beforehand by buffer exchange with 10mM HCl (Centriprep YM-10, MW cut off 10kDa, Millipore, Bedford, MA). BMP-2 was added, where applicable, at a final concentration of 250μg/ml and thoroughly integrated into the collagen mix by passing back and forth between 2 linked syringes. Once BMP-2 was incorporated, the collagen was mixed with HAED, before crosslinking into a hydrogel.

2.1.6 Rheology

The HA-based hydrogel is a good example of a viscoelastic material, that is, one that exhibits both viscous and elastic properties. These characteristics lend themselves to analysis. The starting material, HAED, behaves as a viscous liquid, with elasticity increasing in relation to time as the crosslinking reaction proceeds. By applying a known stress (σ) to the sample through the parallel plate of the rheometer, the resulting deformation (strain, γ) is measured from rotation of the plate. These can be described:

$$\sigma = \frac{F}{A} \quad (1)$$

where F corresponds to the force applied and A is the area of the material, and

$$\gamma = \frac{x}{y} \quad (2)$$

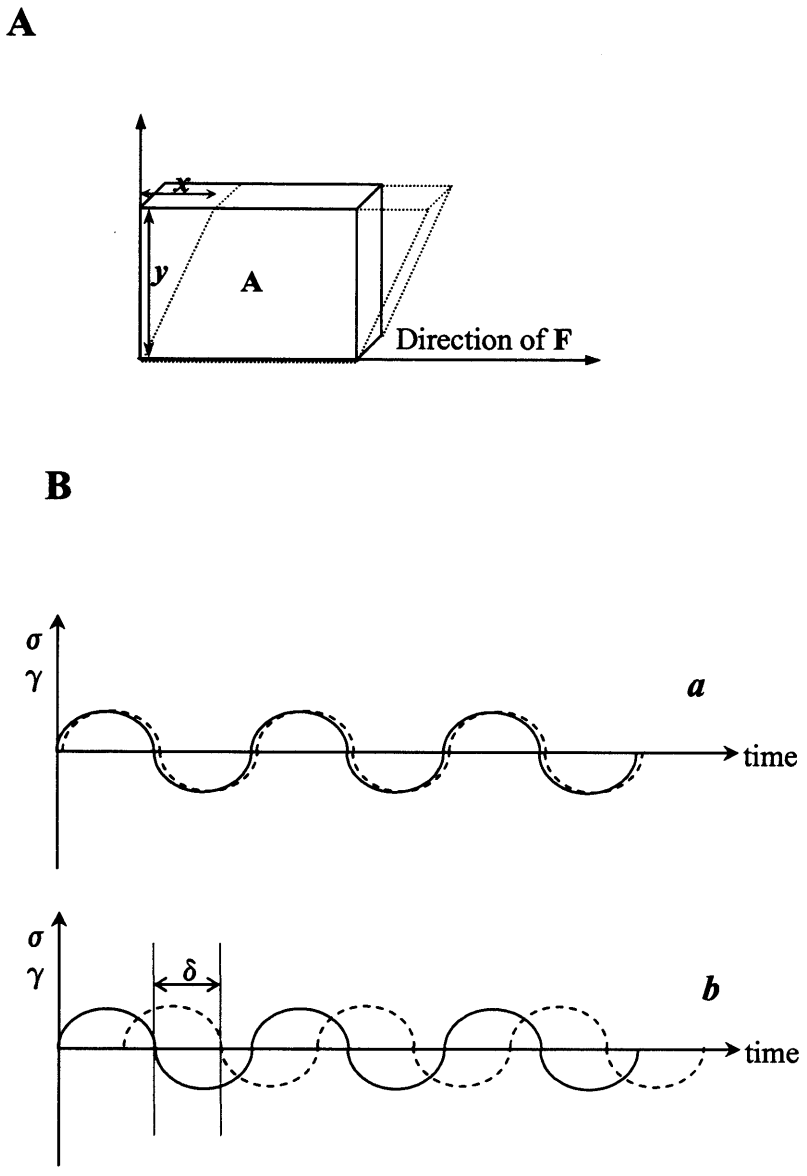

Figure 2.1: Demonstration of the quantities used in rheology. A: : schematic of the deformation of a viscoelastic material in response to an applied force. B: diagram to demonstrate the response of a material (dotted line) to an applied sinusoidal force (solid line). *a*: a typical elastic material, the in-phase component. *b*: a typical viscous material with an increased phase shift δ, representing the out-of-phase component.

where x refers to the deformation of material and y refers to the height of material (Figure 2.1A).

The combined strain and shear is given by the complex shear modulus G*:

$$G^* = \frac{\sigma}{\gamma} \tag{3}$$

A material can be described as having an in-phase or out-of-phase component, which relates to the extent that a material behaves in an elastic or viscous manner, respectively. When a sinusoidal (oscillating) force is applied an elastic material can store the energy and thus transfer the force back. This is known as the in-phase component (figure 2.1B*a*). Conversely, a viscous material cannot store the energy and dissipates it as heat, thus responding out of phase with the applied force (figure 2.1B*b*).

This phase shift is measured as δ, which can be described as:

$$\tan \delta = \frac{G''}{G'} \tag{4}$$

where G′ is known as the "storage modulus" corresponding to the in-phase component, which describes the elastic behaviour of the material, G″ is termed the "loss modulus", corresponding to the out-of-phase component and thus the viscous behaviour. The complex shear modulus (G*) is related to these two moduli as follows:

$$G^*(\omega) = \sqrt{(G'^2 + G''^2)} \tag{5}$$

where ω is the oscillation frequency. In addition, absolute complex viscosity is described as η^* defined as follows:

$$\eta^* = \frac{\sqrt{(G'^2 + G''^2)}}{\omega} \tag{6}$$

Rheological characteristics were measured using an AR500 controlled stress rheometer (TA instruments, Leatherhead, Surrey, UK), with a 40mm standard steel parallel plate fitted. Hydrogels (final volume 550μl) were prepared as described in Section 2.1.4. The component concentrations were kept the same throughout except

where stated. These were 9 mg/ml HAED, 1:1 SPA_4-PEG (20kD) crosslinker to HAED ratio, no collagen, and the measurements taken at 25°C. These were loaded onto the rheometer. The plate was lowered onto the sample to a gap distance of 300μm, except for hydrogels containing collagen, which had a gap distance of 700μm (volume of hydrogel 1.1ml). The plate was oscillated with a torque of 10Pa at a frequency of 5 Hz at 10 second intervals over 15 minutes. The time between the start of integration of the crosslinker into HAED and the start of oscillation was approximately 50 seconds. When the test time was extended from 15 minutes to 1.5 hours the hydrogel was prepared as before, but the readings were taken at 30 second intervals. The "creep" response of the material was analysed by applying a single force of 50Pa to the sample and measuring the responding movement. After 10 minutes, the force was removed and subsequent movement of the sample measured. Calculations of variables were carried out by the rheometer software.

2.1.7 Fourier-Transform infrared spectroscopy

The degree of modification of carboxylic acid groups of HAED was explored by Fourier transform infrared spectroscopy (FT-IR). HAED was prepared as described in Section 2.1.1 and the degree of modification was varied by adjusting the concentration of the carbodiimide catalyst. Percentage modification was determined by the TNBS assay described in Section 2.1.2.

HAED samples were lyophilised overnight and two approaches attempted to produce fine particles:

1. Lyophilised sample was extensively chopped with scissors to produce fine particles.
2. Lyophilised sample was snap-frozen in liquid nitrogen followed by crushing with a piston and eppendorf system. This method produced a less satisfactory powder than the above method.

The sample was used neat and analysed by applying it directly onto the germanium crystal of a Mattson Galaxy 5020 FT-IR, sensIR single reflection ATR. Scans (100) were averaged for each spectrum.

2.1.8 Cell viability assay

Immortalised human foreskin HCA_2 fibroblasts were donated by Dr David Kippling (Cardiff University), and expanded in Dulbecco's Modified Eagle Medium (DMEM) supplemented with 10% foetal bovine serum (FBS), 100 units/ml penicillin, 100μg/ml streptomycin, and 292μg/ml glutamine (Invitrogen). Porcine chondrocytes were extracted from pigs' trotters (kindly donated by Professor Bruce Caterson, Cardiff University) and cultured in DMEM, supplemented as above. All cells were cultured at 37°C with 5% CO_2.

Hydrogels (265μl) were prepared as described in Section 2.1.4. Once the components had been mixed to form a hydrogel the material was immediately transferred to a 15mm dish (Corning, NY, USA), to produce a hydrogel approximately 2 mm thick. The cells were immediately but gently mixed with a pipette tip into the hydrogel during setting. As a control, low melting point agarose (SeaPlaque GTG agarose, FMC BioProducts, Rockland, ME, USA) was dissolved in PBS (pH7.4, Invitrogen) to a concentration of 1% (w/v), by heating. Once the agarose had cooled to approximately 37°C, 265μl was transferred to a 15mm dish and the same number of cells added. This provided a positive control, where cell survival would be expected. Once set, the hydrogels were incubated at 37°C, 5% CO_2 with 0.5ml DMEM, 10% FBS and antibiotics for 24 hours. To provide a dead cell control, methanol (30%, 500μl) was added for 15 minutes at 37°C. Cell survival was determined with an ethidium homodimer/calcein cell cytotoxicity kit (Molecular Probes, Leiden, The Netherlands). Ethidium homodimer and calcein AM (5μM, 200μl) were added to the hydrogels and incubated for 20 minutes at 37°C. The hydrogels were washed twice with 0.5ml PBS and the fibroblasts within were fixed with 4% paraformaldehyde (500μl), for 20 minutes at 37°C. Hydrogels were analysed using a Zeiss Axiovert 35 fluorescence microscope, and photographs were taken using Kodak EktaChrome p1600 film.

2.1.9 Flow cytometry

Hydrogels were prepared as described above and $2x10^5$ HCA_2 fibroblasts were incorporated into each hydrogel. Medium (described above, 0.5ml per hydrogel) was added and the hydrogels incubated for 24 hours at 37°C, 5% CO_2. Each hydrogel was washed with 0.5ml PBS and digested with 2000 units of hyaluronidase (bovine testes, Sigma), in hyaluronidase buffer (Appendix 1.1) for 2 hours at 37°C. The digested hydrogels were centrifuged at 1500xg and the pellet resuspended in 0.5ml PBS. Propidium iodide (Sigma) was added to each sample to a final concentration of 5μg/ml. Samples were analysed by a FACSCaliber (Becton Dickinson, Franklin Lakes, New Jersey), each run measuring 5000 events. Data were analysed using WinMDI v2.8 software.

2.1.10 Ectopic bone formation assay

HAED hydrogels were prepared as described in Section 2.1.4. Hydrogels were allowed to set within the syringe. Hydrogel discs were obtained by slicing the syringe and duplicates were placed into 3 rats for each hydrogel formulation (a total of six hydrogels per formulation). The animal work was carried out in collaboration with Dr Hanne Bentz (Orthogene, USA) as described previously[405]. The implants were excised after 10 days and wax embedded. Sections were stained with haematoxylin and eosin.

2.2. Expression and detection of flt-1(1-3)

2.1 Acquisition of flt-1(1-3) cDNA

Human umbilical vein endothelial cells (HUVECs, Promocell, Heidelberg, Germany) were cultured in endothelial cell growth medium (Promocell, Appendix 2). These were subcultured until confluent by trypinisation (Invitrogen, Paisley), at 37°C, 5% CO_2. Total RNA was extracted from confluent HUVECs using Tri Reagent (Sigma, Poole, Dorset) according to the manufacturer's protocol. The total RNA was purified using amplification grade DNAse I (Invitrogen) to eliminate any residual genomic

DNA from the RNA sample, following the manufacturer's protocol. cDNA was synthesised from 2μg of total RNA by reverse transcription for 1 hour at 42°C using 200 units of Superscript II RNAseH$^-$ reverse transcriptase (Invitrogen) and 0.025μg/μl oligo(dT) primer in a 20μl reaction mixture containing 0.5mM dNTPs and 10mM DTT in first strand buffer.

Polymerase Chain Reaction (PCR) was performed with 1μl of the reverse transcription reaction using one of the following polymerases:

- 1.25 units of Taq polymerase (Promega, Madison, WI).
- 1.7 units Expand Hi-Fi (Boerhinger Mannheim, Indianapolis, IN).
- 0.5 units Vent$_R$ polymerase (New England Biolabs, Beverly, MA).

Polymerase buffers were supplemented with 2mM magnesium chloride, or, in the case of Vent$_R$ polymerase, 2mM magnesium sulphate, except where specified. dNTPS (200μM) and primers (0.5μM each, Invitrogen) were added at a final concentration of 200μM and 0.5μM respectively. The final reaction volume was 50μl. PCR reactions were carried out using a Gene Amp 9600 thermal cycler (Applied Biosystems, Warrington, UK). Each PCR reaction began with a Hot Start step, whereby the polymerase was added after the reaction mix had achieved 95°C to eliminate problems with non-specific binding. Forty cycles were carried out, each consisted of denaturation (95°C) for 45 seconds, annealing (60°C) for 1 minute and elongation (72°C) for 1 minute. An extra elongation step of 10 minutes was applied after 40 cycles. Amplified products were visualised by 1% agarose gels containing 0.13μg/ml ethidium bromide (Sigma).

2.2.2 Cloning of flt-1(1-3) DNA into pCRII vector

Flt-1(1-3) cDNA was subcloned into the pCRII vector (Appendix 3.2) using the TA cloning kit (Invitrogen, Paisley, UK). PCR product (~10ng) was ligated into the pCRII vector (25ng/μl) using T4 DNA ligase (4 units) for 16 hours at 14.5°C. The constructs were transformed into TOP10αF *E.coli* (Invitrogen) according to the manufacturer's protocol. Successful ligation was indicated by disruption of a reporter Lac Z gene in the multiple coding region of pCRII. Resulting loss of the β-galactosidase activity was assessed by addition of X-Gal (5-bromo-4-chloro-3-

indolyl-β-D-galactoside, 20μl of 50mg/ml stock, Promega, Southampton, UK). Selected colonies were seeded into 3 ml of LB broth (Appendix 1.2) containing 50μg/ml kanamycin (Sigma) and cultured for 16 hrs at 37°C. Glycerol (50%) stocks were made up and stored at -80°C. Plasmid DNA was purified using the Wizard Plus SV plasmid prep system (Promega, Madison, WI, USA) following the manufacturer's protocol.

2.2.3 Cloning of flt-1(1-3) into pCEP-Pu vector

The expression vector pCEP-Pu (donated by Neil Smyth, Institute for Biochemistry II, Medical Faculty, University of Cologne, Appendix 3.1) and the pCRII/flt-1(1-3) plasmid (40μl each) were digested with 20 units Hind III and 20 units Not I at 37°C for 2 hours. To avoid recircularisation the 5'phosphate groups of pCEP-Pu were removed by digestion with 1 unit calf intestinal alkaline phosphatase (New England Biolabs) for 30 minutes at 37°C. Fresh phosphatase (1 unit) was added and the reaction was incubated for a further 30 minutes at 37°C. The products were visualised on a 1% agarose gel containing 0.13μl/ml ethidium bromide and extracted using the QIAquick kit (Qiagen Inc., Chatsworth, CA) following the manufacturer's protocol. Equal quantities of flt-1(1-3) and pCEP-Pu (total of 6μl) were ligated with 4 units DNA ligase (Promega) for 16 hours at 14.5°C. The ligation product was transformed into DH5α *E.coli* (Invitrogen) in accordance with the manufacturer's protocol. The transformed bacteria (100μl) were incubated for 16 hours on LB agar plates (Appendix 1.2) containing 30μg/ml ampicillin (Sigma). Colonies were selected and expanded in LB broth with 50μg/ml ampicillin, overnight. Glycerol (50%) stocks were made up and stored at -80°C. Plasmid DNA was purified using the Wizard Plus SV plasmid prep system (Promega) following the manufacturer's protocol.

2.2.4 Confirmatory restriction digests

DNA (1μl) was incubated with 20 units of restriction enzyme and respective buffers (New England Biolabs, Beverly, MA, USA and Promega), with 10mg/ml acetylated bovine serum albumin (BSA). The reactions were incubated at 37°C for 2 hours and visualised on a 1% agarose gel containing 0.13 μl/ml ethidium bromide.

2.2.5 DNA Sequencing

Sequencing reactions were carried out using the dRhodamine dye terminator cycle sequencing kit (Applied Biosystems) according to the manufacturer's protocol, using primers at a concentration of 1.5μM. Briefly, the reaction sequence was 20 seconds at 96°C, 10 seconds at 50°C, 4 minutes at 60°C for 25 cycles (Gene Amp 9600 thermal cycler, Applied Biosystems, Warrington, UK). Excess dye-labelled terminators were removed by ethanol/sodium acetate precipitation and the sequence acquired on an ABI 310 automated sequencer (PE applied biosystems).

2.2.6 Transfection of flt-1(1-3) into 293 EBNA cells

Immortalised HEK 293 EBNA fibroblasts were expanded in Dulbecco's Modified Eagle Medium (DMEM) with 1:1 F-12 nutrient mixture. This was supplemented with 10% foetal bovine serum (FBS), 100 units/ml penicillin, 100μg/ml streptomycin and 292μg/ml glutamine. Geneticin was added to a final concentration of 250μg/ml to select for the EBNA phenotype (all cells and reagents supplied by Invitrogen). Cells were grown on $10cm^2$ and $14cm^2$ tissue culture dishes (Corning and Cellstar, Greiner Bio-one, Kremsmuenster, Austria) and subcultured by trypsinisation with medium changes every 2 – 3 days. Prior to transfection, cells were allowed to reach 80% confluency in 35mm dishes (Greiner Bio-one). The flt(1-3)- pCEP-Pu plasmid (1.25 μg or 2.5 μg) was mixed with 10 μg of lipofectamine (Invitrogen) in 200 μl of serum-free DMEM and allowed to stand for 15 minutes at room temperature. Meanwhile, the cells were washed twice with serum-free DMEM. An additional 800 μl of serum-free DMEM was added to the DNA-lipofectamine mixture, which was then added dropwise to the cells and incubated for 5 hours at 37 °C in a 5% CO_2 incubator. After 48 hours of culture in complete medium, the transfected cells were selected by puromycin resistance (0.5 μg/ml, Sigma). Starting at 0.5μg/ml, the concentration of puromycin was gradually increased to 10μg/ml over the next few media changes, to select for highly expressing transfected cells.

Separate 35mm wells were transfected by the above method with pcDNA3-Lac Z (1.25μg) to determine transfection efficiency. After 48 hours the cells were washed with PBS and fixed with 4% paraformaldehyde for 10 minutes. The following stain was added to the cells (2ml per well).

- X-Gal (Promega), to 1.2 mg/ml
- Potassium ferrocyanide (Sigma), to 8.1 mg/ml
- Potassium ferricyanide (Sigma), to 6.3 mg/ml
- Magnesium chloride (Promega), to 2.4 mM

These were all made up in PBS (at the final concentrations stated). Cells were returned to the incubator, and over the next few hours the extent of blue staining in the Lac Z-transfected cells was assessed. This indicated successful transfection of the plasmid and activity of β-galactosidase arising from expression of the Lac Z gene.

2.2.7 Harvesting of conditioned medium

Once confluent, the cells were washed with PBS twice and incubated in serum-free DMEM (including penicillin, streptomycin and glutamine, but no puromycin nor geneticin added). Conditioned medium was collected over the next few days. At each collection point, protease inhibitors were added (final concentrations of 2mM phenylmethylsulphonyl fluoride (PMSF, made up in ethanol, Sigma), 2mM N-ethyl maleimide (NEM, made up in water, Sigma) and 5mM ethylenediaminetetraacetic acid (EDTA, made up in water, Sigma)) and if the medium was not used immediately, snap-frozen in liquid nitrogen before storage at -20°C.

2.2.8 Cell extraction

Cells were washed twice with PBS. Cells were extracted using an SDS based buffer (Appendix 1.2) containing protease inhibitors, for 5 minutes. Debris was removed by centrifugation at 15,000x g for 10 minutes at 4°C. The supernatant was processed for analysis and the pellet stored at -20°C.

2.2.9 Ultrafiltration of flt-1(1-3)

YM-10 Centriprep concentrators were used (MW cut off 10,000Da, Millipore, Bedford, MA, USA), according to the manufacturer's protocol. The resulting volume of concentrated sample was typically 0.5ml – 1.0ml, depending on the number of centrifugation steps. Concentrated protein was determined by measuring the optical density at 280nm using a Beckman Coulter DU800 spectrophotometer.

2.2.10 Sodium dodecyl sulphate/polyacrylamide gel electrophoresis

An ethanol precipitation of samples was carried out by incubating the sample with 9 volumes of ethanol for 16 hours at 4°C, followed by centrifugation at 10,000x g for 30 minutes. Pellets were resuspended in 8M urea. Samples for sodium dodecyl sulphate/polyacrylamide gel electrophoresis (SDS/PAGE) were mixed with an equal volume of 2X sample buffer (Appendix 1.2) with β-mercaptoethanol (1% v/v, Sigma) and denatured by heating to 100°C for 5 minutes prior to loading. The addition of β-mercaptoethanol and heating steps were omitted when running under non-reducing conditions. Samples were loaded onto a 4-20% polyacrylamide gradient gel (Invitrogen) and run at 125V, 35mA for 2 hours in SDS-PAGE running buffer (Appendix 1.2).

2.2.11 Western blotting

The gel from SDS/PAGE was transferred onto a nitrocellulose membrane (Protran, Schleider and Schuell, Dassel, Germany) using blotting apparatus (Novex, Invitrogen) with transfer buffer (Appendix 1.2), at 25V, 125mA for 2 hours. The membrane was stained for protein by incubation in Ponceau S (Appendix 1.2) for a few seconds, and excess removed with water. The stain was then removed by incubation with tris-buffered saline (TBS, Appendix 1.2). The membrane was blocked with either 5% non-fat dry milk (Marvel, Premier International Foods, Spalding, UK) in TBS for flt-1(1-3), or with 5% casein (Sigma) in TBS for strep-tag detection. Blocking was carried out for 16 hours at 4°C or 1 hour at room temperature. Incubation with primary antibody was carried out at room temperature for 1 hour with one of the following:

- Anti-streptavadin tag polyclonal antiserum raised in rabbits (IBA), 1:2000 dilution in 5% casein in TBS.
- Anti-flt-1 monoclonal antibody from mice (Sigma), 1:500 dilution in 5% milk in TBS.

After three 5-minute washes with TBS/Tween (0.05% Tween-20 (Sigma)) the membrane was incubated for 1 hour at room temperature with the appropriate horseradish peroxidase (HRP)-conjugated secondary antibody:

- Anti-rabbit-HRP, 1:3000 dilution in 5% casein in TBS (for anti-streptavadin, Dako, Glostrup, Denmark).
- Anti-mouse-HRP, 1:1000 dilution in 5% milk in TBS (for anti-flt-1, Dako).

The membrane was washed as above followed by two washes in distilled water. The immunological reaction was revealed using the enhanced chemilluminescence kit (ECL Plus, Amersham Bioscience, Little Chalfont, UK) according to the manufacturer's protocol, and exposed to X-ray film (Hyperfilm, Amersham Bioscience) for 5 minutes before development.

2.2.12 Slot blot

A nitrocellulose membrane (Protran, Schleider and Schuell) was soaked in TBS and transferred to a slot-blot manifold (Hoefer PR 648, Amersham Bioscience). Sample (100μl) was loaded and vacuum applied across the membrane. Each slot was washed 3 times with 1.0ml TBS under vacuum.

Protein was visualised using Ponceau S, and the membrane was probed with antibodies as described by the Western blot method.

2.2.13 Silver stain of polyacrylamide gels

The method described here is based on that of Nesterenko *et al.*[473].

The following solutions were prepared immediately before use:

Fixative: 12ml of 50% acetone (Fisher)
300μl of 50% trichloroacetic acid (Sigma)
5ml of 35% formaldehyde (Sigma)

Stain: 12ml distilled water
160μl of 20% silver nitrate (Sigma)
100μl of 35% formaldehyde
Developer: 2.4g sodium carbonate (Sigma) in 12ml water
5μl of 10% sodium sulphite (BDH)
5μl of 35% formaldehyde
Stop solution: 10ml of 1% acetic acid (Fisher)

The gel was placed in a 10cm plastic dish and fixed for 5 minutes. After 3 washes with distilled water, the gel was placed in water for 5 minutes. The gel was then washed a further 3 times. For the pre-treatment step, the gel was incubated in 50% acetone for 5 minutes. The gel was then placed in 0.0167% sodium sulphite in distilled water for 1 minute and washed 3 times with distilled water. The gel was stained for 8 minutes and washed twice with water. The developer solution was added and as soon as protein staining could be seen on the gel the reaction was stopped. This was left on for at least 30 seconds, and the gel scanned (Umax PowerLook II). The gel was finally dehydrated with 1% glycerol for 30 minutes.

2.2.14 Deglycosylation of flt-1(1-3)

An flt-1(1-3) sample (20μg) was treated with N-Glycosidase F (PNGase F, New England Biolabs, Beverly, MA, USA) according to the manufacturer's instructions. Briefly, it was added to glycoprotein denaturing buffer (New England Biolabs) and boiled for 10 minutes. After addition of G7 and NP-40 buffers (New England Biolabs), 1025 units of N-Glycosidase F was added to the sample and incubated for 1 hour at 37°C.

2.3 Purification and binding affinity of flt-1(1-3)

2.3.1 Strep Tag purification, method 1: Column

Strep-Tactin Macroprep slurry (IBA, Göttingen, Germany) was transferred to a HR5/5 column (Amersham Biosciences), to yield a 1ml bed volume, equilibrated with wash buffer (Appendix 1.2). Flow rate was 1 ml/min and 0.5ml fractions were collected.

Sample (10 column volumes, CV) was applied to the column and after 21 CV of wash buffer a gradient up to 0.5mM desthiobiotin (in elution buffer, Appendix 1.2) was run over 3 CV. The elution buffer (containing 2.5mM desthiobiotin) was passed through the column for a further 80 CV. The column was regenerated according to the manufacturer's instructions.

2.3.2 Strep Tag purification, method 2: Slurry

Conditioned medium (25ml) was incubated with rolling in 1 ml StrepTactin Macroprep slurry in wash buffer (Appendix 1.2) for 30 minutes at 4°C. The slurry was pelleted by centrifugation at 1000xg for 5 minutes and the supernatant removed for storage at -20°C. The slurry was washed by resuspending in 5ml wash buffer and incubating at 4°C for 5 minutes followed by centrifugation at 1000xg, 5 minutes. The supernatant was removed and stored at -20°C. This wash step was repeated to a total of 3 washes, each wash collected. The slurry was incubated with elution buffer (see above, also at 300mM Sodium chloride) overnight at 4°C (Appendix 1.2, also used at 300mM Sodium chloride). The slurry was pelleted by centrifugation and the supernatant stored at -20°C. An additional 1.5ml of elution buffer was added and after briefly mixing, was spun down and the supernatant collected.

2.3.3 Heparin affinity chromatography

Conditioned medium (200ml) was centrifuged at 5000xg for 5 minutes to remove cell debris and loaded onto a HiPrep 16/10 Heparin FF column (Amersham Biosciences). After removing unbound proteins with 2 CV washing buffer bound proteins were eluted by increasing the sodium chloride concentration from 120mM to 1060mM in a linear gradient. Flt-1(1-3) was eluted between sodium chloride concentrations of 277mM and 571mM. The column was regenerated with buffer containing 2000mM sodium chloride and equilibrated in washing buffer (Appendix 1.2 for recipes). Fractions (2.5ml) were collected.

2.3.4 Cation exchange chromatography

Heparin affinity chromatography fractions positive for flt-1 were pooled, concentrated down to 1ml (Section 2.2.9) and dialysed against the Cation exchange start buffer (Spectra/Por 2, Spectrum Labs, Rancho Dominguez, CA, USA, MW cut-off 12-14,000Da). The sample (500μl) was then run through a cation exchange column (Mono S 5/50 GL, Amersham Biosciences) and flt-1(1-3) eluted over a gradient of 100mM to 600mM sodium chloride (Appendix 1.2 for recipes). Fractions (500μl) were collected.

2.3.5 Size exclusion chromatography

Heparin affinity chromatography fractions positive for flt-1 were pooled and concentrated as above. Samples were applied (500μl) to a gel filtration column (Superdex 75 HR10/30, Amersham Biosciences) and proteins separated over 1 CV, using the heparin affinity chromatography washing buffer. Fractions (500μl) were collected.

2.3.6 Protein concentration assays

The BCA protein assay kit (Pierce, Rockford, IL, USA) was employed, using a microtitre plate method. Briefly, a series of bovine serum albumin (BSA) standards were made between 50μg/ml and 2000μg/ml. To these and the test samples the reaction mix was added and the colour reaction developed for 30 minutes at 37°C. Colour intensity was measured at 540nm using a Microplate Autoreader EL311, Bio-Tek instruments. To measure the levels of total flt-1 in the preparations the Quantikine flt-1 immunoassay kit (R & D systems, Minneapolis, MN, USA) was used, according to the manufacturer's instructions, with a soluble flt-1 standard for calibration. Briefly, this involved a sandwich ELISA-type assay. A monoclonal antibody against flt-1 was coated onto the plate. The flt-1(1-3) was added, followed by a polyclonal antibody, conjugated to peroxidase. Tetramethylbenzadine was used to develop a colour reaction.

2.3.7. Flt-1(1-3)/VEGF binding assay

The Biacore 3000 (Biacore, Uppsala, Sweden) and the CM5 sensor chip (Biacore) were used for this work. The system and chip were washed with HBS-EP buffer (Appendix 1.3). Firstly, the optimum pH for interaction of vascular endothelial growth factor (VEGF) with the chip was determined by injecting 5μg/ml VEGF (R&D Systems) dissolved in a number of acidic pH buffers into the system, and satisfactory interaction was found with a 10mM sodium acetate buffer at pH4.5. The VEGF (3μg/ml) was then immobilised onto the 2nd flow cell of the chip using 70μl of 100mM NHS (N-hydroxysuccinimide) and 70μl of 400mM EDC (N-ethyl-N'-(3-diethylaminoprophyl) carbodiimide), with 1M ethanolamine (Biacore) as a block. The 1st flow cell acted as a blank, having received the same treatment minus the VEGF. Test samples were diluted to 82μg/ml in HBS-EP buffer and 20μl passed over the chip. The chip was cleaned with 50mM sodium hydroxide. Data was analysed using the BiaEvaluation software.

2.4 Biological assays of hydrogel with flt-1(1-3)

3.4 Chick chorioallantoic membrane assay

White fertilised chicken eggs were obtained from Henry Stewart Ltd., Louth, UK and incubated at 38°C for 3 days. At day 3 the eggs were windowed as follows: the rounded end of each egg was pierced with a 0.8 mm gauge needle and 2 ml of albumin drained off, care taken not to pierce the yolk sac. The CAM was allowed to drop for 5 – 10 minutes, and a strip of sellotape placed on the upward facing side of the egg. Using fine scissors, a window of approximately 1.5 cm^2 was cut through the sellotape and underlying shell. Unfertilised eggs and those with damaged CAMs were discarded. The window was sealed with a second strip of sellotape, as was the hole in the rounded end of the egg. The eggs were returned to the incubator for a further 4 days. At day 7 the test material was prepared. The test sample (or PBS) was mixed with HAED and crosslinker to produce a hydrogel with final volume of 600μl. The components were mixed as described in Section 2.1.4 and allowed to set for approximately 1 hour inside the syringe. The syringe containing the hydrogel was

sliced into 50μl sections to yield hydrogel discs of diameter 5mm and height 3mm. Eggs were removed from the incubator and the sellotape® seal over the window cut away. Any dead embryos were discarded. One hydrogel disc per egg was gently placed on the CAM, with a negative control of no hydrogel. Images were taken using a Tessovar (Zeiss) dissection microscope coupled to a Leica 35mm camera with Velvia F100 (Fuji) film. The window was resealed with a strip of sellotape®. At day 10 the sellotape® was once again removed, and images taken using the above set-up. A selection of hydrogels was removed from the CAM for histological processing. These were fixed overnight at 4°C in 4% paraformaldehyde, followed by formulin before paraffin wax embedding. The embedding and subsequent sectioning and staining with haematoxylin and eosin were kindly carried out by Ms Kath Allsop. The eggs were destroyed at day 10. Results were obtained from approximately 67% of the originally incubated eggs. The 33% loss arose from unfertilised eggs, dead eggs, damaged CAMs or breakages.

2.4.2 Rat metatarsal bone formation assay

A pregnant female Wistar rat was euthanased 19 days post-conception and developing embryos removed. The hindlimbs of each embryo were excised and the three central metatarsal bones removed to ice cold PBS and kept together. Hydrogels were prepared by mixing the test sample (or PBS) with HAED and crosslinker, which were mixed as described in Section 2.1.4. The hydrogel was allowed to set within the syringe at 4°C 2 days prior to use. The syringe containing the hydrogel was sliced to yield 50μl discs, diameter 5mm, height 3mm. In a 12-well plate (BD Bioscience, San Jose, CA, USA) the isolated metatarsals were placed onto the hydrogel disc, one disc and three metatarsals per well. For each test sample or control six discs (up to 18 metatarsal bones) were set up. α-MEM containing 0.3 % FBS and 5μg/ml ascorbic acid (all ingredients: Sigma, Poole, Dorset) was added at 2 ml per well. Images were taken using an Olympus CK40 microscope attached to a Camedia C-3030 digital camera (Olympus). The hydrogels were incubated at 37°C, 5% CO_2. Every 1-3 days fresh ascorbic acid was applied to each well, but otherwise the medium was not changed. After 3 and 7 days further images were taken. Using Image-Pro Plus v 4.5.1.22 (Media Cybernetics, Inc.) the length of the calcified zone in each metatarsal was measured for days 1, 3 and 7. At 7 days, one set of three metatarsals from each

test group was fixed in 10% formulin (Fisher) and embedded in paraffin wax. An aliquot of the medium was also collected. Some sections (4μm) were made and stained with Haematoxylin and Eosin, by conventional methods. This histology work was kindly carried out by Ms Kath Allsop.

2.4.3 Immunohistochemistry of foetal rat metatarsals

Sections (4μm) were taken of each wax-embedded metatarsal and deparaffinised (incubated for 10 minutes in Xylene twice, 5 minutes in 100% ethanol twice, then 5 minutes sequentially in 90% ethanol, 70% ethanol, 50% ethanol and PBS). The metatarsals were fixed in 4% paraformaldehyde (Fisher) and washed in PBS for 5 minutes. They were then digested with Protease XXIV (Sigma) for 10 minutes at 37°C and washed with PBS. The metatarsals were blocked for 16 hours in 10% FBS, 5% BSA, made up in PBS. The metatarsals were incubated in a 1:20 dilution (in 1% BSA/PBS) of polyclonal anti-von Willebrand Factor antibody (Sigma) for 90 minutes at 37°C and washed 3 times in PBS. They were then incubated in a HRP-conjugated anti-rabbit secondary antibody for 90 minutes at 37°C and then washed 4 times in PBS. The HRP substrate Diaminobenzadine (DAB) (10μl of 15mM) was diluted in 1.99ml of 15mM sodium phosphate buffer, pH6.4, with 2μl of 30% hydrogen peroxide. This substrate mixture was placed on each metatarsal and the reaction allowed to continue for a few minutes until brown staining on the metatarsals could be seen, at which point the reaction was stopped with distilled water. The sections were counterstained with methyl green to enable visualisation of the nuclei of cells within the tissue. Each section was incubated with 1% methyl green (Sigma) in 20% ethanol for approximately one minute. The sections were thoroughly washed with distilled water and the colour developed with 70% ethanol. Once the sections were dry, they were mounted using Entellan (Merck) and analysed on an Olympus AX70 microscope.

3.1 Hydrogel Characterisation Introduction

This chapter describes the construction of hyaluronan (HA)-based hydrogels. It assesses any toxic effects of their formation *in vitro* and the suitability of the hydrogels for the delivery of bioactive agents *in vivo*.

HA is an important constituent of cartilage, not only in a structural role in maintaining the organisation of the tissue, but also as a signalling molecule. Furthermore, its viscoelastic and biocompatible properties, along with its relatively simple structure make HA a good candidate for new biomaterials (Section 1.1.4). HA has a repeating disaccharide structure of D-glucuronic acid and N-acetyl-D-glucosamine residues (Figure 3.1), which can be modified through the amide moiety on the D-glucosamine residues, the carboxyl group on the D-glucuronic acid residues, or the hydroxyl groups[390,410].

Auto-crosslinked polysaccharides (ACP) result from condensation of HA to achieve esterification between the carboxyl and hydroxyl groups on the same or different polymers. The hydrogel thus produced does not contain any different residues from native HA[411]. Hylans arise from HA crosslinked with divinyl sulfone, which does not affect the carboxyl or acetomido groups and represent a family of HA derivatives that can be used in a range of applications (Section 1.6.4)[390,391]. Esterification of the carboxyl groups with an alcohol increases hydrophobicity to produce the group of biomaterials known as HYAFFs, which exhibit different solubility and structural properties compared to HA, despite not technically being classed as hydrogels, as there is no crosslinking between strands[394]. Barbucci *et al.*[400] have reported on a modification to carboxyl groups using tetrabutylammonium and 2-chloro-1-methylpyridinium iodide. To this attaches a large diamine bi-functional crosslinker, which forms a crosslink by simultaneously connecting to another modified carboxyl group and leading to hydrogel formation. This group also revealed that sulphating the molecule further enhanced resistance to enzymatic degradation. A method of crosslinking the hydroxyl groups with a diepoxide such as PEG diglycidyl ether has been developed[413]. This has the advantage of leaving the

carboxyl groups intact for other modifications. This study coupled biotin to the carboxyl groups, suggesting that other agents could be attached to promote a biological effect.

A material that crosslinks *in situ* can be injected as a liquid, to form into a solid in the tissue. This minimises surgical invasion and allows penetration of the resultant scaffold into fissures within the damaged tissue. Pre-prepared thiolated HA can be crosslinked under physiological conditions via the carboxyl groups using esters or amides of poly(ethylene)glycol (PEG)[401]. Alternatively, the carboxyl groups on HA can be modified to methacrylate esters, which upon exposure to the correct wavelength, can be photopolymerised *in situ*[402,412].

However, the altered physical characteristics of some of these biomaterials, or duration time and harsh conditions required to crosslink HA derivatives into a hydrogel, limit the applications of these products. Previous work by this laboratory has developed a method whereby a pre-derivatised HA can be crosslinked under physiological conditions in minutes, without the loss of other functional groups on the molecule, thus retaining many of the original properties of HA[405]. Moreover, this technique has the advantage of allowing *in situ* hydrogel formation and the possible incorporation of cells or bioactive agents during the crosslinking process.

This chapter describes the characterisation of these hydrogels as follows:

- The modification of HA to an ethylenediamine derivative (HAED) and hydrogel formation.
- The structural and mechanical assessment of the hydrogels.
- Testing of the hydrogels for biological effects.

The derivatisation of HA (Figure 3.1B) was carried out using an established method[405], with subsequent crosslinking (via a commercially available crosslinker) into a hydrogel (Figure 3.2). The viscoelastic properties of HA and its derivatives have successfully been investigated by rheology[400,414]. Therefore, this technique was applied herein after the preliminary studies and the optimal concentrations of the hydrogel components were

A

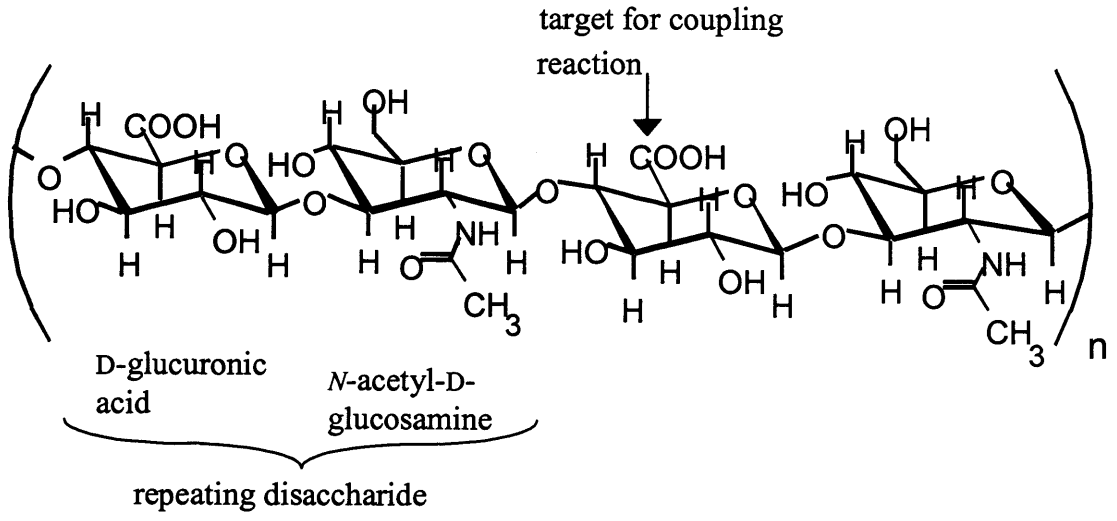

B

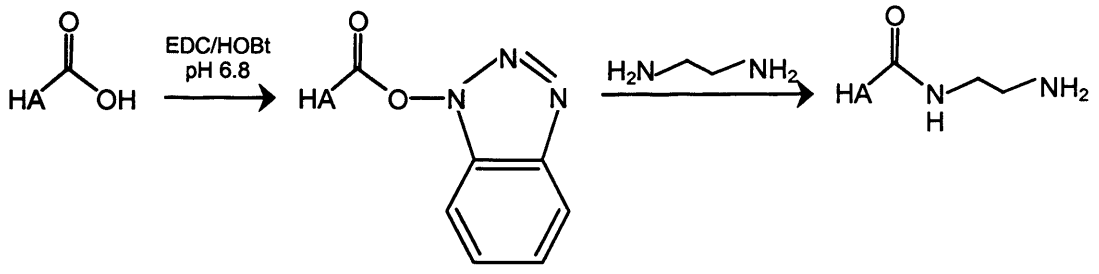

Figure 3.1: Chemical structure and derivatisation of HA. A: Structure of hyaluronan, indicating the sites for subsequent derivatisation. B: Derivatisation of hyaluronan to HAED with ethylenediamine. The intermediate was formed using a carbodiimide (EDC) / hydroxybenzotriazole (HOBt) - catalysed reaction.

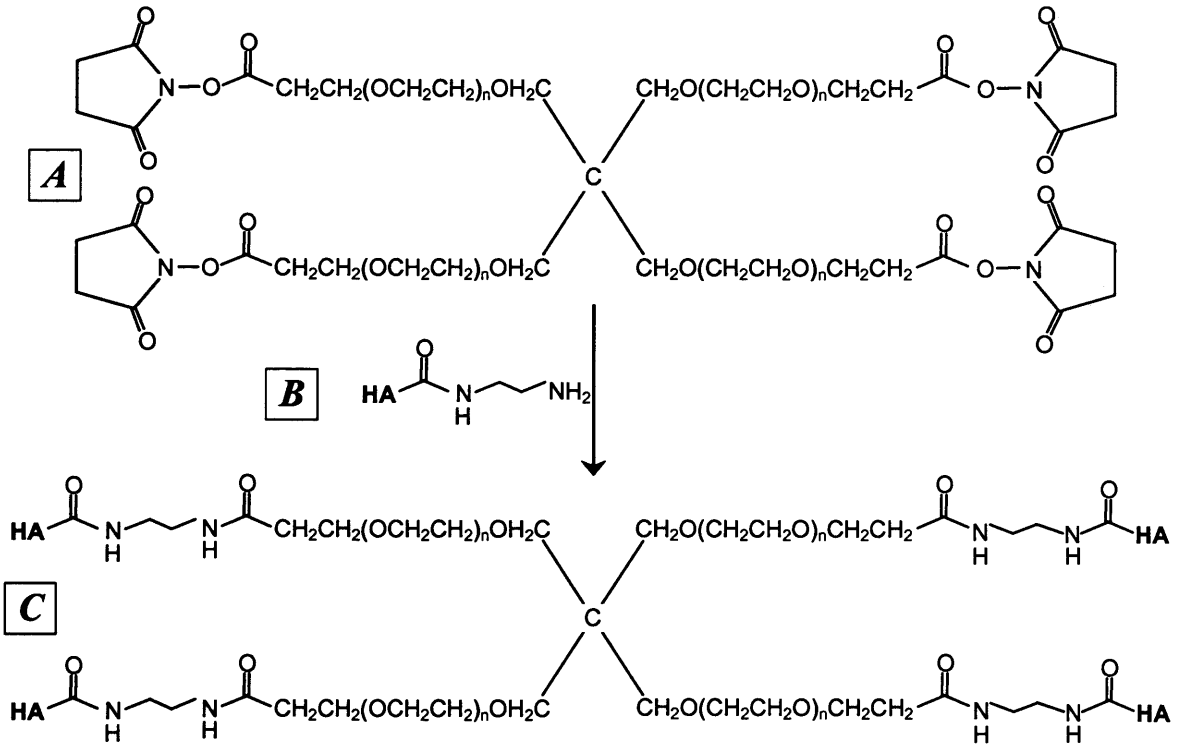

Figure 3.2: Crosslinking of SPA_4-PEG (structure A) with the derivatised side chain of HAED (structure B) to produce a hydrogel (structure C).

determined. Fourier-Transform Infrared Spectroscopy (FT-IR) has previously been employed to detect differences in the functional groups brought about by derivatisation[400]. It was postulated that by measuring the change in the amine functional groups of HAED to an amide as the crosslinking reaction proceeded, the actual, rather than the calculated, extent of crosslinking could be deduced. This would provide information on the average pore size within the resultant hydrogel, an important consideration for *in vivo* applications involving cell delivery or infiltration into the biomaterial.

The *in vitro* cytotoxicity of the crosslinking reaction on cells was assessed by means of a fluorescent live/dead cell cytotoxicity kit, previously used to reveal the toxicity of hydrogels[328,401]. This principle was applied to further quantitatively examine cell survival using flow cytometry. The *in vivo* tolerance of the hydrogel was confirmed with an ectopic bone formation assay following subcutaneous implantation, an established model in material testing[415]. It is of importance that the matrix scaffold supports infiltration of mesenchymal stem cells so that growth factor-induced tissue transformation can occur. If the scaffold is not well tolerated by the surrounding tissue, the presence of inflammatory cells may disrupt infiltration and differentiation of stem cells, resulting in altered tissue regeneration.

This chapter demonstrated that an elastic hydrogel can be formed upon crosslinking of modified HA and the properties of the hydrogel may be manipulated through adjustment of component concentration. Collagen can be incorporated into the hydrogel without loss of crosslinking ability and that the crosslinking reaction is non-toxic to cells in culture. The resultant hydrogel allows infiltration of cells *in vivo* and can induce bone formation when an osteogenic agent is incorporated into the modified HA prior to crosslinking.

3.2 Hydrogel Characterisation Results

3.2.1. Derivatisation of hyaluronan

Hyaluronan (HA, 1.5 million Daltons) was derivatised using a carbodiimide/hydroxybenzotriazole-catalysed reaction to couple ethylenediamine to the carboxyl moiety on the D-glucuronic acid of HA (Figure 3.1)[405]. The ethylenediamine derivative (HAED) formed was purified by ethanol precipitation, following formation of the sodium salt. The concentration of the final HAED was 15mg/ml. A 2, 4, 6-trinitrobenzenesulphonic acid (TNBS) assay for the quantification of amines was employed to determine the extent of derivatisation of the carboxylic acid groups, which was 12.4% ±5 (n=9)[416]. To confirm the findings from the TNBS assay, the change in concentration of D-glucuronic acid was examined utilising the reaction of hexuronic acids with carbazole, which lead to a colour change which could be quantified spectrophotometrically[417]. The decrease in concentration was inversely proportional to the extent of D-glucuronic acid modification to the derivative, and was found to reflect the results of the TNBS assay.

3.2.2. Gross examination of hydrogels

The HAED was crosslinked into hydrogels by mixing with bi- or tetra-functional active ester crosslinkers, which reacted with the derivatised side chains to form a peptide bond (Figure 3.2). Four crosslinkers were investigated:

- 2 - arm polyethylene glycol - succinimidyl propionate (SPA_2-PEG, MW 3.4kDa).
- 4 - arm polyethylene glycol - succinimidyl propionate (SPA_4-PEG, MW 20kDa).
- SPA_4-PEG, MW 10kDa.
- Succinimide ester of carboxymethylated 4 - arm polyethylene glycol (SC_4-PEG, MW 20kDa).

Table 3.1: The effect of the different components on the gel-like quality of the material. For gel score, see text. Each gel consisted of 9mg/ml HAED, 1:1 SPA_4-PEG (20kDa) : HAED, with no collagen, except where stated.

Gel score	0	1	2	3
6mg/ml HAED			✓	
9mg/ml HAED				✓
12mg/ml HAED				✓
15mg/ml HAED				✓
(No crosslinker)	✓			
0.1:1 SPA_4-PEG (20kDa)		✓		
0.5:1 SPA_4-PEG (20kDa)			✓	
1:1 SPA_4-PEG (20kDa)				✓
1.2:1 SPA_4-PEG (20kDa)				✓
1.5:1 SPA_4-PEG (20kDa)				✓
2:1 SPA_4-PEG (20kDa)				✓
1:1 SPA_2-PEG (3.4kDa)				✓
1:1 SC_4-PEG (20kDa)				✓
1:1 SPA_4-PEG (10kDa)	✓			
Pepsinised collagen 6mg/ml			✓	
Pepsinised collagen 9mg/ml				✓
Pepsinised collagen 12mg/ml				✓
Telocollagen 0.5mg/ml			✓	
Telocollagen 1mg/ml				✓
Telocollagen 1.5mg/ml				✓
Telocollagen 1.75mg/ml			✓	
Telocollagen 2.5mg/ml			✓	

Hydrogel quality was defined as a material exhibiting elastic gel-like properties noticeably firmer compared to the viscous non-crosslinked material. This was initially assessed by its ability to retain its structure when smeared with a pipette tip (smeared material indicated the presence of a viscous liquid), to return to its original shape following manual downward pressure onto the hydrogel and to maintain sufficient structural integrity to allow lifting of the whole material with forceps. The material could be scored thus:

- 0: no hydrogel had formed. The material behaved as a viscous fluid, identical to HAED. It could not be lifted with forceps.
- 1: some crosslinking had occurred, but the mixture could be smeared with a pipette tip although some resistance was evident. It could not be lifted with forceps without disintegrating.
- 2: a noticeable hydrogel had formed. The material could be lifted in one piece with forceps and offered resistance to pressure. However, a little smearing was still noticeable.
- 3: a good quality hydrogel, producing a rubbery-like material which could not be smeared and returned to original shape upon depression. This could easily be handled with forceps.

Table 3.1 shows a summary of the effect of each component concentration on the resulting hydrogel. The HAED concentration was not increased above 15mg/ml as this would have been above the physical limit of solubility. Although hydrogels containing 9mg/ml were slightly weaker than with 12mg/ml or 15mg/ml, the lower concentration meant that the fraction of HAED in the total volume of the hydrogel was decreased, allowing other materials such as collagen to be incorporated without affecting the overall volume of the hydrogel, with little compromise in hydrogel quality.

Both the SC_4-PEG (20kDa) and SPA_2-PEG (3.4kDa) crosslinkers yielded firm, type 3 hydrogels after 5 minutes. The crosslinking reaction using SPA_4-PEG (20kDa) proceeded at a slower rate, reaching completion after 10 minutes. However, the SPA_4-PEG (10kDa) crosslinker failed to produce a noticeable hydrogel and it was suspected that a problem with the manufacturing process had rendered this crosslinker

inactive, so it was omitted from further experiments. Alternatively, the side chains of this crosslinker may have been too short to enable crosslinking between HAED molecules. The SC_4-PEG crosslinker produced the best hydrogels, indicating that these crosslinker groups were more reactive. However, this crosslinker was not freely available due to patent protection, so its use was restricted. Figure 3.3 macroscopically illustrates the effects of crosslinker on the properties of the hydrogel. Hydrogel properties could be greatly influenced by changes in crosslinker concentration. The ratio of 1:1 (crosslinker) : (HAED) functional groups resulted in type 3 hydrogels without using as much material as higher concentrations, so was selected for future work.

Two forms of bovine type I collagen were evaluated – pre-fibrillised telocollagen and pre-fibrillised pepsinised collagen. The collagen was sheared through a 450μm diameter needle, to enable greater homogeneity when mixed with HAED. The reasons for incorporating collagen were two-fold. Firstly, it retains collagen-binding factors within the hydrogel, when used as a delivery system. Secondly, the presence of collagen may facilitate the migration of cells into the hydrogel[404]. As collagen was incorporated into HAED prior to addition of the crosslinker, the influence of the amine groups of collagen lysine residues on the crosslinking reaction was considered. At the collagen concentrations used, it was deduced that the presence of lysine would alter the Molar ratio of amine groups available for crosslinking by a maximum of 10%, which would change the total amine group to crosslinker ratio from, for instance, 1:1 to 1.1:1. This change produced little discernable difference in the properties of the hydrogel, and therefore was not taken into account on the inclusion of collagen.

Hydrogels containing higher concentrations of fibrillised telocollagen (Table 3.1) disintegrated when smeared. It was probable that the physical bulk of the collagen disrupted the crosslinking reaction, leading to steric hindrance of the reactive groups. Pepsinised collagen produced smaller and more homogenous fibrils, which could be incorporated at higher concentrations without such disruption to the crosslinking reaction. Telocollagen could not be added at these concentrations and achieve fibrillisation. These hydrogels were very spongy and resistant to pressure. These properties were probably caused by the additional physical properties of the collagen

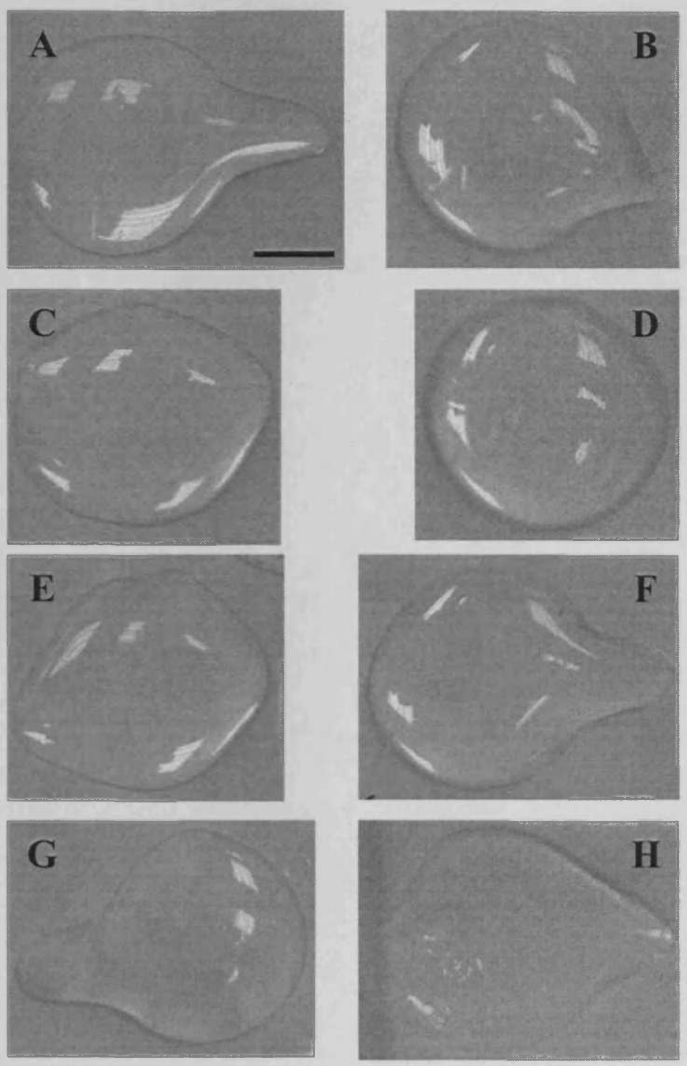

Figure 3.3: Macroscopic examples of HAED hydrogels (500μl) on plastic, which had been probed with a pipette tip 2 minutes after mixing (the protrusion seen in some images) and images taken after 30 minutes. Gels contain 9mg/ml HAED, a crosslinker : HAED ratio of 1:1, SPA_4-PEG (20kDa) crosslinker, except where stated. A: 0.1:1 ratio, which can be smeared at 2 minutes, but as the hydrogel slowly crosslinks it does not allow the smeared region to flow back into the hydrogel. B: 1:1 ratio, the hydrogel has not crosslinked by 2 minutes, but is more resistant to smearing than 0.1:1 and at 30 minutes is much more domed and gel-like. C: SPA_4-PEG (10kDa), with a flattened shape as it behaves as a viscous liquid, and the smeared region flowed back into the rest of the material. D: SC_4-PEG (20kDa), this cannot be smeared at 2 minutes as a hydrogel has formed by this point, resulting in a domed profile. E: SPA_2-PEG (3.4kDa), this can be smeared a little, but has begun to solidify by 2 minutes. F: 6mg/ml HAED, this is not as solid as (A), the smear begins to flow back into material before crosslinking was complete. G: 1.5mg/ml fibrillised telocollagen, the hydrogel is softer and easier to smear. H: 9mg/ml fibrillised pepsinised collagen, has a rougher surface, the hydrogel is more dense and smearing is more difficult. Scale bar = 5mm.

rather than any chemical interaction with the crosslinker. The macroscopic appearance of hydrogels with collagen is illustrated in Figure 3.3.

In summary, the findings of these initial experiments were:

- HAED concentration had to be at least 9mg/ml to form firm hydrogels.
- A ratio of crosslinker : HAED reactive groups of between 0.5:1 and 2:1 produced the firmest hydrogels.
- The SPA_4-PEG (10kDa) crosslinker was inactive, but SPA_4-PEG (20kDa), SC_4-PEG (20kDa) and SPA_2-PEG (3.4kDa) could all form hydrogels.
- The reaction reached completion within 10 minutes, although SC_4-PEG (20kDa) and SPA_2-PEG (3.4kDa) formed hydrogels more rapidly.
- The incorporation of collagen resulted in denser hydrogels that were more brittle.

3.2.3. Rheology

The aforementioned method of hydrogel quality assessment had a number of shortcomings, not least the subjective nature of evaluation and potential for operator variation. Rheological analysis allowed the elastic and viscous characteristics of the hydrogel to be determined, enabling more critical comparison between hydrogels. A hydrogel would be expected to have considerable elastic properties, unlike the highly viscous HAED. The elastic and viscous quantities determined by rheology are described more thoroughly in Section 2.1.6.

The HAED concentration and crosslinker ratio selected yielded firm hydrogels, whilst minimising reagent quantities. The final volume of each hydrogel was established to 550μl with phosphate buffered saline (PBS), except in collagen-containing hydrogels where the volume of each constituent was doubled (explained below). Immediately after mixing, the setting hydrogel was loaded onto the rheometer and the parallel plate lowered to leave a gap of 300μm, or 700μm for collagen-containing hydrogels. For each variable, hydrogels were tested in triplicate.

A plate-style rheometer can apply shear forces equally across a sample (Figure 3.4). Either a coned plate or a parallel plate can be used. A parallel plate was used

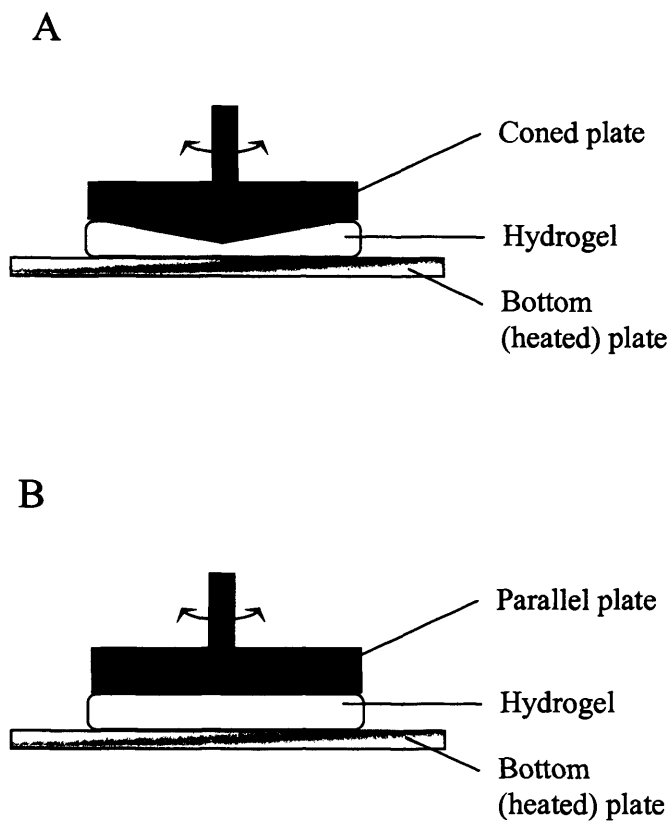

Figure 3.4: Diagrammatic representation of the setup for the rheological measurement of hydrogels, with the oscillation of the upper plate indicated. A: A coned upper plate, illustrating the decrease in gap distance between the point of the cone and the bottom plate. B: A parallel plate, with a uniform gap distance across the sample. The parallel plate setup was used in this study.

in the present study, to avoid complications due to large collagen particles under the point of the cone disrupting measurements[418]. Although collagen was sheared through a 450μm needle before incorporation into a hydrogel, the gap distance between the parallel plates was increased to 700μm, with a relative increase in total hydrogel volume. This increased the homogeneity of the collagen-containing hydrogels.

Briefly, the quantities for studying elastic and viscous properties are as follows:

- G′ is the "Storage Modulus". This describes the elastic properties of the hydrogel, expected to increase with hydrogel formation.
- G″ is the "Loss modulus". This relates to the viscous properties, anticipated to decrease with hydrogel formation.
- Tan δ is the phase shift caused by the response of a material to an applied oscillatory force. This indicates whether the material is behaving in an elastic or viscous manner, with a decrease in tan δ indicating increasing elasticity. Therefore, this value would be expected to decrease as the hydrogel formed.

The definitions of these quantities are discussed in more depth in Section 2.1.6. The arithmetic mean was calculated from the triplicates at each time point.

Figure 3.5 shows the relationship between the three variables in two different samples. Sample A contains HAED only (9 mg/ml), with no hydrogel forming. There appears to be a very slight decrease in elasticity, shown by the drop in tan δ coupled with the increase in G′ (Figure 3.5A). This small change could have resulted from slight dehydration of the hydrogel on the rheometer. In contrast, Figure 3.5B is a hydrogel of crosslinker to HAED ratio of 2:1, showing a marked increase in elasticity. Tan δ decreased in value and although G″ initially increased, it levelled off as the hydrogel became more elastic. Explanations for this are discussed in Section 3.3.2. A sharp increase in G′ was observed as the material became more elastic, so this parameter was selected to describe the characteristics of the hydrogels in subsequent experiments.

Figure 3.6 shows hydrogel elasticity (G′) under different conditions. Figure 3.6A demonstrates the importance of crosslinker concentration in the production of a

hydrogel. There was no increase in elasticity when no crosslinking had occurred (red line), while the elasticity of the material increased with increasing crosslinker concentration, up to 1.5:1. However, very high levels of crosslinker (5:1) led to a reduction in hydrogel quality. The use of high levels of crosslinker was not pursued, as the ability to form hydrogels at low crosslinker concentrations was of more relevance to the study. The rheological data concurred with the previous observations (Section 3.2.2.) that good quality hydrogels are attainable with crosslinker concentrations above 0.5:1.

Predictably, increasing the HAED concentration also increased the elasticity of the hydrogel, as more amine groups were located closer together to ameliorate crosslinking (Figure 3.6B). The fluctuations in the graph at the HAED concentration of 6mg/ml were considered to be caused by drying out of the material. The addition of pepsinised collagen concurred with the observations in Section 3.2.2, with a very firm, rubbery hydrogel formed, as demonstrated by Figure 3.6C. Telocollagen did not have the same effect, in that there was a slight reduction in the quality of the hydrogel. This correlated with the previous findings, where at higher telocollagen concentrations, hydrogels were weaker and more fragile.

The choice of crosslinker also affected these properties of the hydrogels. As reported in section 3.2.2 the SC_4-PEG (20kDa) yielded the firmest hydrogels (Figure 3.6D). The SPA_4-PEG (20kDa) and SPA_2-PEG (3.4kDa) hydrogels were similar, while the SPA_4-PEG (10kDa) did not form hydrogels. Figure 3.6E demonstrated that the crosslinking reaction proceeded more rapidly at an increased temperature. The stutter at approximately 700 seconds was attributed to the hydrogel dehydrating with increased temperature and adherence to the apparatus. This was followed by a sudden release with the next oscillation causing the observed drop in the reading.

Future clinical applications of HAED hydrogels may require the crosslinking reaction to occur *in situ*, in a "wet" environment. The closest approximation to this attainable with the rheometer was accomplished by surrounding the crosslinking hydrogel with PBS prior to the rheometer plate making contact with the sample. During testing, additional PBS was added to the exposed hydrogel around the sides of the plate.

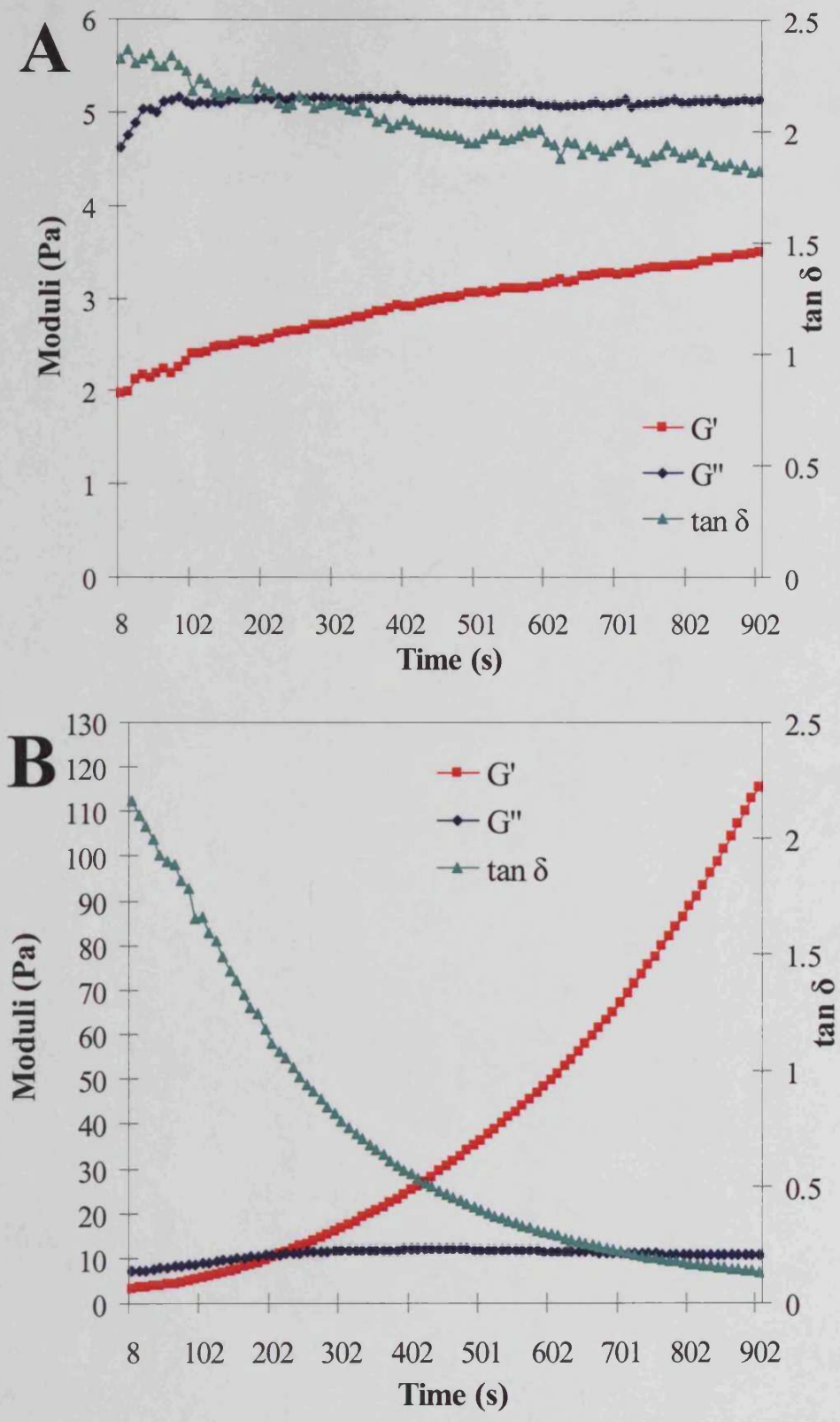

Figure 3.5: Rheological data for two HAED hydrogel preparations. A: HAED only (9mg/ml HAED, no crosslinker added). B: A firm hydrogel (9 mg/ml HAED, crosslinker added (2:1)). This data represents a single run.

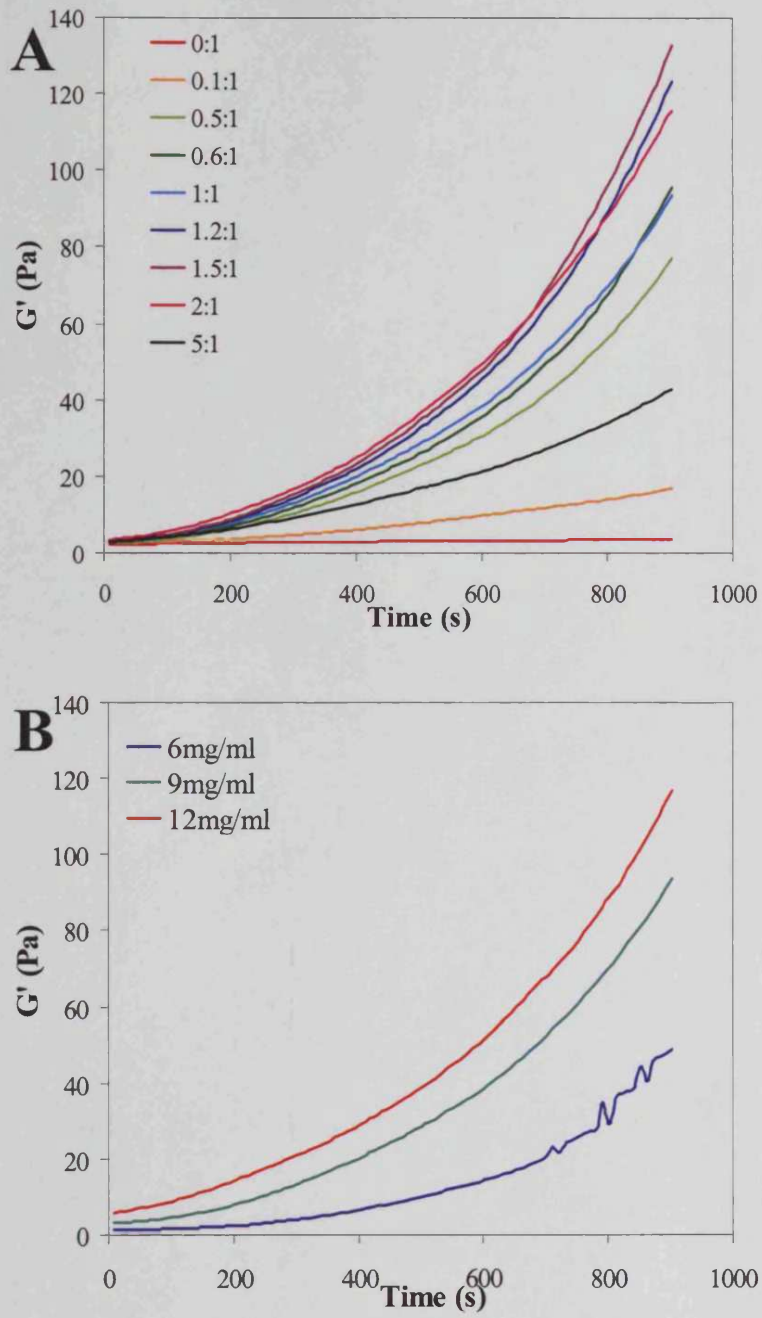

Figure 3.6: The storage modulus indicating elasticity as a function of time, for HAED hydrogels. Conditions except where specified: 9 mg/ml HAED, crosslinker ratio 1:1, crosslinker SPA_4-PEG (20kDa), 25°C, no PBS around the hydrogel. The following conditions were altered: A: crosslinker : HAED groups; B: HAED concentration; C: Collagen concentration; D: type of crosslinker; E: reaction temperature; F: surrounding the hydrogel with PBS. Each plot represents n=3. (Continued over the next two pages.)

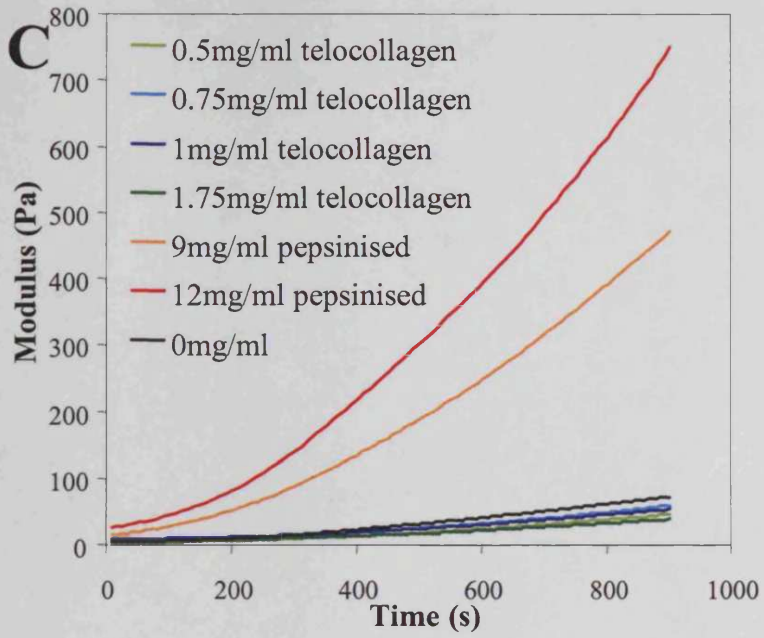

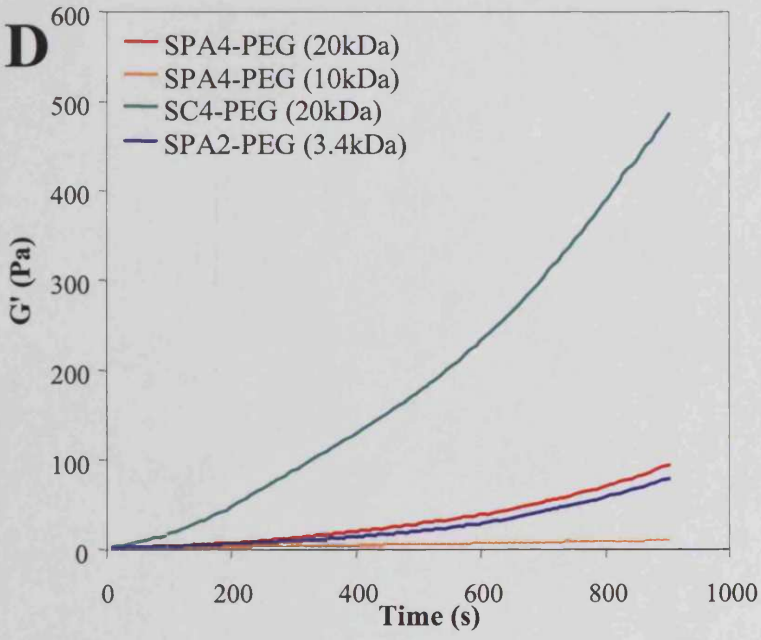

(Figure 3.6 continued.)

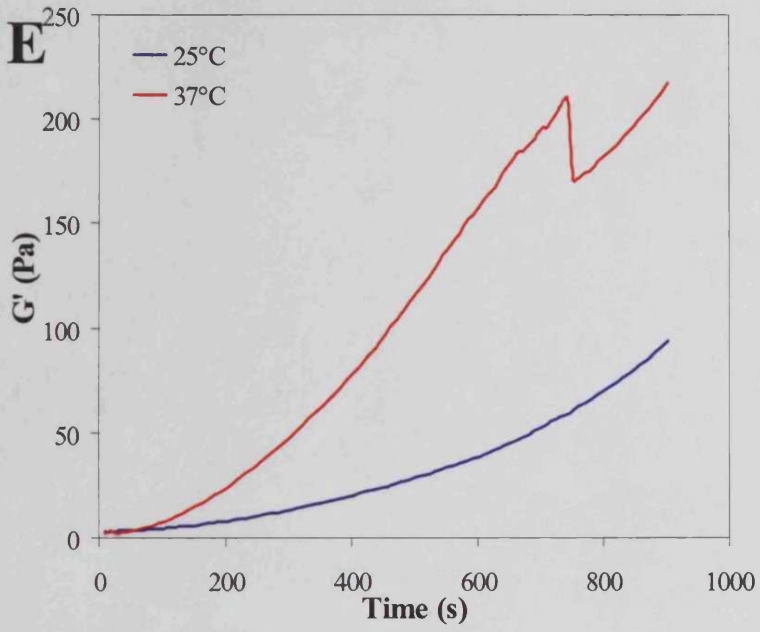

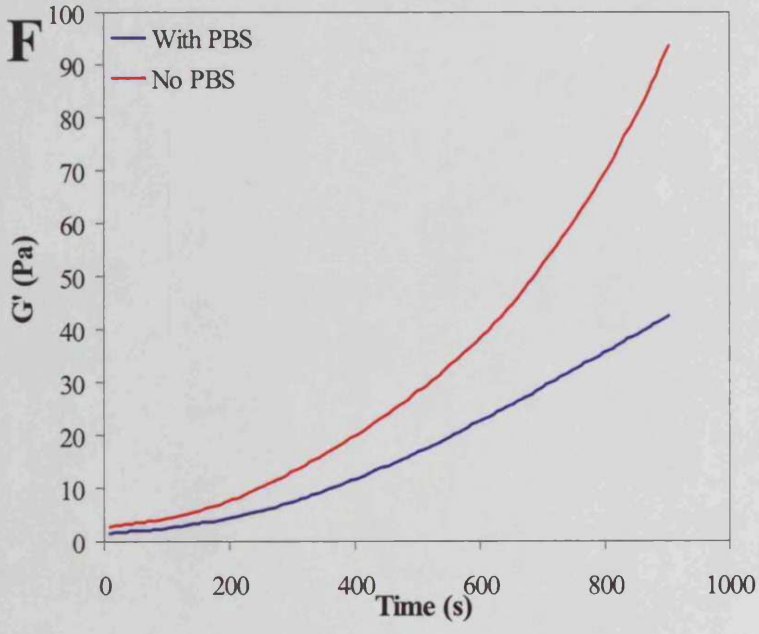

(Figure 3.6 continued.)

Figure 3.6F exhibited a drop in hydrogel elasticity and thus hydrogel formation, upon addition of PBS. Although the previous assessment had implied that the crosslinking reaction reached completion within 10 minutes (Section 3.2.2), the G′ value did not level off as expected at this point (Figure 3.5). This was investigated further by measuring hydrogel crosslinking over 90 minutes, as any longer led to deformation of the hydrogel as a result of dehydration. To limit dehydration over the longer run time, the outer edge of the sample was surrounded by PBS after the plate had been lowered. A levelling off of tan δ was demonstrated after 30 minutes (1600 seconds), indicating that no further change in viscosity occurred within the hydrogel (Figure 3.7).

To further explore the characteristics of the hydrogel using an alternative experimental approach, the "creep" response of the material was investigated. Once the hydrogel had been allowed to crosslink for 15 minutes, a constant shear force was applied and the resulting displacement, or creep, measured. After 10 minutes, the force was removed and the movement of the material to its original position was measured. A viscous material would be expected to show little resistance, allowing the plate to move easily. Conversely, an elastic material would offer resistance with a slower "creep" by the material in reaction to the applied force. However, upon testing of the hydrogels, an interesting observation was made. Instead of a steady creeping of the elastic hydrogel, a ringing-type response occurred (Figure 3.8). Even so, this measurement can be correlated to the oscillation experiments already described previously by the tan δ parameter. The A_n and A_{n+1} values indicated in Figure 3.8 refer to the maximum displacement of each vibration of the hydrogel, and tan δ can be deduced as follows:

$$\Lambda = \ln\left(\frac{A_n}{A_{n+1}}\right) \tag{1}$$

Followed by:

$$\Lambda = \pi \tan \delta \tag{2}$$

At 15 minutes (900 seconds), the tan δ value was already very small (Figure 3.5B). The hydrogel shown in Figure 3.8 yielded a tan δ value at 15 minutes of 0.059,

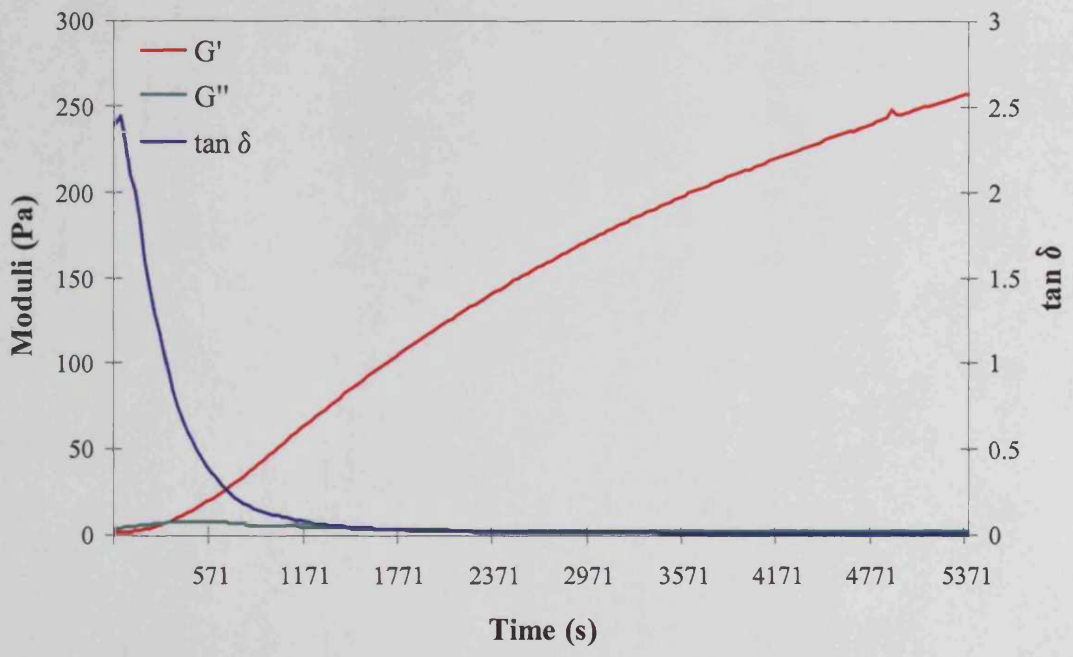

Figure 3.7: Viscoelastic parameters (storage modulus G′, loss modulus G″ and tan δ) over 90 minutes for HAED hydrogel, containing 9mg/ml HAED, 1:1 SPA_4-PEG (20kDa) to HAED, at 25°C.

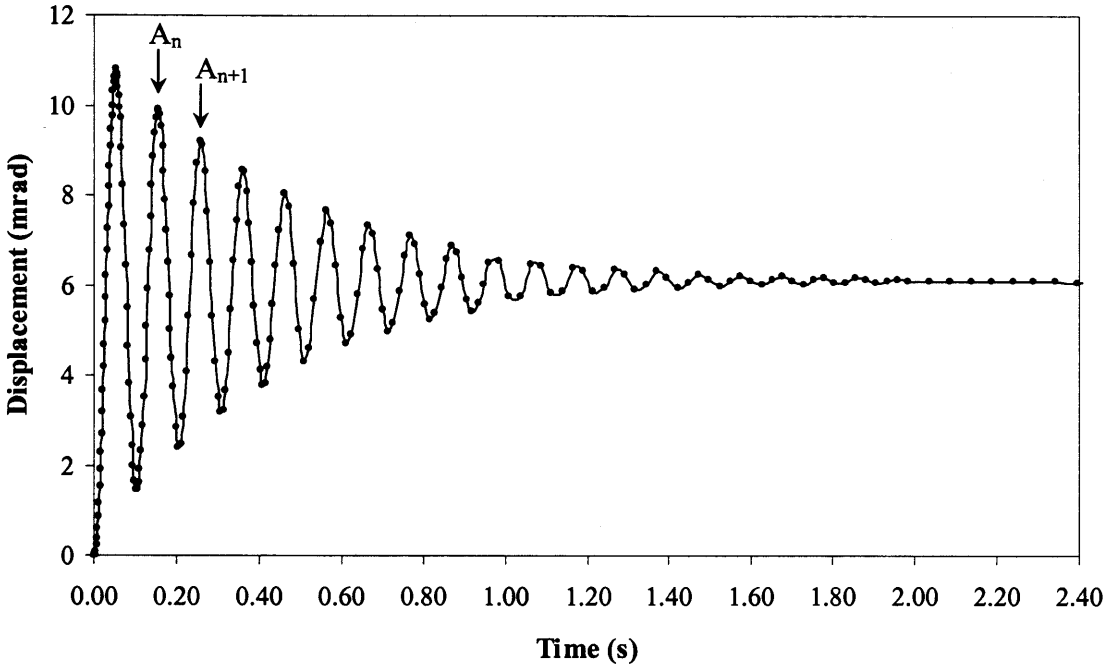

Figure 3.8: The displacement (milliradians) in response to 50Pa applied force, of hydrogel consisting of 9mg/ml HAED, 1:1 SPA4-PEG (20kDa), no collagen. A_n and A_{n+1} indicate points for calculation of the logarithmic decrement (see text).

Table 3.2: Preparation of HAED samples containing different concentrations of carbodiimide to attain a range of percentage modifications of carboxylic acid side chain.

Molar excess of carbodiimide	% Modification
0 X	2.5
0.25 X	2.0
0.65 X	2.2
1.6 X	3.8
4 X	7.0
10 X	18.9

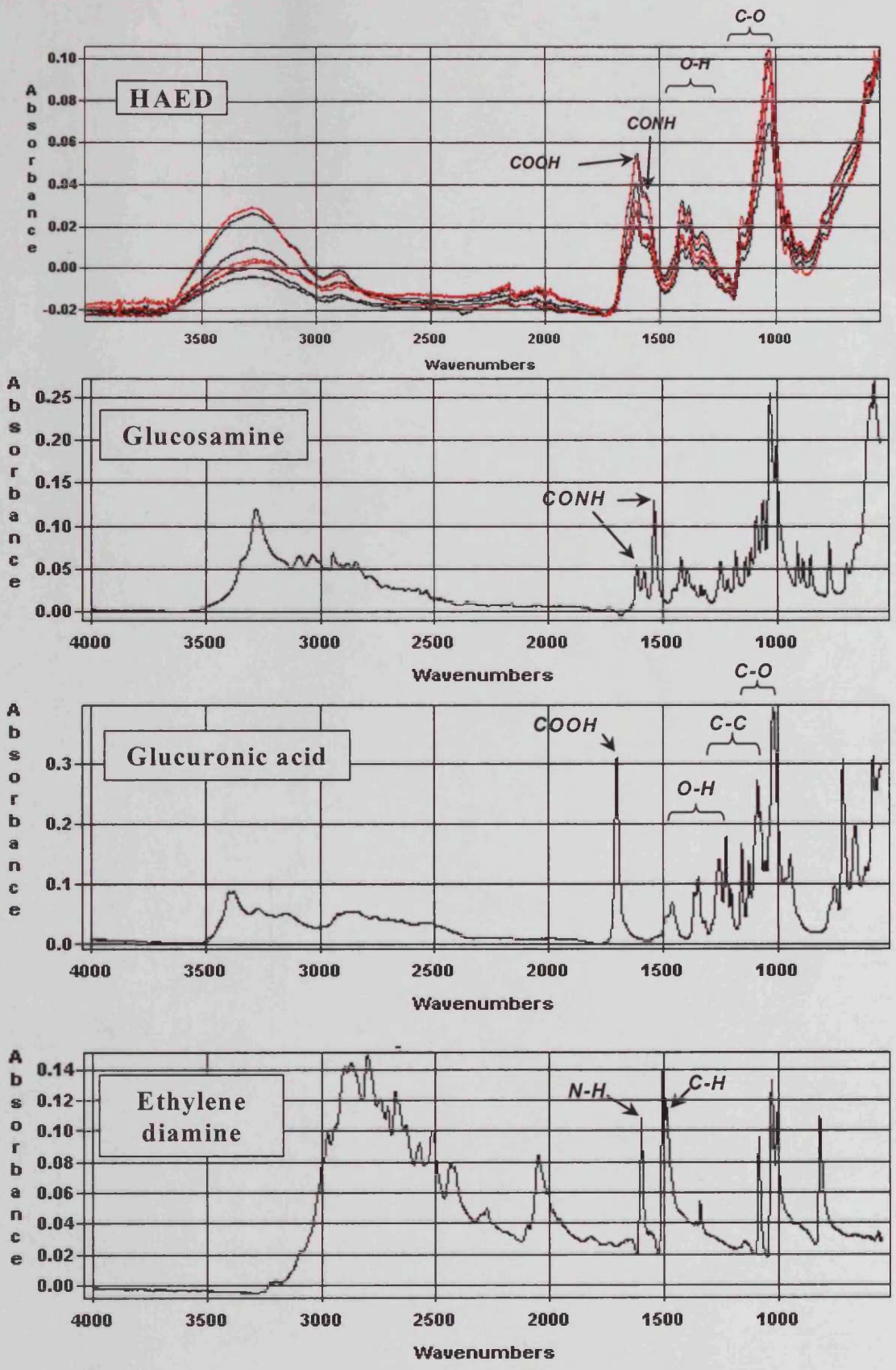

Figure 3.9: FT-IR spectra of HAED samples and control compounds. HAED spectrum: Red refers to HAED samples derivatised 3-20%. Black indicates HAED samples derivatised less than 3%. Wavenumbers measured in cm^{-1}. Neat dry sample applied directly to a germanium crystal.

Table 3.3: The functional groups, with their respective spectrum peaks, of interest to determine the extent of the crosslinking reaction occurring within HAED hydrogels.

Functional group	Identifying spectrum peaks (cm^{-1})
Amine	3500-3300
	2700-2300
	1650-1560
Carboxyl	3000-2500
	1725-1700
Amide	3460-3400
	1700-1670
	1550-1510

3.2.5. Cell viability assay

To examine any toxic effects of the crosslinking reaction on cells, HCA_2 fibroblasts were incorporated into crosslinking hydrogels and incubated for 24 hours at 37°C, with 5% CO_2. The fibroblasts were stained with calcein AM and ethidium homodimer-1. The cell-permeable calcein AM was converted by the esterase activity of live cells to produce fluorescent calcein with a green fluorescence at excitation 495nm and emission 515nm. Ethidium homodimer-1 entered cells with damaged membranes and bound to nucleic acids, producing a red fluorescence at excitation 495nm and emission 635nm. After staining, the cells were fixed and examined.

Figure 3.10 compared the effects of hydrogel density through crosslinker ratio, upon cell viability. It has been previously determined that when very little crosslinker was applied (0.1:1), no hydrogel formed (Section 3.2.2). This resulted in the diffusion of fibroblasts through the HAED to the bottom of the well. The fibroblasts formed a monolayer, with virtually no cells being suspended in the hydrogel (Figure 3.10). There was little indication of cell death. With a firmer hydrogel (1:1), the cells were embedded within the hydrogel matrix, indicated by blurring in the magnification plane. Associated with this was a slight increase in cell death after 24 hours, indicating a potentially toxic effect of the hydrogel. Within a denser hydrogel (2:1), the cells were more dispersed within a three dimensional matrix, with a notable increase in cell death.

For comparison, the SC_4-PEG (20kDa) crosslinker was also tested and exhibited a higher level of cell survival than SPA_4-PEG (20kDa) (Figure 3.11). The SPA_2-PEG (3.4kDa) was not tested as it was proposed that the small pore size generated by the smaller crosslinker would not support cell infiltration, as previously observed[405].

Collagen was incorporated into HAED prior to crosslinking, and the effect of collagen on cell survival and spreading was investigated (Figure 3.12). Cells incubated in hydrogels containing pepsinised collagen exhibited more cell death than those in the absence of collagen, probably as a result of the increased density of the material. Figure 3.12 demonstrated some simultaneous green and red staining by the same cells following treatment with fibrillised telocollagen. This could indicate the early stages of cell death, as the esterases required to trigger calcein fluorescence were still present

but cell membrane integrity was being lost. This would cause the dual staining observed.

As a future purpose of the hydrogels would be to provide a delivery vehicle scaffold in cartilage lesions, the effects of crosslinking hydrogels on porcine chondrocyte survival was investigated (Figure 3.13). It was demonstrated that the cell survival was comparable to that of the HCA_2 fibroblasts, indicating that these hydrogels did not have a particularly detrimental effect on chondrocytes.

In summary, this approach demonstrated that:

- The crosslinking reaction and hydrogel showed early signs of toxicity to fibroblasts after 24 hours, even at relatively high concentrations of crosslinker.
- A lower crosslinker : HAED ratio allowed increased cell survival.
- The presence of collagen reduced cell viability.
- Chondrocytes were comparable with fibroblasts in tolerating the crosslinking reaction.
- This method was not ideal for quantification of cell toxicity.

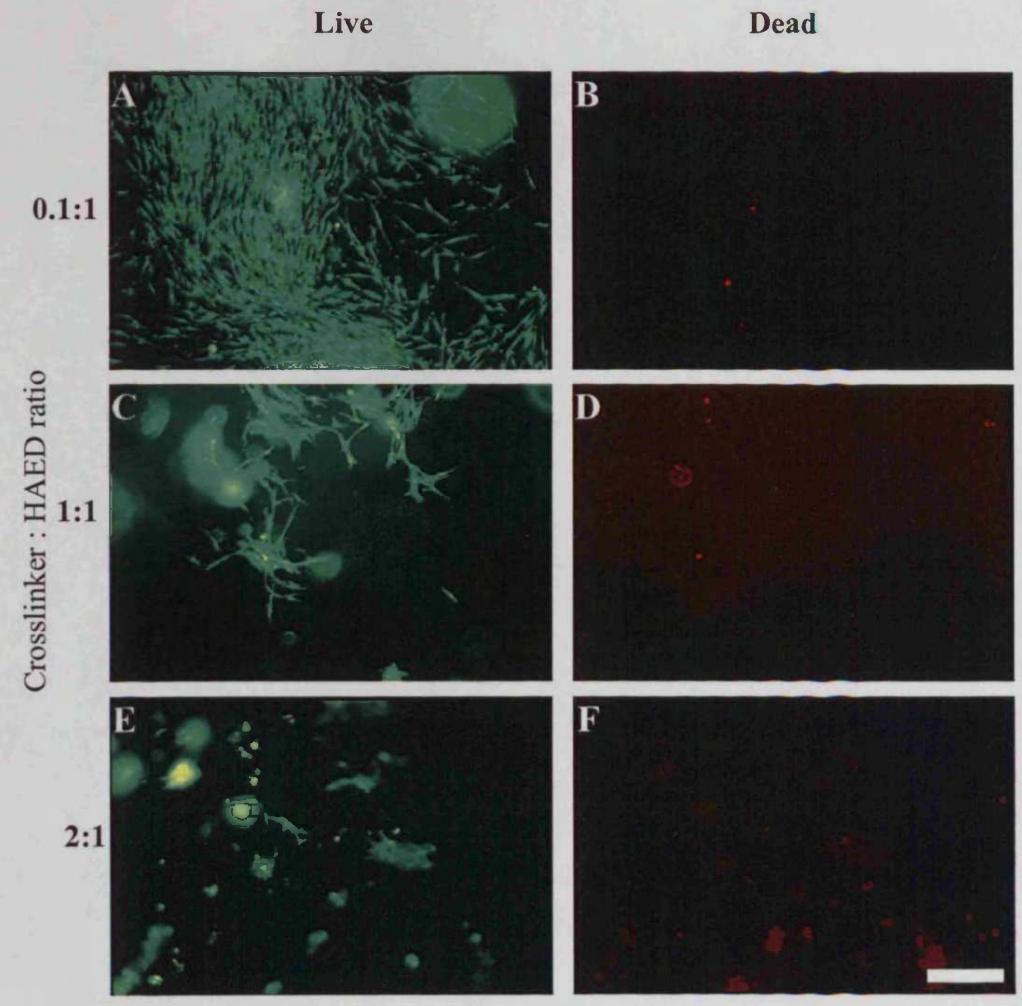

Figure 3.10: Cell viability in HAED hydrogels. Calcein live cell stain (A, C, E) and ethidium homodimer-1 dead cells stain (B, D, F) of $2x10^5$ HCA_2 fibroblasts incorporated into hydrogels of 12mg/ml HAED, 12mg/ml pepsinised collagen, SPA_4-PEG (20kDa) crosslinker at the crosslinker : HAED ratios as shown. Scale bar = 200μm.

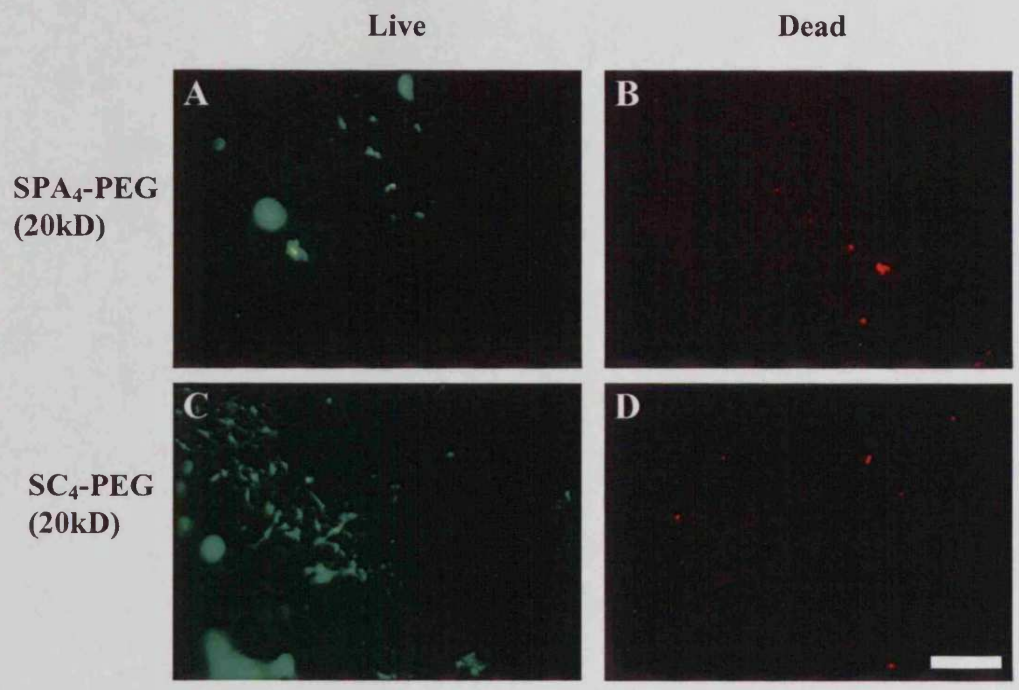

Figure 3.11: Calcein live cell stain (A, C) and ethidium homodimer-1 dead cells stain (B, D) of $2x10^5$ HCA_2 fibroblasts in hydrogels of 12mg/ml HAED, 12mg/ml pepsinised collagen, at the crosslinker : HAED ratio of 0.5:1, the ratio selected as preliminary results showed a good response at this ratio. The type of crosslinker used is indicated on the left. Scale bar = 200μm.

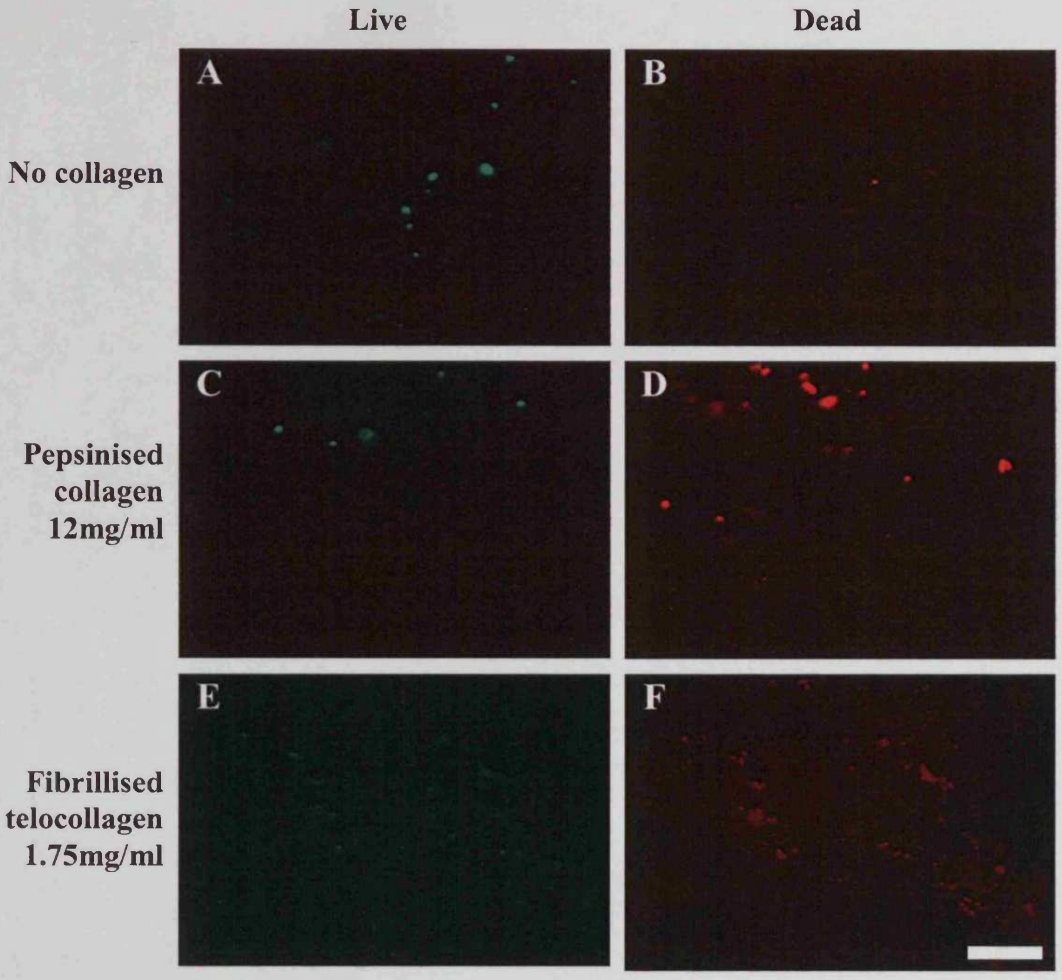

Figure 3.12: Calcein live cell stain (A, C, E) and ethidium homodimer-1 dead cell stain (B, D, F) of $2x10^4$ HCA_2 fibroblasts in hydrogels of 12mg/ml HAED, SPA_4-PEG (20kDa) crosslinker at 0.5:1 ratio with HAED. Scale bar = 200μm.

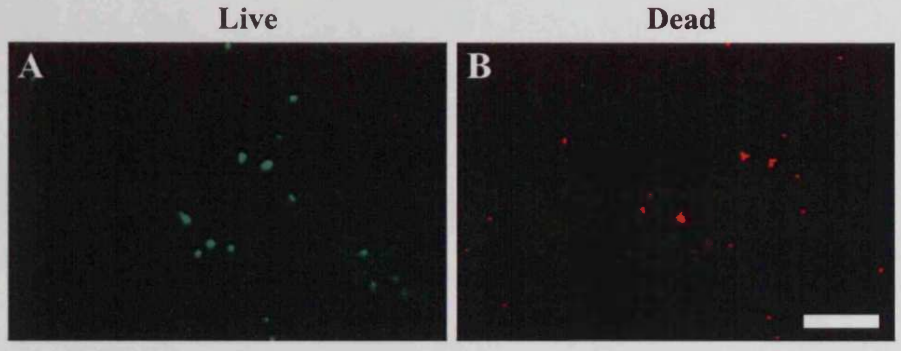

Figure 3.13: Calcein live cell stain (A) and ethidium homodimer-1 dead cell stain (B) of $2x10^4$ porcine chondrocytes in a hydrogel of 12mg/ml HAED, SPA_4-PEG (20kDa) crosslinker at 0.5:1 ratio with HAED. Scale bar = 200μm.

3.2.6. Flow cytometry

Flow cytometry was used as an alternative method to quantify cell survival in the crosslinking hydrogels. HAED-based hydrogels were prepared to test cell toxicity, in response to the following factors: crosslinker concentration, crosslinker type and HAED concentration. Collagen was excluded from this set of experiments for reasons given in Section 3.3.5. HCA_2 fibroblasts were integrated into hydrogels during the crosslinking reaction and incubated for 16 hours. Hyaluronidase digestion liberated the cells from the hydrogel, as described previously[405] and from preliminary experiments in the present study. The cells were pelleted and stained with propidium iodide (PI), as previously used[401,475]. This chromophore integrates into accessible DNA in dead cells, upon which its fluorescence increases 20 - 30-fold. The DNA-PI complex excites at 488nm with maximum emission at 615nm (supplier literature). A positive control was prepared by placing a hydrogel containing cells into toxic methanol, thus producing 100% toxicity. Fibroblasts grown as a monolayer under normal tissue culture conditions provided a negative control with very little PI staining, indicative of good cell survival. For each variable 5 hydrogel/cell complexes were analysed in parallel.

Flow cytometry was performed on 5000 events (cells) per hydrogel. PI was detected using the flow cytometer photomultiplier tube FL3. All HCA_2 fibroblasts naturally exhibit autofluorescence, which was exploited by using the signal from the photomultiplier tube FL1 (whose wavelength settings cannot detect PI) as the x axis when plotting the intensity of the PI signal. Figure 3.14 demonstrates a selection of typical data obtained. Parts A, C, and E show histograms of the intensity of the PI signal in the cells analysed (logarithmically transformed). The live cell control (A) shows a peak of events at a low PI intensity, indicating live cells, with small numbers of dead cells (high intensity). By contrast, part C represents the dead cell control, showing peaks of high PI intensity. Part E represents a hydrogel example showing a mixture of live and dead cells. The corresponding dot plots are of the FL1 readings plotted against PI intensity (FL3).

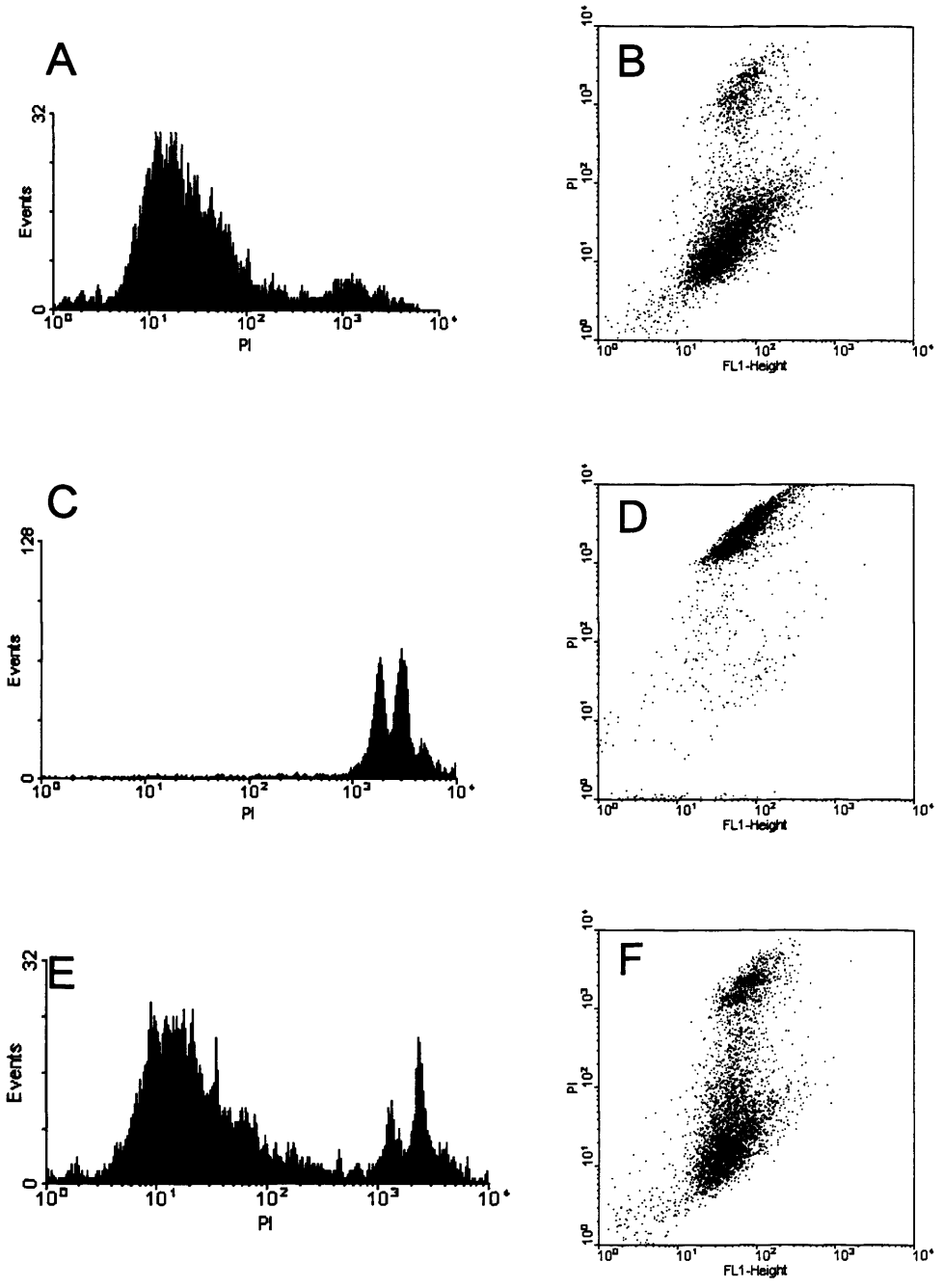

Figure 3.14: Histograms (A, C, E) and dot plots (B, D, F) following flow cytometry, for HCA_2 fibroblasts stained with propidium iodide, to yield fluorescent dead cells. (A, B) Negative control (cells grown in a monolayer). (C, D) Positive control (cells killed). (E, F) Fibroblasts cultured for 16 hours in hydrogel (9mg/ml HAED, SPA_4-PEG (20kDa) crosslinker ratio 1:1), showing both live and dead cells.

The dot-plot depiction provided a more appropriate method to identify and quantify the PI positive populations (in the upper half of the plots) than the histograms. This was described as a percentage of the total events measured, from which the reciprocal percentage of live cells was calculated. The results were statistically analysed to reveal any significant change in cell survival in the hydrogels. The non-paired T-test showed that there was a significant overall reduction in cell survival in the hydrogels compared to those grown in a monolayer ($p<0.05$), although there was significantly less cell death compared to the dead cell control ($p<0.05$) (Appendix 4).

The one-way ANOVA statistical test was employed to determine if there was any difference with respect to cell survival for the following groups of variables:

- Crosslinker ratio – 0:1 to 2:1
- HAED concentration – 6, 9, and 12 mg/ml
- Crosslinker type – SPA_4-PEG (20kDa), SC_4-PEG (20kDa), SPA_2-PEG (3.4kDa)

Figure 3.15 shows the percentage cell survival between hydrogels of different crosslinker ratios. Also shown is the percentage survival of the positive (dead) and negative (live) controls. There was no significant difference between the hydrogels with different ratios of crosslinker ($p>0.05$). Changing the concentration of HAED to alter the density of the hydrogel had no effect on cell toxicity, in that there was no significant difference between the different concentrations ($p>0.05$) (Figure 3.16).

A comparison was made between the three different crosslinkers examined in this study. Figure 3.17 demonstrated once again, no significant difference between the different types of crosslinker, with no significant differences ($p>0.05$) in cell survival between the different crosslinkers.

In summary, flow cytometry revealed:

- The crosslinking reaction was potentially toxic to cells.
- The concentrations of crosslinker and HAED had no effect on toxicity, nor did the type of crosslinker used.

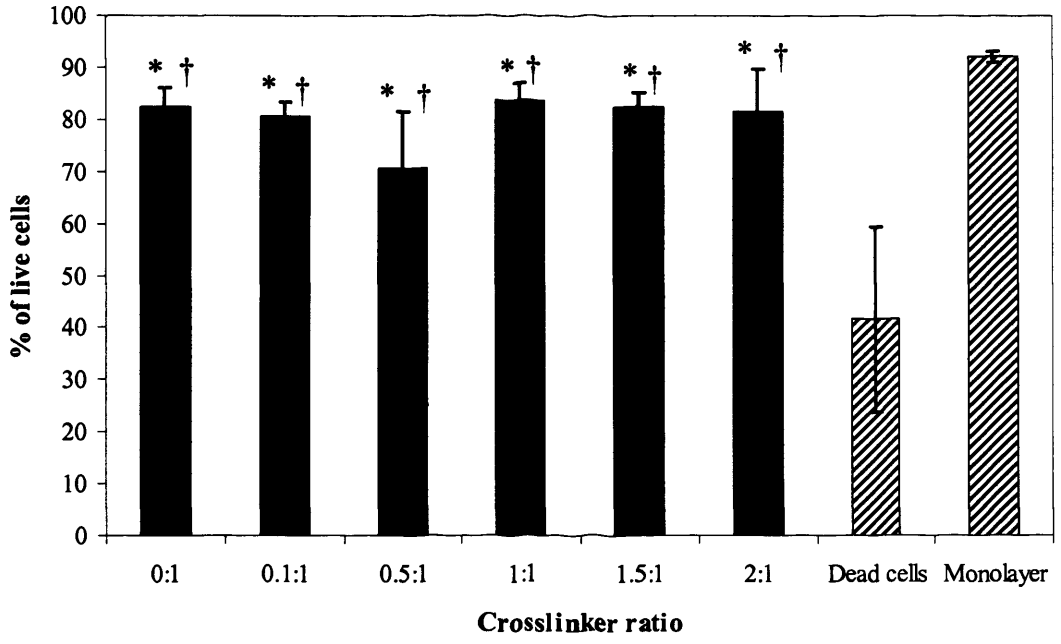

Figure 3.15: HCA_2 fibroblast survival incubated within HAED hydrogels with a range of crosslinker to HAED ratios (9mg/ml HAED, SPA4-PEG (20kDa)). Percentage survival was calculated from propidium iodide positive cells indicating cell death. The two hatched bars represent the positive (dead cells) and negative (monolayer) controls. Error bars represent ± standard deviation (n=5), (*) indicates a significant difference from the dead cell control, (†) indicates a significant difference from the monolayer control.

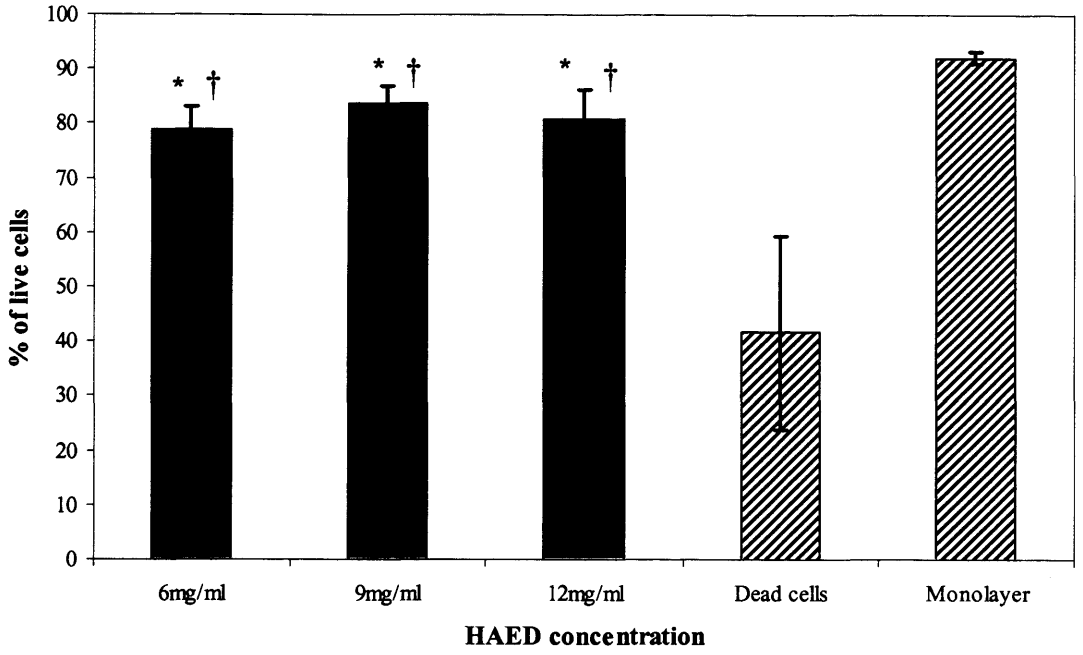

Figure 3.16: Comparison of HAED concentration in the toxicity of resultant hydrogels, (1:1 ratio of SPA_4-PEG (20kDa) to HAED), calculated from propidium iodide – stained HCA_2 fibroblasts. Hatched bars represent positive (dead) and negative (monolayer). Error bars represent standard deviation (n=5), (*) indicates a significant difference from the dead cell control, (†) indicates a significant difference from the monolayer control.

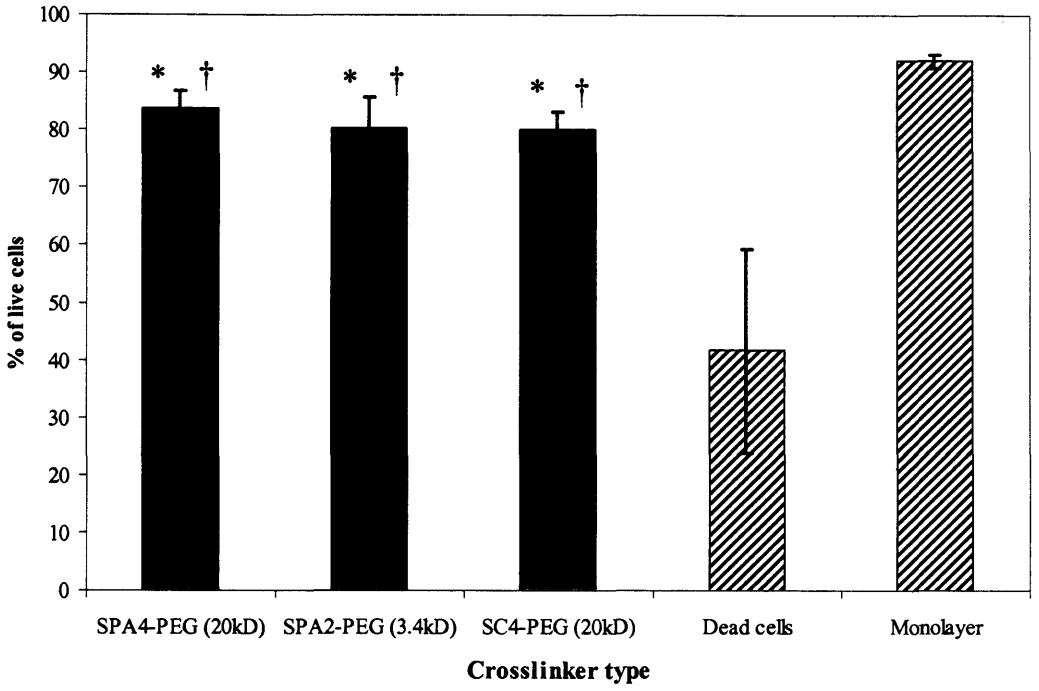

Figure 3.17: The effects of crosslinker on HCA_2 fibroblast toxicity, incorporated into HAED hydrogels (9mg/ml HAED, 1:1 crosslinker to HAED ratio). Percentage survival was derived from the percentage cell death as determined by propidium iodide staining followed by flow cytometry. The hatched bars represent the positive (dead) and negative (live) cells. Error bars represent ± standard deviation (n=5), (*) indicates a significant difference from the dead cell control, (†) indicates a significant difference from the monolayer control.

3.2.7. Ectopic bone formation assay

The *in vitro* cytotoxicity of the crosslinking hydrogel was assessed in Sections 3.2.5 and 3.2.6, but to analyse the response to hydrogels *in vivo,* an ectopic bone formation assay was employed[415]. Hydrogels were prepared as before, however, each hydrogel containing 250μg/ml recombinant bone morphogenetic protein-2 (BMP-2), as previously described[405]. Table 3.3 shows the formulations of hydrogels tested. The chemotactic role of BMP-2 would indicate the formulation requirements for permitting cell infiltration into the hydrogel from the surrounding tissue, an important consideration with respect to the long-term aim of any prospective product.

Six hydrogels of each formulation were implanted into 3 rats, by our collaborating partners. At 10 days post implantation, the implants were analysed histologically for cell infiltration and the presence of inflammatory cells. Figure 3.18 shows a typical specimen from each group. Only hydrogel 1, with 1 mg/ml telocollagen, 9 mg/ml HAED and crosslinker ratio of 1.2:1 showed substantial cell infiltration, (Figure 3.18(1)). This revealed the optimum concentrations of components required to achieve cell infiltration. The infiltration into the hydrogel as a result of BMP-2 stimulation indicates that HAED hydrogels are suitable scaffolds to support tissue regeneration. The pores in the hydrogel created by the large tetra-functional crosslinkers were of a sufficient size to allow cell migration. After 10 days the hydrogel is still present, which demonstrates that the cells did infiltrate into the hydrogel, rather than the hydrogel degrading away.

No cell infiltration was observed with the other formulations, although BMP-2-induced cartilage and bone formation was evident. The bone deposits evident in Figure 3.18 did not only occur in direct contact with the hydrogel, but formed in the surrounding tissue. This indicated that HAED hydrogels could deliver and release growth factors that could influence the surrounding matrix, not only the tissue in direct contact with the hydrogel.

The choice of crosslinker did not exhibit any effect. A fibrotic capsule was evident in the majority of the hydrogels, indicated in Figure 3.18(4). Some preparations exhibited some potential inflammation (for example 3.1(3)), although there was none observed in the hydrogel supporting infiltration. This suggested that the HAED was

hypo- or non-immunogenic, an important factor when inserting a biomaterial into a potentially inflamed environment. The hydrogel had not been degraded within 10 days, allowing it to act as a scaffold for new tissue growth over a longer time scale than that used here.

In summary, the ectopic bone formation assay revealed:

- The hydrogel was an effective delivery system for BMP-2.
- At a low collagen concentration, cell infiltration into the hydrogel could occur.
- The hydrogel was not degraded by day 10.

Table 3.3: Hydrogels implanted in the ectopic bone formation study. All hydrogels contained 250μg/ml BMP-2.

Hydrogel	HAED (mg/ml)	Crosslinker to HAED ratio	Fibrillised telocollagen (mg/ml)	Pepsinised collagen (mg/ml)
1	9	1.2:1 (SPA_4-PEG)	1	
2	12	1.2:1 (SPA_4-PEG)	1.75	
3	9	1.2:1 (SPA_4-PEG)	1.75	
4	12	0.6:1 (SPA_4-PEG)	1.75	
5	12	1.2:1 (SC_4-PEG)	1.75	
6	12	1.75:1 (SPA_4-PEG)		12
7	12	1.75:1 (SPA_4-PEG)		9
8	9	1.6:1 (SPA_4-PEG)		9
9	12	1.5:1 (SPA_4-PEG)		6
10	12	1.75:1 (SC_4-PEG)		12
11	12	0.9:1 (SPA_4-PEG)		12

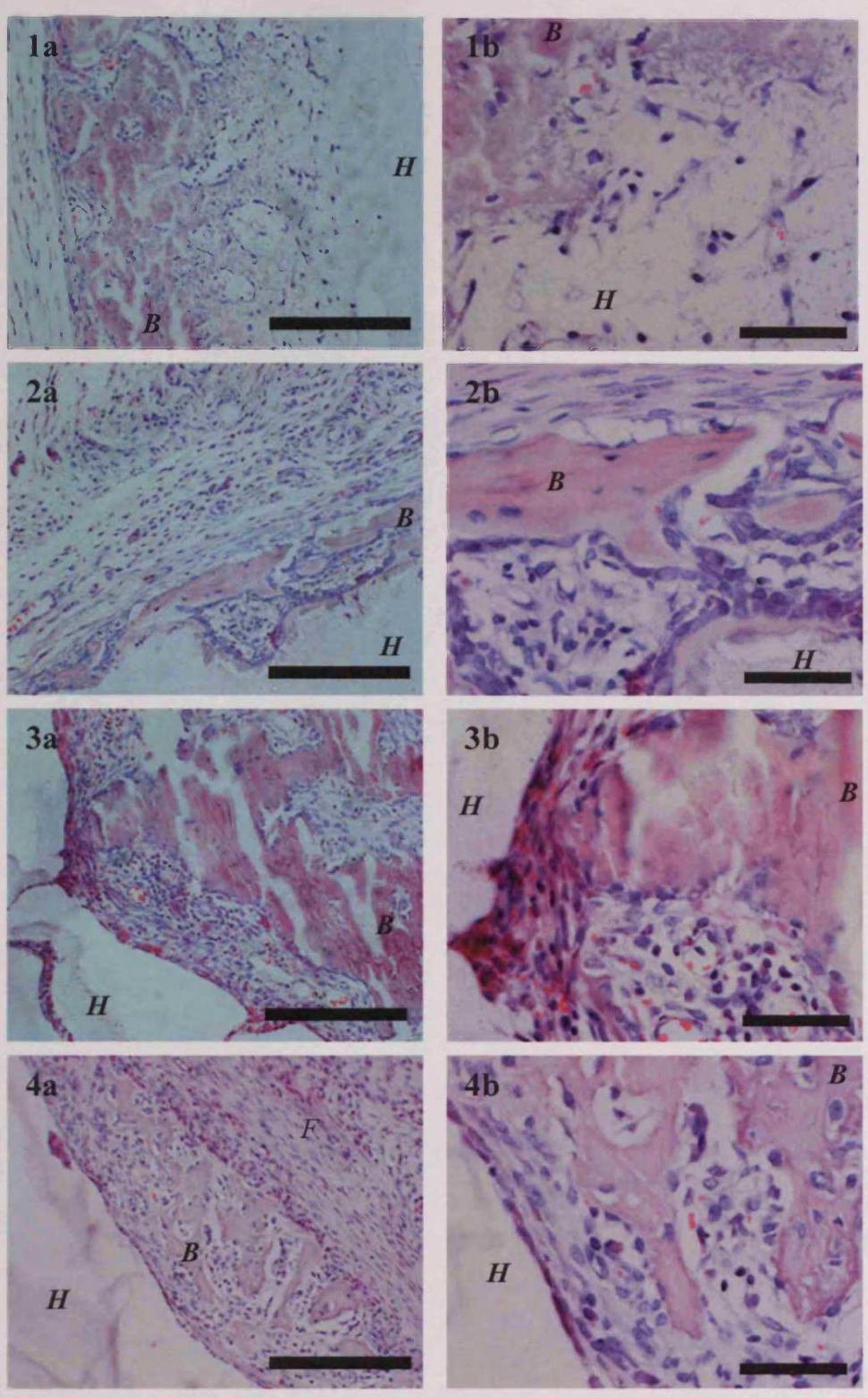

Figure 3.18: Haematoxylin/Eosin staining of tissue following subcutaneous implantation of HAED hydrogels containing 250μg/ml BMP-2. Numbers correspond to the hydrogel formulation in Table 3.3. H: position of hydrogel. B: BMP-2-induced bone formation. F: fibrotic capsule. Scale bars = (a) 200μm, (b) 50μm. (Continued over next two pages.)

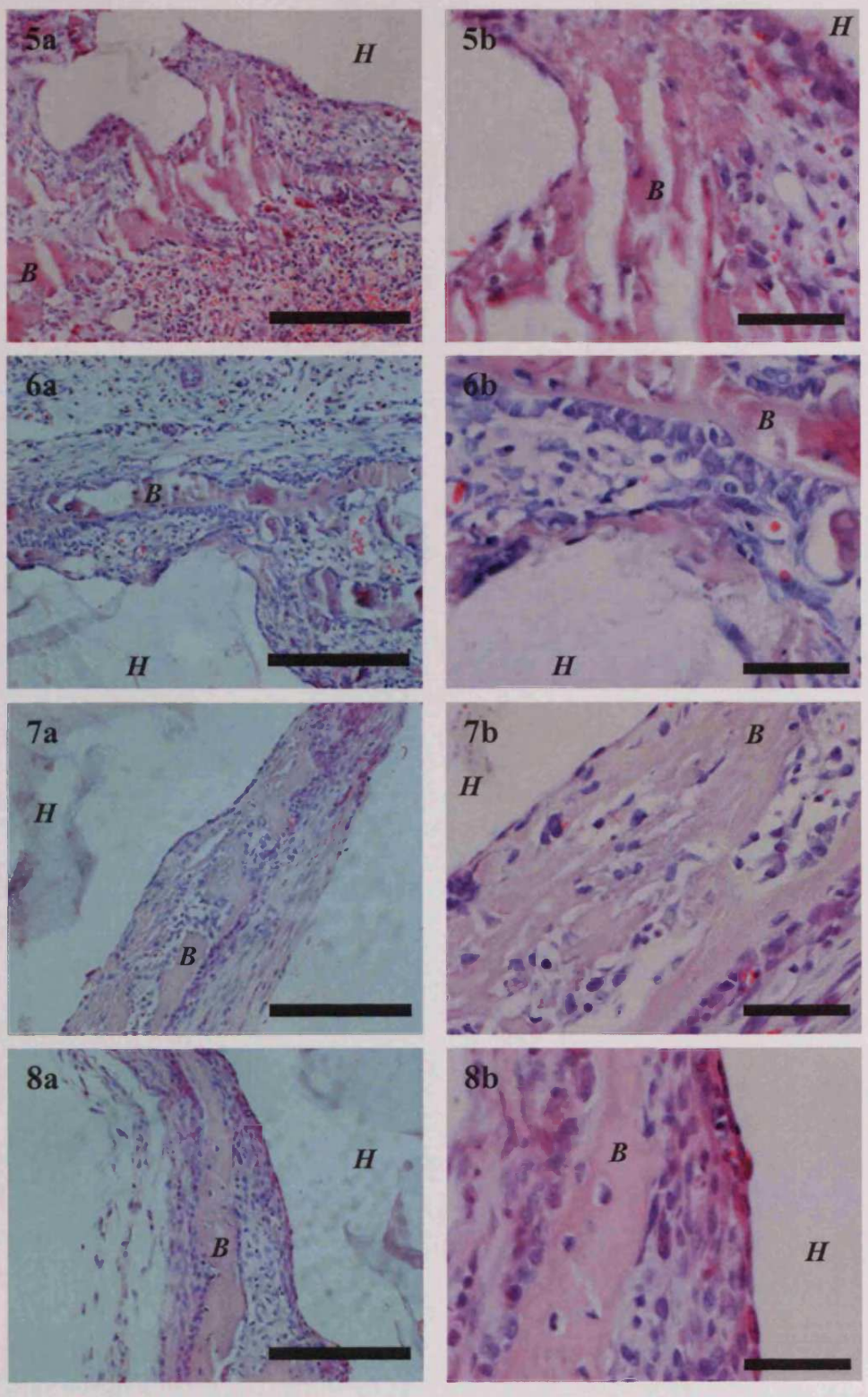

(Figure 3.18 continued)

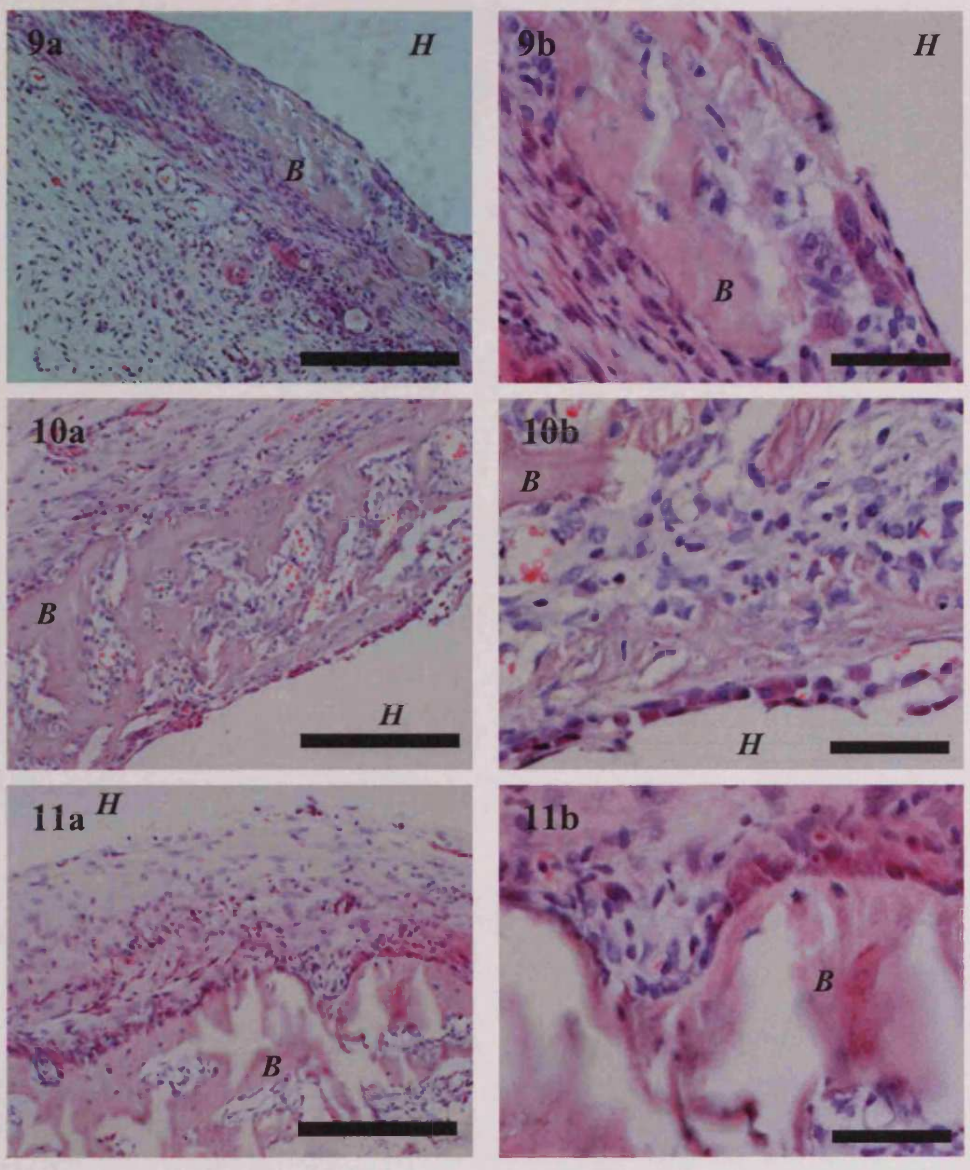

(Figure 3.18 continued)

3.3 Hydrogel Characterisation Discussion

There have been extensive studies into the use of growth factors and cells in the repair of articular cartilage. However, a major problem identified in the use of these factors is the delivery and retention of these agents within the sites of interest. Such difficulties have been countered in part, by the development of biomaterials to provide the delivery of cells and growth factors within a three-dimensional environment in which to lay down matrix[339,341,344]. Experimental work performed using artificial cartilage lesions requires the creation of a neat excision of a section of cartilage into which the sample is placed[339,376]. However, during osteoarthritis, the damage tends to resemble fissures and cracks[134,419]. The importance of an injectible biomaterial to fill such an irregular surface is outlined in Section 3.1.

Fibrin-based biomaterials have been utilised for their ability to be injected as liquid precursors[344,341]. However, fibrin is not endogenous to cartilage and can contract, whereas HA plays a major role in the homeostasis of the tissue and has been used to alleviate the symptoms of osteoarthritis (Section 1.6.4)[389]. Not only does HA provide an opportunity to enhance cartilage repair, but the advantages of an injectable HA-based hydrogel have been recognised by other groups[401,420].

3.3.1. Gross examination

HA was derivatised to HAED and crosslinked into hydrogels. Preliminary assessment of the hydrogels was carried out by this method, which provided an indication of the concentration range of components required for the formation of hydrogels. However, this technique was subjective and could not detect subtle differences between hydrogels. Therefore, a more objective, reproducible technique was required.

3.3.2. Rheology

Rheological assessment provided more quantitative information as to the elasticity of the hydrogels and enabled a more accurate comparison between hydrogels as well as an indication of the extent of gelation. When analysing the chemical crosslinking of a

polymer, the point at which a predominantly liquid material becomes a solid is described as the Gel Point, which is the point at which the average molecular weight diverges to infinity[421]. Although this can occur when the storage modulus (G′, describing elastic properties) equals the loss modulus (G″, describing viscous properties), it is only the case under special cases of crosslinking[421,422]. Moreover, the experimental design employed herein did not involve a frequency sweep, i.e., a range of frequencies applied to the sample. As this measurement is a requirement for the calculation of the Gel Point, the parameter could not be determined. As the Gel Point would reveal the time taken to achieve a hydrogel, this would be very useful if the material were to be injected. Therefore, a continuation of the work would be to determine the Gel Points for HAED hydrogels.

The initial stages of the crosslinking process exhibited a slight initial increase of G″, indicating increased viscosity. This could have arisen in the early stages of the reaction, as the crosslinking of HAED molecules caused an increase in molecular weight. Once the majority of the HAED molecules had crosslinked into a hydrogel, the material would have crossed the Gel Point and behave as an elastic solid. Furthermore, HA forms a loose network of tangled chains above 1mg/ml[414], which would further enhance viscosity. G″ did not decrease with the setting of the hydrogel, although as the hydrogel is largely comprised of water, this would have a significant effect on its rheology and may explain the constant level of viscosity observed. Incomplete crosslinking may also explain why very high levels of crosslinker (5:1) did not produce elastic hydrogels. The reduction in hydrogel quality may have arisen from the 4-arm crosslinker molecule only binding to one or two amine groups on HAED, as other HAED amine groups are effectively blocked by the saturation with crosslinker. This led to optimum ratio range for the most elastic hydrogels of between 0.5:1 and 1.5:1.

However, there were drawbacks with this rheological method for assessing hydrogel strength. Dehydration of the hydrogel on the rheometer may have occurred in all test conditions, but was more obvious at increased temperature or time. This led to adherence to the parallel plates, with stuttering or inaccurate readings. Although the addition of PBS around the sample would alleviate this, it could dilute the

components prior to crosslinking. Indeed, during these PBS experiments, some leakage of HAED into the surrounding fluid was evident, witnessed by an observed increase in viscosity of the PBS. To avoid this, a humidity chamber was set up around the parallel plates, but this did not alleviate the problem. The 1.5 hour rheological assessment showed a steady increase in elasticity (G'). The crosslinking would be expected to have reached completion by this point and may have been reflected by the viscosity, also indicated by the phase shift (tanδ), approaching zero after 30 minutes. This phenomenon could have been a result of partial dehydration. The drop of the phase shift may be more indicative of the crosslinking reaction reaching completion, at approximately 30 minutes. In the future, a comparison of the final hydrogel with a preformed hydrogel kept in humid conditions would further indicate if the reaction had reached completion after 30 minutes. If the hydrogel is to be crosslinked *in situ*, as part of a delivery strategy, this potential for dilution with surrounding fluid must be taken into account. However, this study has demonstrated that the hydrogel can be formed even when bathed in PBS, indicating the ability to crosslink under physiological conditions.

Rheological analysis has previously been applied to HA derivatives. Park *et al.*[402] reported a more rapid gelation of HA with photopolymerisation than described in the present study, with the reaction reaching completion at approximately two minutes. Another group described findings with similarities to those in the present study[413]. They reported an increase in the complex modulus with increased crosslinking of HA and a reduction in the complex modulus with the incorporation of 0.19mg/ml collagen. Although the present study focussed on the elastic modulus (G') instead of the complex modulus, the two parameters gave similar results in the present study, concurring with the study mentioned above. Interestingly, Barbucci *et al.*[400] also revealed that sulphation of HA increased the elastic properties of HA.

3.3.3. Fourier-transform infrared spectroscopy

As this technique has previously been applied to the analysis of HA-based compounds in order to detect structural modifications[400], it was utilised in these investigations. It was anticipated that FT-IR would identify an increase in amine levels resulting from the ethylenediamine modification, followed by a decrease in amines and an increase

in amides due to crosslinking. This would allow for monitoring of the chemical reaction over time, reveal the degree of crosslinking actually taking place and thus provide information on the average pore size within the hydrogel.

To initially test this technique, lyophilised HAED preparations containing varying degrees of derivatisation were analysed by FT-IR to identify any increases in the amine peak levels. Unfortunately, no spectral differences were observed between these. It is possible that a higher level of derivatisation of the carboxyl groups than that used (20%) was required to detect any change in amine levels. Alternatively, the long chains of HAED may have quenched the signal, although this may not be significant, as HA has previously been successfully analysed by FT-IR and demonstrated changes in peaks in response to hydrogel formation[400,413]. Segura *et al.*[413] demonstrated the presence of PEG crosslinkers by IR, suggesting that the PEG element of the crosslinkers used in the present study could be detected by this method. This indicates an alternative for future work.

Further analysis would be required to determine if increasing the extent of derivatisation resulted in increases in the amine signal, or if the degree of crosslinking could be deduced from the levels of PEG groups contained in the crosslinkers used in the present study. However, the latter approach could produce misleading data if the crosslinking reaction is incomplete. Other workers have visualised HA-based hydrogels using scanning electron microscopy[399,413], suggesting that this technique could be applied to the present study, to provide information on the pore size and overall structure of HAED hydrogels.

3.3.4. Cell viability assay

For the hydrogel to be used as a delivery system, it must be able to retain cells in a three-dimensional matrix to allow for the space-filling reconstruction of tissue. It must also be biodegradable to allow eventual replacement by new tissue and biocompatible so as to minimise rejection of the implant and induction of an inflammatory response. Both previous work and the present study have demonstrated that these hydrogels are susceptible to degradation by hyaluronidase[405]. The cell survival was assessed by means of a commercially available live/dead cytotoxicity kit. Cells were incorporated into crosslinking hydrogels, incubated for 24 hours and

fluorescent dyes added to reveal the status of each cell in the hydrogel.

The crosslinking reaction is vital to retain the cells in a 3D environment. This assay indicated some cell tolerance to the hydrogels setting, including chondrocyte tolerance. However, the 24 hour timescale was not sufficient to accurately assess cytotoxicity in response to the materials. There were indications of a toxic effect, demonstrated by some cells simultaneously fluorescing green and red. This pointed to early cell death occurring. To fully elucidate toxic effects of the hydrogels, the cells would need to be incubated for a longer time within the hydrogels. Other studies assessing cytotoxicity of similar biomaterials, incubated cells with the material for 48 hours[412] to 28 days[401]. However, at this stage, it is inconclusive if the HAED hydrogels can be injected, either immediately after addition of crosslinker, or simultaneously with the crosslinker, into a cartilage defect, with minimal cytotoxicity. The density of the hydrogel is an important factor, as denser pepsinised collagen-containing hydrogels would affect the remodelling capabilities of the fibroblasts. This could have had a detrimental effect on their survival, especially in regards to build-up of matrix fragments within the cell.

The three-dimensional nature of each sample made quantification by microscopic means unfeasible. Preliminary work using confocal microscopy led to distorted cell images caused by the surrounding hydrogel. This would require further trouble-shooting, as confocal microscopy has previously been applied to the study of cells within a hydrogel environment[401]. The three-dimensional data generated by confocal microscopy could further answer questions regarding the pattern of cell survival. For instance, it would indicate if there was a difference in cell viability between the edges and the centre of the hydrogel. Preliminary confocal microscopy work was carried out, but it was decided that flow cytometry would provide a more quantifiable overall assessment of the cytotoxicity of the crosslinking reaction.

3.3.5. Flow cytometry

Cells were incubated with crosslinking hydrogels and after 24 hours, the hydrogel was digested with hyaluronidase. The cells stained with propidium iodide to highlight dead cells, before analysis by flow cytometry. This alternative dead cell marker was used as preliminary tests showed dual staining problems with the two fluorescent

markers, calcein and ethidium homodimer, previously used in the cell viability assay. The cell viability could be extrapolated from a count of dead cells, with positive and negative controls being used to verify the accuracy of this staining technique.

The dead cell positive control would be expected to have 0% live cells, but according to the flow cytometry data, had nearer 40% live cells. It was possible that the methanol used to kill the cells did not achieve complete cell death. Alternatively, the methanol may have fixed the cells and reduced cell permeability, to hinder interaction between PI and the nucleic acids. This illustrates the disadvantage of the single dye system over the dual dye system. Nonetheless, all the cells from the hydrogels and the live control showed significant increases in cell survival compared to the methanol-treated cells. There was approximately 10% increase in cell death of fibroblasts in hydrogels compared to the monolayer control. This could have arisen from the additional handling the cells underwent when being integrated into the hydrogels. The pH (6.3) of the hyaluronidase buffer used in the digestion of the hydrogel may have caused some toxicity. Therefore, the monolayer control provided more of a control for the fluorescent label, rather than an indicator of the hydrogel toxicity *per se*. Future work would require this control to be treated in a much closer manner to that of the test samples.

There was otherwise no significant difference in cell survival in relation to the crosslinker type, concentration or HAED concentration. It is interesting to note that the crosslinker SPA_2-PEG (3.4kDa) did not induce an increase in cell death, demonstrating that the theoretically smaller pore size that would be generated by this smaller crosslinker was not detrimental to the cell survival. As the cells were present while crosslinking was taking place, the crosslinks would have formed around them, thus not affecting the cell. However, it is possible that cell infiltration into an already crosslinked hydrogel could be compromised by using the smaller crosslinker. The concentration of crosslinker did not affect cell survival as much as anticipated. It was hypothesised that an increase of amount of crosslinker would increase the hydrogel density, making it less hospitable for cells. However, the crosslinker may not have effected the overall hydrogel density as much as anticipated, discussed more thoroughly in Section 3.3.6.

It is conceivable that the crosslinker could have chemically reacted with the amine groups on cell surface proteins. This did not appear to greatly affect the cell, as metabolism of the calcein AM fluorescent marker by cells in the cell viability test indicated that they were still active. It is possible that attachment of the crosslinker to cells could result in membrane protein dysfunction, but as the crosslinker would not target a particular class of proteins, loss of function of individual proteins may not have much effect on the cell as a whole. However, it must be noted that the lysine amine groups on proteins may have had a different pKa value than that on HAED, indicating different reactivity at a different pH. In conclusion, the flow cytometry data indicated that some cytotoxicity was evident, demonstrated by the significant drop in cell viability compared to the monolayer control. As discussed in the cell viability assay, the cells would need to be incubated in the hydrogels for a longer period to deduce the extent of toxicity. The dual staining observed using calcein and ethidium homodimer further confirms the findings of the cell viability assay, in that early cell death may have been underway.

Other groups have reported good cell tolerance to HA-based biomaterials, as assessed by similar *in vitro* assays[337,395,412]. These studies demonstrate that HA-based biomaterials can be non-toxic to cells and provide good candidates to support cell delivery. The hydrogel characterised in the present study could potentially have advantages over other *in situ* crosslinkable hydrogels. Photocrosslinking of modified macromolecules into hydrogels allows *in situ* gelation[424], but photoinitiators can be cytotoxic. Indeed, in 2002, Trudel and Massia[412] reported a cytotoxic effect of an HA-based hydrogel formed by photocrosslinking, with only approximately 15% cell survival from fibroblasts cultured on the hydrogel compared to the no-hydrogel control.

3.3.6. Ectopic bone formation assay

The *in vitro* cytotoxicity of the hydrogels did not reveal if the hydrogels are suitable for the delivery of bioactive factors and what conditions were required to support cell infiltration. To allow tissue remodelling in a void, the introduced material must either contain cells or attract cells from the surrounding area to infiltrate into the material, differentiate into chondrocytes and synthesis new matrix. The present study addressed this by incorporating BMP-2 into hydrogels of different compositions.

These were placed subcutaneously into rats, explanted after 10 days by our collaborating partners, and assessed by histological analysis.

BMP-2 induced tissue remodelling to cartilage and subsequent bone formation around the implant. Moreover, one hydrogel formulation (9mg/ml HAED, 1.2:1 SPA_4-PEG (20kDa) to HAED ratio of crosslinker, 1mg/ml fibrillised collagen) demonstrated cell infiltration into the hydrogel. It is of note that the hydrogel which allowed infiltration had the lowest collagen concentration of all the prepared samples, but not the lowest crosslinker concentration. This was in agreement with the findings from the flow cytometry, which demonstrated that crosslinker concentration had little effect on toxicity. These results suggest that the extent of crosslinking has more effect on the elasticity than on the density of the material. Theoretically, at a higher crosslinker concentration the density would be affected, but this would fall outside the optimal range of crosslinker concentration and result in a less elastic hydrogel. In contrast, the bulky fibrils of collagen could contribute significantly to the density of the material.

The inclusion of collagen in this experiment was required for the delivery of the collagen-binding BMP-2. A control hydrogel without collagen would have been inappropriate as it was hypothesised that the BMP-2 would have diffused away too rapidly. As cells migrated into the hydrogel at the lowest collagen concentration used, the amount of collagen could be reduced further to below 1mg/ml, which may promote cell infiltration. However, the importance of collagen to the scaffold is two-fold. Firstly, it provides a binding site for BMP-2. Secondly, other studies have shown that cell infiltration and proliferation is increased in HA/collagen matrices, compared to each material on its own[403,404]. Further work is required to determine the optimal concentration of collagen to achieve cell infiltration. Moreover, the type of collagen used may influence the tissue generated. Buma *et al.*[376] revealed that although a type I collagen matrix induced greater progenitor cell migration into a cartilage defect, these cells were more chondrogenic with a type II collagen matrix.

As mentioned above, BMP-2 – induced bone formation was observed. However, the present study did not include a negative control (no BMP-2) to assess the effect of the hydrogel itself. Previous work in our laboratory has demonstrated that HA-based hydrogels using a SPA_2-PEG crosslinker to a similar hydrazide derivative of HA did

not induce osteogenesis nor cellular invasion in the absence of BMP-2[405]. This suggests that the bone formation and cellular infiltration observed in the present study were due to BMP-2.

Although the ectopic bone formation assay indicated the optimal conditions to allow cell infiltration, the cartilage lesion is a very different environment. A partial defect would not enable migration progenitor cells from the subchondral bone, although progenitor cells have been identified in articular cartilage[357]. Furthermore, factors such as pH and the presence of degradative enzymes in OA cartilage, may affect the rate of degradation of the hydrogel and components. The role of the HAED hydrogel as a three-dimensional scaffold during tissue remodelling could be compromised. However, HA-based hydrogels have been applied to OA cartilage and supported cartilage repair[337], suggesting that exogenous HA-based materials can enhance chondrogenesis in OA.

Importantly, after infiltration, there did not appear to be a significant inflammatory response. However, this was not the case with some of the hydrogels that did not support infiltration. Although cartilage is an avascular tissue, there is potential for inflammation from the underlying bone in a full thickness defect, or from the synovium, as apparent during osteoarthritis[318,425]. This underlines the importance of introducing a material that does not encourage inflammation.

In conclusion, we have demonstrated that biocompatible hydrogels can be generated from ethylenediamine-derivatised HA with large tetra-functional crosslinkers. The properties of the hydrogel can be controlled by altering the crosslinker concentration and type and by incorporating collagen. This study has demonstrated that the crosslinking reaction is non-toxic, can be performed *in situ* and under suitable conditions, cell infiltration into the material can be achieved. This also shows that cells can be embedded in a crosslinking hydrogel, either in culture or *in vivo*.

4.1. Production of Fms-like Tyrosine Kinase-1 Domains 1-3

Introduction

This chapter describes the expression and purification of an angiogenesis inhibitor, to function as a decoy receptor for vascular endothelial growth factor (VEGF). This growth factor has an important role in many developmental and pathogenic processes[226]. Its pro-angiogenic role has made it a target for inhibition in angiogenesis-dependent conditions, such as malignant tumours, diabetic retinopathy and osteoarthritis (OA) (Section 1.4.5). Furthermore, growth factors, such as BMP-2, can induce bone formation under angiogenic conditions (Section 1.1.8).

Investigators have approached the issue of VEGF inhibition in several ways. Neutralising antibodies against either a ligand or the ligand binding site on the corresponding receptor have been shown to inhibit VEGF-induced mitogenesis of endothelial cells[270,288,350]. Small length peptides, typically fewer than 50 residues, both based on VEGF[242], the VEGF-binding region of one of its receptors, KDR[426] or from random phage libraries[267,427,428,430] have been demonstrated to attach to the receptor-binding site on VEGF. Each of these approaches has demonstrated an inhibition in the mitogenicity or proliferation of endothelial cells. Work by Siemeister *et al.*[430] showed that VEGF mutants could also disrupt the interaction between ligand and receptor. This was achieved by mutating one of the two binding sites of VEGF, so the mutant bound to the receptor, but prevented receptor dimerisation. Expression of VEGF itself has been blocked by the transfection of an antisense VEGF construct into a highly tumourigenic cell line[269]. This led to a significant reduction in VEGF secretion and decreased tumour growth, therefore confirming the role of VEGF in tumour development, although this may be unsuitable as a treatment tool. The administration of VEGF conjugated to a tumour toxin (gelonin) has been found to reduce tumour growth *in vitro* and *in vivo*[271].

An endogenous potent inhibitor of VEGF-mediated angiogenesis has been identified, consisting of the extracellular Ig-like domains of the VEGF receptor fms-like tyrosine kinase-1 (flt-1)[315], termed sflt-1 (Section 1.4.9). Administration of recombinant sflt-1

has been shown to reduce the severity of induced arthritis in animal models[318]. This inhibitor provides a means of VEGF inhibition with advantages over the above approaches. As it is naturally occurring, toxicity concerns are reduced. Unlike antibodies or peptides, it can act in a dominant negative fashion, by binding VEGF and interacting with full-length receptors.

This chapter aimed to develop a modified form of sflt-1, as the flt-1 receptor has a higher affinity for VEGF than KDR[280,281]. The first three extracellular domains have been identified as a requirement for VEGF binding and have been demonstrated to inhibit VEGF-mediated endothelial proliferation[287,290,432]. More relevant to this study, these regions have been demonstrated to halt VEGF-mediated endochondral ossification[112]. For this reason, the research described in the present study aimed to design a 'decoy receptor' based on the first three extracellular domains in an attempt to inhibit the activity of VEGF.

By incorporating this truncated form of flt-1 into a hydrogel and injecting the hydrogel into osteoarthritic cartilage, this 'decoy receptor' could act by two mechanisms. The first would be to bind and thus sequester the VEGF present, minimising the interaction of VEGF with endogenous receptors. The second would be to form heterodimers with native receptors in the presence of VEGF, as sflt-1 has been shown to inhibit VEGF by this mechanism[315]. The decoy was chosen over the full six domains of sflt-1 for two reasons. Firstly, for easier incorporation into the hydrogel, and secondly, because peptides consisting of only the first three domains have been found to have a longer half-life *in vivo* than the larger sflt-1[112]. The advantage of this approach rather than receptor-specific antibodies or peptides is that VEGF interaction with both KDR and flt-1 receptors can be inhibited[290].

The sequence of flt-1 has been reported[433] and the boundary between the third and fourth domain has been deduced from crystallographic data[290,434]. For the purpose of this investigation, the end of domain three was deemed to be 341 amino acids (1023 base pairs) downstream from the methionine (ATG) start site, between two glutamine residues.

To produce the recombinant flt-1(1-3), a cDNA construct was generated and transfected into a human embryonic kidney cell line. As the gene encodes for the extracellular region of the receptor, conditioned medium from the cell culture was collected and partially purified. Affinity of flt-1(1-3) with VEGF was established using Surface Plasmon Resonance technology.

4.2. Production of fms-like tyrosine kinase-1 domains 1-3 (flt-1(1-3))

Results

4.2.1. Isolation and amplification of flt-1(1-3) cDNA

Total RNA was obtained from human umbilical vein endothelial cells (HUVECs) and reverse transcribed into cDNA using an oligo dT oligonucleotide method. The cDNA sequence of the first 3 extracellular domains of the receptor flt-1 (flt-1(1-3)) was amplified by PCR. Primers containing restriction sites were used to incorporate these sites at each end of the amplified flt-1(1-3) sequence (Figure 4.1). This allowed subsequent directional in frame insertion of the flt-1(1-3) sequence into the expression vector. These restriction sites were Hind III (5′ end) and Not I (3′ end).

However, an initial polymerase chain reaction (PCR) using these restriction site primers did not yield a product visible by agarose gel electrophoresis, possibly due to low copy numbers, indicating that the primers were not very efficient. The presence of flt-1 cDNA was confirmed using primers P2 and P5, which yielded the expected 300bp fragment (Figure 4.2). To increase the number of copies of the flt-1(1-3) target sequence prior to amplification with the restriction site primers, an additional PCR step was undertaken beforehand with completely complementary primers located slightly outside the target sequence (represented by P3 and P4 in the Figure 4.1 schematic). A second, nested, PCR from this reaction using the restriction site-containing primers yielded an amplicon of ~1030bp in length. This was ligated into the cloning vector pCRII using the A overhang generated by the Taq polymerase, expanded in Top10αF *E.coli*.

Sequencing of the purified DNA was carried out using primers from the pCRII vector to ensure that flt-1(1-3) was the amplification product and the restriction sites were incorporated correctly (see Appendix 3.2 for vector map). The results indicated that flt-1(1-3) had been amplified, but by coincidence the P1 primer was complementary to a short sequence in the reverse primer binding region at the 3′ end of the flt-1(1-3) sequence and had out-competed the P2 primer. This resulted in the PCR product

A

Primer	Sequence (5′ - 3′)	Position from ATG start site	Description
P1	ATTAAGCTTGCGCTC ACC**ATG**GTCAGCTA C	-9 (5′ end of primer, plus restriction site extension)	Forward primer, with a Hind III site, start site indicated in **bold**.
P2	TAAGCGGCCGCCTGT TTTCGATGTTTCACA GTGATG	998 (3′ end of primer)	Original reverse primer with Not I site. Region annealing with sequence is towards the 3′ end of the primer.
P2a	AACCCGGCTCGAGC GGCCGCTACGGTTTC AAGCACCTGCTG	1021 (3′ end of primer)	Optimised reverse primer with Not I site.
P3	CAGGCCACGTCGCG CTCACCA	-19 (5′ end of primer)	Forward first round primer.
P4	CTACGGTTTCAAGCA CCTGCTG	1023 (3′ end of primer)	Reverse first round primer.
P5	CACTCCCAGTCAAAT TACTTAGAGGC	710 (5′ end of primer)	Forward internal primer. Substitution to avoid hairpins indicated in **bold**.

B

Figure 4.1: Primers used for flt-1(1-3) amplification. A: the primer sequences (restriction sites are underlined). B: schematic showing the relative position of the primers. The flt-1 (1-3) cDNA sequence encoding the 3 N-terminal IgG domains is shown in grey.

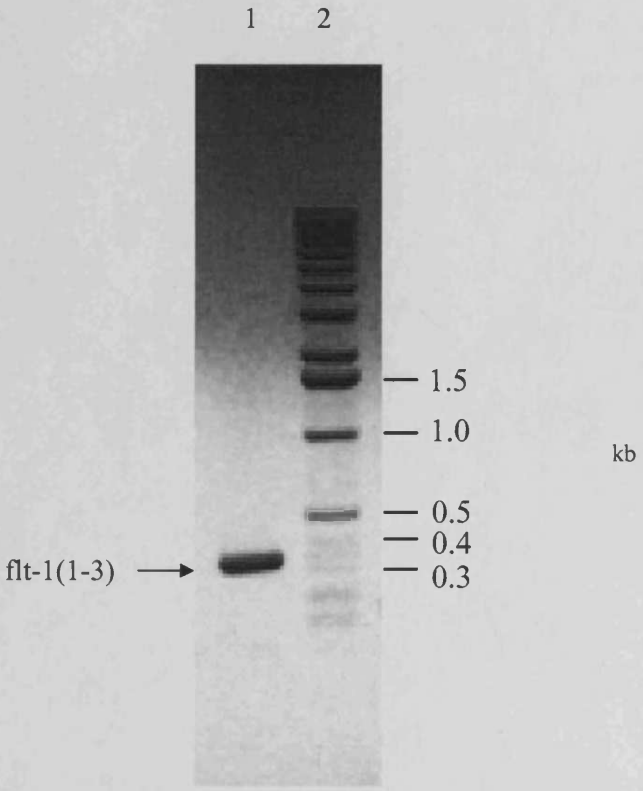

Figure 4.2: Analysis of PCR product by agarose gel electrophoresis. PCR product visualised by 1% agarose gel electrophoresis, visualised with ethidium bromide staining, calibrated with 1 kb ladder (lane 2). Lane 1 shows a control PCR using primers P2 and P5 to yield a ~300bp fragment. This provided early confirmation of the presence of flt-1.

containing a new introduced Hind III site at the 3′ end, instead of Not I. This product could not be used for digestion and ligation into the expression vector, as the construct downstream of flt-1(1-3) would have been out of frame. Several approaches were undertaken to eliminate this problem. The annealing temperature and magnesium chloride concentration were adjusted to improve P2 attachment, but was found not to reduce the binding of P1 to the sequence in question. A restriction digest was carried out on the template, to remove the complementary sequence on flt-1(1-3), but failed to remove this sequence. An alternative first round primer was designed, to prevent the amplification of the complementary sequence. This did not alleviate the problem, due to low levels of the original template in the starting material coupled with very efficient binding by the P1 primer. A subsequent dilution of the starting material did not remove these low levels of original template. A re-design of the primer P2 solved the problem and the new primer P2a (Figure 4.1) successfully incorporated a Not I site at the 3′ end of the flt-1(1-3) sequence. In summary, the first round of PCR was carried out with primers P3 and P4, followed by a second round using P1 and P2a. This resulted in successful amplification of flt-1(1-3) (Figure 4.3) with the correct insertion of the restriction sites. The final PCR product was ligated into pCRII and expanded in *E.coli.*

DNA sequencing highlighted up to 5 mutations per clone, which had occurred during the second PCR, using a Taq Polymerase enzyme. This PCR step was repeated using Expand Hi-Fidelity and VentR polymerases, both of which have exonuclease (proof-reading) activities. Again, several mutations occurred at different locations, probably as a result of repetitive motifs within the sequence. Ironically, the sequence with the least mutations was from a Taq Polymerase reaction, which contained only three. Two were silent and a third substituted a histidine residue for a glutamine at position 864 that was deemed to be conservative enough to use this sequence for further investigations.

The expression vector pCEP-Pu was selected to allow for episomal expression of flt-1(1-3), described in more detail in Section 4.3. It included a sequence between the Not I and Xho I restriction sites of the multiple cloning region coding for a Streptavadin-based tag, or strep tag, which would be added to the C-terminus of the

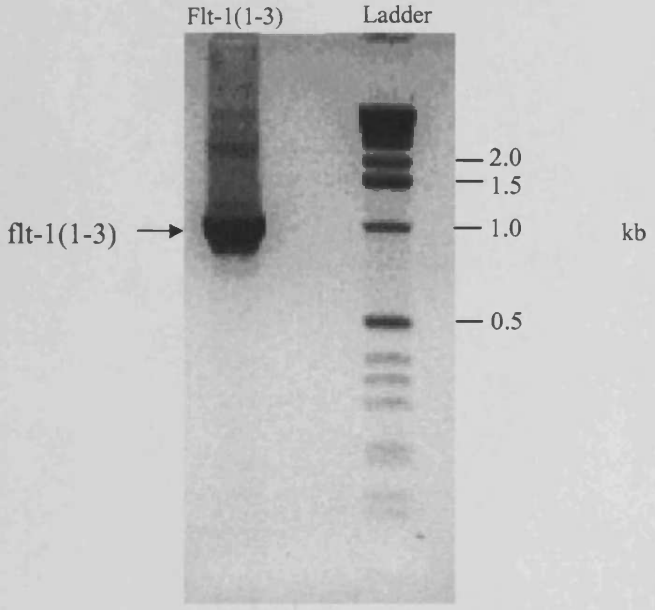

Figure 4.3: Second round PCR product visualised by 1% agarose gel electrophoresis with ethidium bromide, calibrated with 1 kb ladder. Band shows successful amplification of flt-1(1-3), size approximately 1030bp.

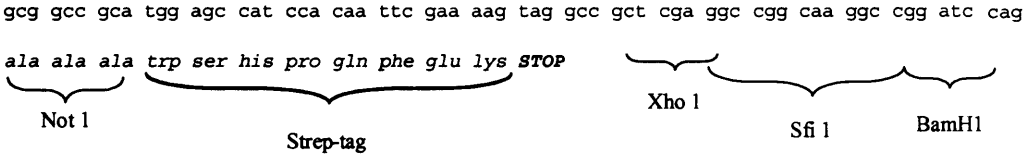

Figure 4.4: Sequence of part of the pCEP-Pu vector, showing the strep tag, Not 1 site used for ligating flt-1(1-3) and the downstream components. The Hind III restriction site is approximately 1000bp upstream from the Not 1 site in the vector.

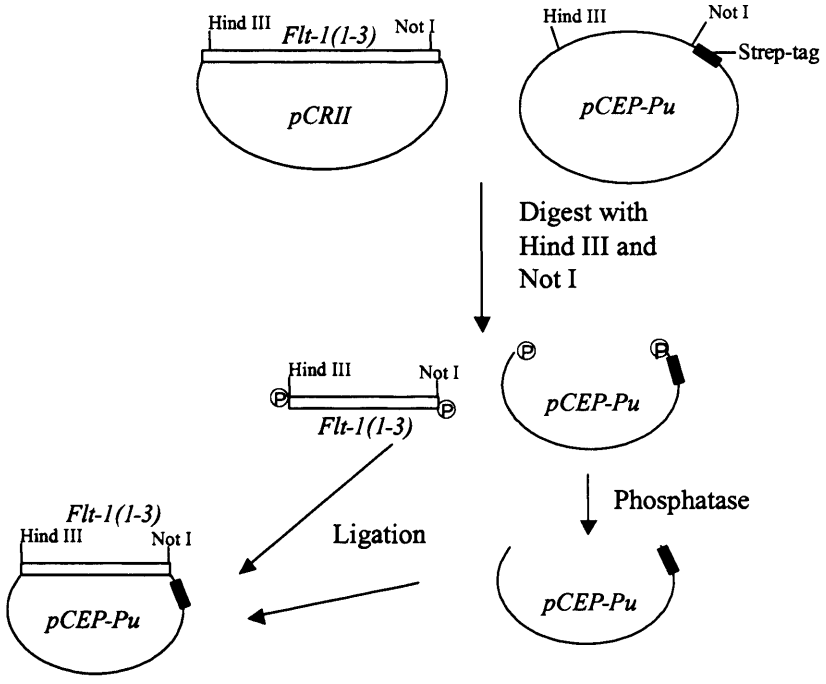

Figure 4.5: Schematic demonstrating the insertion of flt-1(1-3) cDNA into the expression vector pCEP-Pu for transfection into 293 EBNA cells.

A

Primer	Sequence	Position from insert	Description
P6	CACTGCATTCTAGTTGTGG	92	For sequencing Hind III join with insert
P7	GGTAGGCGTGTACGGTGGG	76	For sequencing Not I join with insert

B

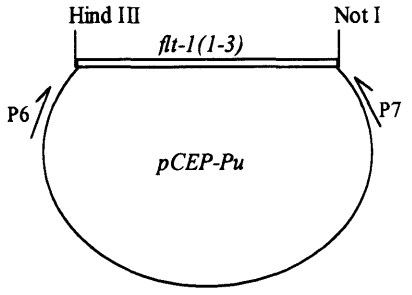

Figure 4.6: Design of primers primers (A) and their position on the vector (B) for sequencing of the junction between vector and insert.

expressed protein to aid in future identification and purification (Figure 4.4, Appendix 3.1 for vector information). The flt-1(1-3) sequence was digested from the pCRII and ligated into pCEP-Pu as detailed in Figure 4.5, and expanded in DH5α *E.coli.* Sequencing with the primers in Figure 4.6 confirmed the correct integration of the flt-1(1-3) into pCEP-Pu, and that the Strep-tag downstream from the flt-1(1-3) sequence was in frame (Appendix 5).

4.2.2. Expression of flt-1(1-3)

The pCEP-Pu/flt-1(1-3) construct was liposomally transfected into human embryonic kidney 293 EBNA cells. Efficiency of transfection was assessed by a parallel transfection of a LacZ gene-containing vector. Detection of β-galactosidase activity led to a cell colour change to blue upon addition of its substrate X-Gal (5-bromo-4-chloro-3-indolyl-β-D-galactoside). The transfection efficiency was determined to be 5% (data not shown). Optimum concentration of the selection antibiotic puromycin was 0.5μg/ml, as determined previously[435]. Therefore, puromycin was included at this dosage for selection and verified to kill wild-type cells within 10 days.

As flt-1(1-3) is part of the extracellular N-terminal region of the receptor and contained the signal peptide, it was expected to be excreted into the cell culture medium. This was confirmed by carrying out a cell extraction of the cell layer followed by Western blotting. No flt-1(1-3) was detected (data not shown). Prior to collection of the conditioned medium, confluent cells were transferred into serum-free medium to reduce purification difficulties arising from excess serum derived protein. Presence of flt-1(1-3) in the medium was detected by Western blotting using two different commercially available antibodies. Anti-flt-1 was a polyclonal antibody raised against the first three domains of the extracellular region. Anti-strep tag was a polyclonal antibody raised against the strep tag incorporated onto the C terminal of flt-1(1-3). The primary antibodies were detected with horseradish peroxidase-conjugated secondary antibodies and visualised by chemiluminescence using the ECL+ system.

The anti-strep tag antibody failed to specifically detect any flt-1(1-3) in conditioned medium (discussed in Section 4.3), but the anti-flt-1 revealed flt-1(1-3) at approximately 50kDa, as shown in Figure 4.7. The faint larger band observed was

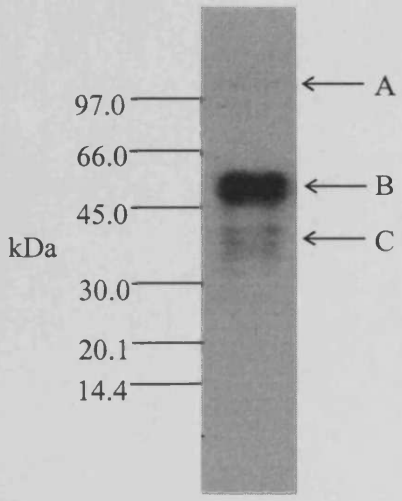

Figure 4.7: Analysis of conditioned medium of cells transfected with flt-1(1-3) construct. Proteins in 100μl conditioned medium were concentrated by ethanol precipitation and separated on a 4-20% SDS/PAGE gel (reducing conditions). Proteins were transferred onto a nitrocellulose membrane and detected with anti-flt-1 antibodies. This was visualised by chemiluminescence. Band A: very faint endogenous soluble flt-1. Band B: flt-1(1-3), at 50kDa. Bands at C: possible variability in glycosylation or degradation product.

A

Primer	Sequence	5' position from Not I site	Description
P8	GAAATAGGGCTTCTGACCTGTG	440	Flt-1(1-3) forward primer in the middle of the sequence
P9	GATTTGAATGATGGTCCACTCC	79	Flt-1(1-3) reverse primer towards 3' end of insert
P10	CTGCATTCTAGTTGTGGTTTGTC	108	Reverse primer aimed at pCEP-Pu sequence downstream from flt-1(1-3) insert

B

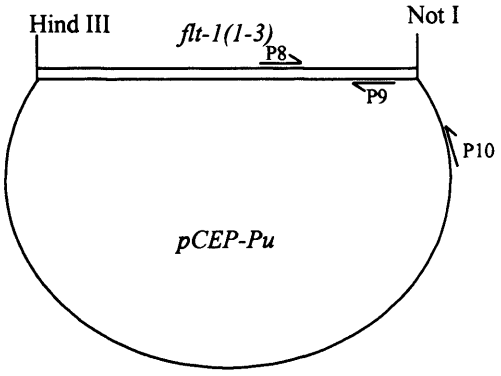

Figure 4.8: Design of the primers (A) and their approximate location (B) within the vector that were used in PCR reactions, for determination if the vector had been lost.

proposed to be low levels of endogenous soluble flt-1, which has previously been identified at 85-90 kDa following expression in Sf9 cells[290]. The smaller bands (C) may have been the result of variable glycosylation of the protein or degradation products. Western blotting of conditioned medium from wild-type (WT) cells did not reveal any flt-1(1-3) (Figure 4.24).

However, the expression levels of flt-1(1-3) were low and an ethanol precipitation step was required to increase protein concentration ten-fold, to visualise the protein by Western blotting. To increase expression, the puromycin concentration was increased to 10μg/ml for more stringent selection, allowing only highly expressing cells to remain alive. Furthermore, the conditioned medium was collected at different time points to increase flt-1(1-3) and cells were grown on insulin/transferrin/selenite (ITS) to increase expression. Culturing cells with 10μg/ml puromycin and collection of medium from 100% confluent cells every 2 days for up to 12 days (no ITS) produced the most flt-1(1-3). However, after approximately 4 months there was a complete loss of flt-1(1-3) expression, although the transfected cells were still resistant to puromycin. To reveal if the pCEP-Pu/flt-1(1-3) construct was still retained within the cells, cDNA from transfected cells and wild-type (WT) cells were subjected to PCR using the primers listed in Figure 4.8. In addition, cell stocks prepared immediately after transfection were tested. Figure 4.9 shows that the flt-1(1-3) primers P8 and P9 produced the expected fragment of 361 base pairs (A) and the flt-1(1-3) primer P8 with pCEP-Pu primer P10 produced a fragment that was calculated to be 556 base pairs in size (B). The presence of a band in the first 4 lanes of the gel may have been due to endogenous flt-1, either full-length or as the truncated soluble form (Section 1.4.9). Lanes 5 to 8 show PCR products that should have only arisen in the presence of the pCEP-Pu/flt-1(1-3) construct, as the DNA amplified straddled the join between insert and vector. The absence of a band in lane 5 indicates that the plasmid may have partially integrated into the genome, or lost part of its original sequence, which explained why no expression was detected. Frozen stocks made shortly after the original transfection of the construct into the 293 EBNA cells still contained the intact plasmid. These cells were expanded and used for subsequent expression work. Figure 4.10 confirms expression of flt-1(1-3) in the restored cell population by Western blotting. The fibroblasts could maintain flt-1(1-3)

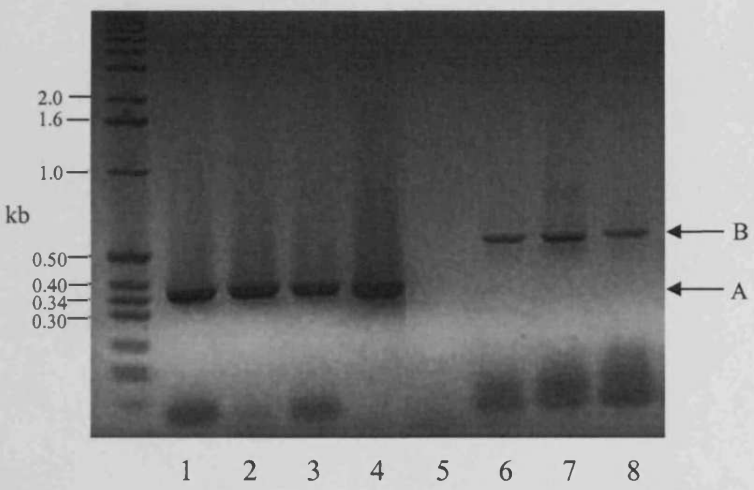

Figure 4.9: 1% agarose gel electrophoresis visualised with ethidium bromide, following PCR of cDNA of flt-1(1-3)-transfected 293 cells. Lanes 1 – 4: Primers P8 and P9, to amplify flt-1(1-3), or endogenous flt-1. Lanes 5 – 8: Primers P8 and P10, to amplify a sequence composed partially of vector and flt-(1-3) (Figure 4.8), to confirm the presence of the construct in the cells. Lanes 1, 5: Transfected cells. Lanes 2, 6: Transfected cells (cells frozen after 5 passages following transfection). Lanes 3, 7: WT cells. Presence of bands suggested potential contamination. Lanes 4, 8: construct control. A: 361bp flt-1(1-3) fragment. B: 560bp flt-1(1-3) fragment.

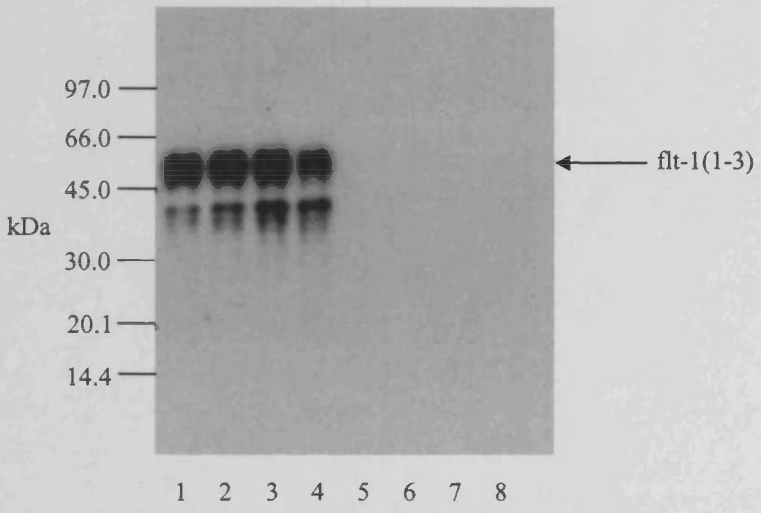

Figure 4.10: Western blot assessing loss of flt-1(1-3) expression. Proteins in conditioned medium (100μl) were concentrated by ethanol precipitation and run on a 4-20% PAGE gel (reducing conditions). It was transferred onto nitrocellulose membrane and probed with anti-flt-1 antibody, followed by visualisation by chemiluminescence. Lanes 1 – 4: transfected cells, frozen stocks made after 5 passages from transfection. Lanes 5 – 8: the cells that lost expression after 4 months. Media were collected from cells 2 days (lanes 4, 8), 4 days (lanes 3, 7), 6 days (lanes 2, 6) and 8 days (lanes 1, 5) after transfer onto serum-free medium.

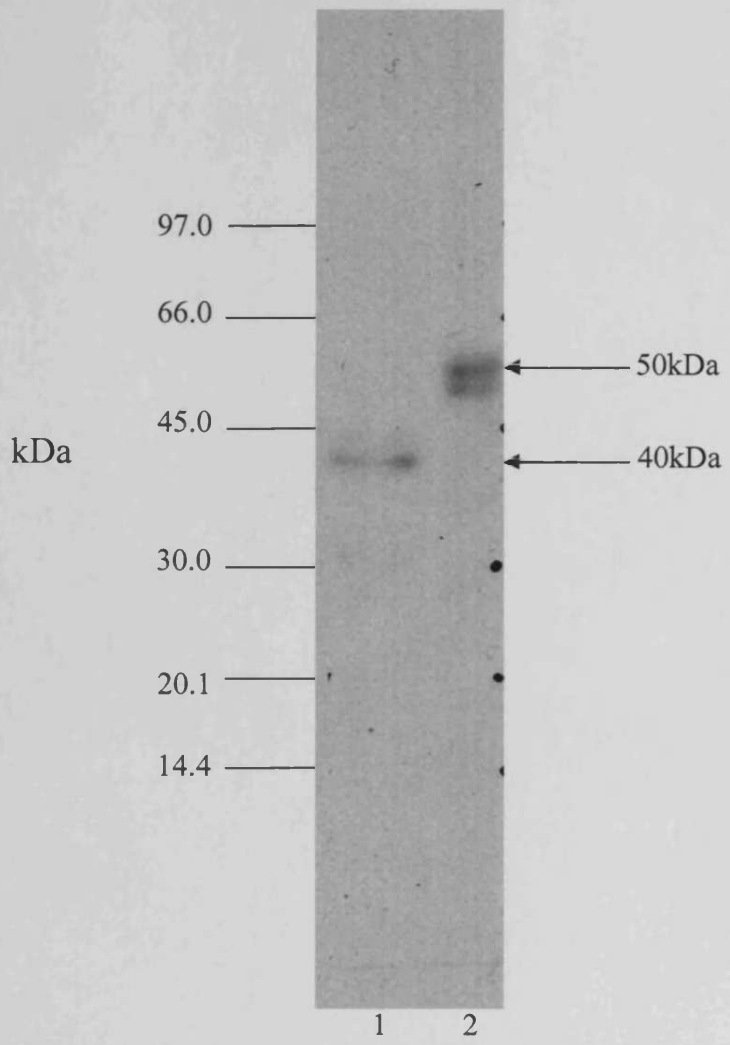

Figure 4.11: Western blot, comparing glycosylated and deglycosylated flt-1(1-3). Samples (100μl) were concentrated by ethanol precipitation and run on a 4-20% PAGE gel (reducing conditions), followed by transfer onto nitrocellulose and probed with anti-flt-1. Visualised by chemiluminescence. Lane 1: conditioned medium from transfected 293 cells subjected to deglycosylation. Lane 2: the same conditioned medium not treated.

expression for up to 13 days after transfer onto serum-free medium (in preparation for medium collection) after which the cell viability decreased.

Figures 4.7 and 4.10 illustrate flt-1(1-3) migrating on an SDS/PAGE gel as a band at 50kDa. This size was determined based on a standard curve from the distance travelled by molecular weight markers run simultaneously (not shown). The calculated molecular mass deduced from the amino acid sequence was 40kDa, but the sflt-1 protein is also known to contain 11 putative N-linked glycosylation sites[290], which may account for the difference in molecular mass. To confirm that this size difference was due to glycosylation, conditioned medium was treated with N-Glycosidase F. The deglycosylated protein was detected at 40kDa, compared to the glycosylated form (50kDa), shown in Figure 4.11. This indicated that the extra mass was indeed due to glycosylation. The band at 50kDa actually migrated as 2 very close bands, perhaps due to differential glycosylation, as indicated by the fact that only a single band is obtained after deglycosylation.

4.2.3. Purification of flt-1(1-3)

4.2.3.1. Strep tag affinity purification

The first purification strategy utilised the incorporated carboxyl terminal strep tag. Conditioned medium (300ml ultrafiltrated to 3ml) was centrifuged to remove any particular matter and passed through a strep-Tactin - affinity column. This streptavadin-based resin has a strong affinity for the strep tag. Bound samples were eluted by competition with desthiobiotin and the fractions collected were tested for flt-1(1-3) by Western blotting. Lanes 1-8 in Figure 4.12 show no evidence of flt-1(1-3) in the elution fractions. It appeared that flt-1(1-3) did not bind effectively to the column, as some flt-1(1-3) was detected in the wash step prior to elution (lane 9). This approach was performed three times, with changing the elution gradient, but with the same conclusions drawn from each run.

As the strep tag did not appear to be binding the strep-Tactin column with high affinity, conditioned medium was incubated for 30 minutes with the strep-Tactin matrix using a batch incubation approach to ensure maximum contact between proteins and the affinity matrix. After washing, desthiobiotin was added to remove the tagged protein from the matrix. A second elution step was carried out to increase

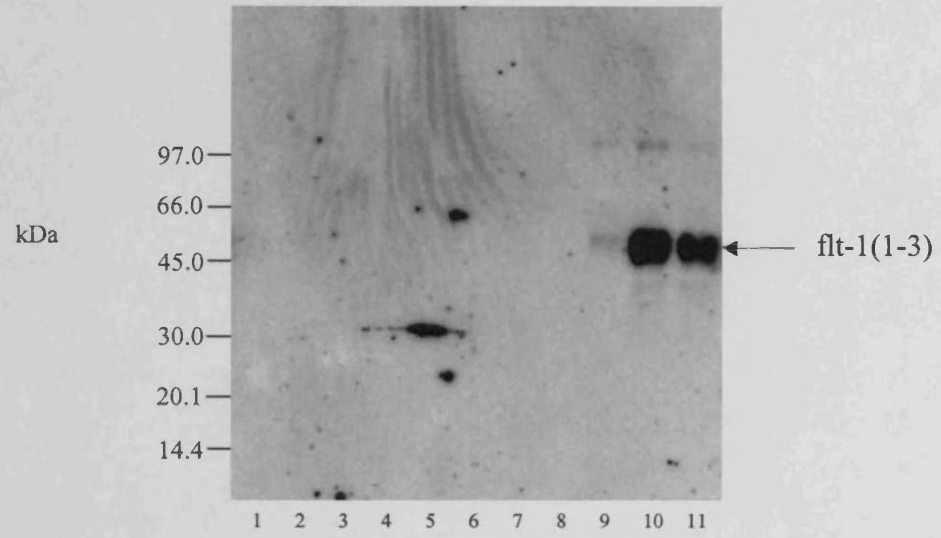

Figure 4.12: Detection of flt-1(1-3) following strep tag affinity purification. Fractions (0.5ml) were collected and proteins in each fraction (100μl) were concentrated by ethanol precipitation, followed by running on a 4-20% PAGE gel (reducing conditions). They were transferred to nitrocellulose, probed with anti-flt-1 and visualised by chemiluminescence. Lanes 1 – 8: fractions eluted from the column. Lane 9: fractions from wash step prior to elution step. Lane 10: conditioned medium from flt-1(1-3) – transfected cells. Lane 11: conditioned medium loaded onto the affinity column (after centrifugation). Putative bands at 30kDa could represent a breakdown product, but were not visible in other fractions assessed by the same method, suggesting that these were artefactual.

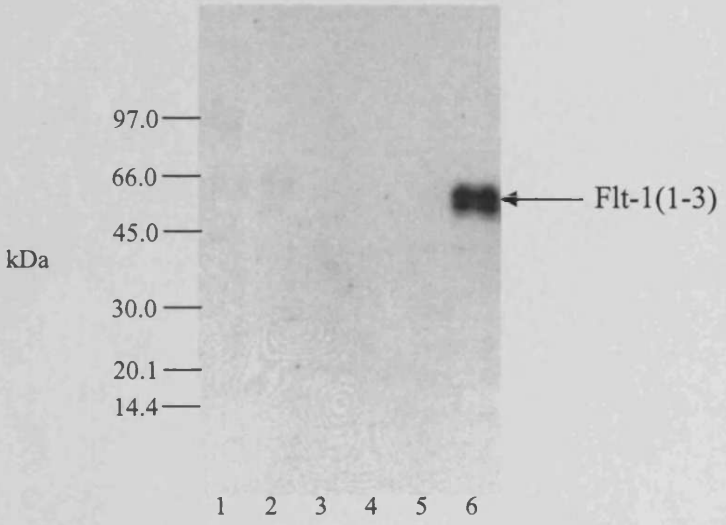

Figure 4.13: Western blotting to assess the strep tag affinity purification after 30 minutes incubation with strep-Tactin. Proteins in each sample (100μl) were concentrated by ethanol precipitation and run on a 4-20% PAGE gel (reducing conditions). They were transferred onto nitrocellulose membrane and probed with anti-flt-1 antibody, followed by visualisation by chemiluminescence. Lane 1: initial buffer wash. Lane 2: initial elution step. Lane 3: 2nd buffer wash. Lane 4: 2nd elution step. Lane 5: strep-Tactin matrix. Lane 6: conditioned medium that was the starting material.

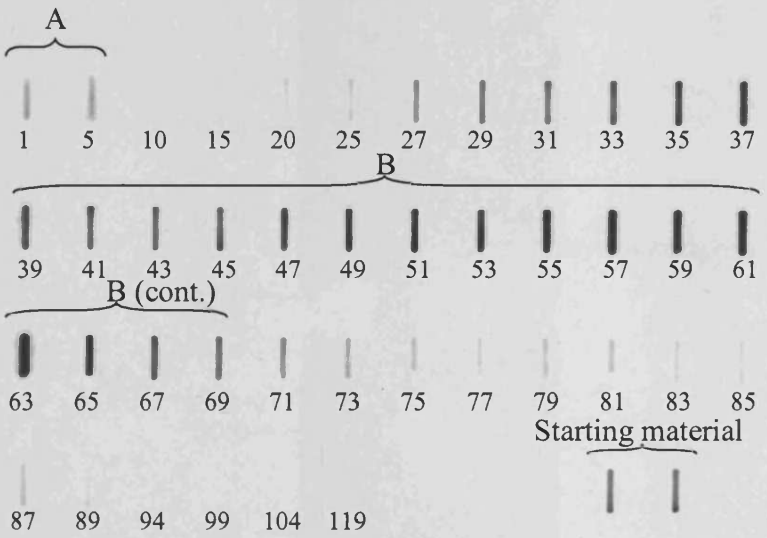

Figure 4.15: Slot blot probed with anti-flt-1 antibodies and visualised by chemiluminescence, of fractions (2.5ml) from heparin affinity chromatography. A: wash through step – unbound flt-1(1-3). B: elution of flt-1(1-3). Starting material: conditioned medium loaded onto column.

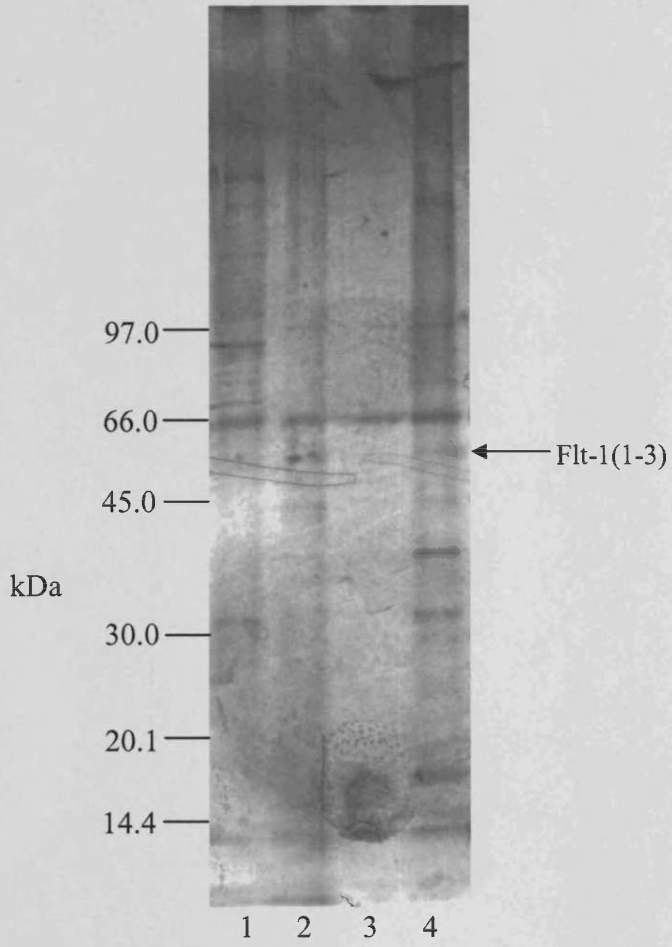

Figure 4.16: SDS/PAGE followed by silver stain, to assess purity of heparin sepharose chromatography fractions. From each fraction (2.5ml), proteins (100μl) were ethanol precipitated and run on a 4-20% PAGE gel (reducing conditions), followed by a silver stain. Lane 1: conditioned medium. Lane 2: pooled flt-1(1-3) positive fractions following heparin affinity chromatography. Lane 3: the buffer filtrate following ultrafiltration concentration, showing that the membrane in the centriprep cartridge did not leak any protein over 10 kDa through, although some contamination is evident possibly caused by albumin, which is 66kDa. Lane 4: ultrafiltration-concentrated pooled flt-1 positive fractions, following heparin affinity chromatography, with putative flt-1(1-3) indicated. A number of proteins were present in the concentrated sample and appeared to be co-purifying with flt-1(1-3).

not yield pure flt-1(1-3). To achieve better separation from co-eluting proteins, the salt gradient during the chromatography run was flattened but this caused flt-1(1-3) to elute over more fractions and did not increase purity. Comparison of lanes 2 and 4 in Figure 4.16 shows successful concentration of the protein, so this technique was applied to all subsequent material eluted from heparin affinity chromatography. A total of sixty such runs confirmed the reproducibility of this approach.

4.2.3.3. Cation exchange chromatography

Amino acid sequence analysis of flt-1(1-3) revealed the isoelectric point (pI) to be 9.73, not taking glycosylation into account. This indicated that at low pH the protein would become increasingly protonated, therefore positively charged. A flt-1(1-3) sample that had been semi-purified by heparin affinity chromatography was dialysed for 16 hours against 2-(N-morpholino) ethanesulphonic acid (MES) buffer, pH6.0 (Appendix 1.2), with 3 changes of buffer. This ensured an overall positive charge on flt-1(1-3). A cation exchange column (MonoS) containing negatively charged sulphate groups coupled to the matrix was equilibrated with the same buffer. The sample was loaded (1ml) and the sodium chloride concentration increased via a gradient up to 600mM to elute bound protein. The fractions were assessed for the presence of flt-1(1-3) by slot blot. The majority of the protein in the sample did not adhere to the column and eluted straight through (Figure 4.17), including some flt-1(1-3) (Figure 4.18 fraction 3). Positive staining in fractions 10-15 indicate that some flt-1(1-3) did interact with the column, although this was substantially less than the flt-1(1-3) loaded onto the column (Figure 4.17A, Figure 4.18). This suggested that some of the protein may be retained on the column after elution. Fractions that potentially contained flt-1(1-3), which had eluted over the salt gradient from three such runs were pooled, further concentrated by ultrafiltration and analysed by Western blotting. However, no flt-1(1-3) could be detected in these fractions by Western blotting (Figure 4.19). Cation exchange was attempted seven times, using different flt-1(1-3) preparations and elution gradients, with the same result. Following these runs, the column was washed with 2M salt, which did not remove any flt-1(1-3) from the column (Figure 4.20). A subsequent wash with 8M urea resulted in elution of flt-1(1-3) from the column (Figure 4.20), demonstrating that flt-1(1-3) had

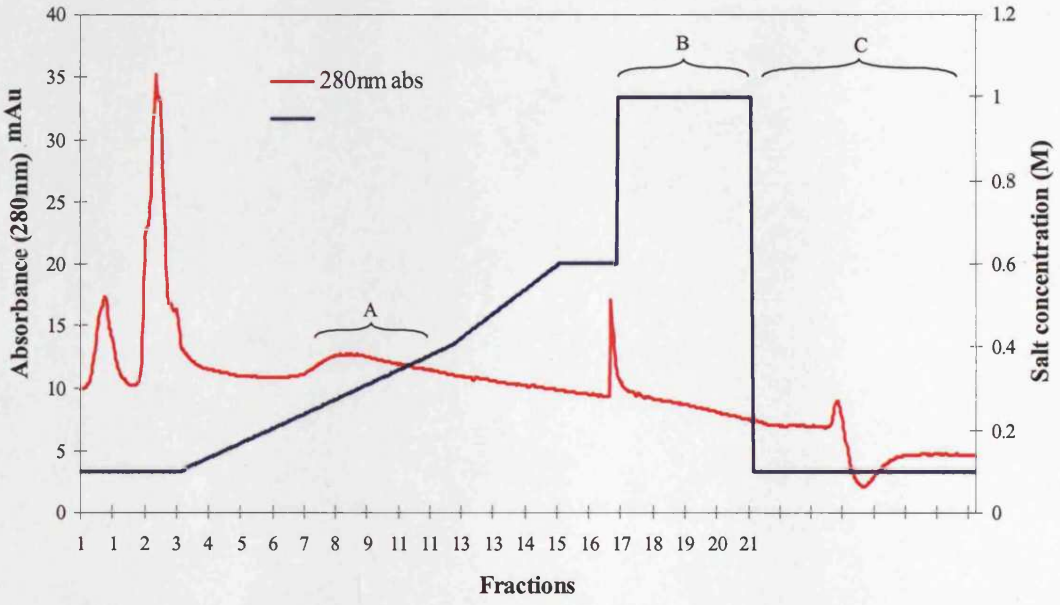

Figure 4.17: Chromatogram of cation exchange purification of concentrated heparin affinity fractions affinity fractions positive for flt-1(1-3). The salt gradient and absorbance at 280nm is shown. A: region where low levels of flt-1(1-3) were detected. B: clean out of the column with 1M sodium chloride. C: re-equilibration of the column.

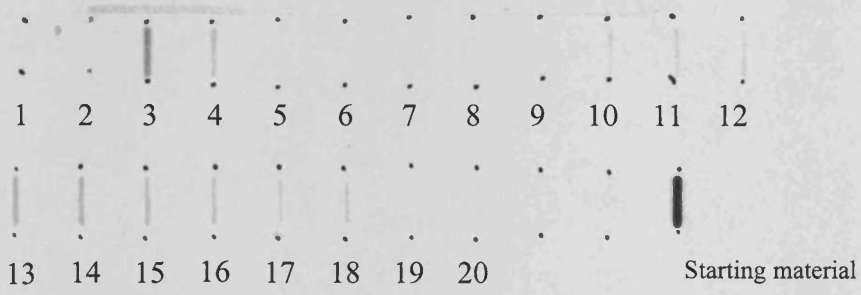

Figure 4.18: Slot blot of cation exchange fractions (50μl), probed with anti-flt-1. Starting material refers to the sample loaded onto the column. Fractions 1-4: wash through prior to gradient. Fractions 5-20: over a salt gradient up to 600mM.

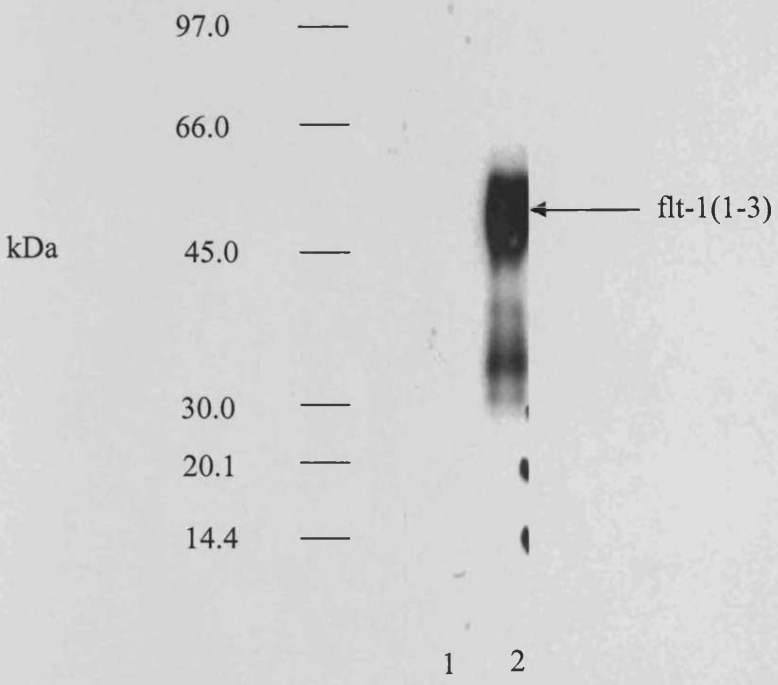

Figure 4.19: Western blot of cation exchange fractions. Proteins (100μl) were concentrated by ethanol precipitation and run on a 4-20% PAGE gel (reducing conditions). They were transferred to a nitrocellulose membrane, probed with anti-flt-1 and visualised by chemiluminesensce. Lane 1: concentrated positive cation exchange fractions. Lane 2: the sample that was loaded onto the cation exchange column.

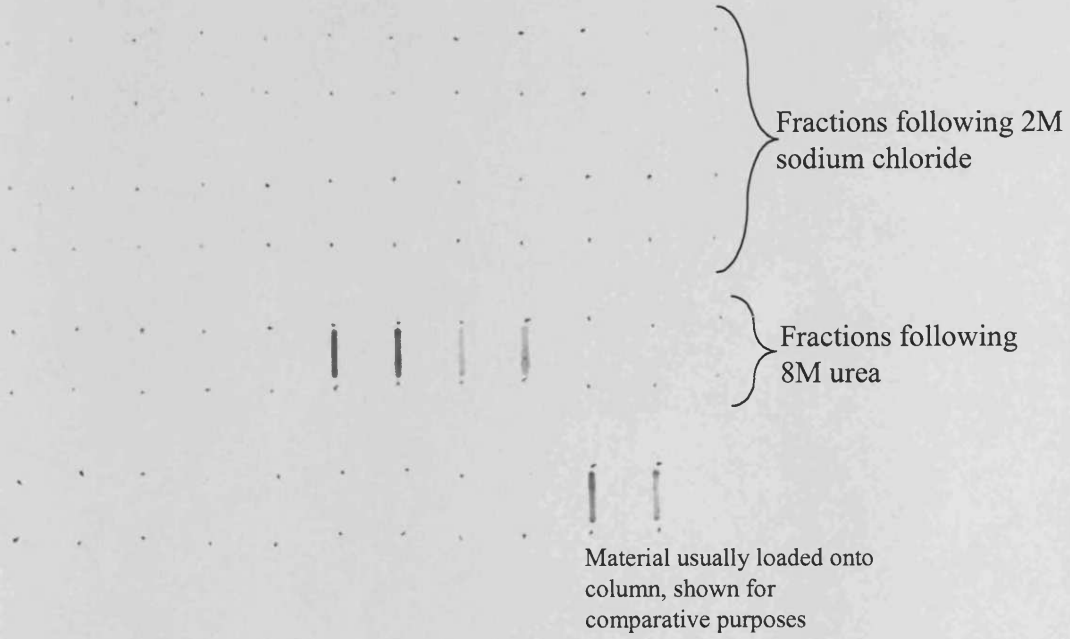

Figure 4.20: Slot blot of fractions (50μl) collected after cleaning the cation exchange column with 2M sodium chloride followed by 8M urea, probed with anti-flt-1. Visualised by chemiluminescence. Retention of flt-1(1-3) on the column is confirmed by the denaturing conditions (8M urea) required to remove it.

remained bound to the column. This may be due to non-specific adsorption rather than specific interaction. As the denaturing properties of 8M urea were deemed to be too harsh to yield functional flt-1(1-3), this purification method was abandoned.

4.2.3.4. Size exclusion chromatography

Study of lane 4 of Figure 4.16 shows that some of the contaminating proteins are of different molecular sizes as compared to flt-1(1-3). To exploit this, concentrated flt-1(1-3) from heparin affinity chromatography was separated on a high resolution gel filtration column (Superdex-75, fractionation range 3-70kDa) and the presence of flt-1 (1-3) in the collected fractions was assessed by slot blot. Figure 4.21 demonstrates 2 peaks (A and B) and slot blot analysis revealed that flt-1(1-3)-positive fractions were identified in both of these, as labelled in Figure 4.22. This was consistent across thirty such runs. It is possible that the earlier peak A contained the endogenous soluble flt-1 due to its larger mass and flt-1(1-3) was believed to be contained in the second peak B. To confirm this, the two sets of positive fractions were separately pooled with the corresponding fractions from 4 other runs, ultrafiltrated and separated on a SDS/PAGE gel, followed by Western blotting and a silver stain. The Western blot shown in Figure 4.23a demonstrated that flt-1(1-3) was present in peak B. It was hypothesised that flt-1(1-3) was forming a precipitate at the top of the column, causing a drop in recovery and the later elution. It was also proposed that the peak A may have been the void volume (V_0), and peak B may be the total volume (V_t), of the column. However, this would need further work to confirm this.

Due to time limitations, subsequent testing of flt-1(1-3) activity was undertaken using ultrafiltrated partially purified flt-1(1-3) from the heparin affinity chromatography. To take into account possible effects of the other proteins present, medium from non-transfected (wild-type) cells was also purified and concentrated by the same method, to act as a negative control. Western blotting verified that no flt-1(1-3) was present in the WT control (Figure 4.24), although expression of other proteins remained the same (Figure 4.25). There was no evidence of endogenous soluble flt-1 in either the WT or flt-1(1-3) preparations. The levels of this protein may have been too low to detect.

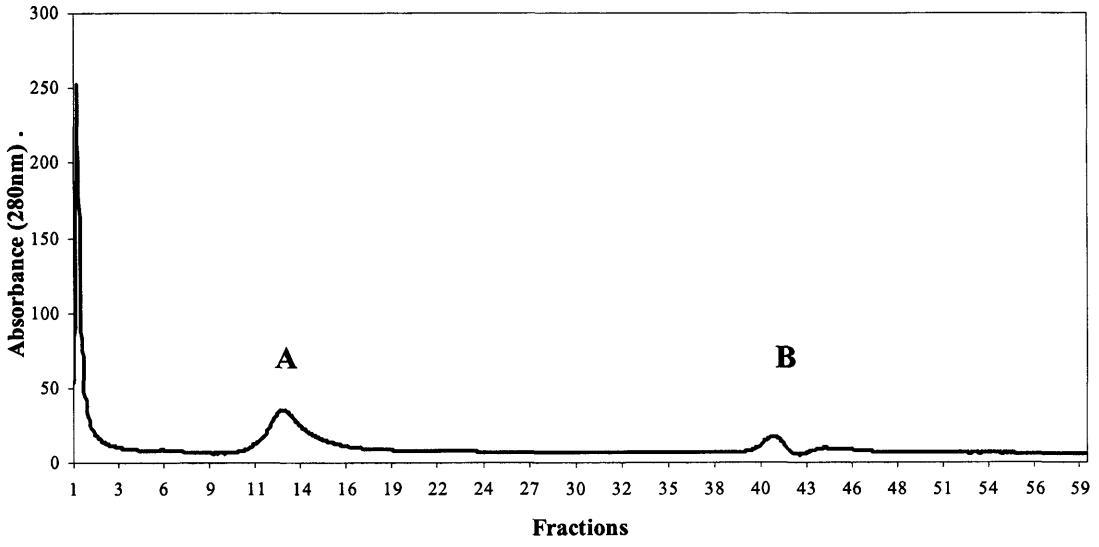

Figure 4.21: Chromatogram of size exclusion purification of fractions from heparin affinity purification positive for flt-1(1-3), showing the absorbance by proteins at 280nm. Sample (500μl) was loaded on a Superdex 75 column and 500μl fractions were collected.

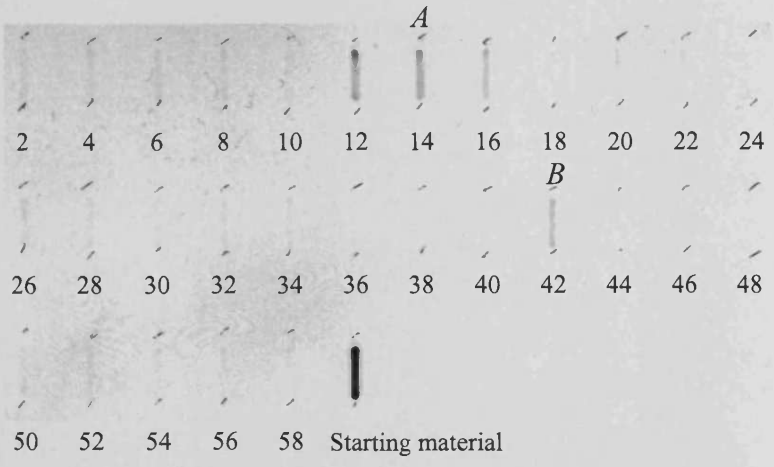

Figure 4.22: Slot blot of size exclusion chromatography fractions, probed with anti-flt-1, visualised by chemiluminescence. Starting material refers to the sample loaded onto this column.

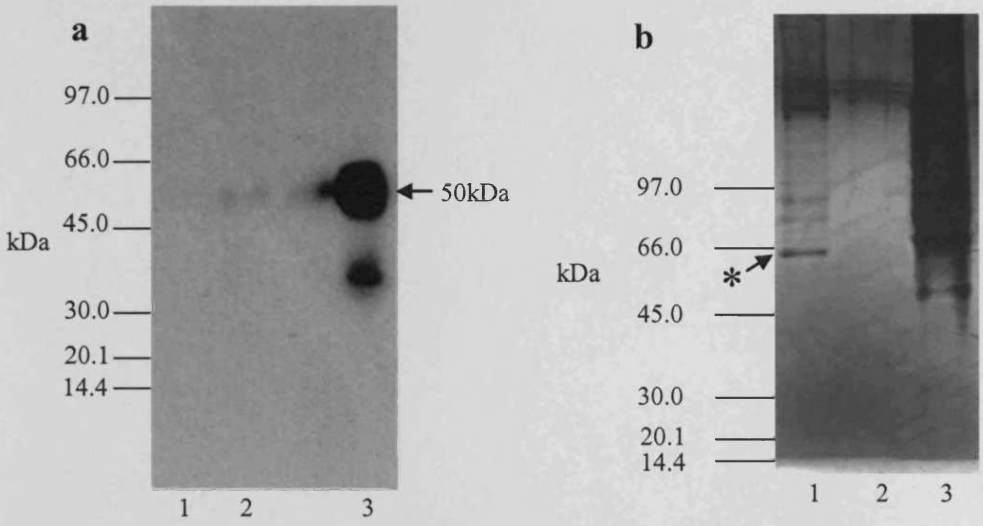

Figure 4.23: Western blot (a) (probed with anti-flt-1, visualised by autoradiography) and silver stain of SDS-PAGE (b), of concentrated flt-1 positive fractions following size exclusion chromatography. Proteins were concentrated by ethanol precipitation and run on a PAGE gel (reducing conditions). For Western blotting, they were transferred to a nitrocellulose membrane and probed with anti-flt-1, visualised by chemiluminescence. Silver stain was carried out on the PAGE gel. Lanes 1: Fractions of peak A (Figure 4.21), fraction 42 (Figure 4.22). Lanes 2: Fractions of peak B (Figure 4.21), fraction 12 (Figure 4.22). Lanes 3: Starting material loaded onto the gel filtration column. The asterisk indicates an unidentified protein of similar molecular mass to flt-1(1-3). The extra, smaller band in lane 3 of the Western blot was assumed to be a result of degradation.

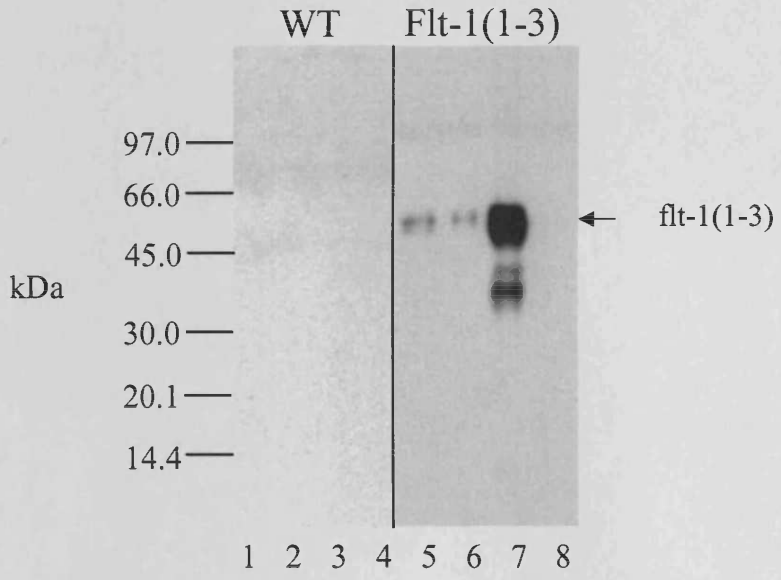

Figure 4.24: Western blot to assess expression, purification and concentration of flt-1(1-3) and WT transfected media. Proteins (100μl) were concentrated by ethanol precipitation, run on a 4-20% PAGE gel, transferred to nitrocellulose and probed with anti-flt-1 antibody. Visualised by chemiluminescence. Samples were WT (lanes 1-4) and flt-1(1-3) (lanes 5 -8). Lanes 1 and 5: conditioned medium. Lanes 2 and 6: pooled heparin affinity chromatography fractions before concentration. Lanes 3 and 7: concentrated pooled fractions. Lanes 4 and 8: filtrate from concentration step, to confirm that no flt-1(1-3) was lost during ultrafiltration.

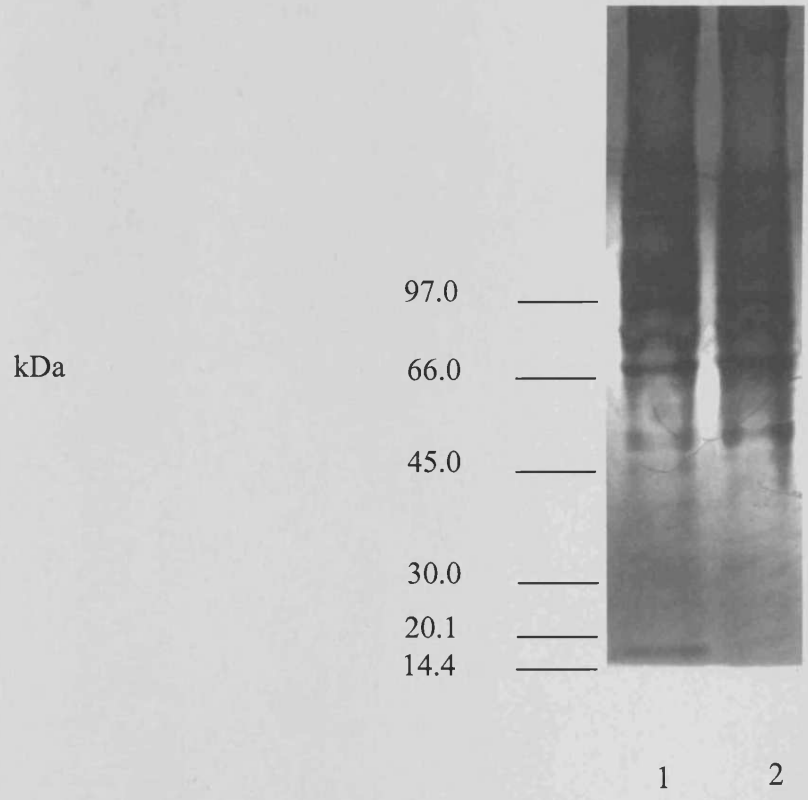

Figure 4.25: SDS/PAGE and silver stain of concentrated heparin affinity chromatography fractions. Proteins (100μl) were concentrated by ethanol precipitatation and run on a 4-20% PAGE gel, followed by silver staining. Lane 1: fractions originating from WT (non-transfected) conditioned medium. Lane 2: fractions from flt-1(1-3) transfected cell medium.

It is noticeable, however, that there was no visual difference in the pattern of bands following silver staining of WT and flt-1(1-3) preparations, which suggests that the levels of flt-1(1-3) were either too low to be detected in a silver stain, or ran to the same point as other proteins. The low level of expression probably exacerbated the difficulties experienced with purification.

In summary, expression and purification approaches revealed that:

- Flt-1(1-3) could be expressed using the pCEP-Pu vector and 293 EBNA fibroblasts, although expression was not as high as anticipated.
- The affinity of flt-1 for heparin could be exploited to partially purify flt-1(1-3).

4.2.4. Concentration of flt-1(1-3)

A Quantikine immunoassay kit was employed to determine the concentration of flt-1(1-3) in the partially purified flt-1 preparations tested in biological assays (Chapter 5). The calculated concentrations also included endogenous forms of flt-1, but by comparison with the WT control, these levels were too low to exert a significant influence. In addition, a BCA protein assay revealed the total protein concentration of these fractions.

Eight concentrates (corresponding to 1.6L conditioned medium) were pooled and the average concentrations summarised in Table 4.1. This was carried out a total of three times. From this the average flt-1(1-3) concentration in the conditioned medium was calculated at 0.335μg/L, although some flt-1(1-3) may have been lost during fraction selection, following heparin affinity chromatography. Individual preparations of flt-1(1-3) were prepared for each of the biological assays (Chapter 5).

4.2.5. Flt-1(1-3)/VEGF binding assay

Surface plasmon resonance, using Biacore technology, was used to examine the affinity of flt-1(1-3) to VEGF. Recombinant human $VEGF_{165}$ (2.98μg/ml) was immobilised by amino-coupling to a Biacore CM5 chip at a density of 3593 response units (RU). A WT negative control, of 82μg/ml total protein, was passed over the

chip. This was followed by a flt-1(1-3) preparation, consisting of 109ng/ml flt-1(1-3) in the same total protein concentration. A polyclonal anti-VEGF antibody (10μg/ml) was passed over the chip and provided a positive control to confirm the activity of VEGF. A rise in the response units indicated interaction of the sample with the immobilised VEGF on the chip, as an increase in immobilised protein size was detected by the refraction of light applied to the sensor chip. This was carried out 3 times, and Figure 4.26 shows one of these runs.

Figure 4.26 demonstrates the change in response units following the application of each sample to the chip containing immobilised VEGF. At point 1, the WT negative control was injected, leading to a decrease in response units (pale blue region), until the injection finished (point 2) and the baseline levelled off. This drop demonstrated that there was no interaction between the negative WT control and VEGF. The flt-1(1-3) sample was injected at point 3 and the injection finished at point 4 (dark blue line). The increase in response of approximately 40 units shows that there was specific interaction with the immobilised VEGF. Furthermore, when compared to the baseline at point 3, the elevated plateau after point 4 demonstrates that flt-1(1-3) was retained on the chip after injection, denoting that specific binding of flt-1(1-3) to VEGF took place. After cleaning the chip, a similar pattern was observed when the antibody against VEGF (positive control) was injected (point 6). This also exhibited specific binding after point 7 (brown line), indicated by the elevated plateau. There did not appear to be interactions from other proteins in the samples, highlighted by the lack of reactivity of the negative control.

In summary, surface plasmon resonance demonstrated that:

- Partially purified flt-1(1-3) bound to VEGF.
- This observation was not caused by contaminating proteins, as no similar response was observed in the WT negative control.

Table 4.1: Concentrations of the test and WT control samples analysed by surface plasmon resonance, as determined by a BCA protein assay (total protein concentration) and by flt-1 immunoassay (flt-1 concentration). The samples were obtained by partial purification by heparin affinity chromatography and ultrafiltration. The 370-fold increase in flt-1 from transfected cells indicates that the flt-1 concentration stated correlates to flt-1(1-3).

Sample	Total protein concentration (μg/ml)	Flt-1 concentration (μg/ml)	Increase in flt-1(1-3) expression compared to WT
Flt-1(1-3)	446.6 ± 235	0.31 ± 0.15	370 x
WT control	446.6 ± 235	(below detection limit)	

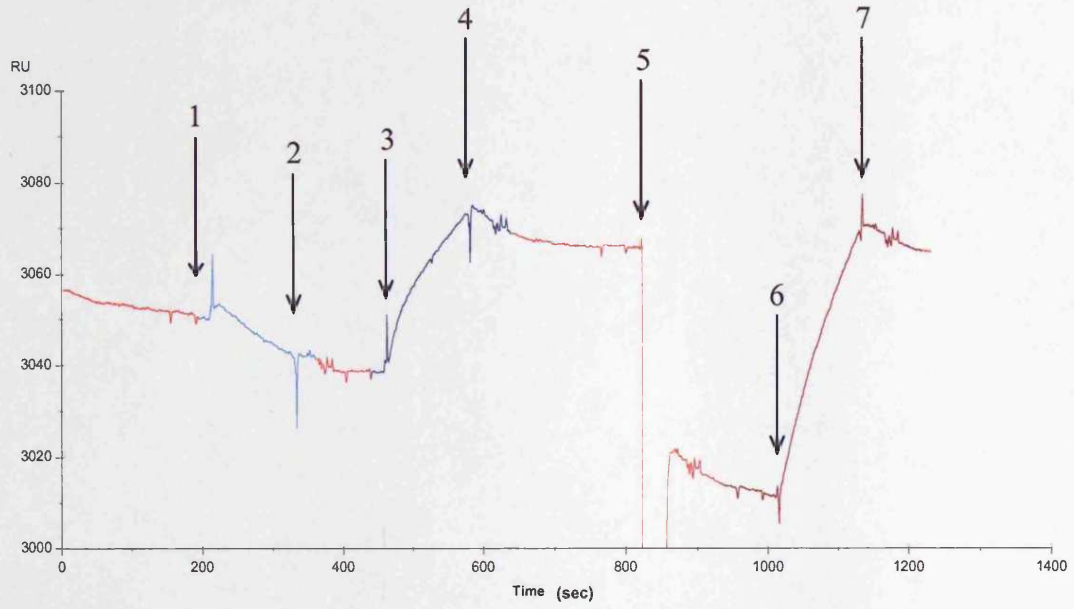

Figure 4.26: BIAcore analysis of binding of partially purified flt-1(1-3), a WT control and anti-VEGF to VEGF immobilised on a sensor chip. **1**: start of injection of the WT negative control (82μg/ml total protein) onto the chip. **2**: end of injection of the WT negative control. **3**: start of injection of flt-1(1-3) (109ng/ml flt-1(1-3), 82μg/ml total protein) onto the chip. **4**: end of injection of flt-1(1-3), the increase in RU indicating interaction with VEGF. **5**: a brief cleaning step of 50mM sodium hydroxide. **6**: start of injection of the polyclonal antibody against VEGF (10μg/ml) onto the chip. **7**: end of injection of the antibody.

4.3 Production of fms-like tyrosine kinase receptor domains 1-3 Discussion

The cDNA of the 3 N-terminal extracellular domains of flt-1 (flt-1(1-3)) was successfully isolated from human umbilical vein endothelial cells (HUVECs) and expressed in human embryonic kidney 293 EBNA fibroblasts. The recombinant flt-1(1-3) was capable of binding VEGF.

4.3.1. Expression of flt-1(1-3)

A mammalian expression system was selected because flt-1(1-3) contains important sulphur bridges and is glycosylated, although it appears that glycosylation is not required for successful VEGF binding[290]. An episomal (extrachromosomal) expression approach was taken using the pCEP-Pu vector[436], whereby several pCEP-Pu/flt-1(1-3) plasmids could be sustained in the nucleus of the host cell without incorporation into the host genome. Theoretically, this would allow stable, high expression of protein[440]. To achieve constant episomal maintenance of viral DNA in the cell, viral elements of the Epstein-Barr Virus (EBV) were required, namely the EBV origin of replication (*OriP*) and the Epstein-Barr Nuclear Antigen-1 (EBNA-1)[437]. The 293 EBNA cells used for transfection already contained a pCMV/EBNA vector, which conferred resistance to geneticin, supplemented to the culture medium[435,437]. The *OriP* component was supplied by the pCEP-Pu vector (Appendix 3.1) and in conjunction with EBNA-1, ensured that the pCEP-Pu/flt-1(1-3) construct was retained by the host cell. The pCEP-Pu/flt-1(1-3) was retained by selection with puromycin. Continual selection was important because there have been reports of a slow loss of vector over time[437]. However, despite the selection of puromycin-positive cells, after a few months there was a loss of flt-1(1-3) expression in this study. It is possible that the vector lost part of its sequence or became partially integrated.

Bacterial expression of truncated flt-1 has yielded a product capable of binding VEGF[290,438] with bacterially expressed flt-1 domains 1-3 showing a comparable binding affinity to its equivalent expressed in insect cells[290]. In both these studies,

procedures were performed to ensure the correct folding and formation of disulphide bridges within the protein, as these bridges are integral to the tertiary structure of flt-1 (Figure 1.8 in Section 1.4.6). It was anticipated that bacterial expression of flt-1(1-3) would achieve greater expression and increased purity through a His tag. However, ligation of the flt-1(1-3) cDNA into the vector proved unsuccessful. Future work would concentrate on further optimising the restriction digest conditions using different restriction sites, such as the Hind III sites incorporated in flt-1(1-3) cDNA and in the vector. Alternatively, a different bacterial expression vector would be selected.

The purification of expressed flt-1(1-3) was important, for future assessment of the ability of flt-1(1-3) to block VEGF-mediated events, with minimal interference from contaminating proteins. For this reason, several different approaches were taken to achieve this. Figure 4.27 summarises the purification approaches used.

4.3.2. Strep tag purification

Fusion tags have been successfully applied in the purification of proteins, consisting of a short amino acid sequence to either act as an affinity ligand or as an epitope for an antibody. The His tag has previously been used in the purification of flt-1 and VEGF[438,439]. In this study, a strep tag of 8 amino acids was used, which exhibits high affinity binding to streptavadin in the same region as biotin, previously termed Strep II[435]. This was contained in the pCEP-Pu vector and by the controlled insertion of the flt-1(1-3) cDNA, the strep-tag was incorporated onto the C-terminal end of the flt-1(1-3). The strep tag was selected as it has enabled the purification of proteins under gentle conditions following expression using 293 EBNA cells[435].

Western blots showed that the strep-tag could not be detected with a polyclonal anti-strep-tag antibody, known to be active during other work in our laboratory. To eliminate other sources of biotin that may have interfered with the interaction, casein rather than milk powder as a blocking agent was implemented during Western blotting. Furthermore, a Strep-Tactin matrix, failed to bind the flt-1(1-3) (Strep-Tactin being a variant of streptavadin, but with greater affinity for the tag[435]). This

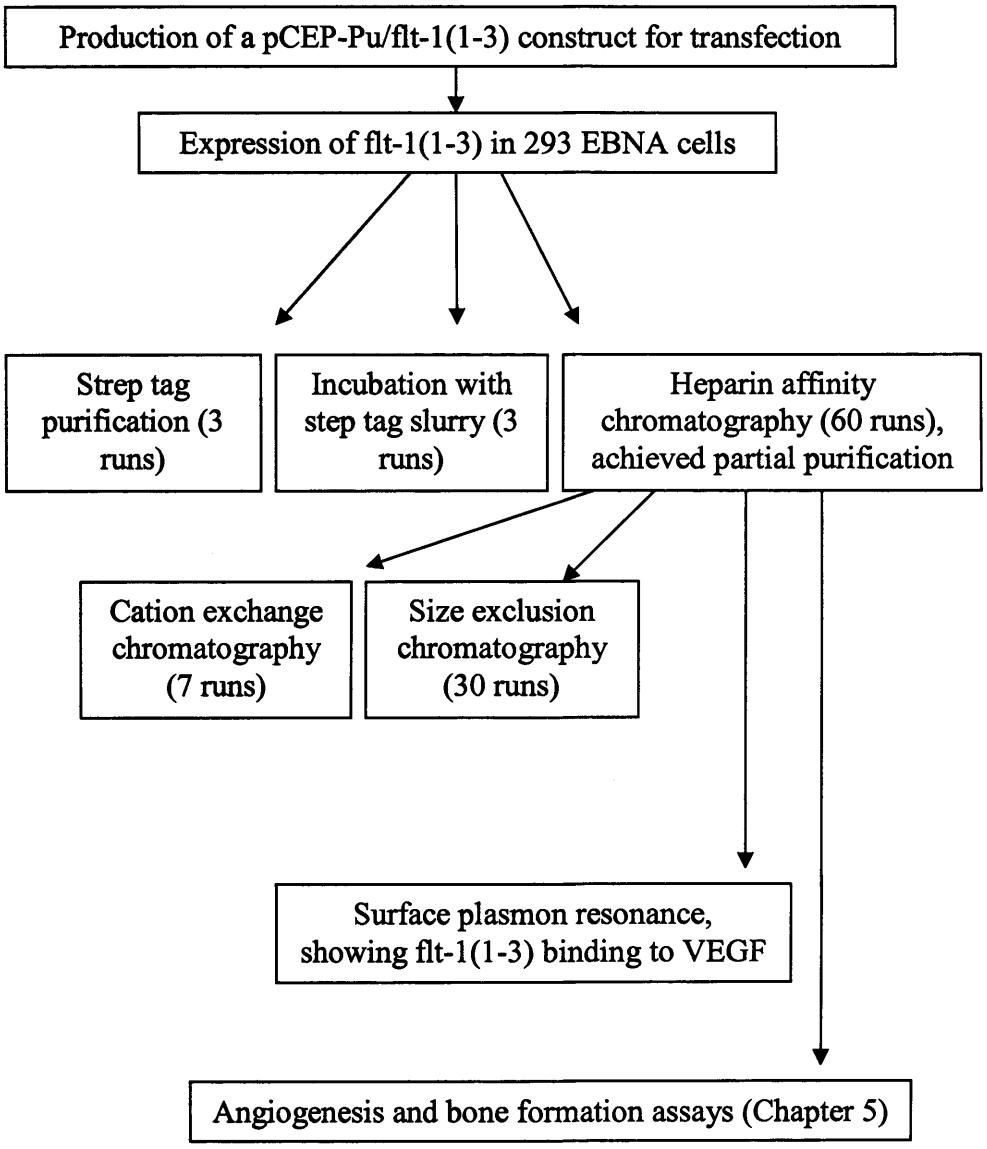

Figure 4.27: A flow diagram summarising the steps taken in this Chapter, to produce and purify flt-1(1-3), with subsequent assays to assess the VEGF-binding activity of flt-1(1-3).

suggested that either the tag was internalised, out of frame, or cleaved. The reducing conditions under which the SDS/PAGE prior to the Western blot was performed would have revealed any internalised strep-tag, and the strep tag cDNA in pCEP-Pu/flt-1(1-3) was still in frame. Therefore, it is likely that the strep tag was cleaved by limited proteolysis. This implies that the strep-tag must have been lost during expression and therefore an alternative approach was adopted.

4.3.3. Heparin affinity chromatography

Flt-1 is known to have a high affinity for heparin[315] and this property has previously been exploited when purifying truncated flt-1[290,315-8]. Workers have reported the elution of truncated flt-1 at sodium chloride concentrations above 0.4M, whereas the present study could detect a fraction of flt-1(1-3) eluting at low salt concentrations (from 0.28M). The long elution range of the flt-1(1-3) suggests that there may have been heterogeneity in the tertiary structure of the protein leading to different degrees of availability of the heparin-binding region to interact with the column. Previously reported purification methods have used heparin affinity chromatography to purify conditioned medium from insect or mammalian cell lines of at least 1 litre over a heparin affinity column[316,318], whereas this method only used 200ml. Interestingly, other groups have also stated that only a partially pure sample of truncated flt-1 was obtained by this method[290,316,441]. This indicates that truncated flt-1 may be difficult to purify and that the results obtained in the present study were in fact successful and comparable to other published data.

4. Cation exchange chromatography

Although ion exchange chromatography has previously been applied to flt-1 purification[316], it was unsuccessful in the experiments described here due to the retention of flt-1(1-3) on the column. The flt-1(1-3) amino acid sequence has a high isoelectric point of 9.73, but this could be influenced by the 11 glycosylation sites in flt-1(1-3)[290]. It was speculated that the interaction of flt-1(1-3) with the anionic matrix was too strong for it to be eluted with 1M sodium chloride. However, some flt-1(1-3) remained on the column, even after elution of 2M sodium chloride (Figure 4.20, Section 4.2.3.3). The chromatogram obtained showed peaks before the start of, and during, the elution gradient, probably caused by other proteins present (Figure 4.17, Section 4.2.3.3). Faint flt-1(1-3) staining was observed in the same fractions of

the salt gradient using slot blot. It is conceivable that the apparently positive fractions were caused more by background staining of other proteins and not by specific detection of flt-1(1-3). This would also explain why no flt-1(1-3) was detected in subsequent Western blots after the proteins were separated by SDS/PAGE (Figure 4.19, Section 4.2.3.3), compared to slot blots, which had no such separation (Figure 4.18, Section 4.2.3.3).

4.3.5. Size exclusion chromatography

This method, in combination with the cation exchange chromatography strategy, has previously yielded a high (90%) purity of sflt-1[442] and was therefore applied here to further purify flt-1(1-3). The size exclusion column was selected as it provided good resolution between 3kDa and 70kDa (supplier literature).

Fractions eluting close to the void volume of the column contained flt-1(1-3), as demonstrated by slot blotting (Figure 4.22, Section 4.2.3.4). The elution position was not consistent with the molecular weight of flt-1(1-3) and fractions at this stage contained high molecular weight proteins. Sflt-1 can form heterodimers with KDR in the absence of VEGF, albeit not to the same extent as when VEGF is present[316]. VEGF could not be detected in conditioned medium nor concentrated heparin affinity fractions by Western blotting (data not shown). However, it was possible that flt-1(1-3) was binding to itself, in the absence of VEGF. Alternatively, the overall shape of flt-1(1-3) may have affected the rate of elution.

Similar to the cation exchange separation attempt, there was significantly less flt-1(1-3) detected in the fractions compared to the sample loaded onto the column. Despite careful analysis of each handling step we were unable to identify the reason for this apparent loss of recombinant protein. If flt-1(1-3) was interacting with other proteins, it may have eluted over a longer period. This could have meant that the amount flt-1(1-3) in each fraction was too diluted to detect.

The purification approaches used in the present study were likely to be partially hampered because of the low expression level of flt-1(1-3). The selection antibiotic was increased 20-fold in a bid to raise protein expression, ensuring that only cells containing a higher number of plasmids remained viable. This did, indeed, increase

production. Other groups producing truncated flt-1 have used a baculovirus transfection and expression system in an insect cell line and achieved higher yields of truncated flt-1 than in the present study, which suggests an alternative future approach[290,315,318,432,438,441]. However, the expression system used in the present study has been previously shown to achieve high levels of expression with some proteins[440]. Moreover, post-translational modification of the expressed protein in the HEK fibroblast cell line used here would represent that of the endogenous protein in humans more closely than an insect cell line.

6. Concentration of flt-1(1-3)

Following partial purification by heparin affinity chromatography, flt-1(1-3) was concentrated by ultrafiltration and measured (Table 4.1, Section 4.2.4). The level of flt-1 detected in non-transfected cells may have been due to the endogenous soluble receptor. The increase in concentration of flt-1(1-3) in transfected cells (in comparison to total protein) clearly showed that the transfected cells were expressing the protein. The approximate concentration of flt-1(1-3) in the conditioned medium was calculated at 0.335μg/L. Miotla *et al.*[318] reported achieving 2-10mg/L of sflt-1 in conditioned medium using the baculovirus expression system in high5 insect cells, but required 5L of conditioned medium. This suggests that the yield of flt-1(1-3) in the present study could be increased by purifying an increased volume of conditioned medium.

4.3.7. Flt-1(1-3)/VEGF binding assay

Previously, binding of truncated flt-1 to VEGF has been assessed using ^{125}I-VEGF complexes in competition or ELISA-type assays[242,267,290,297,315,426,442]. Surface Plasmon Resonance (SPR) has been used here as this technology provides a more rapid, sensitive method for studying the binding kinetics of VEGF with its receptors[350,427]. The technique immobilises either the receptor or ligand on a carboxymethylated dextran and gold – coated sensor chip, followed by passing the corresponding ligand or receptor in solution over the chip. Interaction of a protein with the immobilised protein is detectable as a change in the size of immobilised protein, as determined by the refraction of a directed light beam.

SPR demonstrated successful binding of flt-1(1-3) to VEGF (Figure 4.26, Section 4.2.5). This finding is consistent with other published work[290,442]. It demonstrates that the expression system used here can produce active flt-1(1-3). Moreover, the binding of flt-1(1-3) to VEGF suggests that although the extracellular domain 4 of flt-1 is required for dimerisation, it may not be required for stable binding. Ma *et al.*[442] demonstrated that the first 3 extracellular domains of flt-1 block VEGF-mediated blood vessel formation *in vivo*, indicating that domain 4 of flt-1 is not required to bind VEGF with high affinity.

The contaminating proteins in the flt-1(1-3) preparation did not block the interaction, which indicates that flt-1(1-3) retains binding affinity to VEGF in the presence of other proteins. This is of importance for the potential application of flt-1(1-3) as a decoy receptor for VEGF in biological assays. The presence of other proteins in the flt-1(1-3) preparation meant that further kinetic analyses were not feasible, as these proteins may have influenced flt-1(1-3) binding to VEGF. For instance, contaminating proteins could have non-specifically coated the dextran strands on the surface of the chip, thus partially blocking the immobilised VEGF from the soluble flt-1(1-3). A purer preparation of flt-1(1-3) would reduce this issue and reveal if flt-1(1-3) has a comparable affinity for VEGF as full-length flt-1. Furthermore, a comparison of the binding affinity of flt-1(1-3) with full-length flt-1 would indicate any differences in VEGF-binding. The dissociation constant (K_d) value for the full-length receptor has been reported as 10-30pM[278], with a similar affinity with the truncated form sflt-1 containing all 7 extracellular domains[287,315,316]. Furthermore, domains 1-3 of flt-1 exhibited only a slight change in K_d, to around 26pM[287]. This truncated form has been reported to block VEGF-mediated DNA synthesis[290,442], inhibit blood vessel formation *in vivo*[442] and halt endochondral ossification[112]. These studies suggest that the expression of flt-1(1-3) described herein may be capable of inhibiting angiogenesis and VEGF-induced bone formation, as part of a treatment strategy in OA. Chapter 5 describes work carried out to further evaluation this.

In conclusion, we have successfully used an episomal expression system to produce an partially pure recombinant flt-1(1-3) that is capable of binding to its ligand, VEGF. However, more work is necessary to improve purity of the expressed protein by the methods used in this study. Preliminary work has been conducted in the use of a

bacterial expression system for flt-1(1-3), as Baerleon *et al.*[290] have reported high-affinity binding of truncated flt-1 expressed in a bacterial system. Furthermore, preliminary experiments using a bioreactor have been carried out, as this enables a higher yield of protein and cell density in a relatively small volume of medium. The commercially available antibody used to probe the Western blots in this Chapter could be utilised to purify flt-1, either by immunoprecipitation or by an affinity chromatography approach. However, the relatively harsh conditions that would be required to elute the protein may cause loss of activity.

5.1 Biological Assays Introduction

A three-dimensional matrix as a delivery system has been used in a number of studies to investigate wound healing and cartilage repair (Section 1.6). Further to the delivery of a bioactive agent, such a matrix can interact with the surrounding tissue or support cell infiltration and thus, enhance void-filling tissue regeneration. Generally, it is preferable to use a material that is biodegradable that can be broken down by normal metabolic pathways, thus avoiding a potential accumulation and subsequent toxic effects.

Endogenous macromolecules have received much interest due to their inherent biocompatibility and biodegradability. For example, fibrin-based matrices have been applied to the delivery of basic fibroblast growth factor (bFGF), via heparin sites incorporated into the matrix[378]. This reproduces the retention of growth factors by extracellular matrix (ECM) components *in vivo*. Hyaluronan (HA) is a natural candidate as a delivery system in cartilage, as it is abundant in this tissue and contributes to tissue integrity (Section 1.1.4). As such, HA-based materials have been used alone[338], or for the delivery of cells[339]. Chapter 3 describes an injectable HA-based hydrogel using an ethylenediamine derivative of HA (HAED). This was shown to crosslink under physiological conditions and was used to deliver active bone morphogenetic protein-2 (BMP-2). The density and elastic properties of this hydrogel could be modified easily, contributing to the hydrogels versatility.

The overall hypothesis of this project is that a matrix that supports angiogenesis will, in the presence of, for example, BMP-2, induce rapid osteogenesis, while a matrix that inhibits angiogenesis will only undergo chondrogenesis (Section 1.7). It has been demonstrated that the inhibition of angiogenesis by suramin allowed the transforming growth factor-β_1 (TGF-β_1) and bone morphogenetic protein-2 (BMP-2)-induced formation of cartilage, with no bone invasion[342]. Indeed, the subcutaneous implantation of recombinant human bone morphogenetic protein-2 (rhBMP-2), in the presence of an

angiogenesis inhibitor, has been reported to decrease bone formation, but to enhance cartilage formation[443].

Vascular endothelial growth factor (VEGF) is a potent angiogenic agent with a pathological role during osteoarthritis (OA), outlined in Section 1.4.5. Chapter 4 describes the expression and partial purification of a decoy receptor based on the VEGF-binding domains of fms-like tyrosine kinase-1 (flt-1), termed flt-1(1-3). It is speculated that by sequestering VEGF and interfering with the interactions between VEGF and endogenous receptors, chondrocyte differentiation will be arrested and vascular ingrowth prevented. This method of angiogenesis inhibition would provide a more precise mechanism than suramin and avoid the potentially toxic side effects associated with suramin[444]. Furthermore, a truncated form of flt-1 is endogenously expressed and inhibits angiogenesis[317]. This lends further support to the viability of this approach as it mimics a physiological process.

This Chapter describes the combination of the delivery system of the HAED hydrogel with the flt-1(1-3) decoy receptor, as a method of inhibiting angiogenesis and reducing bone formation. $VEGF_{165}$ and suramin were used as positive and negative controls for the angiogenesis assay, respectively.

Several *in vitro* and *in vivo* angiogenesis assays have been applied to investigations of VEGF and its receptors. To study VEGF-mediated effects on cells *in vitro*, incorporation of radiolabelled thymidine as a marker of cell proliferation, in response to VEGF has been used extensively[242,267,290,294,315,427,430] , although this technique does not indicate angiogenesis *per se*. As it has been observed that endothelial cells cultured *in vitro* can form tubules to indicate angiogenesis[445], this has also been used to study VEGF-mediated angiogenesis[446,447]. However, angiogenesis does not arise solely from endothelial cell proliferation, but also involves other cell types (Section 1.3.1). To address this, organ culture assays have been developed, such as the rat aortic ring assay[448]. To study angiogenesis in the organism, the corneal pocket assay[244,267,446] and the Matrigel plug assay[449] have been developed. A less technically demanding assessment of angiogenesis

is the chick chorioallantoic membrane (CAM) assay, a tissue used for years by embryologists before being applied to angiogenesis studies. However, inter-species differences in response to agents and morphological changes in the developing embryo must be taken into account, when studying angiogenesis by this method. Quantification of this technique has further been a challenge, but image analysis software and biochemical methods have addressed this problem[406]. The foetal rat metatarsal assay has received much attention, since it provides a whole organ culture approach for the study of endochondral ossification[450]. The foetal metatarsal provides a useful model for the present study, as OA cartilage seems to share characteristics with the foetal growth plate, such as chondrocytes entering hypertrophy (Section 1.2).

HAED hydrogels containing flt-1(1-3) were assessed for anti-angiogenic activity in the CAM assay. They were assessed for inhibitory effects on bone formation, using the foetal rat metatarsal bone formation assay.

5.2 Biological Assays Results

5.2.1. Chick chorioallantoic membrane assay

This assay was employed to determine if flt-1(1-3) could block angiogenesis. Flt-1(1-3) was partially purified from transfected 293 EBNA cells medium by heparin affinity chromatography, and the total protein and flt-1 concentrations were determined, as described in Chapter 4. To account for any effects of contaminating proteins, an additional sample was prepared in an identical manner from non-flt-1(1-3)-transfected cells. This was termed the 'WT preparation'.

Hydrogels were prepared to 9mg/ml hyaluronan ethylene diamine derivative (HAED), with a ratio of 1:1 (functional groups) SPA_4-PEG (20kDa) crosslinker to HAED, with no collagen included. The bioactive agents were incorporated in place of phosphate-buffered saline (PBS), when diluting the hydrogel components to the correct concentration (20μl added). This small volume of sample that could be incorporated by this method placed limits on the final concentrations obtainable. An alternative method of lyophilising the hydrogel and rehydrating it with a larger volume of test sample did not produce homogenous hydrogel discs, as the lyophilisation step damaged hydrogel shape and structure. Another method involving the injection of test sample into a pre-existing hydrogel merely resulted in loss of sample through seepage and a weakened, more dilute hydrogel. Both methods were aborted, in favour of the PBS replacement method, described above.

Table 5.1 summarises the quantities of bioactive agents that were incorporated into each hydrogel disc placed on the CAM. As VEGF has been shown to stimulate angiogenesis in the CAM[407], it was included as a pro-angiogenic control. $VEGF_{165}$ (100ng) was incorporated into hydrogel discs, as previous work has reported that a tenth of this amount can elicit a strong angiogenic effect[407], thus ensuring that an effect would be observed in the present study. As an anti-angiogenic control, suramin (500μg) was added to a 50μl hydrogel, as this level had been previously shown to inhibit angiogenesis[405].

Windows were cut into the shells of chicken eggs at developmental day 3, and re-sealed with sellotape®. The hydrogels were added onto the CAMs at day 7 of development and angiogenesis assessed at developmental day 10, as illustrated in Figure 5.1. Eight hydrogels for each variable were placed on the corresponding number of CAMs. An additional 8 CAMs did not receive any hydrogels, to detect any potential effects of the hydrogels themselves. Figure 5.2 shows an example from each group.

As, expected, there was an increase in general blood vessel diameter over the three days and the hydrogel itself did not affect the blood vessel formation. $VEGF_{165}$-containing hydrogels did not produce an observable angiogenic effect in any of the 8 eggs and consequently failed as a positive control. However, the clouding of the hydrogel in Figure 5.2 implies that there was a biological response to VEGF. Perhaps the concentration was too high to elicit a recognisable angiogenic response. However, 2 of the 8 CAMs treated with suramin-containing hydrogels contained a ring around the hydrogel, which was absent in new blood vessel growth, just visible in Figure 5.2. No such ring formed around the hydrogels with flt-1(1-3), indicating that no inhibition of angiogenesis occurred. In addition, there is no difference between the flt-1(1-3) and WT preparation responses. The HAED hydrogels did not appear to influence angiogenesis. However, as VEGF did not produce an angiogenic effect, further experimentation is required to assess any influence the hydrogels may have on angiogenesis.

The movement of the embryo within each egg caused distortions in the CAM and caused the hydrogel to shift from its original position on the membrane. These factors made comparisons of blood vessel formation, between eggs and from day 7 to day 10 difficult. Furthermore, histological examination of the hydrogels showed no blood vessel invasion into the biomaterials (data not shown).

In summary, the CAM assay demonstrated that:

- The HAED hydrogels can deliver active agents that influence angiogenesis.
- The concentration of flt-1(1-3) used in this study did not effect angiogenesis.

Table 5.1: Hydrogels with test samples investigated in the CAM assay. Compounds were incorporated immediately prior to crosslinking of the hydrogel.

Test sample	Final amount in each 50µl hydrogel
$VEGF_{165}$	100ng
Suramin	500µg
Flt-1(1-3) preparation	2.3ng flt-1 and flt-1(1-3) (in 2.74µg total protein)
WT preparation	0.02ng flt-1 (in 2.74µg total protein)

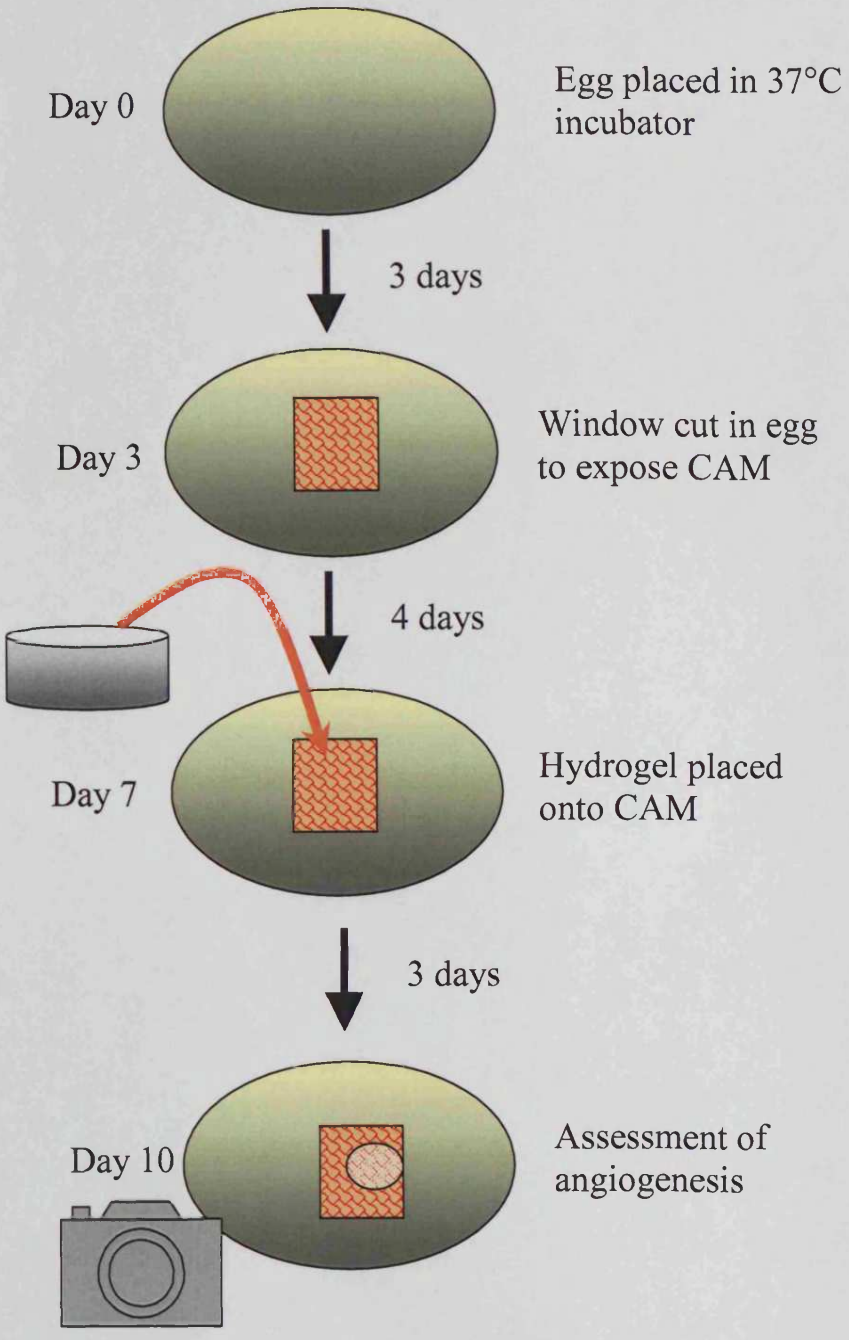

Figure 5.1: Schematic diagram of the CAM assay.

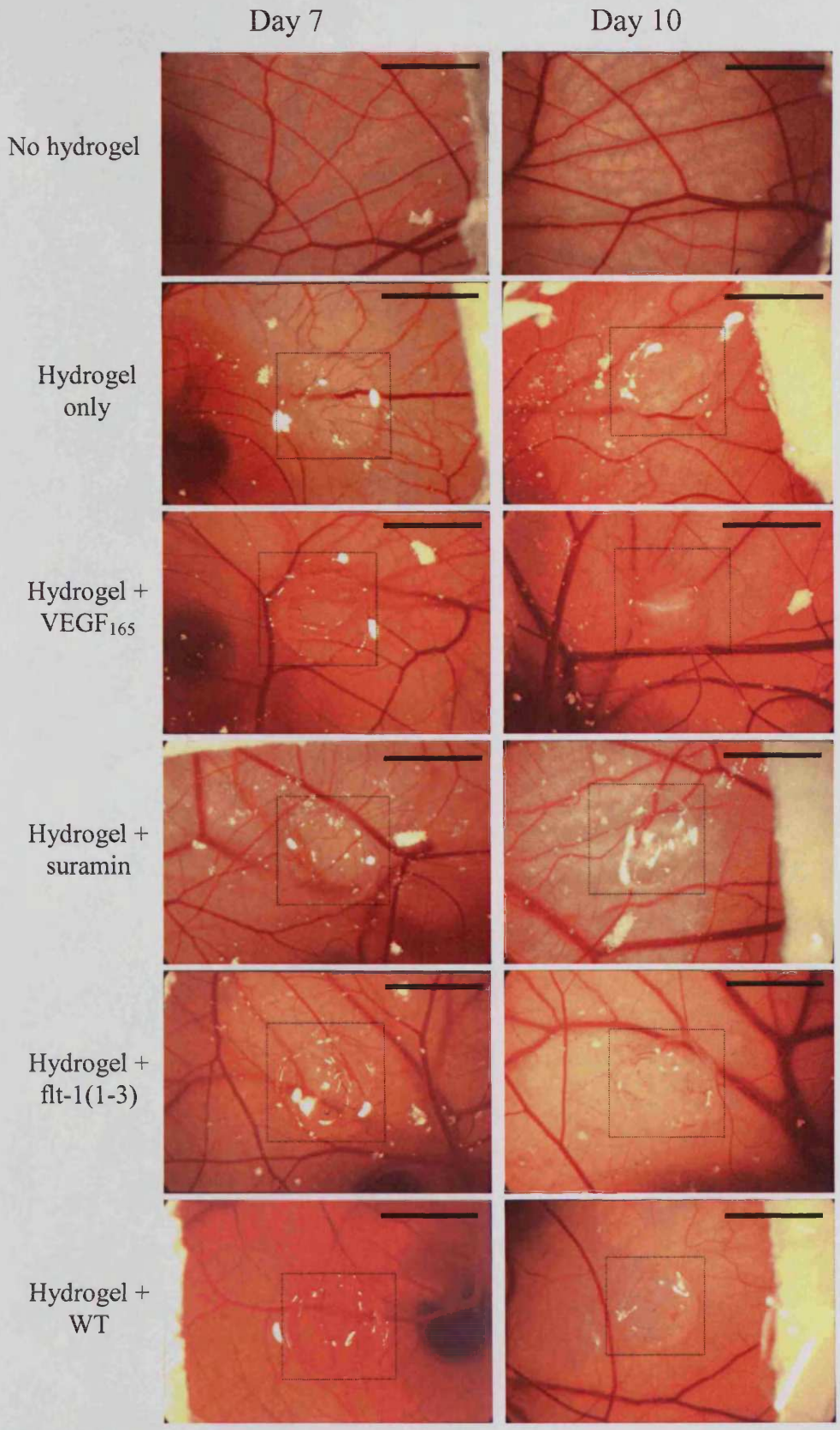

Figure 5.2: Chick chorioallantoic membranes at developmental days 7 and 10 in the same eggs. HAED hydrogels containing one or none of the factors listed in Table 5.1 were added on day 7 (left images) and changes in angiogenesis assessed at day 10 (right images). A box surrounds the position of each hydrogel to aid visualisation. With the addition of suramin there is a reduction in small blood vessels around the hydrogel. No other changes, compared to the absence of hydrogel, were observed. Scale bars = 5mm

5.2.2. Foetal rat metatarsal bone formation assay

5.2.2.1. Preparation of test materials

This assay was used to assess any potential chondrogenic and anti-osteogenic effects of flt-1(1-3). Due to time constraints, this assay could only be carried out once. Flt-1(1-3) was partially purified as described in Chapter 4. To take into account impurities in the test sample, a parallel sample was prepared from non-transfected WT 293 EBNA fibroblasts, which was expected to have an identical protein content when used at the same total protein concentration, but with no flt-1(1-3).

Hydrogels were prepared in the same manner as those for the CAM assays, to a final concentration of 9mg/ml HAED, 1:1 SPA_4-PEG (20kDa) to HAED ratio, with no collagen added. The factors listed in Table 5.2 were added. The VEGF concentration in hydrogel 2 was the highest quantity that could be incorporated for such a small volume, when following the supplier's instructions, regarding resuspension of the lyophilised compound provided. The lower level of VEGF in one of the hydrogels served as a comparison for hydrogels with flt-1(1-3) or WT preparations. The suramin quantity used was previously reported to inhibit angiogenesis[405]. The soluble flt-1 standard was comprised of the 7 Ig-like extracellular regions of flt-1, was obtained from the supplier of the immunoassay kit that had been used to determine flt-1 concentration. This was included as an additional control and the low level was incorporated due to availability.

5.2.2.2. Preparation of metatarsals

The central 3 metatarsals were dissected from rat foetuses 19 days after conception and were kept in their groups of 3 upon placement onto the hydrogel discs. There were between 13 and 18 metatarsals per treatment group listed in Table 5.2, as some metatarsals were damaged during handling. The metatarsals were cultured and assessed after 3 and 7 days.

Western blotting was carried out on the metatarsal culture medium at day 7 and no flt-1(1-3), nor VEGF, was detected. This indicated that the concentration of any factor that may have been released from the hydrogel was too low to detect.

Table 5.2: Hydrogels with test samples investigated in the rat metatarsal bone formation assay. Samples were incorporated immediately prior to crosslinking of the hydrogel.

Test sample	Final amount in 50µl hydrogel
VEGF	100ng
Flt-1(1-3)	8.02ng flt-1 and flt-1(1-3) (12.14µg total protein)
VEGF + Flt-1(1-3)	27.8ng VEGF and 8.02ng flt-1 and flt-1(1-3) (12.14µg total protein in flt-1(1-3) preparation)
Suramin	500µg
WT control	0.01ng flt-1 (12.14µg total protein)
VEGF + WT control	25ng VEGF 0.01ng flt-1 (12.14µg total protein in WT preparation)
Soluble flt-1 standard	0.2ng
VEGF	27.8ng

5.2.2.3. Observations and measurement of calcified zone

The length of calcified zone in the centre of each metatarsal was measured using image analysis software, at these time points and assessed for signs of change. Figure 5.3 illustrates the metatarsals over the 7 days. The calcified zone is visible as a band in the centre of each metatarsal. At day 7, the paler zones either side of the calcified zone show expansion following VEGF treatment and the hydrogel alone, but no such expansion in the metatarsals treated with partially purified conditioned medium (ie. flt-1(1-3) and WT). This indicated an overall arrest in growth of the metatarsal. The measurement of the calcified zone provided an indication as to the extent of endochondral ossification. In some cases the calcified zone had shrunk by day 3, to increase again by day 7, as observed in Figure 5.4. This phenomenon has been observed by other workers in the laboratory of Smith & Nephew, although the precise reason for this remains unknown. In metatarsals treated with hydrogel 5 (suramin), swelling of the epiphysis region of the metatarsal was observed, with the calcified zone appearing 'pinched'. This phenomenon could have influenced the calcified zone length by constricting expansion and is discussed in Section 5.3.

Statistical analysis

The paired T-test was selected to test for significant changes in calcified zone length from day 0 to days 3 and 7 of each metatarsal (Appendix 6). Figure 5.4 shows the changes in calcified zone length over 3 and 7 days. Over 7 days, hydrogels containing suramin and the WT control demonstrated a significant reduction in calcified zone length. The WT control with VEGF showed an increase. Although the hydrogels with flt-1(1-3) and flt-1(1-3) with VEGF initially exhibited a decrease in calcified zone length, this difference had disappeared by day 7. The increase in calcified zone length with the WT control and VEGF did not appear to be caused solely by VEGF, as the VEGF (100ng) control did not cause a statistically significant increase in calcification. The decrease in calcified zone length from the suramin–containing hydrogel was accompanied by swelling of the cartilaginous regions towards the ends of the metatarsal, which appeared to be increased by suramin.

The percentage change in calcified length in response to hydrogels from the treatment groups, compared to that of the hydrogel only, was statistically analysed using the

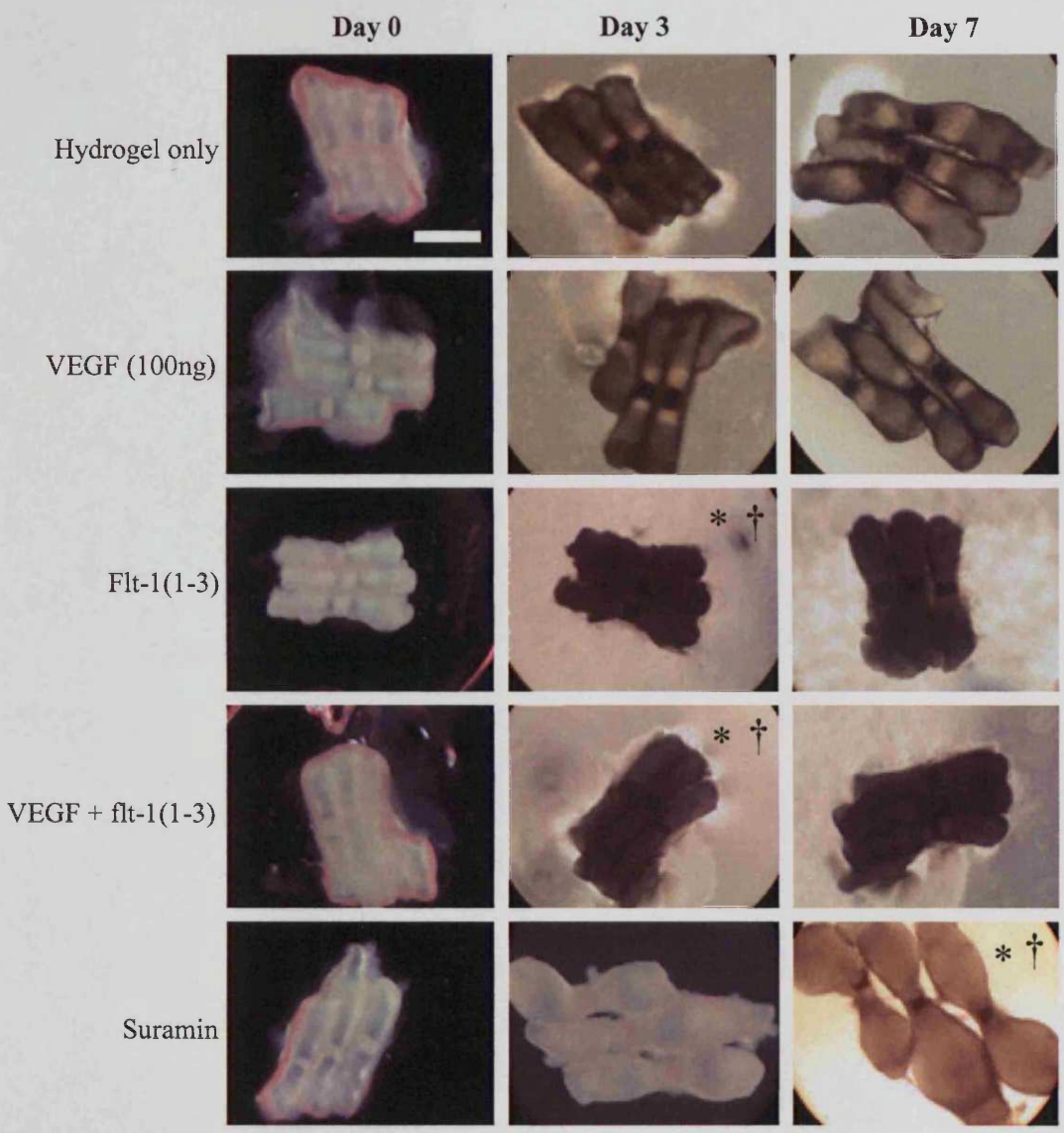

Figure 5.3: The central 3 metatarsals dissected from rat foetuses at developmental day 19. Day 0: immediately after removal. Days 3, 7: after spending 3 or 7 days on a hydrogel disc containing the factors listed in Table 1. The pale pink/white band (with dark image background) or dark band (with pale image background) in the centre of each metatarsal is the calcified zone, the length of which was measured. * = A significant difference in the length of the calcified zone compared to the metatarsals from the same treatment group at day 0. † = A significant difference in the change of calcified zone length compared to the 'hydrogel only' control over the same time period. These are illustrated graphically in Figure 5.4. The different colours were caused by different illumination settings and did not affect the results. Scale bar = 1mm. (Continued on next page.)

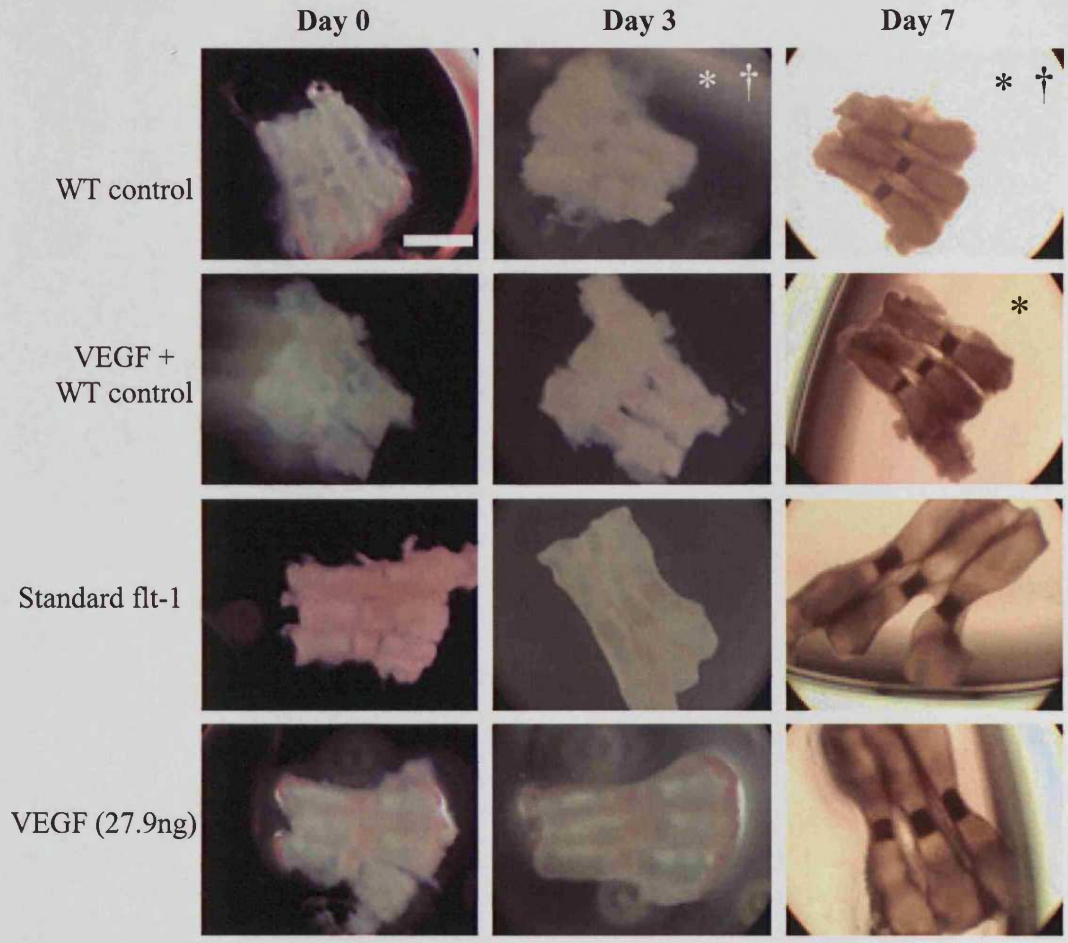

(Figure 5.3 continued)

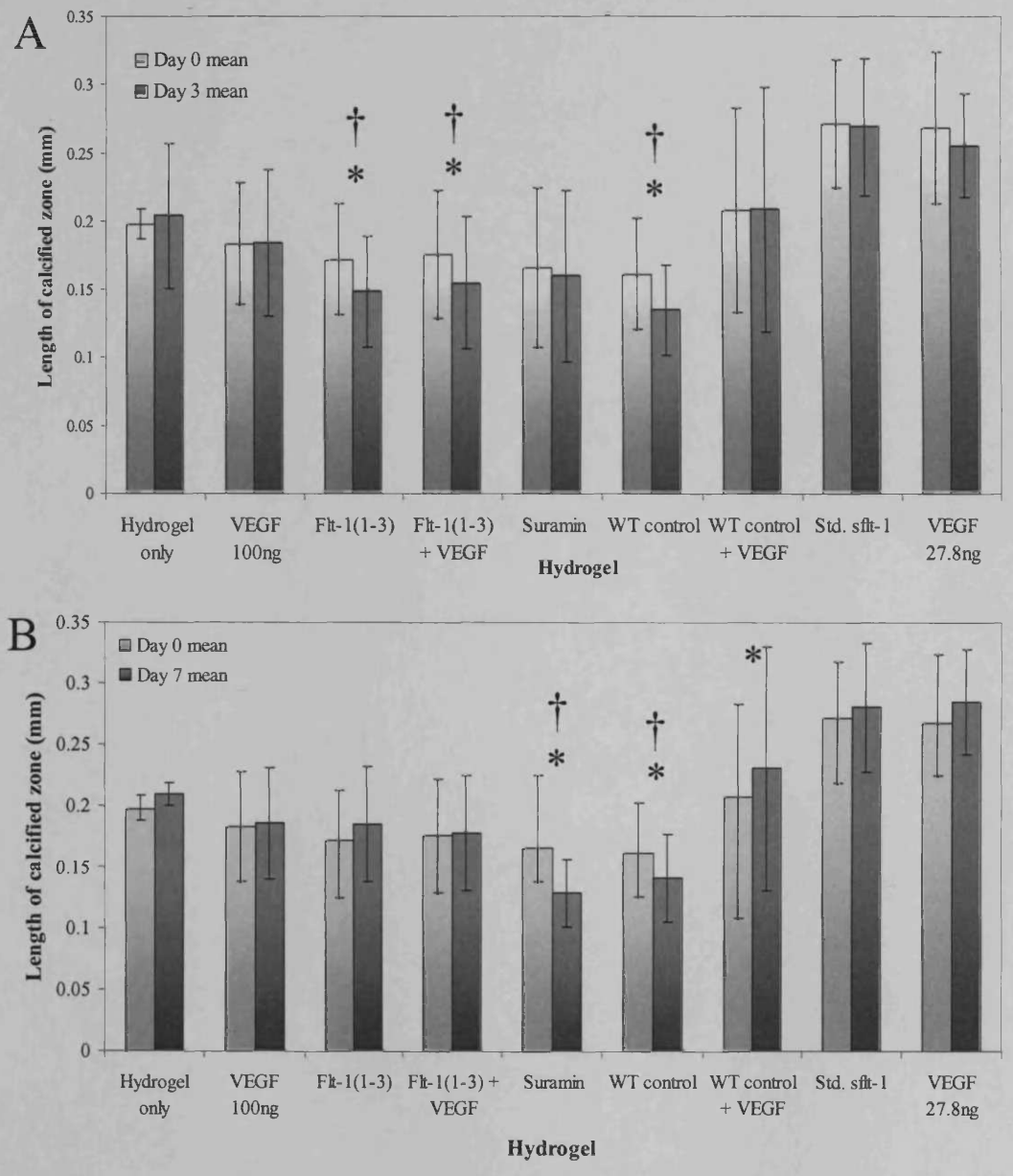

Figure 5.4: The lengths of the calcified zones in foetal rat metatarsals before and 3 days (A) or 7 days (B) after incubation with HAED-based hydrogels containing the factors listed in Table 5.2. The error bars represent the standard deviation. * = A significant difference in the length of the calcified zone of metatarsals compared to those from the same treatment group at day 0, determined by the paired T-test ($p<0.05$). † = A significant difference in the change in length of calcified zones compared to the 'hydrogel only' control over the same time period, determined by the non-paired T-test ($p<0.05$).

non-paired T-test (Appendix 6). Figure 5.4A shows that although flt-1(1-3) treatment showed an initial decrease in metatarsal length, only suramin and the WT control demonstrated a decrease over 7 days (Figure 5.4B).

5.2.2.4. Haematoxylin & Eosin staining and Immunolabelling of metatarsals

The most intact metatarsals from each treatment group were paraffin wax embedded after day 7, followed by sectioning and immunostaining. Haematoxylin and Eosin (H & E) staining gave an overview of the differentiation stages of chondrocytes within the metatarsals and the calcified hypertrophic zone, which is macroscopically visible (Figure 5.5). Immunostaining was carried out using a polyclonal antibody raised against von Willebrand Factor (vWF), a plasma glycoprotein[21]. Positive staining would highlight the presence of blood vessels, illustrated by a brown stain. The tissue was counterstained with methyl green to visualise cell nuclei. The presence of blood vessels in the perichondrium was revealed by brown staining. This confirmed that the staining was specific, as this membrane is known to be vascularised[120]. Interestingly, positive vWF staining is evident around the hypertrophic chondrocytes, although blood vessels are not visible in this zone. Metatarsals treated with no bioactive agents and VEGF (27.8ng) demonstrated bone growth (Figure 5.5A and F). Angiogenesis appears to be further advanced following VEGF treatment, indicated by vascular invasion into the primary ossification centre and more intense staining in Figure 5.11. This is accompanied by early signs of trabicular bone formation (Figure 5.5F). These observations are consistent with the measurements of the calcified zone, which demonstrated a slight (albeit not statistically significant) increase in bone formation (Figure 5.4). Moreover, the metatarsal treated with VEGF demonstrates putative secondary ossification of the epiphyseal regions, indicated by the areas of brown staining around hypertrophic chondrocytes (Figure 5.11). Interestingly, the metatarsal treated with 100ng VEGF did not show such a pronounced response as that treated with the lower amount of VEGF (Figure 5.12). However, sections of the whole metatarsal would need to be studied to verify this.

In contrast, the metatarsals incubated on hydrogels containing flt-1(1-3) or the WT control did not show expansion of the hypertrophic zone towards the epiphyseal regions, nor progressive ossification (Figures 5.5B-E, 5.7-5.10). Furthermore, vWF labelling was limited to the hypertrophic region in these metatarsals, indicating that

there was no metatarsal growth. The presence of VEGF did not counteract this effect (Figures 5.8 and 5.10). The flattened chondrocytes in columns evident in metatarsals treated with VEGF or the hydrogel only were not as organised in the samples treated with conditioned medium. These observations could not be attributed to flt-1(1-3), as they occurred in the metatarsal treated with the WT control (Figure 5.9), suggesting that other factors in the preparation may have been involved. The addition of the soluble flt-1 standard to a hydrogel did not prevent endochondral ossification, as bone formation is apparent in Figures 5.5H and 5.13. However, the hypertrophic zone did not spread outwards to the same extent as that of the metatarsal incubated on a hydrogel containing no agents, suggesting a soluble flt-1-mediated effect. Figure 5.14 shows that suramin severely disrupted the cellular and structural organisation of the metatarsal, with only the calcified hypertrophic zone retaining an identifiable structure (Figures 5.5I and 5.14). It is likely that these cells were already hypertrophic at the point of dissection (day 0). No intense vWF labelling was present outside the hypertrophic zone. This suggests that suramin at this concentration compromises chondrocyte viability.

The effects of VEGF and suramin on the metatarsals demonstrated that the HAED hydrogels could deliver these agents without compromising their activity. As the agents were not anchored into the matrix, they may have slowly diffused out to elicit a biological effect. Moreover, the hydrogels did not degrade or dissolve after 7 days in culture medium. A technique to assess the diffusion of agents out of the hydrogels is discussed in Chapter 6.

In summary, the foetal rat metatarsal assay revealed that:

- VEGF stimulated endochondral ossification.
- The preparations from 293 EBNA fibroblasts, purified by heparin affinity chromatography, had the ability to prevent further metatarsal growth, possibly through an anti-angiogenic mechanism, although it was doubtful that this was mediated by flt-1(1-3).
- The HAED hydrogels released bioactive factors, to induce a biological response.

Hydrogel with no bioactive agent

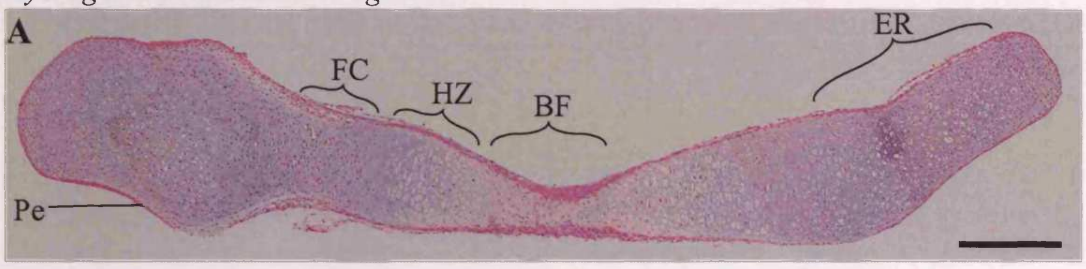

Hydrogel with flt-1(1-3)

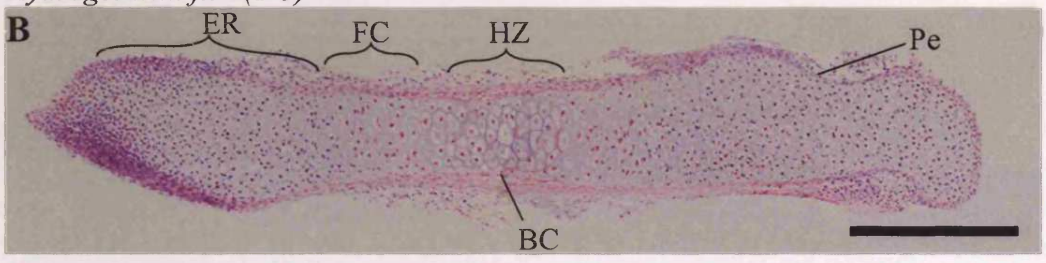

Hydrogel with flt-1(1-3) and VEGF

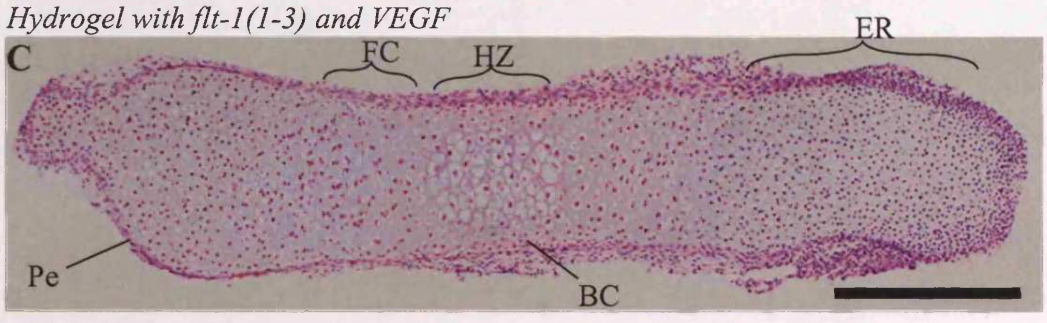

Hydrogel with WT control

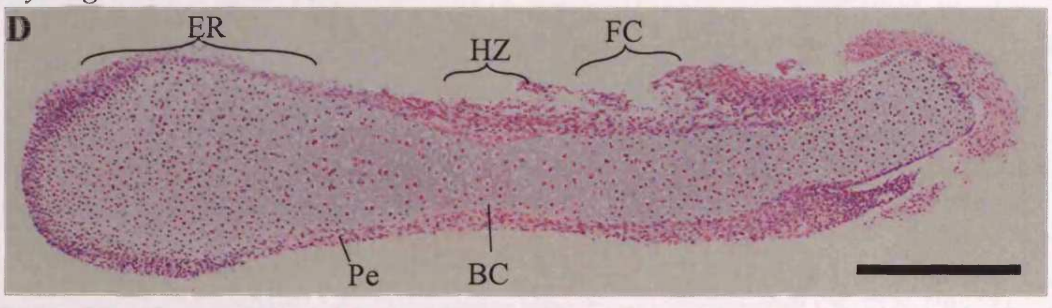

Figure 5.5: Haematoxylin and Eosin staining of foetal rat metatarsals explanted at day 19 after conception and cultured on HAED hydrogels (each of which contained one of the test samples listed in Table 5.2) for 7 days, followed by fixation and embedding in paraffin wax. Parts G and H show half metatarsals. BF: bone formation, BC: bone collar, HZ: hypertrophic zone, FC: flattened chondrocyte zone, ER: epiphyseal region, with most proliferation, Pe: perichondrium. A decrease in ossification, progression of hypertrophy and proliferation are evident in metatarsals cultured on hydrogels containing the flt-1(1-3) and WT control preparations. Scale bars = 300μm. (Continued on the next page.)

Hydrogel with WT control and VEGF

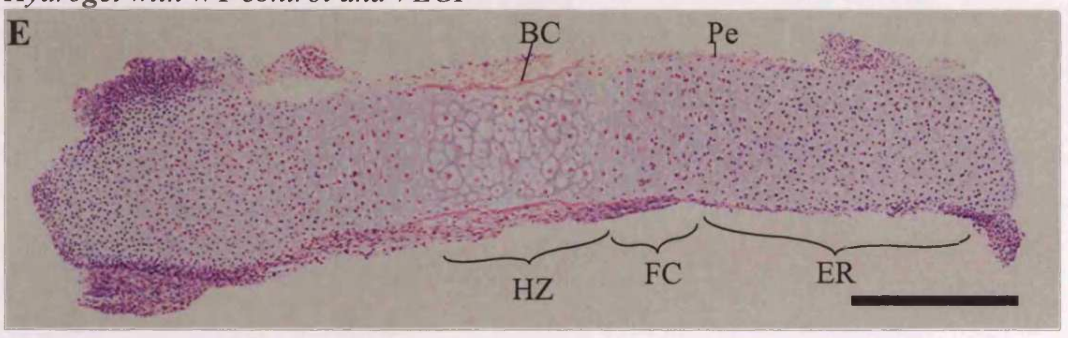

Hydrogel with VEGF (27.8ng)

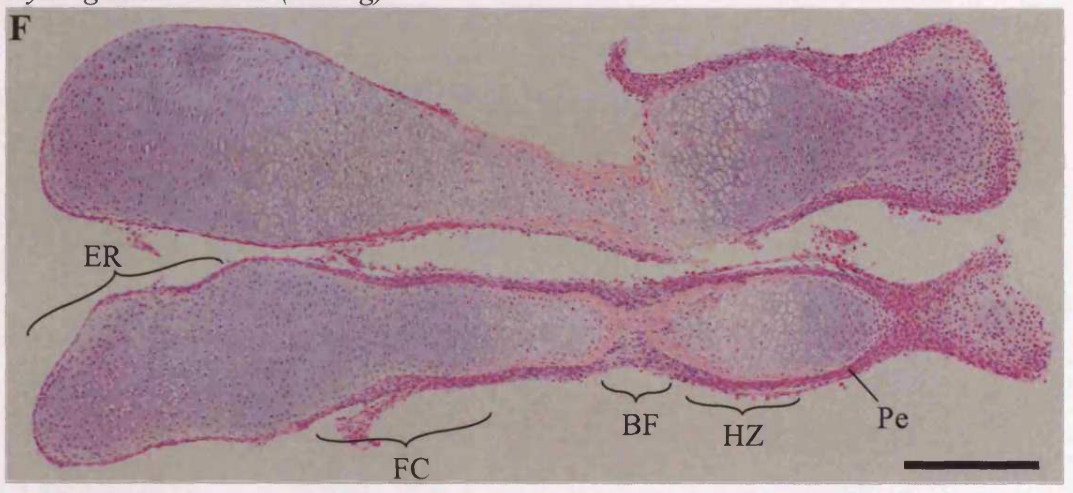

Hydrogel with VEGF (100ng)

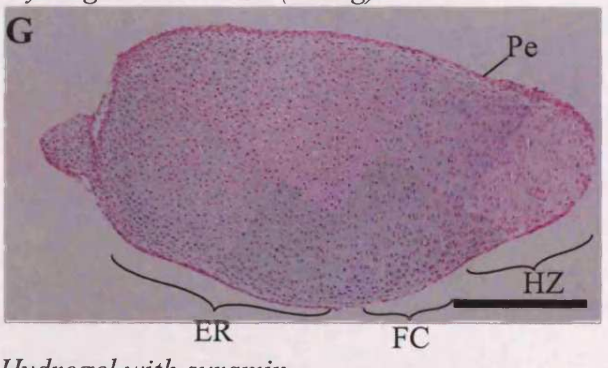

Hydrogel with soluble flt-1

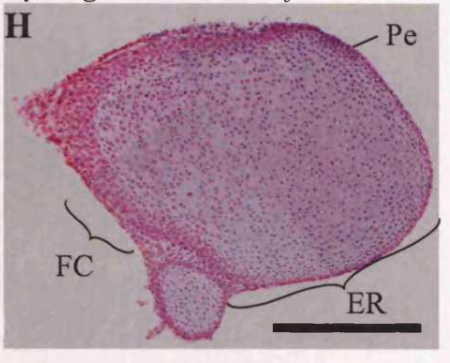

Hydrogel with suramin

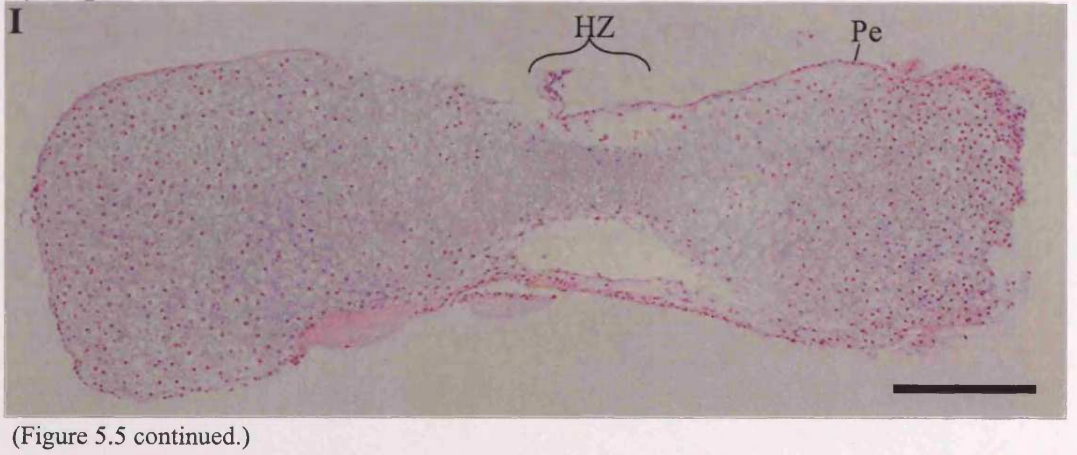

(Figure 5.5 continued.)

Hydrogel with no bioactive agents

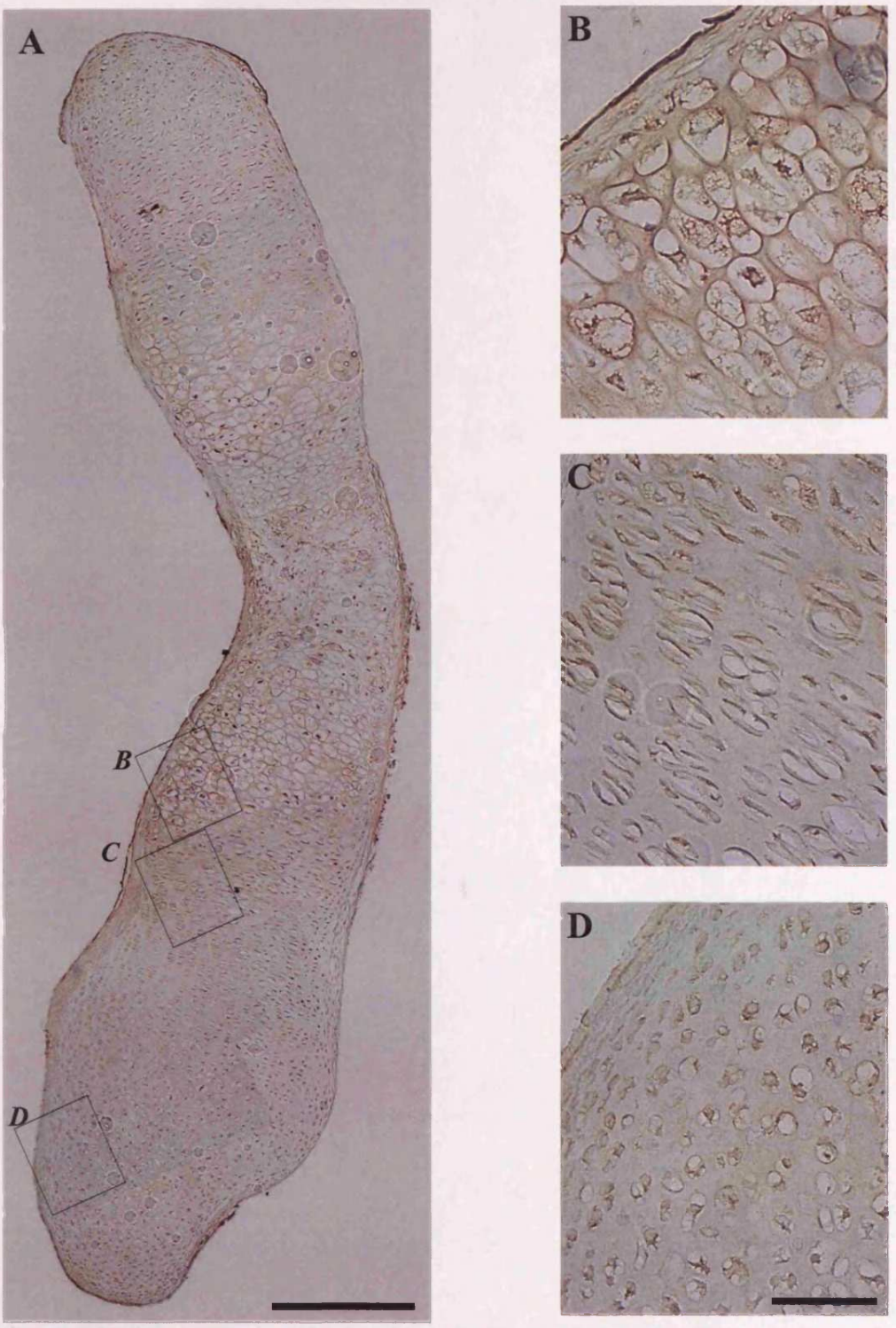

Figure 5.6: Immunostaining of a foetal rat metatarsal with anti-von Willebrand Factor (brown), counterstained with methyl green. The metatarsal was cultured for 7 days on a hydrogel that did not contain any additional substances. Selected areas of the hypertrophic zone (B), proliferating zone (C) and epiphyseal region (D) are shown at a higher magnification. The zones formed during endochondral ossification are illustrated in the corresponding image in Figure 5.5A. Scale bars = 300μm (A) and 50μm (B-D).

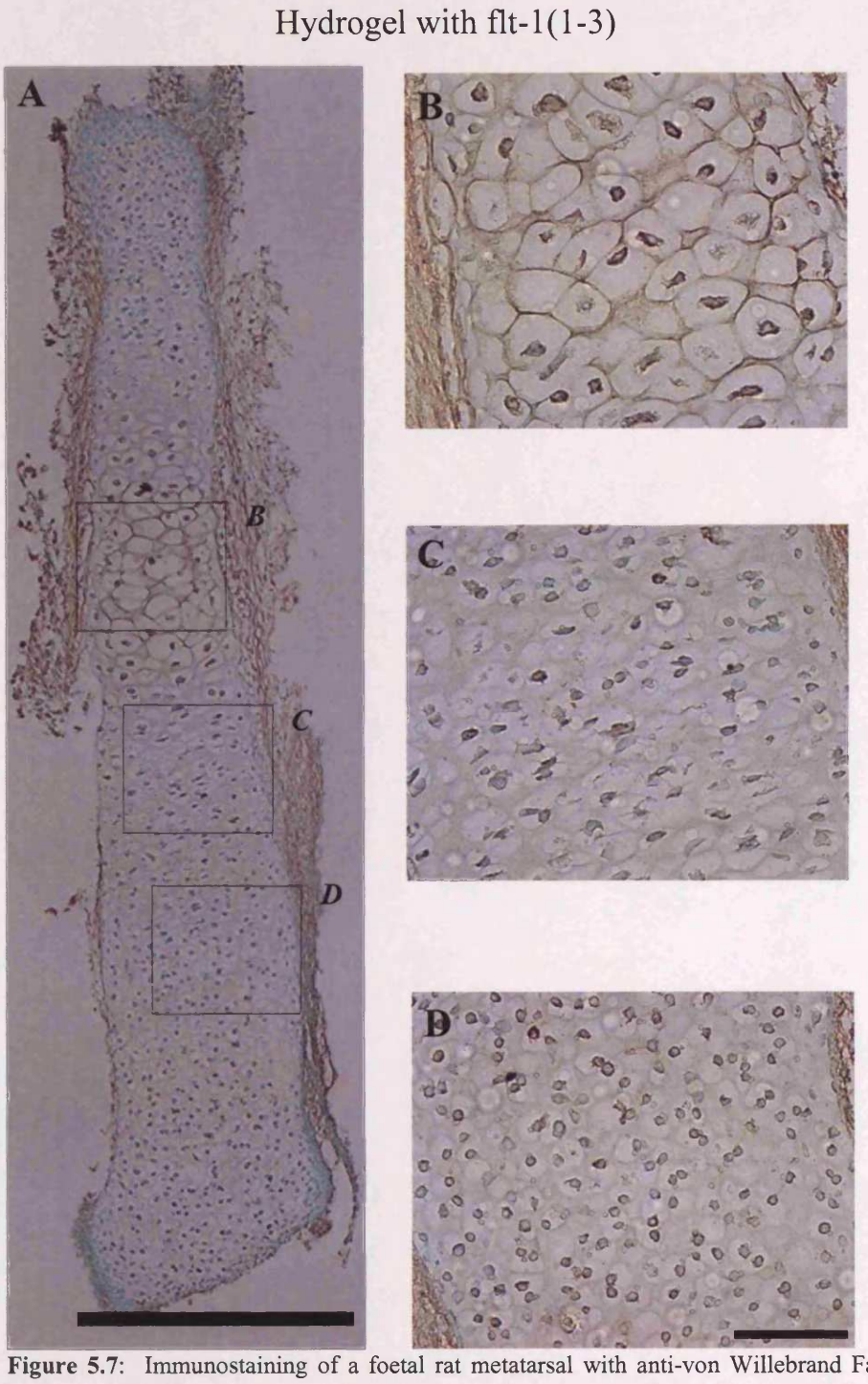

Figure 5.7: Immunostaining of a foetal rat metatarsal with anti-von Willebrand Factor (brown), counterstained with methyl green. The metatarsal was cultured for 7 days on a hydrogel containing flt-1(1-3) (8.02ng). Selected areas of the hypertrophic zone (B), proliferating zone (C) and epiphyseal region (D) are shown at a higher magnification. The zones formed during endochondral ossification are illustrated in the corresponding image in Figure 5.5B. Scale bars = 300μm (A) and 50μm (B-D).

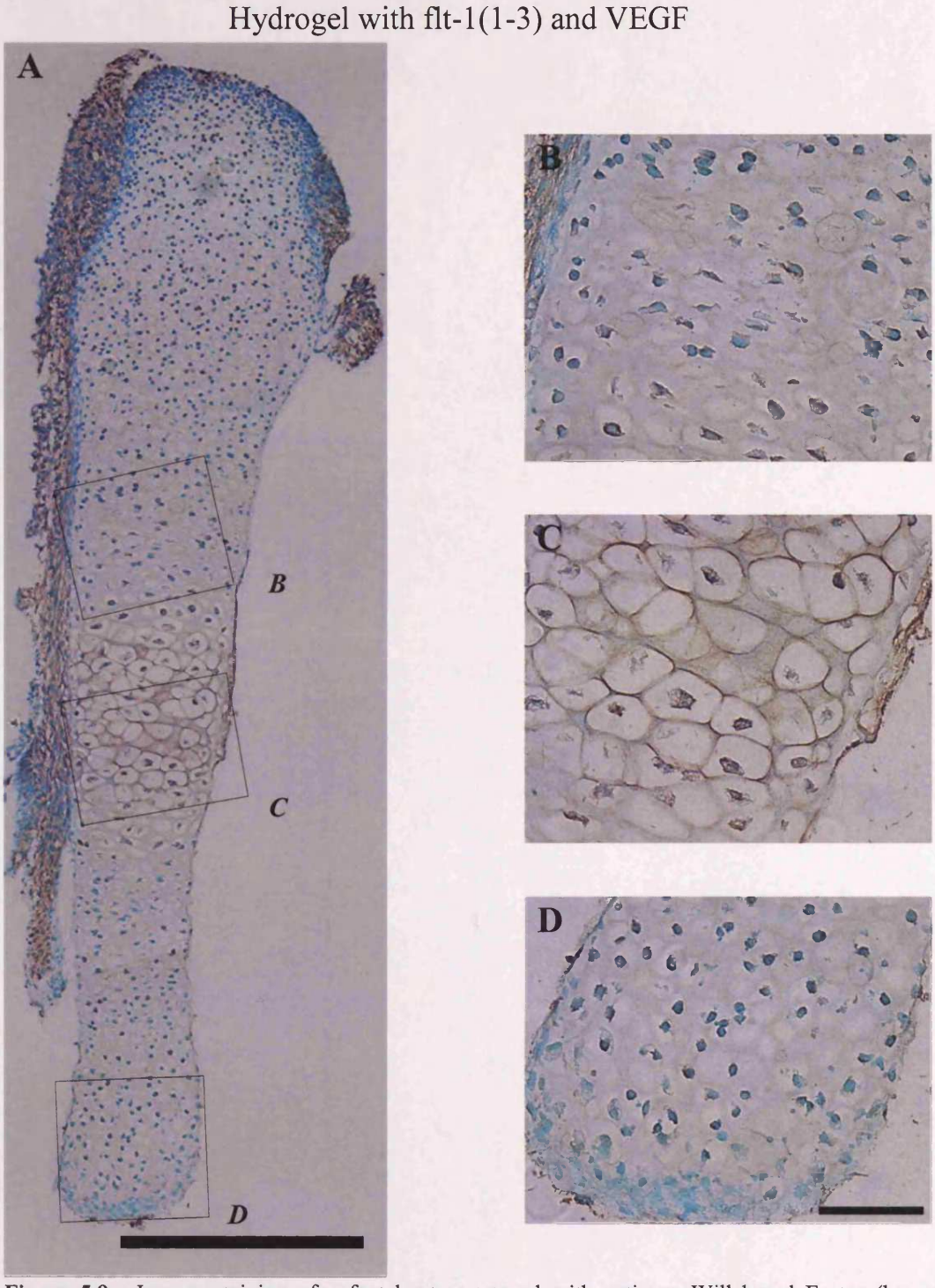

Figure 5.8: Immunostaining of a foetal rat metatarsal with anti-von Willebrand Factor (brown), counterstained with methyl green. The metatarsal was cultured for 7 days on a hydrogel containing flt-1(1-3) (8.02ng) and VEGF (27.8ng). Selected areas of the proliferating zone (B), hypertrophic zone (C) and epiphyseal region (D) are shown at a higher magnification. The zones formed during endochondral ossification are illustrated in the corresponding image in Figure 5.5C. Scale bars = 300μm (A) and 50μm (B-D).

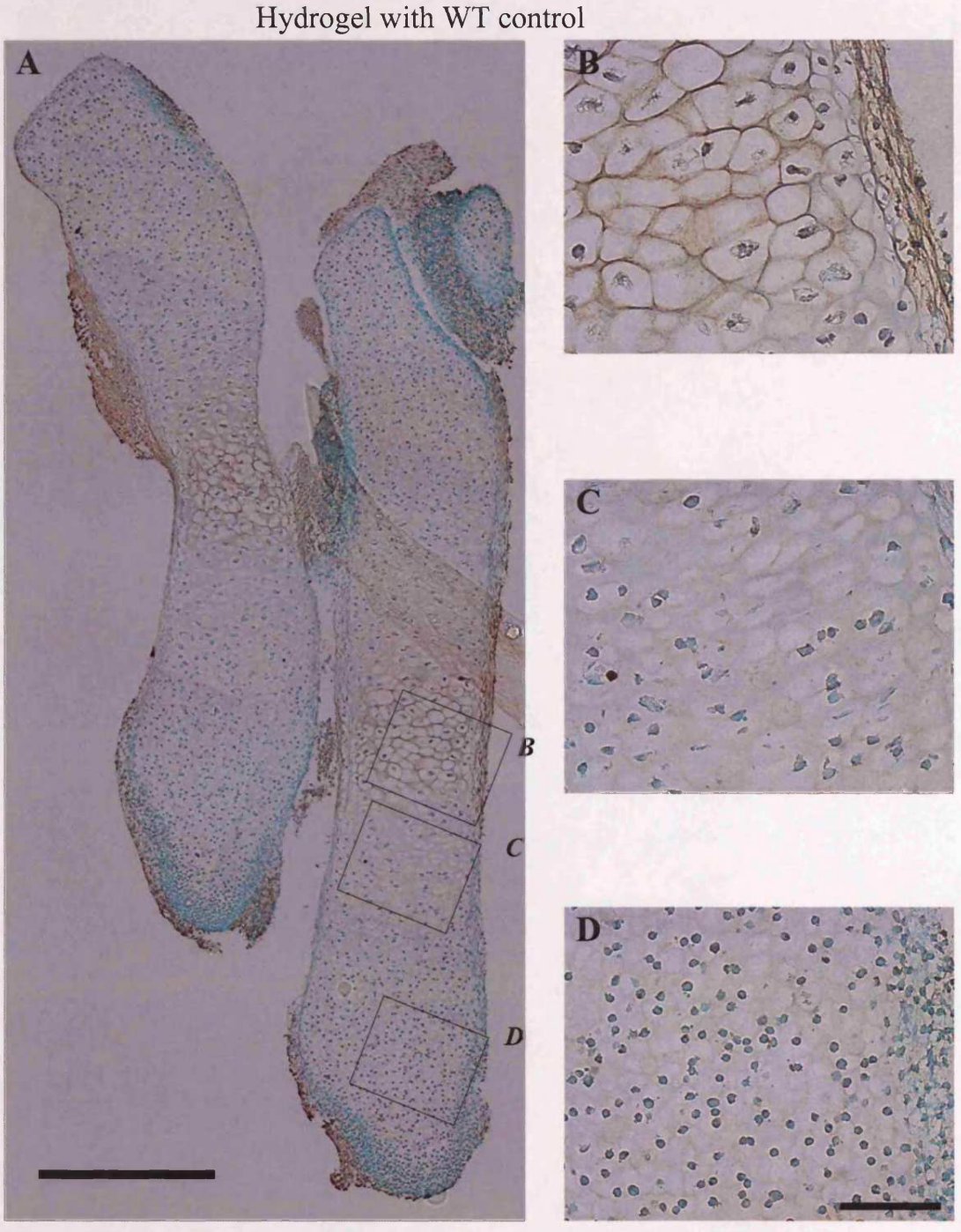

Figure 5.9: Immunostaining of foetal rat metatarsals with anti-von Willebrand Factor (brown), counterstained with methyl green. The metatarsals were cultured for 7 days on a hydrogel containing the WT control (0.01ng flt-1(1-3)). Selected areas of the hypertrophic zone (B), proliferating zone (C) and epiphyseal region (D) are shown at a higher magnification. The zones formed during endochondral ossification are illustrated in the corresponding image in Figure 5.5D. Scale bars = 300μm (A) and 50μm (B-D).

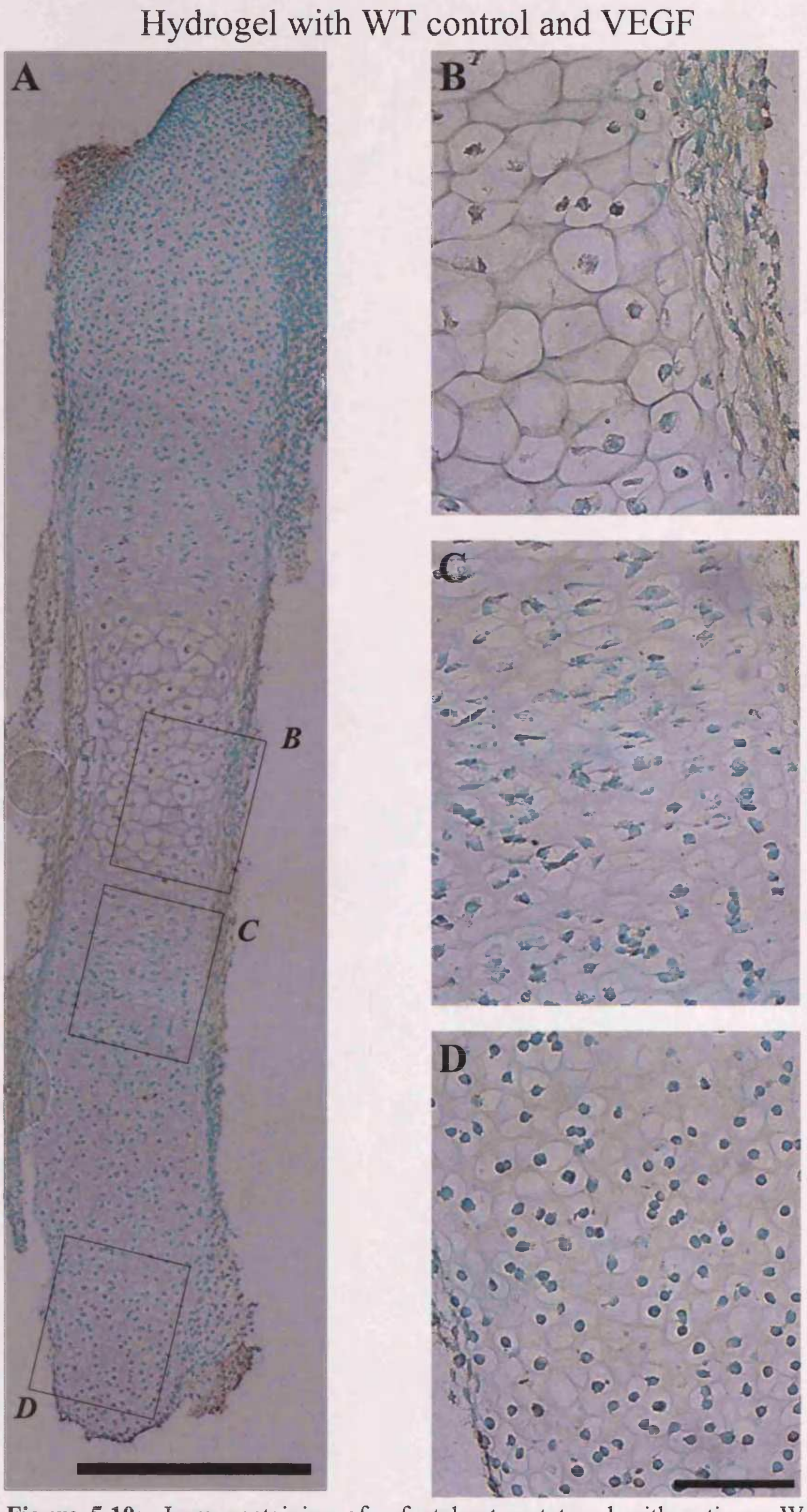

Figure 5.10: Immunostaining of a foetal rat metatarsal with anti-von Willebrand Factor (brown), counterstained with methyl green. The metatarsal was cultured for 7 days on a hydrogel containing the WT control (0.01ng flt-1(1-3)) and VEGF (27.8ng). Selected areas of the hypertrophic zone (B), proliferating zone (C) and epiphyseal region (D) are shown at a higher magnification. The zones formed during endochondral ossification are illustrated in the corresponding image in Figure 5.5E. Scale bars = 300μm (A) and 50μm (B-D).

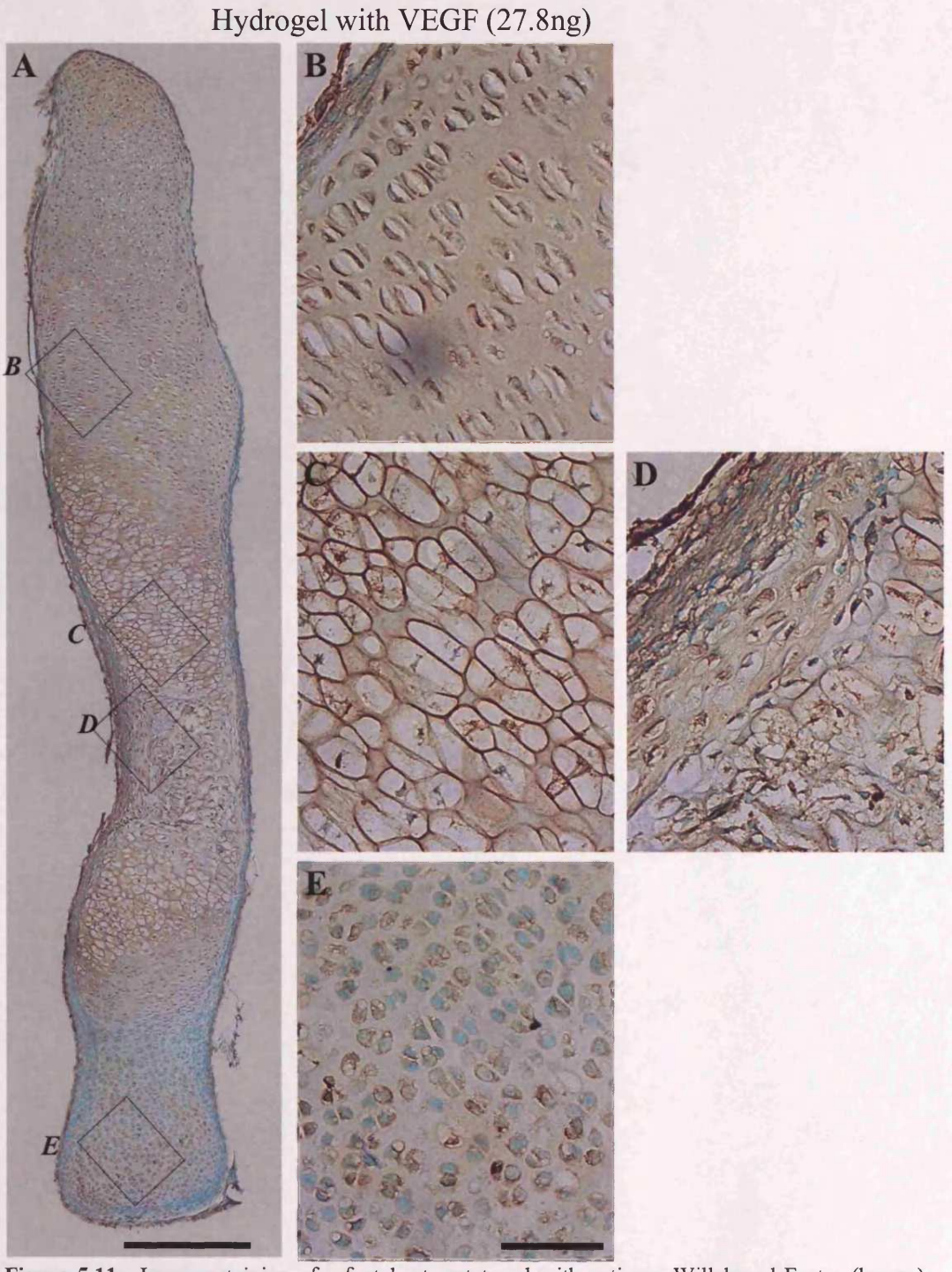

Figure 5.11: Immunostaining of a foetal rat metatarsal with anti-von Willebrand Factor (brown), counterstained with methyl green. The metatarsal was cultured for 7 days on a hydrogel containing VEGF (27.8ng). Selected areas of the proliferating zone (B), hypertrophic zone (C), bone collar (D) and epiphyseal region (E) are shown at a higher magnification. The zones formed during endochondral ossification are illustrated in the corresponding image in Figure 5.5F. Scale bars = 300μm (A) and 50μm (B-E).

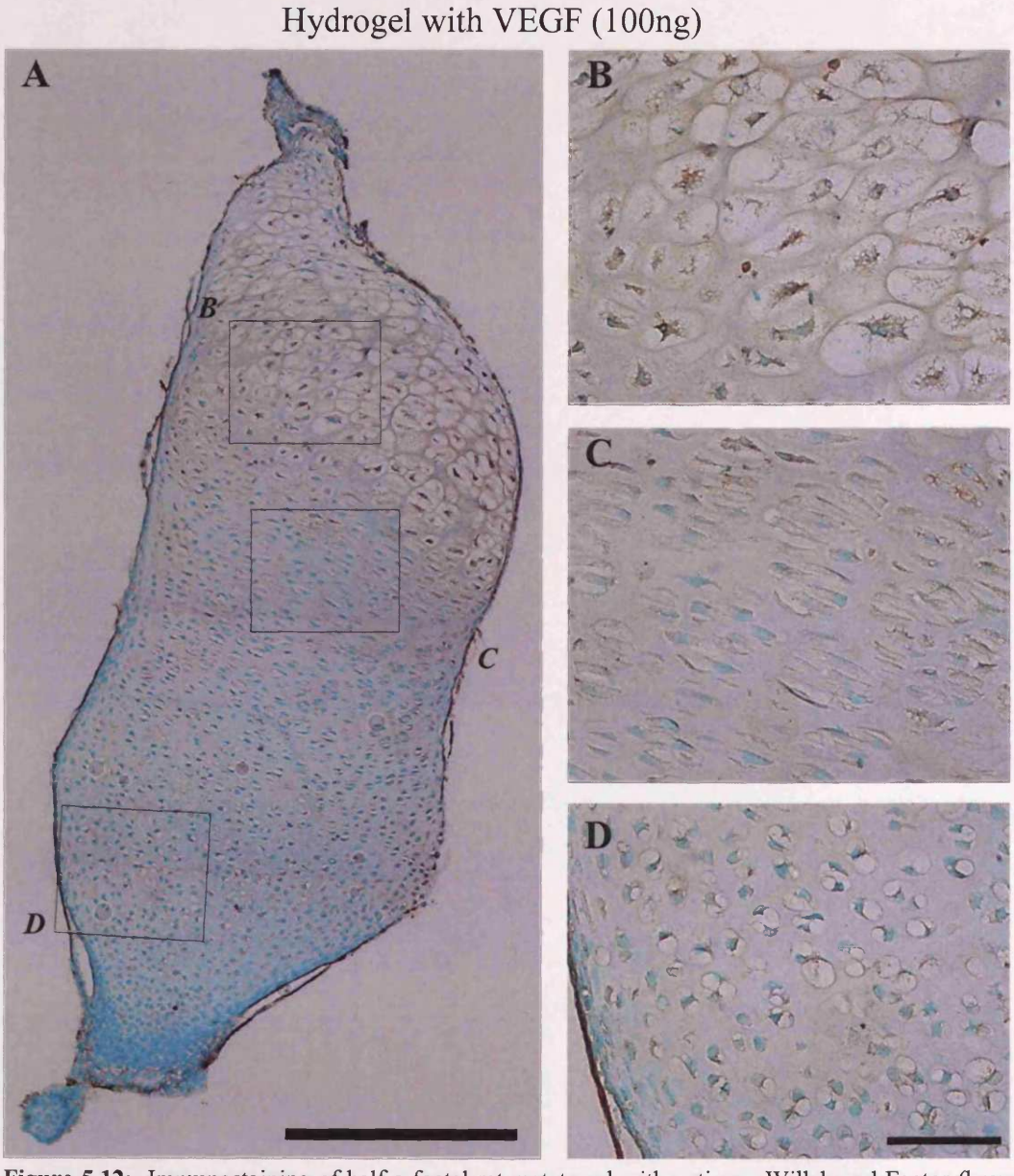

Figure 5.12: Immunostaining of half a foetal rat metatarsal with anti-von Willebrand Factor (brown), counterstained with methyl green. The metatarsal was cultured for 7 days on a hydrogel containing VEGF (100ng). Selected areas of the hypertrophic zone (B), proliferating zone (C) and epiphyseal region (D) are shown at a higher magnification. The zones formed during endochondral ossification are illustrated in the corresponding image in Figure 5.5G. Scale bars = 300μm (A) and 50μm (B-D).

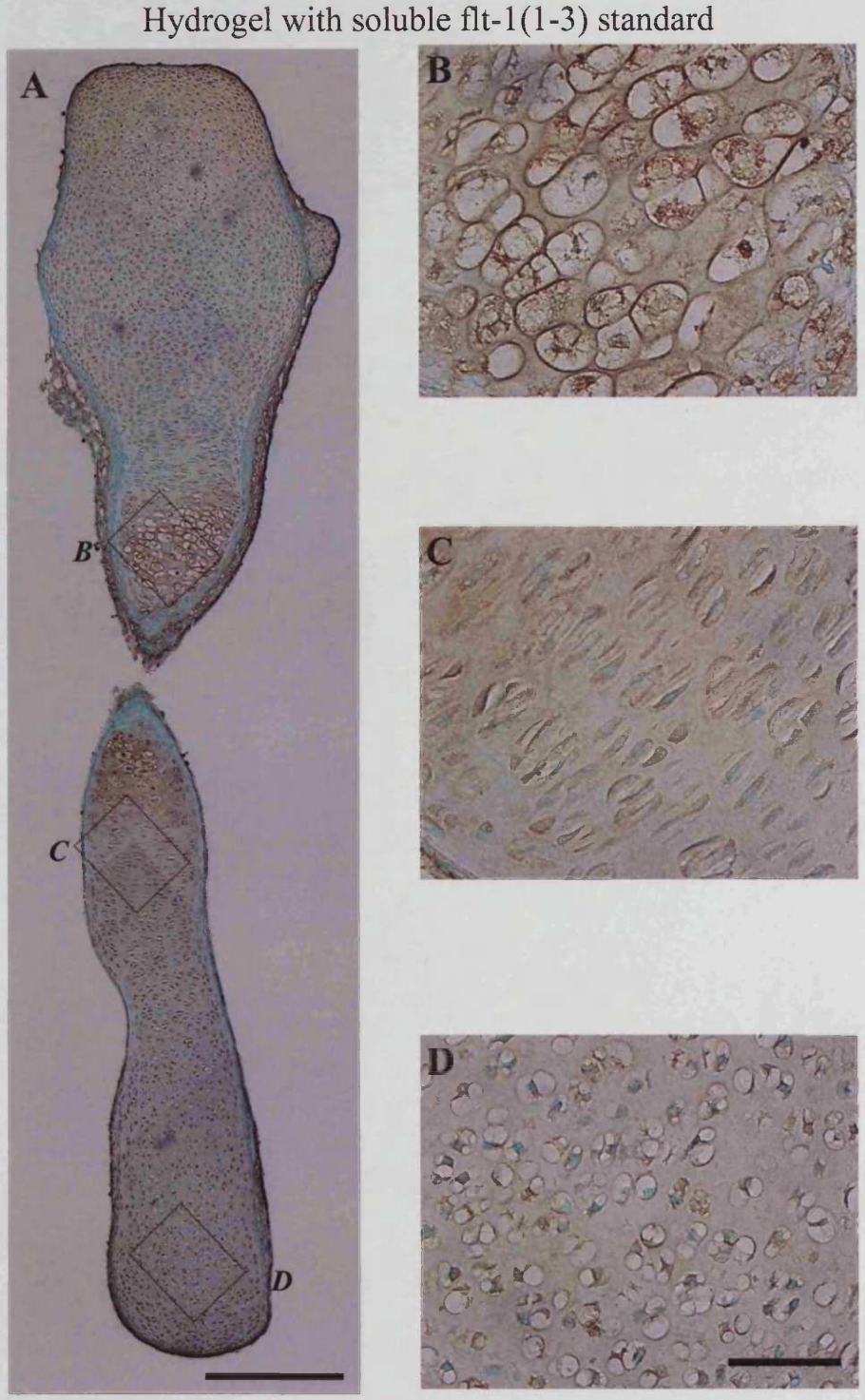

Figure 5.13: Immunostaining of a foetal rat metatarsal with anti-von Willebrand Factor (brown), counterstained with methyl green. The metatarsal was cultured for 7 days on a hydrogel containing the soluble flt-1 standard (0.2ng). Selected areas of the hypertrophic zone (B), proliferating zone (C) and epiphyseal region (D) are shown at a higher magnification. The zones formed during endochondral ossification are illustrated in the corresponding image in Figure 5.5H. Scale bars = 300μm (A) and 50μm (B-D).

assess this and is discussed in Chapter 6. VEGF has been reported to induce angiogenesis in the CAM assay at levels of 200ng (via Sephadex G-200 beads[230]) or by drying 10ng of VEGF onto a cover slip, which was subsequently placed on the CAM[267]. This cover slip approach could be applied to the application of flt-1(1-3) alone to assess anti-angiogenic properties.

There was no noticeable difference between hydrogels containing flt-1(1-3), the WT control, and PBS alone. The concentration of flt-1(1-3) may have been too low to elicit a response. Other workers have reported that soluble forms of flt-1 inhibit VEGF-induced proliferation of cells at concentrations of 25ng/ml[290,442]. Although 2.3ng of flt-1(1-3) was added in the present study, it was added in a hydrogel, rather than directly, unlike the studies referred to. Furthermore, the concentrations with which inhibition of VEGF is observed are likely to be different between *in vitro* cell proliferation studies and the *in vivo* CAM assay, undertaken in the present study. *In vivo* intraperitoneal administration into mice[318] or intramuscular administration into rabbits[442] of soluble flt-1 required much higher levels of 300μg and 1000μg, respectively. Although the flt-1(1-3)-containing hydrogel was applied directly onto the CAM, it was possible that the concentration of flt-1(1-3) used in the present study was too low to block VEGF-mediated effects. It was anticipated that there would be minimal interference from contaminating proteins in the flt-1(1-3) preparation, as this did not prevent flt-1(1-3) binding to VEGF (Section 4.3.7). However, it is possible that the other constituents in the preparation may have partially hindered the action of flt-1(1-3) on the CAM.

It could be argued that the recombinant human flt-1(1-3) used herein did not interact with high affinity with avian growth factors due to species difference. However, both Zilberberg *et al.*[272] and Bae *et al.*[267] reported angiogenic responses in the CAM assay using recombinant human VEGF, suggesting that there is species cross-reactivity. Moreover, a VEGF inhibition study using the CAM assay involved mixing a peptide inhibitor with VEGF, prior to the addition of both agents onto the CAM[272]. Future work could involve an adaptation of this approach, by combining VEGF and flt-1(1-3)

beforehand. This would bypass any species specificity issues of flt-1(1-3), to establish if flt-1(1-3) can inhibit VEGF-mediated angiogenesis.

Methods for quantifying blood vessel formation in this assay have received attention[406]. A method developed by our collaborating laboratory involves analysis of the images of the CAM. Briefly, the number of pixels deduced to form part of a blood vessel is calculated, to provide an indication of a change in the area occupied by blood vessels compared to a control. This method was applied to the images obtained in the present study, but further optimisation of data acquisition is required to utilise this technique.

An alternative *in vitro* assay previously mentioned is the endothelial cell tubule forming assay. It was anticipated that flt-1(1-3) would be tested for angiogenesis using this approach, but time constraints meant that only preliminary studies were carried out.

5.3.2. Foetal rat metatarsal assay

This organ culture technique has been applied to the study of several factors involved in bone growth, as it provides a microenvironment similar to the *in vivo* setting, as it allows intercellular interactions between the different types of cell in the developing bone[63,105,450,455]. For this study, it provided a useful model of endochondral ossification to test the hypothesis that a matrix inhibiting angiogenesis, will also block bone formation. VEGF is known to promote endochondral ossification[112], which has been formerly blocked in this model[451]. Previously published work have cultured metatarsals for 3 or 4 days and measured the length of the entire metatarsal[63,105,450,455]. Curving of the metatarsals over the longer time course of the present study meant that this not feasible. Furthermore, some of the metatarsals still had proximal phalanges attached, which would have provided false measurements. Therefore, measurement of the calcified zone indicated the extent of bone formation. However, this method did not indicate expansion of the metatarsals due to chondrocyte proliferation.

Blood vessel invasion into the proliferating chondrocytes and mineralisation were detected in both VEGF-stimulated and non-stimulated metatarsals, demonstrating that the

metatarsals were metabolically active after dissection. Metatarsals treated with flt-1(1-3) or the WT control exhibited no mineralisation compared to the hydrogel-only control and the VEGF-treated samples. There was reduced angiogenesis into the cartilage and the band of hypertrophic chondrocytes did not advance towards the epiphysis. Furthermore, there was no evidence of a secondary ossification centre, further confirming that angiogenesis is a prerequisite for this process.

These observations occurred in metatarsals incubated with both flt-1(1-3) and WT control-containing hydrogels, which suggest that the agent responsible was derived from the other protein(s) that had co-purified with flt-1(1-3) from the conditioned medium. Several growth factors that regulate different stages of endochondral ossification contain heparin-binding domains, such as TGF-β[36], BMP-2[456], bFGF[457], platelet-derived growth factor-BB (PDGF-BB[458]) and IGF-1 binding protein, responsible for the modulation of IGF-1 action and increasing the half-life of IGF-1[459], outlined in Section 1.1.8. A role of heparin in the ECM is to bind these growth factors, enabling the tightly controlled, location-specific, release and limits growth factor diffusion[35]. However, as the flt-1(1-3) and WT control were partially purified by heparin affinity chromatography, the preparations would have contained heparin-binding proteins. The introduced proteins may have competed with endogenous growth factors for heparin in the cartilage matrix, or provided such a high concentration of growth factors to overload biological responses. This would have interfered with the regulation of endochondral ossification, which may account for the observed effect.

The observations reported from the inhibition of single growth factors were not in accordance with the present findings. For instance, inhibition of VEGF or matrix metalloproteinases (MMPs) exhibited an increase in the number of hypertrophic chondrocytes, as progression to apoptosis and vascular invasion were blocked[108,111,112]. This was not observed in the present study. Moreover, inhibition studies with parathyroid hormone-related protein (PTHrP) resulted in shrinkage of the epiphyseal region and an increased number of non-hypertrophic chondrocytes amongst hypertrophic chondrocytes[99]. In this study, there did not appear to be such a specific response.

These preliminary results have shown that an agent or combination of agents in the applied treatments, other than flt-1(1-3), caused an arrest in metatarsal growth. To confirm this would require assessment of other metatarsals from the same treatment group, which could not be evaluated in the present study due to time constraints. Gerber *et al.*[290] demonstrated inhibition of ossification using a decoy receptor consisting of the first 3 extracellular domains of flt-1. This implies that the flt-1(1-3) produced in the present study should exhibit a similar effect. A preparation containing a more pure, higher concentration of flt-1(1-3) is required to confirm this. In addition, a future approach could involve incubating the metatarsal between two hydrogels. This would increase metatarsal exposure to the bioactive factors and prevent metatarsals drifting away from the hydrogel during culture.

Limitations of an anti-vWF antibody to detect invading blood vessels was evident, as labelling appeared throughout some metatarsals. The polyclonal antibody was raised against the whole protein, which would include the "A" domains. These are found in a number of extracellular molecules present in epiphyseal cartilage, including matrilins and collagens[54,476]. It is probable that the antibody cross-reacted with these to generate the effect observed. A continuation of this study would utilise an antibody raised against the cell surface receptor CD31 (platelet endothelial cell adhesion molecule-1, PECAM-1), expressed on the cell surface of vascular cells[477].

The metatarsals treated with suramin exhibited extensive disruption of the cartilage, and no bone formation (Figure 5.14, Section 5.2.2.4). Suramin has been shown to be anti-angiogenic[453]. Furthermore, it inhibits the action of growth factors, such as TGF-β, PDGF and bFGF, by inhibiting interactions with their respective receptors, in addition to disrupting proteoglycan catabolism[460,461]. Inhibition of proteoglycan catabolism in the ECM may explain the swelling and distortion observed in suramin-treated metatarsals, as a higher level of polyanionic glycosaminoglycans (GAGs) would cause movement of water into the tissue. The loss of the overall form of the metatarsal indicated that collagen breakdown had occurred, thus losing the structure and strength of the tissue.

This would also explain the disordered ECM observed. In addition, suramin has been reported to inhibit the proliferation and division of osteosarcoma cells[462], which may have contributed to the prevention of ossification by osteoblasts.

The apparent shrinkage of the calcified zones was unexpected, as it was rather unlikely that the metatarsals would actually de-calcify. This phenomenon may have arisen from handling, but to determine the cause of this, microscopic analysis would have to be conducted on metatarsals around 3 days after explantation.

In conclusion, the studies carried out in this Chapter have demonstrated the suitability of HAED hydrogels in the delivery of growth factors. To assess the biological activity of flt-1(1-3), a more concentrated preparation is required. However, previous studies suggest that flt-1(1-3) provides inhibition of VEGF-mediated angiogenesis, with prevention of subsequent bone formation. This is of relevance in the treatment of OA, where angiogenesis, accompanied by new bone growth, is one of the contributing factors to cartilage degradation (Section 1.3.2).

6. Overall Discussion

The limited capacity of cartilage to self-repair following injury has led to the development of cartilage repair strategies (Section 1.5). Such an approach may require bioactive factors to stimulate matrix synthesis or cell proliferation, or an inhibitor of a pathological pathway. A space-filling scaffold has been shown to enhance cartilage repair[338]. Cells are an important component of the repair response and can be either introduced[327] or attracted from surrounding tissues by chemotactic agents[341].

The present study was based on the hypothesis that a matrix which supports angiogenesis, will, in the presence of bioactive factors such as bone morphogenetic protein-2 (BMP-2), induce rapid bone formation, while a matrix that inhibits angiogenesis, will promote chondrogenesis. Chapter 3 describes the characterisation of a hyaluronan (HA)-based hydrogel to deliver growth factors and provide a three-dimensional scaffold to support cartilage remodelling. Chapter 4 describes the production of a decoy receptor to inhibit vascular endothelial growth factor (VEGF)-mediated angiogenesis and subsequent bone formation. Chapter 5 evaluates the combination of hydrogel and decoy receptor as an anti-angiogenic material and as an inhibitor of ossification.

Previously, this laboratory has developed a hydrogel based on an ethylenediamine derivative of HA (HAED), which exhibited potential for tissue repair applications[405]. The present study revealed the optimum component concentrations required to achieve a hydrogel with appropriate viscoelastic properties. The hydrogels supported the delivery of bioactive agents, either incorporated into the crosslinking hydrogels, or via collagen that was included in the hydrogels. Moreover, cell infiltration into the material indicated the suitability of this hydrogel in tissue remodelling. However, potential cytotoxicity of the hydrogels requires further investigation. If non-toxic, these HAED hydrogels can be used in other applications, such as bone growth, skin treatments or eye surgery. Indeed, the Hylan biomaterials have shown potential in soft tissue augmentation[391]. HA-based biomaterials have been developed for delivery of drugs in the eye[420]. Furthermore, HA and collagen matrices have been shown to promote bone healing[404].

Ibusuki *et al.*[333] defined nine essential requirements important for scaffolds in cartilage repair. These are injectability; rapid solidification *in situ*; no subsequent shrinkage of the scaffold; biodegradability; non-toxicity; ability to withstand mechanical force in cartilage; high cell viability; support of cell re-differentiation and resulting in phenotypic expression of chondrocyte markers, such as collagen type II. The present study has demonstrated that the HAED hydrogel fulfils many of these requirements, although it was not designed as a cartilage replacement *per se* and therefore, does not match cartilage for mechanical strength. It is anticipated that administration of this hydrogel in a clinical setting would be followed by minimal weight bearing for a few weeks, until tissue remodelling is complete. This raises the question as to the quality of the replacement tissue that would be synthesised in a non-weight bearing environment. One solution to this could be the use of ultrasound, which has been shown to promote proteoglycan synthesis[463].

To block angiogenesis, the present study describes the expression of a decoy receptor, consisting of the first 3 extracellular domains of the VEGF receptor, fms-like tyrosine kinase-1 (flt-1), termed flt-1(1-3). It was proposed that this would be incorporated into the hydrogel to sequester endogenous VEGF. Flt-1(1-3) was shown to bind VEGF, but the low concentration of flt-1(1-3) meant that anti-angiogenic activity could not be confirmed. Furthermore, a purer and more concentrated preparation is required to demonstrate inhibition of ossification. Previous work has identified pro-angiogenic effects of HA oligosaccharides[72,75]. This is a potential factor regarding degradation products of the hydrogel. However, the HAED hydrogel did not appear to induce angiogenesis in the present study, although this requires confirmation. Moreover, other studies involving HA-based biomaterials in cartilage remodelling have not reported angiogenic effects as a consequence of HA degradation in cartilage partial- and full-thickness defects[337,338,464]. However, Peattie *et al.*[465] reported a synergistic effect between high molecular mass HA-based hydrogels and vascular endothelial growth factor (VEGF) in neovascularisation, following subcutaneous implantation into rats. As advanced OA

chondrocytes express VEGF[224], these findings would be a consideration when applying the HAED hydrogel to OA cartilage.

In a cartilage repair strategy following on from the present study, a HAED hydrogel containing collagen, BMP-2 and flt-1(1-3) would be injected into a cartilage lesion immediately after the crosslinker was supplemented, whereupon it would form a space-filling three-dimensional scaffold. It is anticipated that the presence of BMP-2 would stimulate the migration of mesenchymal stem cells (MSCs) from the surrounding synovium, periosteum or subchondral bone into the scaffold. It is believed that the MSCs would then undergo differentiation into chondrocytes with associated matrix synthesis further enhanced by the HA-based hydrogel. Meanwhile, flt-1(1-3) would block the pathogenic function of VEGF. MSCs have been demonstrated to migrate from synovial tissues into a partial-thickness cartilage defect[341]. Furthermore, Iwata *et al.*[470] reported that BMPs can induce MSCs to differentiate into chondrocytes. As chondrocytes have very limited capacities for migration[341], the migration and differentiation of MSCs would be required for matrix synthesis. Inhibition of angiogenesis has been shown to prevent bone invasion into a cartilaginous repair tissue following implantation of a matrix containing IGF-1, BMP-2 or TGF-β1[342]. This study used suramin in the matrix to block angiogenesis and further demonstrated that slow release of the angiogenesis inhibitor promoted cartilage growth more effectively than rapid diffusion. This is in agreement with the future objectives of the present study.

The cartilage model for hydrogel assessment requires some consideration. A partial defect in otherwise healthy cartilage may not represent the osteoarthritic state, as VEGF would be at much lower levels. In contrast, advanced OA exhibits inflammation of the synovial membrane, with increased VEGF activity in the synovial membrane and within cartilage itself[224]. Animal models which exhibit the spontaneous development of OA[467] provide a means of investigating at which stage of injury the material is most effective.

The potential inhibition of angiogenesis to promote cartilage repair has been illustrated by Takita *et al.*[443], who combined BMP-2 and an anti-angiogenic polyphenol,

epigallocatechin 3-gallate, into scaffolds of fibrous glass membranes. The study revealed that in the presence of BMP-2 and the angiogenesis inhibitor, cartilage was still produced with decreased bone formation, whereas in the presence of BMP-2 alone, bone formation was predominant. This supports findings in the present study, which demonstrated BMP-2-induced bone formation following subcutaneous implantation. Kim *et al.*[467] demonstrated that a BMP-2-containing Hyaff-11 biomaterial induced osteogenesis of seeded fibroblasts. Interestingly, the group also revealed that Hyaff-11 maintained a more prolonged, slower release of BMP-2 than collagen gels, which was proposed to be caused by electrostatic interactions between the basic N-terminus of BMP-2 and the carboxyl groups on HA. This suggests that the incorporation of collagen may not be required for delivery of BMP-2. In addition, synergy between administered growth factors can be exploited for cartilage repair. An *in vitro* study[468] demonstrated that a combination of BMP-7 and IGF-1 achieved greater proteoglycan synthesis than each individually, which could be a consideration in a continuation of the present study. In addition, the more chondrogenic BMP-7 may be more applicable to cartilage repair than the osteogenic BMP-2. It does not induce cell proliferation, which may be considered a drawback, but this does risk proliferating chondrocytes progressing to hypertrophy and subsequent osteogenesis[62].

A study conducted by Diefenderfer *et al.*[64] revealed that adult human MSCs did not respond to BMP-2, BMP-4 and BMP-7 as effectively as rat MSCs in culture. These findings present obvious issues regarding a BMP-2 approach. An alternative growth factor, platelet-derived growth factor-BB (PDGF-BB), has received much interest, as it can promote proteoglycan synthesis, but does not induce chondrocyte differentiation[469]. However, one study found that the pre-treatment of chondrocytes with PDGF-BB led to the formation of fibrous connective tissue, rather than hyaline cartilage following implantation[373].

The rate of diffusion of bioactive factors from the hydrogel may have influenced the biological responses observed in this study. Time constraints meant that methods of coupling flt-1(1-3) to the HAED hydrogel could not be addressed. Stable attachment of

flt-1(1-3) may result in an accumulation of VEGF within the hydrogel until it were degraded, which could also allow slow, sustained release of flt-1(1-3). The rate of scaffold degradation would thus influence the biological response. A stable attachment within the hydrogel may also provide some protection against metabolic inactivation[390]. Alternatively, a hydrolysable link may enable a more rapid diffusion of flt-1(1-3), which would enable the inhibitor to interact with surrounding tissue. However, this could have the added risk of diffusion away from the target site. Enzymatic cleavage offers a more tissue-specific mechanism and oligopeptide links between the scaffold and attached agent have been used to achieve this[410]. The method of coupling should take into account the nature of the bioactive factor. For instance, a permanent bond would not be suitable for the delivery of intracellular signalling molecules[410]. The rate of diffusion could be assessed by the use of radiolabelled proteins and the measurement of radioactivity in fluid surrounding a range of HAED hydrogels of different component concentrations.

Modification of the carboxyl moiety of HA could introduce a peptide link to couple flt-1(1-3), with enzymatic release. However, there is the potential risk of enzymatic degradation of flt-1(1-3). Heparin immobilised on a fibrin scaffold has also been successfully used to deliver growth factors, such as basic fibroblast growth factor (bFGF)[378], which suggests a mechanism for not only the delivery of the heparin-binding flt-1(1-3), but also for the sequestering of VEGF. However, many growth factors have heparin-binding sites and cartilage repair may be affected if chondrogenic growth factors are trapped within the delivery scaffold.

Assessment of the HAED hydrogel (with BMP-2 and flt-1(1-3)) in a cartilage lesion, would reveal if the anti-angiogenic signal is only required while a cartilaginous matrix is being synthesised, or if sustained inhibition is required to prevent bone invasion, after the hydrogel has been degraded. BMP-2 induces chondrocyte proliferation during endochondral ossification, where the end result for these chondrocytes is hypertrophy and cell death, accompanied by angiogenesis (Section 1.1.8). The role of VEGF in endochondral ossification[112] suggests that inhibition of VEGF action may be required long-term. There has been considerable interest in the delivery of MSCs transfected with

chondrogenic agents to regenerate cartilage[471]. The transfection of MSCs *in vitro* with flt-1(1-3) cDNA, followed by implantation, may provide a slow release over a longer time, especially if the MSCs are retrovirally transduced. In combination with the HAED hydrogel and BMP-2, this would provide progenitor cells for matrix synthesis and offer long-term inhibition of VEGF activity. Moreover, transfection of MSCs with BMP-2 cDNA has resulted in increased biological response compared to administration of the BMP-2 protein[472]. However, future results from the effectiveness of coupling of flt-1(1-3) to the HAED hydrogel would reveal if flt-1(1-3) inhibits VEGF more efficiently in a free state, or immobilised on a scaffold.

In conclusion, the application of an inhibitor to VEGF, in a BMP-2-containing HAED hydrogel, into damaged cartilage, offers a potential solution to cartilage degradation. This study characterised the HAED hydrogels and demonstrated their suitability in the delivery of growth factors. It was also shown that the hydrogels could support cell infiltration, although the toxicity of the materials remains to be elucidated. The development of a VEGF inhibitor can bind this growth factor, but further work is required to reveal if it can block VEGF-induced angiogenesis and osteogenesis.

7. References

1. Bobic, V. and Noble, J. Articular cartilage – to repair or not to repair. J. Bone Joint Surg. **82-B**, 165-166 (2000).
2. Newman, A.P. Articular cartilage repair. Am. J. Sports Med. **26**, 309-324 (1998).
3. Tortora, G.J. and Grabowski, S.R. Principles of anatomy and physiology. New York: John Wiley & Sons (2000).
4. Hunziker, E.B. Articular cartilage structure in humans and experimental animals. In: Ed. Kuettner, K.E., Schleyerbach, R., Peyron, J.G. and Hascall, V.C. Articular cartilage and osteoarthritis. New York: Raven Press, ch. 13 (1992).
5. Poole, A.R., Kojima, T., Yasuda, T., Mwale, F., Kobayashi, M. and Laverty, S. Composition and structure of articular cartilage. A template for tissue repair. Clin. Orthop. Rel. Res. **391S**, 26-33 (2001).
6. Schumacher, B.L., Block, J.A., Schmid, T.M., Aydelotte, M.B. and Kuettner, K.E. A novel proteoglycan synthesized and secreted by chondrocytes of the superficial zone of articular cartilage. Arch. Biochem. Biophys. **311**, 144-152 (1994).
7. Temenoff, J.S. and Mikos, A.G. Review: tissue engineering of articular cartilage. Biomaterials **21**, 431-440 (2000).
8. Lorenzo, P., Bayliss, M.T. and Heinegård, D. A novel cartilage protein (CILP) present in the mid-zone of human articular cartilage increases with age. J. Biol. Chem. **273**, 23463-23468 (1998).
9. Oegema Jr., T.R. and Thompson Jr., R.C. The zone of calcified cartilage: its role in osteoarthritis. In: Ed. Kuettner, K.E., Schleyerbach, R., Peyron, J.G. and Hascall, V.C. Articular cartilage and osteoarthritis. New York: Raven Press, ch. 22 (1992).
10. Eyre, D.R., Wu, J-J. and Woods, P. Cartilage-specific collagens: structural studies. In: Ed. Kuettner, K.E., Schleyerbach, R., Peyron, J.G. and Hascall, V.C. Articular cartilage and osteoarthritis. New York: Raven Press, ch. 9 (1992).
11. Rucklidge, G.J., Milne, G. and Robins, S.P. Collagen type X: a component of the surface of normal human, pig, and rat articular cartilage. Biochem. Biophys. Res. Comm. **224**, 297-302 (1996).
12. Olsen, B.R. Molecular biology of cartilage collagens. In: Ed. Kuettner, K.E., Schleyerbach, R., Peyron, J.G. and Hascall, V.C. Articular cartilage and osteoarthritis. New York: Raven Press, ch. 11 (1992).
13. van der Kraan, P.M., Stoop, R., Meijers, T.H.M., Poole, A.R. and van den Berg, W.B. Expression of type X collagen in young and old C57Bl/6 and Balb/c mice. Relation with articular cartilage degeneration. Osteoarthritis Cartilage **9**, 92-100 (2001).
14. Luckman, S.P., Rees, E. and Kwan, A.P.L. Partial characterization of cell-type X collagen interactions. Biochem. J. **372**, 485-493 (2003).
15. Wiberg, C., Heinegård, D., Wenglén,C., Timpl, R. and Mörgelin, M. Biglycan organizes collagen VI into hexagonal-like networks resembling tissue structures. J. Biol. Chem. **277**, 49120-49126 (2002).
16. Eikenberry, E.F., Mendler, M., Bürgin, R., Winterhalter, K.H. and Bruckner, P. Fibrillar organization in cartilage. In: Ed. Kuettner, K.E., Schleyerbach,

R., Peyron, J.G. and Hascall, V.C. Articular cartilage and osteoarthritis. New York: Raven Press, ch. 10 (1992).

17. Connon, C.J., Siegler, V., Meek, K.M., Hodson, S.A., Caterson, B., Kinoshita, S. and Quantock, A.J. Proteoglycan alterations and collagen reorganisation in the secondary avian cornea during development. Ophthalmic Res. **35**, 177-184 (2003).
18. Blaschke, U.K., Eikenberry, E.F., Hulmes, D.J.S., Galla, H-J. and Bruckner, P. Collagen XI nucleates self-assembly and limits lateral growth of cartilage fibrils. J. Biol. Chem. **275**, 10370-10378 (2000).
19. Kiani, C., Chen, L., Wu, Y.J., Yee, A.J. and Yang, B.B. Structure and function of aggrecan. Cell Res. **12**, 19-32 (2002).
20. Alberts, B., Bray, D., Lewis, J., Raff, M., Roberts, K. and Watson, J.D. Molecular biology of the cell. New York: Garland Publishing (1994).
21. Voet, D. and Voet, J.G. Biochemistry. New York: John Wiley & Sons (1995).
22. Hardingham, T.E., Fosang, A.J. and Dudhia, J. Aggrecan, the chondroitin sulphate/keratan sulphate proteoglycan from cartilage. In: Ed. Kuettner, K.E., Schleyerbach, R., Peyron, J.G. and Hascall, V.C. Articular cartilage and osteoarthritis. New York: Raven Press, ch. 1 (1992).
23. Iozzo, R.V. The biology of the small leucine-rich proteoglycans. Functional network of interactive proteins. J. Biol. Chem. **274**, 18843-18846 (1999).
24. Rosenberg, L.C. Structure and function of dermatan sulphate proteoglycans in articular cartilage. In: Ed. Kuettner, K.E., Schleyerbach, R., Peyron, J.G. and Hascall, V.C. Articular cartilage and osteoarthritis. New York: Raven Press, ch. 4 (1992).
25. Danielson, K.G., Baribault, H., Holmes, D.F., Graham, H., Kadler, K.E. and Iozzo, R.V. Targeted disruption of decorin leads to abnormal collagen fibril morphology and skin fragility. J. Cell Biol. **136**, 729-743 (1997).
26. Xu, T., Bianco, P., Fisher, L.W., Longenecker, G., Smith, E., Goldstein, S., Bonadio, J., Boskey, A., Heegard, A-M., Sommer, B., Satomura, K., Dominguez, P., Zhao, C., Kulkarni, A.B., Robey, P.G. and Young, M.F. Targeted disruption of the biglycan gene leads to an osteoporosis-like phenotype in mice. Nature Gen. **20**, 78-82 (1998).
27. Kinsella, M.G., Fischer, J.W., Mason, D.P. and Wight, T.N. Retrovirally mediated expression of decorin by macrovascular endothelial cells. Effects on cellular migration and fibronectin fibrillogenesis *in vitro*. J. Biol. Chem. **275**, 13924-13932 (2000).
28. Wiberg, C., Klatt, A.R., Wagener, R., Paulsson, M., Bateman, J.F., Heinegård, D. and Mörgelin, M. Complexes of matrilin-1 and biglycan or decorin connect collagen VI microfibrils to both collagen II and aggrecan. J. Biol. Chem. **278**, 37698-37704 (2003).
29. Jepsen, K.J., Wu, F., Peragallo, J.H., Paul, J., Roberts, L., Ezura, Y., Oldberg, A., Birk, D.E. and Chakravarti, S. A syndrome of joint laxity and impaired tendon integrity in lumican- and fibromodulin-deficient mice. J. Biol. Chem. **277**, 35532-35540 (2002).
30. Ameye, L., Aria, D., Jepsen, K., Oldberg, A., Xu, T. and Young, M.F. Abnormal collagen fibrils in tendons of biglycan/fibromodulin-deficient mice lead to gait impairment, ectopic ossification, and osteoarthritis. FASEB J. **16**, 673-680 (2002).

31. SunderRaj, N., Fite, D., Ledbetter, S., Chakravarti, S. and Hassell, J.R. Perlecan is a component of cartilage matrix and promotes chondrocyte attachment. J. Cell Sci. **108**, 2663-2672 (1995).
32. Vaughan-Thomas, A., Young, R.D., Phillips, A.C. and Duance, V.C. Characterization of type XI collagen-glycosaminoglycan interactions. J. Biol. Chem. **276**, 5303-5309 (2001).
33. Gitay-Goran, H., Soker, S., Vlodavsky, I. and Neufeld, G. The binding of vascular endothelial growth factor to its receptors is dependent on cell surface-associated heparin-like molecules. J. Biol. Chem. **267**, 6093-6098 (1992).
34. Folkman, J., Klagsbrun, M., Sasse, J., Wadzinski, M., Inger, D. and Vlodavsky, I. A heparin-binding angiogenic protein – basic fibroblast growth factor – is stored within basement membrane. Am. J. Pathol. **130**, 393-400 (1988).
35. Vlodavsky, I., Miao, H-Q., Atzmon, R., Levi, E., Zimmerman, J., Bar-Shavit, R., Peretz, T. and Ben-Sasson, S.A. Control of cell proliferation by heparan sulphate and heparin-binding growth factors. Thrombosis Haemostasis **74**, 534-540 (1995).
36. McCaffrey, T.A., Falcone, D.J. and Du, B. Transforming growth factor-β1 is a heparin-binding protein: identification of putative heparin-binding regions and isolation of heparins with varying affinity for TGF-β1. J. Cell. Physiol. **152**, 430-440 (1992).
37. Meyer, K. and Palmer, J.W. The polysaccharide of the vitreous humor. J. Biol .Chem. **107**, 629-634 (1934).
38. Toole, B.P. Hyaluronan is not just a goo! J. Clin. Invest. **106**, 335-336 (2000).
39. Laurent, T.C. and Fraser, J.R.E. Hyaluronan. FASEB J. **6**, 2397-2404 (1992).
40. Toole, B.P. Hyaluronan in morphogenesis. J. Internal Med. **242**, 35-40 (1997).
41. Cao, L., Lee, V., Adams, M.E., Kiani, C., Zhang, Y., Hu, W. and Yang, B.B. β_1-integrin-collagen interaction reduces chondrocyte apoptosis. Matrix Biol. 18, 343-355 (1999).
42. Knudson, C.B. and Knudson, W. Hyaluronan-binding proteins in development, tissue homeostasis, and disease. FASEB. J. **7**, 1233-1241 (1993).
43. Lee, J.Y., Spicer, A.P. Hyaluronan: a multifunctional, megaDalton, stealth molecule. Curr. Op. Cell Biol. **12**, 581-586 (2000).
44. Day, A.J. The structure and regulation of hyaluronan-binding proteins. Biochem. Soc. Trans. **27**, 115-121 (1999).
45. Levick, J.R. Synovial fluid: determinants of volume turnover and material concentration. In: Ed. Kuettner, K.E., Schleyerbach, R., Peyron, J.G. and Hascall, V.C. Articular cartilage and osteoarthritis. New York: Raven Press, ch. 37 (1992).
46. Weiss, C. Why viscoelasticity is important for the medical uses of hyaluronan and hylans. In: Ed. Abatangelo, G. and Weigel, P.H. New Frontiers in Medical Sciences: refining hyaluronan. Elsevier Science B.V. 89-103 (2000).
47. Kvam, B.J., Fragonas, E., Degrassi, A., Kvam, C., Matulova, M., Pollesello, P., Zanetti, F. and Vittur, F. Oxygen-derived free radical (ODFR) action on

hyaluronan (HA), on two HA ester derivatives, and on the metabolism of articular chondrocytes. Exp. Cell Res. **218**, 79-86 (1995).

48. Gendelman, R., Burton-Wurster, N.I., MacLeod, J.N. and Lust, G. The cartilage-specific fibronectin isoform has a high affinity binding site for the small proteoglycan decorin. J. Biol. Chem. **278**, 11175-11181 (2003).
49. Flannery, C.R., Hughes, C.E., Schumacher, B.L., Tudor, D., Aydelotte, M.B., Kuettner, K.E. and Caterson, B. Articular cartilage superficial zone protein (SZP) is homologous to megakaryocyte stimulating factor precursor and is a multifunctional proteoglycan with potential growth-promoting, cytoprotective, and lubricating properties in cartilage metabolism. Biochem. Biophys. Res. Comm. **254**, 535-541 (1999).
50. Bornstein, P., Armstrong, L.C., Hankenson, K.D., Kyriakides, T.R. and Yang, Z. Thrombospondin-2, a matricellular protein with diverse functions. Matrix Biol. **19**, 557-568 (2000).
51. Thur, J., Rosenberg, K., Nitsche, D.P., Pihlajamaa, T., Ala-Kokko, L., Heinegård, D., Paulsson, M. and Maurer, P. Mutations in cartilage oligomeric matrix protein causing pseudoachondroplasia and multiple epiphyseal dysplasia affect binding of calcium and collagen I, II, and IX. J. Biol. Chem. **273**, 6083-6092 (2001).
52. Neidhart, M., Hauser, N., Paulsson, M., Dicesare, P.E., Michel, B.A. and Häuselmann, H.J. Small fragments of cartilage oligomeric matrix protein in synovial fluid and serum as markers for cartilage degradation. Br. J. Rheumatol. **36**, 1151-1160 (1997).
53. Neame, P.J., Sommarin, Y., Boynton, R.E. and Heinegård, D. The structure of a 38-kDa leucine-rich protein (chondroadherin) isolated from bovine cartilage. J. Biol. Chem. **269**, 21547-21654 (1994).
54. Deák, F., Wagener, R., Kiss, I. and Paulsson, M. The matrillins: a novel family of oligomeric extracellular matrix proteins. Matrix Biol. **18**, 55-64 (1999).
55. Moses, M.A., Wiederschain, D., Wu, I., Fernandez, C.A., Ghazizadeh, V., Lane, W.S., Flynn, E., Sytkowski, A., Tao, T. and Langer, R. Troponin I is present in human cartilage and inhibits angiogenesis. Proc. Natl. Acad. Sci. USA **96**, 2645-2650 (1999).
56. Ellis, A.J., Curry, V.A., Powell, E.K. and Cawston, T.E. The prevention of collagen breakdown by TIMP, TIMP-2 and a low molecular weight synthetic inhibitor. Biochem. Biophys. Res. Comm. **201**, 94-101 (1994).
57. Gendron, C., Kashiwagi, M., Hughes, C., Caterson, B. and Nagase, H. TIMP-3 inhibits aggrecanase-mediated glycosaminoglycan release from cartilage explants stimulated by catabolic factors. FEBS lett. **555**, 431-436 (2003).
58. Qi, J.H., Ebrahem, Q., Moore, N., Murphy, G., Claesson-Welsh, L., Bond, M., Baker, A. and Anand-Apte, B. A novel function for tissue inhibitor of metalloproteinases-3 (TIMP3): inhibition of angiogenesis by blockage of VEGF binding to VEGF receptor-2. Nature Med. **9**, 407-415 (2003).
59. Ohba, Y., Goto, Y., Kimura, Y., Suzuki, F., Hisa, T., Takahashi, K. and Takigawa, M. Purification of an angiogenesis inhibitor from culture medium conditioned by a human chondrosarcoma-derived chondrocytic cell line, HCS-2/8. Biochim. Biophys. Acta **1245**, 1-8 (1995).
60. Keene, D.R., Jordan, C.D., Reinhardt, D.P., Ridgway, C.C., Ono, R.N., Corson, G.M., Fairhurst, M., Sussman, M.D., Memoli, V.A. and Sakai, L.Y.

Fibrillin-1 in human cartilage: developmental expression and formation of special banded fibers. J. Histochem. Cytochem. **45**, 1069-1082 (1997).

61. Grimaud, E., Heymann, D. and Rédini, F. Recent advances in TGF-β effects on chondrocyte metabolism. Potential therapeutic roles of TGF-β in cartilage disorders. Cytokine Growth Factor Rev. **13**, 241-257 (2002).
62. Chubinskaya, S. and Kuettner, K.E. Regulation of osteogenic proteins by chondrocytes. Int. J. Biochem. Cell Biol. **35**, 1323-1340 (2003).
63. De Luca, F., Barnes, K.M., Uyeda, J.A., De-Levi, S., Abad, V., Palese, T., Mericq, V. and Baron, J. Regulation of growth plate chondrogenesis by bone morphogenetic protein-2. Endocrinol. **142**, 430-436 (2001).
64. Diefenderfer, D.L., Osyczka, A.M., Reilly, G.C. and Leboy, P.S. BMP responsiveness in human mesenchymal stem cells. Connect. Tiss. Res. **44** suppl. 1, 305-311 (2003).
65. Chubinskaya, S., Merrihew, C., Cs-Szabo, G., Mollenhauer, J., McCartney, J., Rueger, D.C. and Kuettner, K.E. Human articular chondrocytes express osteogenic protein-1. J. Histochem. Cytochem. **48**, 239-250 (2000).
66. Sampath, T.K., Maliakal, J.C., Hauschka, P.V., Jones, W.K., Sasak, H., Tucker, R.F., White, K.H., Coughlin, J.E., Tucker, M.M., Pang, R.H.L., Corbett, C., Özkaynak, E., Oppermann, H. and Rueger, D.C. Recombinant human osteogenic protein-1 (hOP-1) induces new bone formation *in vivo* with a specific activity comparable with natural bovine osteogenic protein and stimulates osteoblast proliferation and differentiation *in vitro*. J. Biol. Chem. **267**, 20352-20362 (1992).
67. Chang. S.C., Hoang, B., Thomas, J.T., Vukicevic, S., Luyten, F.P., Ryba, N.J.P., Kozak, C.A., Reddi, A.H. and Moos Jr., M. Cartilage-derived morphogenetic proteins. New members of the transforming growth factor-β subfamily redominantly expressed in long bones during human embryonic development. J. Biol. Chem. **269**, 28227-28234 (1994).
68. Erlacher, L., Ng, C-K., Ullrich, R., Krieger, S. and Luyten, F.P. Presence of cartilage-derived morphogenetic proteins in articular cartilage and enhancement of matrix replacement in vitro. Athritis Rheumatism **41**, 263-273 (1998).
69. Holmes, M.W.A., Bayliss, M.T. and Muir, H. Hyaluronic acid in human articular cartilage. Age-related changes in content and size. Biochem. J. **250**, 435-441 (1988).
70. Moseley, R., Leaver, M., Walker, M., Waddington, R.J., Parsons, D., Chen, W.Y.J. and Embery, G. Comparison of the antioxidant properties of HYAFF®-11p75, AQUACEL® and hyaluronan towards reactive oxygen species in vitro. Biomaterials **23**, 2255-2264 (2002).
71. Cortivo, R., Brun, P., Cardarelli, L., O'Regan, M., Radice, M. and Abatangelo, G. Antioxidant effects of hyaluronan and its α-methyl-prednisolone derivative in chondrocyte and cartilage cultures. Semin. Arthritis Rheum. **26**, 492-501 (1996).
72. West, D.C., Hampson, I.N., Arnold, F. and Kumar, S. Angiogenesis induced by degradation products of hyaluronic acid. Science **228**, 1324-1326 (1985).
73. West, D.C. and Kumar, S. Endothelial cell proliferation and diabetic retinopathy. The Lancet 1(8587), 715-716 (1988).

74. Montesano, R., Kumar, S., Orci, L. and Pepper, M.S. Synergistic effect of hyaluronan oligosaccharides and vascular endothelial growth factor on angiogenesis in vitro. Lab. Invest. **75**, 249-262 (1996).
75. Fieber, C., Baumann, P., Vallon, R., Termeer, C., Simon, J.C., Hofmann, M., Angel, P., Herrlich, P. and Sleeman, J.P. Hyaluronan-oligosaccharide-induced transcription of metalloproteinases. J. Cell Sci. **117**, 359-367 (2004).
76. Lawler, J. The functions of thrombospondin-1 and –2. Curr. Op. Cell Biol. **12**, 634-640 (2000).
77. Baker, A.H., Edwards, D.R. and Murphy, G. Metalloproteinase inhibitors: biological actions and therapeutic opportunities. J. Cell Sci. **115**, 3719-3727 (2002).
78. Urist, M.R., Mikulshi, A. and Lietze, A. Solubilized and insolubilized bone morphogenetic protein. Proc. Natl. Acad. Sci. USA **76**, 1828-1832 (1979).
79. Anderson, H.C., Hodges, P.T., Aguilera, X.M., Missana, L. and Moylan, P.E. Bone morphogenetic protein (BMP) localization in developing human and rat growth plate, metaphysic, epiphysis, and articular cartilage. Histochem. Cytochem. **48**, 1493-1502 (2000).
80. Sellers, R.S., Zhang, R., Glasson, S.S., Kim, H.D., Peluso, D., D'Augusta, D.A., Beckwith, K. and Morris, E.A. Repair of articular cartilage defects one year after treatment with recombinant human bone morphogenetic protein-2 (rhBMP-2). J. Bone Joint Surg. **82-A**, 151-160 (2000).
81. Sailor, L.Z., Hewick, R.M. and Morris, E.A. Recombinant human bone morphogenetic protein-2 maintains the articular chondrocyte phenotype in long-term culture. J. Orthop. Res. **14**, 937-945 (1996).
82. Archer, C.W. and Francis-West, P. The chondrocyte. Int. J. Biochem. Cell Biol. **35**, 401-404 (2003).
83. van der Kraan, P.M., Buma, P., van Kuppevelt, T. and van den Berg, W.B. Interaction of chondrocytes, extracellular matrix and growth factors: relevance for articular cartilage tissue engineering. Osteoarthritis Cartilage **10**, 631-637 (2002).
84. Wilkins, R.J., Browning, J.A. and Ellory, J.C. Surviving in a matrix: membrane transport in articular chondrocytes. J. Membrane Biol. **177**, 95-108 (2000).
85. Aydelotte, M.B., Schumacher, B.L. and Kuettner, K.E. Heterogeneity of articular chondrocytes. In: Ed. Kuettner, K.E., Schleyerbach, R., Peyron, J.G. and Hascall, V.C. Articular cartilage and osteoarthritis. New York: Raven Press, ch. 16 (1992).
86. Williams, J.M., Uebelhart, D., Ongchi, D.R., Kuettner, K.E. and Thonar, E.J-M.A. Animal models of articular cartilage repair. In: Ed. Kuettner, K.E., Schleyerbach, R., Peyron, J.G. and Hascall, V.C. Articular cartilage and osteoarthritis. New York: Raven Press, ch. 36 (1992).
87. Mollenhauer, J., Mok, M.T., King, K.B., Gupta, M., Chubinskaya, S., Koepp, H. and Cole, A.A. Expression of anchorin CII (cartilage annexin V) in human young, normal adult, and osteoarthritic cartilage. Histochem. Cytochem. **47**, 209-220 (1999).
88. Kühn, K., D'Lima, D.D., Hashimoto, S. and Lotz, M. Cell death in cartilage. Osteoarthritis Cartilage **12**, 1-16 (2004).
89. Erlebacher, A., Filvaroff, E.H., Gitelman, S.E. and Derynck, R. Toward a molecular understanding of skeletal development. Cell **80**, 371-378 (1995).

90. Urist, M.R. Bone morphogenetic protein: the molecularization of skeletal system development. J. Bone Miner. Res. 12, 343-346 (1997)
91. Arteaga-Solis, E., Gayraud, B., Lee, S.Y., Shum, L., Sakai, L. and Ramirez, F. Regulation of limb patterning by extracellular microfibrils. J. Cell Biol. 154, 275-281 (2001).
92. Behonick, D.J. and Werb, Z. A bit of give and take: the relationship between the extracellular matrix and the developing chondrocyte. Mech. Dev. 120, 1327-1336 (2003).
93. Gould, S.E., Upholt, W.B. and Kosher, R.A. Syndecan 3: a member of the syndecan family of membrane-intercalated proteoglycans that is expressed in high amounts at the onset of chicken limb cartilage differentiation. Proc. Natl. Acad. Sci. USA 89, 3271-3275 (1992).
94. Arikawa-Hirasawa, E., Watanabe, H., Takami, H., Hassell, J.R. and Yamada, Y. Perlecan is essential for cartilage and cephalic development. Nature Gen. **23**, 354-358 (1999).
95. Lefebvre, V., Huang, W., Harley, V.R., Goodfellow, P.N. and De Crombrugghe, B. SOX9 is a potent activator of the chondrocyte-specific enhancer of the Proα1 (II) collagen gene. Mol. Cell. Biol. **17**, 2336-2346 (1997).
96. Lefebvre, V., Li, P. and de Crombrugghe. A new long form of Sox5 (L-Sox5), Sox6 and Sox9 are coexpressed in chondrogenesis and cooperatively activate the type II collagen gene. EMBO J. **17**, 5718-5733 (1998).
97. de Combrugghe, B., Lefebvre, V., Behringer, R.R., Bi, W., Murakami, S. and Huang, W. Transcriptional mechanisms of chondrocyte differentiation. Matrix Biol. **19**, 389-394 (2000).
98. St-Jacques, B., Hammerschmidt, M. and McMahon, A.P. Indian hedgehog signalling regulates proliferation and differentiation of chondrocytes and is essential for bone formation. Genes Dev. **13**, 2072-2086 (1999).
99. Amizuka, N., Warshawsky, H., Henderson, J.E., Goltzman, D. and Karaplis, A.C. Parathyroid hormone-related peptide-depleted mice show abnormal epiphyseal cartilage development and altered endochondral bone formation. J. Cell Biol. **126**, 1611-1623 (1994).
100. Karaplis, A.C., Luz, A., Glowacki, J., Bronson, R.T., Tybulewicz, V.L.J., Kronenberg, H.M. and Mulligan, R.C. Lethal skeletal dysplasia from targeted disruption of the parathyroid hormone-related peptide gene. Genes Dev. **8**, 277-289 (1994).
101. Bakre, M.M., Zhu, Y., Yin, H., Burton, D.W., Terkeltaub, R., Deftos, L.J. and Varner, J.A. Parathyroid hormone-related peptide is a naturally occurring, protein kinase A-dependent angiogenesis inhibitor. Nature Med. **8**, 995-1003 (2002).
102. Hiraki, Y, Inoue, H., Iyama, K-I., Kamizono, A., Ochiai, M., Shukunami, C., Iijima, S., Suzuki, F. and Kondo, J. Identification of chondromodulin I as a novel endothelial cell growth inhibitor. Purification and its localization in the avascular zone of epiphyseal cartilage. J. Biol. Chem. **272**, 32419-32426 (1997).
103. Hiaki, Y., Inoue, H., Kondo, J., Kamizono, A., Yoshitake, Y., Shukunami, C. and Suzuki, F. A novel growth-promoting factor derived from fetal bovine cartilage, chondromodulin II. Purification and amino acid sequence. J. Biol. Chem. **271**, 22657-22662 (1996).

104. Wing-hoi, C., Kwong-man, L., Kwok-pui, F., Po-yee, L. and Kwok-sui, L. TGF-β1 is the factor secreted by proliferative chondrocytes to inhibit neo-angiogenesis. J. Cell. Biochem. Suppl. **36**, 79-88 (2001).
105. Mancilla, E.E., De Luca, F., Uyeda, J.A., Czerwiec, F.S. and Baron, J. Effects of fibroblast growth factor-2 on longitudinal bone growth. Endocrinol. **139**, 2900-2904 (1998).
106. Baker, J., Liu, J-P., Robertson, E.J. and Efstratiadis, A. Role of insulin-like growth factors in embryonic and postnatal growth. Cell **75**, 73-82 (1993).
107. Newman, B., Gigout, L.I., Sudre, L., Grant, M.E. and Wallis, G.A. Coordinated expression of matrix Gla protein is required during endochondral ossification for chondrocyte survival. J. Cell Biol. **154**, 659-666 (2001).
108. Zhou, Z., Apte, S.S., Soininen, R., Cao, R., Baaklini, G.Y., Rauser, R.W., Wang, J., Cao, Y. and Tryggvason, K. Impaired endochondral ossification and angiogenesis in mice deficient in membrane-type matrix metalloproteinase I. Proc. Natl. Acad. Sci. USA **97**, 4052-4057 (2000).
109. Vu, T.H. and Werb, Z. Matrix metalloproteinases: effectors of development and normal physiology. Gene. Dev. **14**, 2123-2133 (2000).
110. Babarina, A.V., Möllers, U., Bittner, K., Vischer, P. and Bruckner, P. Role of the subchondral vascular system in endochondral ossification: endothelial cell-derived proteinases derepress late cartilage differentiation in vitro. Matrix Biol. **20**, 205-213 (2001).
111. Vu, T.H., Shipley, J.M., Bergers, G., Berger, J.E., Helms, J.A., Hanahan, D., Shapiro, S.D., Senior, R.M. and Werb, Z. MMP-9/gelatinase B is a key regulator of growth plate angiogenesis and apoptosis of hypertrophic chondrocytes. Cell **93**, 411-422 (1998).
112. Gerber, H-P., Vu, T.H., Ryan, A.M., Kowalski, J., Werb, Z. and Ferrara, N. VEGF couples hypertrophic cartilage remodelling, ossification and angiogenesis during endochondral bone formation. Nature Med., **5**, 623-628 (1999).
113. Midy, V. and Plouët, J. Vasculotropin/vascular endothelial growth factor induces differentiation in cultured osteoblasts. Biochem. Biophys. Res. Comm. **199**, 380-386 (1994).
114. Carlevaro, M.F., Cermelli, S., Cancedda, R. and Cancedda, F.D. Vascular endothelial growth factor (VEGF) in cartilage neovascularization and chondrocyte differentiation: auto-paracrine role during endochondral bone formation. J. Cell Science **113**, 59-69 (2000).
115. Wang, D.S., Miura, M., Demura, H. and Sato, K. Anabolic effects of 1,25-dihydroxyvitamin D_3 on osteoblasts are enhanced by vascular endothelial growth factor produced by osteoblasts and by growth factors produced by endothelial cells. Endocrin. **138**, 2953-2962 (1997).
116. Carlevaro, M.F., Albini, A., Ribatti, D., Gentili, C., Benelli, R., Cermelli, S., Cancedda, R. and Candedda, F.D. Transferrin promotes endothelial cell migration and invasion: implication in cartilage neovscularization. J. Cell Biol. **136**, 1375-1384 (1997).
117. Archer, C.W. Skeletal development and osteoarthritis. Ann. Rheum. Dis. **53**, 624-630 (1994).
118. Mundlos, S. and Olsen, B.R. Heritable diseases of the skeleton. Part I: molecular insights into skeletal development-transcription factors and signalling pathways. FASEB J. **11**, 125-132 (1997).

119. Sandell, L.J., Morris, N., Robbins, J.R. and Goldring, M.B. Alternatively spliced type II procollagen mRNAs define distinct populations of cells during vertebral development: differential expression of the amino-propeptide. J. Cell Biol. **114**, 1307-1319 (1991).
120. Olsen, B.R., Reginato, A.M. and Wang, W. Bone development. Annu. Rev. Cell Dev. Biol. **16**, 191-220 (2000).
121. Hall, B.K. and Miyake, T. All for one and one for all: condensations and the initiation of skeletal development. Bioessays **22**, 138-147 (2000).
122. Dowthwaite, G.P., Bishop, J.C., Redman, S.N., Khan, I.M., Rooney, P., Evans, D.J.R., Haughton, L., Bayram, Z., Boyer, S., Thomson, B., Wolfe, M.S. and Archer, C.W. The surface of articular cartilage contains a progenitor cell population. J. Cell Sci. **117**, 889-897 (2003).
123. Hunter, W. Of the structure and diseases of articulating cartilages. Phil. Trans. **470**, 514-521 (1743).
124. Bank, R.A., Bayliss, M.T., Lafeber, P.J.G., Maroudas, A. and Tekoppele, J.M. Ageing and zonal variation in post-translational modification of collagen in normal human articular cartilage. The age-related increase in non-enzymatic glycation affects biomechanical properties of cartilage. Biochem. J. **330**, 345-351 (1998).
125. Sztrolovics, R., Alini, M., Roughley, P.J. and Mort, J.S. Aggrecan degradation in human intervertebral disc and articular cartilage. Biochem. J. **326**, 235-241 (1997).
126. Melching, L.I. and Roughley, P.J. The synthesis of dermatan sulphate proteoglycans by fetal and adult human articular cartilage. Biochem. J. **261**, 501-508 (1989).
127. Roughley, P.J. Age-associated changes in cartilage matrix. Implications for tissue repair. Clin. Orthop. Rel. Res. **391S**, 153-160 (2001).
128. Mayne, R. and von der Mark, K. Collagens of cartilage. In: Ed: Hall, B.K. Cartilage volume 1. Structure, function and biochemistry. New York: Harcourt Brace Jovanovich, ch. 7 (1983).
129. Lee, D.M. and Weinblatt, M.E. Rheumatoid arthritis. The Lancet **358**, 903-911 (2001).
130. Pritzker, K.P.H. Cartilage histopathology in human and rhesus macaque osteoarthritis. In: Ed. Kuettner, K.E., Schleyerbach, R., Peyron, J.G. and Hascall, V.C. Articular cartilage and osteoarthritis. New York: Raven Press, ch. 33 (1992).
131. Menkes, C-J. and Lane, N.E. Are osteophytes good or bad? Osteoarthritis Cartilage **12**, S53-54 (2004).
132. Lowther, D.A., Sriratana, A. and Baker, M.S. Effect of inflammation on cartilage metabolism. In: Ed. Kuettner, K.E., Schleyerbach, R., Peyron, J.G. and Hascall, V.C. Articular cartilage and osteoarthritis. New York: Raven Press, ch. 38 (1992).
133. Yuan, G-H., Tanaka, M., Masuko-Hongo, K., Shibakawa, A., Kato, T., Nishioka, K. and Nakamura, H. Characterization of cells from pannus-like tissue over articular cartilage of advanced osteoarthritis. Osteoarthritis Cartilage **12**, 38-45 (2004).
134. Minns, R.J., Steven, F.S. and Hardinge, K. Osteoathrotic articular cartilage lesions of the femoral head observed in the scanning electron microscope. J. Pathol. **122**, 63-70 (1977).

135. Mitchell, N. and Shepard, N. The resurfacing of adult rabbit articular cartilage by multiple perforations through the subchondral bone. J. Bone Joint Surg. **58-A**, 230-233 (1976).
136. LeBaron, R.G. and Athanasiou, K.A. Ex vivo synthesis of articular cartilage. Biomaterials **21**, 2575-2587 (2000).
137. Sandell, L.J. and Aigner, T. Articular cartilage and changes in arthritis an introduction: cell biology of osteoarthritis. Arthritis Res. **3**, 107-113 (2001).
138. Spector, T.D. and MacGregor, A.J. Risk factors for osteoarthritis: genetics. Osteoarthritis Cartilage **12**, S39-44 (2004).
139. Nakase, T., Miyaji, T., Tomita, T., Kaneko, M., Kuriyama, K., Myoui, A., Sugamoto, K., Ochi, T. and Yoshikawa, H. Localization of bone morphogenetic protein-2 in human osteoarthritic cartilage and osteophyte. Osteoarthritis Cartilage **11**, 278-284 (2003).
140. Aigner, T., Vornehm, S.I., Zeiler, G., Dudhia, J., von der Mark, K. and Bayliss, M.T. Suppression of cartilage matrix gene expression in upper zone chondrocytes of osteoarthritic cartilage. Arthritis Rheumatism **40**, 562-569 (1997).
141. D'Lima, D.D., Hashimoto, S., Chen, P.C., Colwell Jr., C.W. and Lotz, M.K. Impact of mechanical trauma on matrix and cells. Clin. Orthop. Rel. Res. **391S**, 90-99 (2001).
142. Oyajobi, B.O. and Russell, R.G.G. Bone remodelling, cytokines, and joint disease. In: Ed. Kuettner, K.E., Schleyerbach, R., Peyron, J.G. and Hascall, V.C. Articular cartilage and osteoarthritis. New York: Raven Press, ch. 23 (1992).
143. Attur, M.G., Dave, M., Cipolletta, C., Kang, P., Goldring, M.B., Patel, I.R., Abramson, S.B. and Amin, A.R. Reversal of autocrine and paracrine effecs of interleukin 1 (IL-1) in human arthritis by type II IL-1 decoy receptor. Potential for pharmacological intervention. J. Biol. Chem. **275**, 40307-40315 (2000).
144. Homandberg, G.A., Hui, F., Wen, C., Purple, C., Bewsey, K., Koepp, H., Huch, K. and Harris, A. Fibronectin-fragment-induced cartilage chondrolysis is associated with release of catabolic cytokines. Biochem. J. **321**, 751-757 (1997).
145. Xie, D., Hui, F., Meyers, R. and Homandberg, G.A. Cartilage chondrolysis by fibronectin fragments is associated with release of several proteinases: stromelysin plays a major role in chondrolysis. Arch. Biochem. Biophys. **311**, 205-212 (1994).
146. Jennings, L., Wu, L., King, K.B., Hämmerle, H., Cs-Szabo, G. and Mollenhauer, J. The effects of collagen fragments on the extracellular matrix metabolism of bovine and human chondrocytes. Connective Tissue Res. **42**, 71-86 (2001).
147. Nishida, Y., Knudson, C.B. and Knudson, W. Osteogenic protein-1 inhibits matrix depletion in a hyaluronan hexasaccharide-induced model of osteoarthritis. Osteoarthritis Cartilage **12**, 374-382 (2004).
148. Liu, H., McKenna, L.A. and Dean, M.F. An N-terminal peptide from link protein can stimulate biosynthesis of collagen by human articular cartilage. Arch. Biochem. Biophys. **378**, 116-122 (2000).
149. Olee, T., Hashimoto, S., Quach, J. and Lotz, M. IL-18 is produced by articular chondrocytes and induces proinflammatory and catabolic responses. J. Immunol. **162**, 1096-1100 (1999).

150. Raz, A., Wyche, A., Siegel, N. and Needleman, P. Regulation of fibroblast cyclooxygenase synthesis by interleukin-1. J. Biol. Chem. **263**, 3022-3028 (1988).
151. Lyons-Giordano, R., Pratta, M-A., Galbraith, W., Davis, G.L. and Arner, E.C. Interleukin-1 differentially modulates chondrocyte expression of cyclooxygenase-2 and phospholipase A_2. Exp. Cell Res. **206**, 58-62 (1993).
152. Stadler, J., Stefanovic-Racic, M., Billiar, T.R., Curran, R.D., McIntyre, L.A., Georgescu, H.I., Simmons, R.L. and Evans, C.H. Articular chondrocytes synthesize nitric oxide in response to cytokines and lipopolysaccharide. J. Immunol. **147**, 3915-3920 (1991).
153. Kashiwagi, M., Enghild, J.J., Gendron, C., Hughes, C., Caterson, B., Itoh, Y. and Nagase, H. Altered proteolytic activities of ADAMTS-4 expressed by C-terminal processing. J. Biol. Chem. **279**, 10109-10119 (2004).
154. Kolettas, E., Muir, H.I., Barrett, J.C. and Hardingham, T.E. Chondrocyte phenotype and cell survival are regulated by culture conditions and by specific cytokines through the expression of Sox-9 transcription factor. Rheumatol. **40**, 1146-1156 (2001).
155. Li, J., Perrella, M.A., Tsai, J-C., Yet, S-F., Hsieh, C-M., Yoshizumi, M., Patterson, C., Endege, W.O., Zhou, F. and Lee, M-E. Induction of vascular endothelial growth factor gene expression by interleukin-1β in rat aortic smooth muscle cells. J. Biol. Chem. **270**, 308-312 (1995).
156. Kato, Y., Nakashima, K., Iwamoto, M., Murakami, H., Hiranuma, H., Koike, T., Suzuki, F., Fuchihata, H., Ikehara, Y., Noshiro, M. and Jikko, A. Effects of interleukin-1 on syntheses of alkaline phosphatase, type X collagen, and 1,25-dihydroxyvitamin D_3 receptor, and matrix calcification in rabbit chondrocyte cultures. J. Clin. Invest. 92, 2323-2330 (1993).
157. Tetlow, L.C. and Woolley, D.E. Comparative immunolocalization studies of collagenase 1 and collagenase 3 production in the rheumatoid lesion, and by human chondrocytes and synoviocytes *in vitro*. Br. J. Rheumatol. **37**, 64-70 (1998).
158. Pelletier, J-P., McCollum, R., Cloutier, J-M. and Martel-Pelletier, J. Synthesis of metalloproteases and interleukin 6 (IL-6) in human osteoarthritic synovial membrane is an IL-1 mediated process. J. Rheumatol. **22**, suppl. 43, 109-114 (1995).
159. Lotz, M. and Guerne, P-A. Interleukin-6 induces the synthesis of tissue inhibitor of metalloproteinases-1/erythroid potentiating activity (TIMP-1/EPA). J. Biol. Chem. **266**, 2017-2020 (1991).
160. Rodenburg, R.J.T., van den Hoogen, F.H., Barrera, P., van Venrooij, W.J., van de Putte, L.B.A. Superinduction of interleukin 8 mRNA in activated monocyte derived macrophages from rheumatoid arthritis patients. Ann. Rheum. Dis. **58**, 648-652 (1999).
161. Jovanovic, D.V., Di Battista, J.A., Martel-Pelletier, J., Jolicoeur, F.C., He, Y., Zhang, M., Mineau, F. and Pelletier, J-P. IL-17 stimulates the production and expression of proinflammatory cytokines, IL-1β and TNF-α, by human macrophages. J. Immunol. **160**, 3513-3521 (1998).
162. Cai, L., Yin, J., Starovasnik, M.A., Hogue, D.A., Hillan, K.J., Mort, J.S. and Filvaroff, E.H. Pathways by which interleukin 17 induces articular cartilage breakdown in vitro and in vivo. Cytokine **16**, 10-21 (2001).

163. Lotz, M., Blanco, F.J., von Kempis, J., Dudler, J., Maier, R., Villiger, P.M. and Geng, Y. Cytokine regulation of chondrocyte functions. J. Rheumatol. **22**, suppl. 43, 104-108 (1995).
164. Lo, Y.Y.C. and Cruz, T. Involvement of reactive oxygen species in cytokine and growth factor induction of c-*fos* expression in chondrocytes. J. Biol. Chem. 270, 11727-11730 (1995).
165. Henrotin, Y.E., Bruckner, P. and Pujol, J-P. L. The role of reactive oxygen species in homeostasis and degradation of cartilage. Osteoarthritis Cartilage **11**, 747-755 (2003).
166. Firestein, G.S. Starving the synovium: angiogenesis and inflammation in rheumatoid arthritis. J. Clin. Invest. **103**, 3-4 (1999).
167. Frank, S., Hübner, G., Breier, G., Longaker, M.T., Greenhalgh, D.G. and Werner, S. Regulation of vascular endothelial growth factor expression in cultured keratinocytes. Implications for normal and impaired wound healing. J. Biol. Chem. **270**, 12607-12613 (1995).
168. Blanco, F.J., Ochs, R.L., Schwartz, H. and Lotz, M. Chondrocyte apoptosis induced by nitric oxide. Am. J. Pathol. **146**, 75-86 (1995).
169. Mendes, A.F., Caramona, M.M., Carvalho, A.P. and Lopes, M.C. Differential roles of hydrogen peroxide and superoxide in mediating IL-1-induced NF-κB activation and iNOS expression in bovine articular chondrocytes. J. Cell. Biochem. **88**, 783-793 (2003).
170. Mathy-Hartert, M., Martin, G., Devel, P., Deby-Dupont, G., Pujol, J-P., Reginster, J-Y. and Henrotin, Y. Reactive oxygen species downregulate the expression of pro-inflammatory genes by human chondrocytes. Inflamm. Res. **52**, 111-118 (2003).
171. Li, W.Q., Qureshi, H.Y., Liacini, A., Dehnade, F. and Zafarullah, M. Transforming growth factor β1 induction of tissue inhibitor of metalloproteinases 3 in articular chondrocytes is mediated by reactive oxygen species. Free Rad. Biol. Med. **37**, 196-207 (2004).
172. Baker, A.H., Edwards, D.R. and Murphy, G. Metalloproteinase inhibitors: biological actions and therapeutic opportunities. J. Cell Sci. **115**, 3719-3727 (2002).
173. Wu, J-J., Lark, M.W., Chun, L.E. and Eyre, D.R. Sites of stromelysin cleavage in collagen types II, IX, X, and XI of cartilage. J. Biol. Chem. **266**, 5625-5628 (1991).
174. Maeda, S., Dean, D.D., Gay, I., Schwartz, Z. and Boyan, B. Activation of latent transforming growth factor β1 by stromelysin in extracts of growth plate chondrocyte-derived matrix vesicles. J. Bone Joint Surg. 16, 1281-1290 (2001).
175. Mohtai, M., Lane Smith, R., Schurman, D.J., Tsuji, Y., Torti, F.M., Hutchinson, N.I., Stetler-Stevenson, W.G. and Goldberg, G.I. Expression of 92-kD type IV collagenase/gelatinase in normal human articular cartilage by interleukin 1. J. Clin. Invest. **92**, 179-185 (1993).
176. Billinghurst, R.C., Dahlberg, L., Ionescu, M., Reiner, A., Bourne, R., Rorabeck, C., Mitchell, P., Hambor, J., Diekmann, O., Tschesche, H., Chen, J., Van Wart, H. and Poole, A.R. Enhanced cleavage of type II collagen by collagenases in osteoarthritic articular cartilage. J. Clin. Invest. **99**, 1534-1545 (1997).

177. Hiraoka, N., Allen, E., Apel, I.J., Gyetko, M.R. and Weiss, S.J. Matrix metalloproteinases regulate neovascularization by acting as pericellular fibrinolysins. Cell **95**, 365-377 (1998).
178. Sounni, N.E., Hajitou, D.A., Frankenne, F., Munaut, C., Gilles, C., Deroanne, C., Thompson, E.W., Foidart, J.M. and Noel, A. MT1-MMP expression promotes tumor growth and angiogenesis through an up-regulation of vascular endothelial growth factor expression. FASEB J. **16**, 555-564 (2002).
179. Tortorella, M.D., Burn, T.C., Pratta, M.A., Abbaszade, I., Hollis, J.M., Liu, R., Rosenfeld, S.A., Copeland, R.A., Decicco, C.P., Wynn, R., Rockwell, A., Yang, F., Duke, J.L., Solomon, K., George, H., Bruckner, R., Nagase, H., Itoh, Y., Ellis, D.M., Ross, H., Wiswall, B.H., Murphy, K., Hillman Jr., M.C., Hollis, G.F., Newton, R.C., Magolda, R.L., Trzaskos, J.M. and Arner, E.C. Purification and cloning of aggrecanase-1: a member of the ADAMTS family of proteins. Science **284**, 1664-1666 (1999).
180. Abbaszade, I., Liu, R-Q., Yang, F., Rosenfeld, S.A., Ross, O.H., Link, J.R., Ellis, D.M., Tortorella, M.D., Pratta, M.A., Hollis, J.M., Wynn, R., Duke, J.L., George, H.J., Hillman Jr., M.C., Murphy, K., Wiswall, B.H., Copeland, R.A., Decicco, C.P., Bruckner, R., Nagase, H., Itoh, Y., Newton, R.C., Magolda, R.L., Trzaskos, J.M., Hollis, G.F., Arner, E.C. and Burn, T.C. Cloning and characterization of *ADAMTS11*, an aggrecanase from the ADAMTS family. J. Biol. Chem. **274**, 23443-23450 (1999).
181. Tortorella, M., Pratta, M., Liu, R-Q., Abbaszade, I., Ross, H., Burn, T. and Arner, E. The thrombospondin motif of aggrecanase-1 (ADAMTS-4) is critical for aggrecan substrate recognition and cleavage. J. Biol. Chem. 275, 25791-25797 (2000).
182. Mort, J.S. and Buttle, D.J. Cathepsin B. Int. J. Biochem. Cell Biol. **29**, 715-720 (1997).
183. Mort, J.S., Magny, M-C. and Lee, E.R. Cathepsin B: an alternative protease for the generation of an aggrecan 'metalloproteinase' cleavage neoepitope. Biochem. J. **335**, 491-494 (1998).
184. Kostoulas, G., Lang, A., Nagase, H. and Baici, A. Stimulation of angiogenesis through cathepsin B inactivation of the tissue inhibitors of matrix metalloproteinases. FEBS Lett. **455**, 286-290 (1999).
185. Sires, U.I., Schmid, T.M., Fliszar, C.J., Wang, Z-Q., Gluck, S.L. and Welgus, H.G. Complete degradation of type X collagen requires the combined action of interstitial collagenase and osteoclast-derived cathepsin-B. J. Clin. Invest. **95**, 2089-2095 (1995).
186. Anderson, G.D., Hauser, S.D., McGarity, K.L., Bremer, M.E., Isakson, P.C. and Gregory, S.A. Selective inhibition of cyclooxygenase (COX)-2 reverses inflammation and expression of COX-2 and interleukin 6 in rat adjuvant arthritis. J. Clin. Invest. **97**, 2672-2679 (1996).
187. Lotz, M. Cytokines in cartilage injury and repair. Clin. Orthop. Rel. Res. **391S**, 108-115 (2001).
188. Narumiya, S., Sugimoto, Y. and Ushikubi, F. Prostanoid receptors: structures, properties, and functions. Physiol. Rev. 79, 1193-1226 (1999).
189. Marks Jr., S.C. and Miller, S. Local infusion of prostaglandin E_1 stimulates mandibular bone formation *in vivo*. J. Oral Pathol. 17, 500-505 (1988).
190. Harada, S-I., Nagy, J.A., Sullivan, K.A., Thomas, K.A., Endo, N., Rodan, G.A. and Rodan, S.B. Induction of vascular endothelial growth factor

expression by prostaglandin E_2 and E_1 in osteoblasts. J. Clin. Invest. **93**, 2490-2496 (1994).

191. Morales, T.I. Polypeptide regulators of matrix homeostasis in articular cartilage. In: Ed. Kuettner, K.E., Schleyerbach, R., Peyron, J.G. and Hascall, V.C. Articular cartilage and osteoarthritis. New York: Raven Press, ch. 18 (1992).
192. Shlopov, B.V., Smith Jr., G.N., Cole, A.A. and Hasty, K.A. Differential patterns of response to doxycycline and transforming growth factor β1 in the down-regulation of collagenases in osteoarthritic and normal human chondrocytes. Arthritis Rheum. **42**, 719-727 (1999).
193. Thompson, C.C.M., Clegg, P.D. and Carter, S.D. Differential regulation of gelatinases by transforming growth factor beta-1 in normal equine chondrocytes. Osteoarthritis Cartilage **9**, 325-331 (2001).
194. Günther, M., Haubeck, H-D., van de Leur, E., Bläser, J., Bender, S., Gütgemann, I., Fischer, D-C., Tschesche, H., Greiling, H., Heinrich, P.C. and Graeve, L. Transforming growth factor β1 regulates tissue inhibitor of metalloproteinases-1 expression in differentiated human articular chondrocytes. Arthritis Rheumatism **37**, 395-405 (1994).
195. Leco, K.J., Khokha, R., Pavloff, N., Hawkes, S.P. and Edwards, D.R. Tissue inhibitor of metalloproteinases-1 (TIMP-3) is an extracellular matrix-associated protein with a distinctive pattern of expression in mouse cells and tissues. J. Biol. Chem. **269**, 9352-9360 (1994).
196. Lo, M.Y. and Kim, H.T. Chondrocyte apoptosis induced by collagen degradation: inhibition by caspase inhibitors and IGF-1. J. Orthop. Res. **22**, 140-144 (2004).
197. van Beuningen, H.M., Glansbeek, H.L., van der Kraan, P.M. and van den Berg, W.B. Differential effects of local application of BMP-2 or TGF-β1 on both articular cartilage composition and osteophyte formation. Osteoarthritis Cartilage **6**, 306-317 (1998).
198. Chubinskaya, S., Kumar, B., Merrihew, C., Heretis, K., Rueger, D.C. and Kuettner, K.E. Age-related changes in cartilage endogenous osteogenic protein-1 (OP-1). Biochim. Biophys. Acta **1588**, 126-134 (2002).
199. Manabe, N., Oda, H., Nakamura, K., Kuga, Y., Uchida, S. and Kawaguchi, H. Involvement of fibroblast growth factor-2 in joint destruction of rheumatoid arthritis patients. Rheum. **38**, 714-720 (1999).
200. Walsh, D.A. Angiogenesis and arthritis. Rheumatol. **38**, 103-112 (1999).
201. Parkar, A.A., Kahmann, J.D., Howat, S.L.T., Bayliss, M.T. and Day, A.J. TSG-6 interacts with hyaluronan and aggrecan in a pH-dependent manner via a common functional element: implications for its regulation in inflamed cartilage. FEBS Lett. **428**, 171-176 (1998).
202. Glant, T.T., Kamath, R.V., Bárdos, T., Gál, I., Szántó, S., Murad, Y.M., Sandy, J.D., Mort, J.S., Roughley, P.J. and Mikecz, K. Cartilage-specific constitutive expression of TSG-6 protein (product of tumor necrosis factor α-stimulated gene 6) provides a chondroprotective, but not anti-inflammatory, effect in antigen-induced arthritis. Arthritis Rheum. **46**, 2207-2218 (2002).
203. van Beuningen, H.M., Glansbeek, H.L., van der Kraan, P.M. and van den Berg, W.B. Osteoarthritis-like changes in the murine knee joint resulting from intra-articular transforming growth factor-β injections. Osteoarthritis Cartilage **8**, 25-33 (2000).

204. Girkontaite, I., Frischholz, S., Lammi, P., Wagner, K., Swoboda, B., Aigner, T. and von der Mark, K. Immunolocalization of type X collagen in normal fetal and adult osteoarthritic cartilage with monoclonal antibodies. Matrix Biol. **15**, 231-238 (1996).
205. Pullig, O., Weseloh, G., Gauer, S. and Swoboda, B. Osteopontin is expressed by adult human osteoarthritic chondrocytes: protein and mRNA analysis of normal and osteoarthritic cartilage. Matrix Biol. **19**, 245-255 (2000).
206. Pullig, O., Weseloh, G., Ronneberger, D-L., Käkönen, S-M. and Swoboda, B. Chondrocyte differentiation in human osteoarthritis: expression of osteocalcin in normal and osteoarthritic cartilage and bone. Calcif. Tissue Int. **67**, 230-240 (2000).
207. Rees, J.A. and Ali, S.Y. Ultrastructural localisation of alkaline phosphate activity in osteoarthritic human articular cartilage. Ann. Rheum. Dis. **47**, 747-753 (1988).
208. Caterson, B., Hughes, C.E., Johnstone, B. and Mort, J.S. Immunological markers of cartilage proteoglycan metabolism in animal and human osteoarthritis. In: Ed. Kuettner, K.E., Schleyerbach, R., Peyron, J.G. and Hascall, V.C. Articular cartilage and osteoarthritis. New York: Raven Press, ch. 29 (1992).
209. Poole, C.A. Chondrons: the chondrocyte and its pericellular microenvironment. In: Ed. Kuettner, K.E., Schleyerbach, R., Peyron, J.G. and Hascall, V.C. Articular cartilage and osteoarthritis. New York: Raven Press, ch. 14 (1992).
210. Vailhé, B., Vittet, D. and Feige, J-J. In vitro models of vasculogenesis and angiogenesis. Lab. Invest. **81**, 439-452 (2001).
211. Carmeliet, P. Angiogenesis in health and disease. Nature Med. **9**, 653-660 (2003).
212. Folkman, J. and Shing, Y. Angiogenesis. J. Biol. Chem. **267**, 10931-10934 (1992).
213. Thurston, G., Rudge, J.S., Ioffe, E., Zhou, H., Ross, L., Croll, S.D., Glazer, N., Holash, J., McDonald, D.M. and Yancopoulos, G.D. Angiopoietin-1 protects the adult vasculature against plasma leakage. Nature Med. **6**, 460-463 (2000).
214. Hangai, M., Kitaya, N., Xu, J., Chan, C.K., Kim, J.J., Werb, Z., Ryan, S.J. and Brooks, P.C. Matrix metalloproteinase-9-dependent exposure of a cryptic migratory control site in collagen is required before retinal angiogenesis. Am. J. Path. **161**, 1429-1437 (2002).
215. Jain, R.K. Molecular regulation of vessel maturation. Nature Med. **9**, 685-693 (2003).
216. Szekanecz, Z., Koch, A.E. Cell-cell interactions in synovitis. Endothelial cells and immune cell migration. Arthritis Res. **2**, 368-373 (2000).
217. Walsh, D.A., Wade, M., Mapp, P.I. and Blake, D.R. Focally regulated endothelial proliferation and cell death in human synovium. Am. J. Pathol. **152**, 691-702 (1998).
218. Stevens, C.R., Blake, D.R., Merry, P., Revell, P.A. and Levick, J.R. A comparative study by morphometry of the microvascular in normal and rheumatoid synovium. Arthritis Rheumatism **34**, 1508-1513 (1991).
219. Naughton, D., Whelan, M., Smith, E.C., Williams, R., Blake, D.R. and Grootveld, M. An investigation of the abnormal metabolic status of synovial

fluid from patients with rheumatoid arthritis by high field proton nuclear magnetic resonance spectroscopy. FEBS Lett. **317**, 135-138 (1993).

220. Shahrara, S., Volin, M.V., Connors, M.A., Haines, G.K. and Koch, A.E. Differential expression of the angiogenic Tie receptor family in arthritic and normal synovial tissue. Arthritis Res. **4**, 201-208 (2002).
221. Walsh, D.A. and Pearson, C.I. Angiogenesis in the pathogenesis of inflammatory joint and lung diseases. Arthritis Res. **3**, 147-153 (2001).
222. Walsh, D.A. and Haywood, L. Angiogenesis: a therapeutic target in arthritis. Curr. Opin. Invest. Drugs **2**, 1054-1063 (2001).
223. Fenwick, S.A., Gregg, P.J. and Rooney, P. Osteoarthritic cartilage loses its ability to remain avascular. Osteoarthritis Cartilage **7**, 441-452 (1999).
224. Enomoto, H., Inoki, I., Komiya, K., Shiomi, T., Ikeda, E., Obata, K-I., Matsumoto, H., Toyama, Y. and Okada, Y. Vascular endothelial growth factor isoforms and their receptors are expressed in human osteoarthritic cartilage. Am. J. Path. **162**, 171-181 (2003).
225. Unemori, E.N., Ferrara, N., Bauer, E.A. and Amento, E.P. Vascular endothelial growth factor induces interstitial collagenase expression in human endothelial cells. J. Cell. Physiol. **153**, 557-562 (1992).
226. Pufe, T., Peterson, W., Tillmann, B. and Mentlein, R. The splice variants $VEGF_{121}$ and $VEGF_{189}$ of the angiogenic peptide vascular endothelial growth factor are expressed in osteoarthritic cartilage. Arthritis Rheum. **44**, 1082-1088 (2001).
227. Hashimoto, G., Inoki, I., Fujii, Y., Aoki, T., Ikeda, E. and Okada, Y. Matrix metalloproteinases cleave connective tissue growth factor and reactivate angiogenic activity of vascular endothelial growth factor 165. J. Biol. Chem. **277**, 36288-36295 (2002).
228. Hayami, T., Funaki, H., Yaoeda, K., Mitui, K., Yamagiwa, H., Tokunaga, K., Hatano, H., Kondo, J., Hiraki, Y., Yamamoto, T., Duong, L.T. and Endo, N. Expression of the cartilage derived anti-angiogenic factor chondromodulin-I decreases in the early stage of experimental osteoarthritis. J. Rheumatol. **30**, 2207-2217 (2003).
229. Michaelson, I.C. The mode of development of the vascular system of the retina, with some observations on its significance for certain retinal diseases. Trans. Ophthalmol. Soc. UK. **68**, 137-180 (1948).
230. Plouët, J., Schilling, J. and Gospodarowicz, D. Isolation and characterization of a newly identified endothelial cell mitogen produced by AtT-20 cells. EMBO J. **8**, 3801-3806 (1989).
231. Ferrara, N. and Henzel, W.J. Pituitary follicular cells secrete a novel heparin-binding growth factor specific for vascular endothelial cells. Biochem. Biophys. Res. Comm. **161**, 851-858 (1989).
232. Connolly, D.T., Olander, J.V., Heuvelman, D., Nelson, R., Monsell, R., Siegel, N., Haymore, B.L., Leimgruber, R. and Feder, J. Human vascular permeability factor. Isolation from U937 cells. J. Biol. Chem. **264**, 20017-20024 (1989).
233. Ferrara, N., Gerber, H-N. and LeCouter, J. The biology of VEGF and its receptors. Nature Med. **9**, 669-676 (2003).
234. Tischer, E., Mitchell, R., Hartman, T., Silva, M., Gospodarowicz, D., Fiddes, J.C. and Abraham, J.A. The human gene for vascular endothelial growth factor. Multiple protein forms are encoded through alternative exon splicing. J. Biol. Chem. **266**, 11947-11954 (1991).

235. Muller, Y.A., Li, B., Christinger, H.W., Wells, J.A., Cunningham, B.C. and de Vos, A.M. Vascular endothelial growth factor: crystal structure and functional mapping of the kinase domain receptor binding site. Proc. Natl. Acad. Sci. USA **94**, 7192-7197 (1997).
236. Peretz, D., Gitay-Goran, H., Safran, M., Kimmel, N., Gospodarowicz, D. and Neufeld, G. Glycosylation of vascular endothelial growth factor is not required for its mitogenic activity. Biochem. Biophys. Res. Comm. **182**, 1340-1347 (1992).
237. Houck, K.A., Ferrara, N., Winer, J., Cachianes, G., Li, B. and Leung, D.W. The vascular endothelial growth factor family: identification of a fourth molecular species and characterization of alternative splicing of RNA. Mol. Endocrin. **5**, 1806-1814 (1991).
238. Poltorak, Z., Cohen, T., Sivan, R., Kandelis, Y., Spira, G., Vlodavsky, I., Keshet, E. and Neufeld, G. VEGF145, a secreted vascular endothelial growth factor isoform that binds to extracellular matrix. J. Biol. Chem. **272**, 7151-7158 (1997).
239. Houck, K.A., Leung, D.W., Rowland, A.M., Winer, J. and Ferrara, N. Dual regulation of vascular endothelial growth factor bioavailability by genetic and proteolytic mechanisms. J. Biol. Chem. **267**, 26031-26037 (1992).
240. Neufeld, G., Cohen, T., Gengrinovitch, S. and Poltorak, Z. Vascular endothelial growth factor (VEGF) and its receptors. FASEB J., **13**, 9-22 (1999).
241. Keyt, B.A., Berleau, L.T., Nguyen, H.V., Chen, H., Heinsohn, H., Vandlen, R. and Ferrara, N. The carboxyl-terminal domain (111-165) of vascular endothelial growth factor is critical for its mitogenic potency. J. Biol. Chem., **271**, 7788-7795 (1996).
242. Soker, S., Gollamudi-Payne, S., Fidder, H., Charmahelli, H. and Klagsbrun, M. Inhibition of vascular endothelial growth factor (VEGF)-induced endothelial cell proliferation by a peptide corresponding to the exon 7-encoded domain of $VEGF_{165}$. J. Biol. Chem., **272**, 31582-31588 (1997).
243. Maglione, D., Guerriero, V., Viglietto, G., Delli-Bovi, P. and Persico, M.G. Isolation of a human placenta cDNA coding for a protein related to the vascular permeability factor. Proc. Natl. Acad. Sci. USA **88**, 9267-9271 (1991).
244. Cao, Y., Linden, P., Shima, D., Browne, F. and Folkman, J. In vivo angiogenic activity and hypoxia induction of heterodimers of placenta growth factor/vascular endothelial growth factor. J. Clin. Invest. **98**, 2507-2511 (1996).
245. Olofsson, B., Pajusola, K., Kaipainen, A., von Euler, G., Joukov, V., Saksela, O., Orpana, A., Pettersson, R.F., Alitalo, K. and Eriksson, U. Vascular endothelial growth factor B, a novel growth factor for endothelial cells. Proc. Natl. Acad. Sci. USA **93**, 2576-2581 (1996).
246. Lee, J., Gray, A., Yuan, J., Luoh, S-M., Avraham, H. and Wood, W.I. Vascular endothelial growth factor-related protein: a ligand and specific activator of the tyrosine kinase receptor Flt4. Proc. Natl. Acad. Sci. USA **93**, 1988-1992 (1996).
247. Achen, M.G., Jeltsch, M., Kukk, E., Mäkinen, T., Vitali, A., Wilks, A.F., Alitalo, K. and Stacker, S.A. Vascular endothelial growth factor D (VEGF-D) is a ligand for the tyrosine kinases VEGF receptor 2 (Flk1) and VEGF receptor 3 (Flt4). Proc. Natl. Acad. Sci. USA **95**, 548-553 (1998).

248. Ogawa, S., Oku, A., Sawano, A., Yamaguchi, S., Yazaki, Y. and Shibuya, M. A novel type of vascular endothelial growth factor, VEGF-E (NZ-7 VEGF), preferentially utilizes KDR/Flk-1 receptor and carries a potent mitotic activity without heparin-binding domain. J. Biol. Chem. **273**, 31273-31282 (1998).
249. Dor, Y., Porat, R. and Keshet, E. Vascular endothelial growth factor and vascular adjustments to perturbations in oxygen homeostasis. Am. J. Physiol. Cell Physiol. **280**, C1367-1374 (2001).
250. Gerber, H-P., Hillan, K.J., Ryan, A.M., Kowalski, J., Keller, G-A., Rangell, L., Wright, B.D., Radtke, F., Aguet, M. and Ferrara, N. VEGF is required for growth and survival in neonatal mice. Dev. **126**, 1149-1159 (1999).
251. Carmeliet, P., Ferreira, V., Breler, G., Pollefeyt, S., Kieckens, L., Gertsenstein, M., Fahrig, M., Vandenhoeck, A., Harpal, K., Eberhardt, C., Declercq, C., Pawling, J., Moons, L., Collen, D., Risau, W. and Nagy, A. Abnormal blood vessel development and lethality in embryos lacking a single VEGF allele. Nature **380**, 435-439 (1996).
252. Senger, D.R., Galli, S.J., Dvorak, A.M., Perruzzi, C.A., Harvey, V.S. and Dvorak, H.F. Tumor cells secrete a vascular permeability factor that promotes accumulation of ascites fluid. Science **219**, 983-985 (1983).
253. Koch, A.E., Harlow, L.A., Haines, G.K., Amento, E.P., Unemori, E.N., Lee Wong, W., Pope, R.M. and Ferrara, N. Vascular endothelial growth factor. A cytokine modulating endothelial function in rheumatoid arthritis. J. Immunol. **152**, 4149-4156 (1994).
254. Mandriota, S.J., Seghezzi, G., Vassalli, J-D., Ferrara, N., Wasi, S., Mazzieri, R., Mignatti, P. and Pepper, M.S. Vascular endothelial growth factor increases urokinase receptor expression in vascular endothelial cells. J. Biol. Chem. **270**, 9709-9716 (1995).
255. Gerber, H-P., Dixit, V. and Ferrara, N. Vascular endothelial growth factor induces expression of the antiapoptotic proteins Bcl-2 and A1in vascular endothelial cells. J. Biol. Chem. **273**, 13313-13316 (1998).
256. Zachary, I. Signaling mechanisms mediating vascular protective actions of vascular endothelial growth factor. Am. J. Physiol. Cell Physiol. **280**, C1375-1386 (2001).
257. Gerber, H-P., Malik, A.K., Solar, G.P., Sherman, D., Liang, X.H., Meng, G., Hong, K., Marsters, J.C. and Ferrara, N. VEGF regulates haematopoietic stem cell survival by an internal autocrine loop mechanism. Nature **417**, 954-958 (2002).
258. Barleon, B., Sozzani, S., Zhou, D., Weich, H.A., Mantovani, A. and Marmé, D. Migration of human monocytes in response to vascular endothelial growth factor (VEGF) is mediated via the VEGF receptor flt-1. Blood **87**, 3338-3343 (1996).
259. Brown, L.F., Detmar, M., Tognazzi, K., Abu-Jawdeh, G. and Iruela-Arispe, M.L. Uterine smooth muscle cells express functional receptors (flt-1 and KDR) for vascular permeability factor/vascular endothelial growth factor. Lab. Invest. **76**, 245-255 (1997).
260. Ahmed, A., Dunk, C., Kniss, D. and Wilkes, M. Role of VEGF receptor-1 (flt-1) in mediating calcium-dependent nitric oxide release and limiting DNA synthesis in human trophoblast cells. Lab. Invest. **76**, 779-791 (1997).
261. Millauer, B., Wizigmann-Voos, S., Schnürch, H., Martinez, R., Møller, N.P.H., Risau, W. and Ullrich, A. High affinity VEGF binding and

developmental expression suggest Flk-1 as a major regulator of vasculogenesis and angiogenesis. Cell **72**, 835-846 (1993).

262. Lambrechts, D., Storkebaum, E., Morimoto, M., Del-Favero, J., Desmet, F., Marklund, S.L., Wyns ,S., Thijs, V., Andersson, J., von Marion, I., Al-Chalabi, A., Bornes, S., Musson, R., Hanson, V., Beckman, L., Adolfsson, R., Singh Pall, H., Prats, H., Vermeire, S., Rutgeerts, P., Katayama, S., Awata, T., Leigh, N., Lang-Lazdunski, L., Dewerchin, M., Shaw, C., Moons, L., Vlietinck, R., Morrison, K.E., Robberecht, W., Van Broeckhoven, C., Collen, D., Anderson, P.M. and Carmeliet, P. VEGF is a modifier of amyotrophic lateral sclerosis in mice and humans and protects motoneurons against ischaemic death. Nature Gen. **34**, 383-394 (2003).
263. Zhang, H-T, Croft, P., Scott, P.A.E., Ziche, M., Weich, H.A., Harris, A.L. and Bicknell, R. Enhancement of tumor growth and vascular density by transfection of vascular endothelial cell growth factor into MCF-7 human breast carcinoma cells. J. Natl. Cancer Inst. **87**, 213-219 (1995).
264. Shweiki, D., Itin, A., Soffer, D. and Keshet, E. Vascular endothelial growth factor induced by hypoxia may mediate hypoxia-initiated angiogenesis. Nature **359**, 843-845 (1992).
265. Mihich, E. and Croce, C.M. Ninth annual Pezcoller symposium: the biology of tumors. Cancer Res. **59**, 491-497 (1999).
266. Bellamy, W.T., Richter, L., Sirjani, D., Roxas, C., Glinsmann-Gibson, B., Frutiger, Y., Grogan, T.M. and List, A.F. Vascular endothelial cell growth factor is an autocrine promoter of abnormal localized immature myeloid precursors and leukemia progenitor formation in myelodysplastic syndromes. Blood **97**, 1427-1434 (2001).
267. Bae, D-G., Gho, Y-S., Yoon, W-H. and Chae, C-B. Arginine-rich anti-vascular endothelial growth factor peptides inhibit tumor growth and metastasis by blocking angiogenesis. J. Biol. Chem., **275**, 13588-13596 (2000).
268. Niethammer, A.G., Xiang, R., Becker, J.C., Woodrich, H., Pertl, U., Karsten, G., Eliceiri, B.P. and Reisfeld, R.A. A DNA vaccine against VEGF receptor-2 prevents effective angiogenesis and inhibits tumor growth. Nature Med. **8**, 1369-1375 (2002).
269. Cheng, S-Y., Huang, H-J.S., Nagane, M., Ji, X-D., Wang, D., Shih, C-Y., Arap, W., Huang, C-M. and Cavanee, W.K. Suppression of glioblastoma angiogenicity and tumorigenicity by inhibition of endogenous expression of vascular endothelial growth factor. Proc. Natl. Acad. Sci. USA **93**, 8502-8507 (1996).
270. Witte, L., Hicklin, D.J., Zhu, Z., Pytowski, B., Kotanides, H., Rockwell, P. and Böhlen, P. Monoclonal antibodies targeting the VEGF receptor-2 (Flk1/KDR) as an anti-angiogenic therapeutic strategy. Cancer Metastasis Rev. **17**, 155-161 (1998).
271. Veenendaal, L.M., Jin, H., Ran, S., Cheung, L., Navone, N., Marks, J.W., Waltenberger, J., Thorpe, P. and Rosenblum, M.G. *In vitro* and *in vivo* studies of a $VEGF_{121}$/rGelonin chimeric fusion toxin targeting the neovasculature of solid tumors. Proc. Natl. Acad. Sci. USA **99**, 786607871 (2002).
272. Zilberberg, L., Shinkaruk, S., Lequin, O., Rousseau, B., Hagedorn, M., Costa, F., Caronzolo, D., Balke, M., Canron, X., Convert, O., Laïn, G., Gionnet, K., Gonçalvès, M., Bayle, M., Bello, L., Chassaing, G., Deleris, G. and Bikfalvi,

A. Structure and inhibitory effects on angiogenesis and tumor development of a new vascular endothelial growth inhibitor. J. Biol. Chem. **278**, 35564-35573 (2003).

273. Aiello, L.P., Avery, R.L., Arrigg, P.G., Keyt, B.A., Jampel, H.D., Shah, S.T., Pasquale, L.R., Thieme, H., Iwamoto, M.A., Park, J.E., Nguyen, H.V., Aiello, L.M., Ferrara, N. and King, G.L. Vascular endothelial growth factor in ocular fluid of patients with diabetic retinopathy and other retinal disorders. New Eng. J. Med. **331**, 1480-1487 (1994).
274. Celletti, F.L., Waugh, J.M., Amabile, P.G., Brendolan, A., Hilfiker, P.R. and Dake, M.D. Vascular endothelial growth factor enhances atherosclerotic plaque progression. Nature Med., **7**, 425-429 (2001).
275. Detmar, M., Brown, L.F., Claffey, K.P., Yeo, K-T., Kocher, O., Jackman, R.W., Berse, B. and Dvorak, H.F. Overexpression of vascular permeability factor/vascular endothelial growth factor and its receptors in psoriasis. J. Exp. Med. **180**, 1141-1146 (1994).
276. Brown, L.F., Olbricht, S.M., Berse, B., Jackman, R.W., Matsueda, G., Tognazzi, K.A., Manseau, E.J., Dvorak, H.F. and Van De Water, L. Overexpression of vascular permeability factor (VPF/VEGF) and its endothelial cell receptors in delayed hypersensitivity skin reactions. J. Immunol. **154**, 2801-2807 (1995).
277. Vaisman, N., Gospodarowicz, D. and Neufeld, G. Characterization of the receptors for vascular endothelial growth factor. J. Biol. Chem. **265**, 19461-19466 (1990).
278. Shibuya, M. Structure and dual function of vascular endothelial growth factor receptor-1 (flt-1). Int. J. Biochem. Cell Biol. **33**, 409-420 (2001).
279. Stewart, M., Turley, H., Cook, N., Pezzella, F., Pillai, G., Ogilvie, D., Cartlidge, S., Paterson, D., Copley, C., Kendrew, J., Barnes, C., Harris, A.L. and Gatter, K.C. The angiogenic receptor KDR is widely distributed in human tissues and tumours and relocates intracellularly on phosphorylation. An immunohistochemical study. Histopath. **43**, 33-39 (2003).
280. De Vries, C., Escobedo, J.A., Ueno, H., Houck, K., Ferrara, N. and Williams, L.T. The fms-like tyrosine kinase, a receptor for vascular endothelial growth factor. Science **255**, 989-991 (1992).
281. Terman, B.I., Dougher-Vermazen, M., Carrion, M.E., Dimitrov, D., Armellino, D.C., Gospodarowicz, D. and Böhlen, P. Identification of the KDR tyrosine kinase as a receptor for vascular endothelial cell growth factor. Biochem. Biophys. Res. Comm. 187, 1579-1586 (1992).
282. Wang, F., Kan, M., Xu, J., Yan, G. and McKeehan, W.L. Ligand-specific structural domains in the fibroblast growth factor receptor. J. Biol. Chem. **270**, 10222-10230 (1995).
283. Blechman, J.M., Lev, S., Barg, J., Eisenstein, M., Vaks, B., Vogel, Z., Givol, D. and Yarden, Y. The fourth immunoglobulin domain of the stem cell factor receptor couples ligand binding to signal transduction. Cell **80**, 103-113 (1995).
284. Mahadevan, D., Yu, J-C., Saldanha, J.W., Thanki, N., McPhie, P., Uren, A., LaRochelle, W.J. and Heidaran, M.A. Structural role of extracellular domain 1 of α-platelet-derived growth factor (PDGF) receptor for PDGF-AA and PDGF-BB binding. J. Biol. Chem. **270**, 27595-27600 (1995).

285. Davis-Smyth, T., Chen, H., Park, J., Presta, L.G. and Ferrara, N. The second immunoglobulin-like domain of the VEGF tyrosine kinase receptor flt-1 determines ligand binding and may initiate a signal transduction cascade. EMBO J. **15**, 4919-4927 (1996).
286. Fuh, G., Li, B., Crowley, C., Cunningham, B. and Wells, J.A. Requirements for binding and signaling of the kinase domain receptor for vascular endothelial growth factor. J. Biol. Chem., **273**, 11197-11204 (1998).
287. Wiesmann, C., Fuh, G., Christinger, H.W., Eigenbrot, C., Wells, J.A. and de Vos, A.M. Crystal structure at 1.7 Å resolution of VEGF in complex with domain 2 of the Flt-1 receptor. Cell, **91**, 695-704 (1997).
288. Lu, D., Kussie, P., Pytowski, B., Persaud, K., Bohlen, P., Witte, L. and Zhu, Z. Identification of the residues in the extracellular region of KDR important for interaction with vascular endothelial growth factor and neutralizing anti-KDR antibodies. J. Biol. Chem., **275**, 14321-14330 (2000).
289. Shinkai, A., Ito, M., Anazawa, H., Yamaguchi, S., Shitara, K. and Shibuya, M. Mapping of the sites involved in ligand association and dissociation at the extracellular domain of the kinase insert domain-containing receptor for vascular endothelial growth factor. J. Biol. Chem., **273**, 31283-31288 (1998).
290. Barleon, B., Totzke, F., Herzog, C., Blanke, S., Kremmer, E., Siemeister, G., Marmé, D. and Martiny-Baron, G. Mapping of the sites for ligand binding and receptor dimerization at the extracellular domain of the vascular endothelial growth factor receptor FLT-1. J. Biol. Chem., **272**, 10382-10388 (1997).
291. Waltenberger, J., Claesson-Welsh, L., Siegbahn, A., Shibuya, M. and Heldin, C-H. Different signal transduction properties of KDR and Flt-1, two receptors for vascular endothelial growth factor. J. Biol. Chem. **260**, 26988-26995 (1994).
292. Kroll, J. and Waltenberger, J. The vascular endothelial growth factor receptor KDR activates multiple signal transduction pathways in porcine aortic endothelial cells. J. Biol. Chem. **272**, 32521-32527 (1997).
293. Ito, N., Wernstedt, C., Engström, U. and Claesson-Welsh, L. Identification of vascular endothelial growth factor receptor-1 tyrosine phosphorylation sites and binding of SH2 domain-containing molecules. J. Biol. Chem. **273**, 23410-23418 (1998).
294. Rahimi, N., Dayanir, V. and Lashkari, K. Receptor chimeras indicate that the vascular endothelial growth factor receptor-1 (VEGFR-1) modulates mitogenic activity of VEGFR-2 in endothelial cells. J. Biol. Chem., **275**, 16986-16992 (2000).
295. Takahashi, T. and Shibuya, M. The 230 kDa mature form of KDR/Flk-1 (VEGF receptor-2) activates the PLC-γ pathway and partially induces mitotic signals in NIH3T3 fibroblasts. Oncogene 14, 2079-2089 (1997).
296. Sawano, A., Takahashi, T., Yamaguchi, S. and Shibuya, M. The phosphorylated 1169-tyrosine containing region of flt-1 kinase (VEGFR-1) is a major binding site for PLCγ. Biochem. Biophys. Res. Comm. **238**, 487-491 (1997).
297. Takahashi, T., Ueno, H. and Shibuya, M. VEGF activates protein kinase C-dependent, but Ras-independent Raf-MEK-MAP kinase pathway for DNA synthesis in primary endothelial cells. Oncogene **18**, 2221-2230 (1999).

298. Eliceiri, B.P., Paul, R., Schwartzberg, P.L., Hood, J.D., Leng, J. and Cheresh, D.A. Selective requirement for Src kinases during VEGF-induced angiogenesis and vascular permeability. Mol. Cell **4**, 915-924 (1999).
299. Meadows, K.N., Bryant, P. and Pumiglia, K. Vascular endothelial growth factor induction of the angiogenic phenotype requires Ras activation. J. Biol. Chem. **276**, 49289-49298 (2001).
300. Kolodkin, A.L., Levengood, D.V., Rowe, E.G., Tai, Y-T., Giger, R.J. and Ginty, D.D. Neuropilin is a semaphorin III receptor. Cell 90, 753-762 (1997).
301. Soker, S., Takashima, S., Miao, H.Q., Neufeld, G. and Klagsbrun, M. Neuropilin-1 is expressed by endothelial and tumor cells as an isoform-specific receptor for vascular endothelial growth factor. Cell **92**, 735-745 (1998).
302. Soker, S., Fidder, H., Neufeld, G. and Klagsbrun, M. Characterization of novel vascular endothelial growth factor (VEGF) receptors on tumor cells that bind $VEGF_{165}$ via its exon 7-encoded domain. J. Biol. Chem. **271**, 5761-5767 (1996).
303. Shalaby, F., Rossant, J., Yamaguchi, T.P., Gertsenstein, M., Wu, X-F., Breitman, M.L. and Schuh, A.C. Failure of blood-island formation and vasculogenesis in Flk-1-deficient mice. Nature **376**, 62-66 (1995).
304. Fong, G-H., Rossant, J., Gertsenstein, M. and Breitman, M.L. Role of the Flt-1 receptor tyrosine kinase in regulating the assembly of vascular endothelium. Nature **376**, 66-70 (1995).
305. Fong, G-H., Zhang, L., Bryce, D-M. and Peng, J. Increased hemangioblast commitment, not vascular disorganization, is the primary defect in flt-1knock-out mice. Dev. **126**, 3015-3025 (1999).
306. Hiratsuka, S., Minowa, O., Kuno, J., Noda, T. and Shibuya, M. Flt-1 lacking the tyrosine kinase domain is sufficient for normal development and angiogenesis in mice. Proc. Natl. Acad. USA **95**, 9349-9354 (1998).
307. Carmeliet, P., Moons, L., Lutton, A., Vincenti, V., Compernolle, V., De Mol, M., Wu, Y., Bono, F., Devy, L., Beck, H., Scholz, D., Acker, T., DiPalma, T., Dewerchin, M., Noel, A., Stalmans, I., Barra, A., Blacher, S., Vandendriessche, T., Ponten, A., Eriksson, U., Plate, K.H., Foidart, J-M., Schaper, W., Charnock-Jones, D.S., Hicklin, D.J., Herbert, J-M., Collen, D. and Persico, M.G. Synergism between vascular endothelial growth factor and placental growth factor contributes to angiogenesis and plasma extravasation in pathological conditions. Nature Med. **7**, 575-583 (2001).
308. Luttun, A., Tjwa, M., Moons, L., Wu, Y., Angelillo-Scherrer, A., Liao, F., Nagy, J.A., Hooper, A., Priller, J., De Klerck, B., Compernolle, V., Daci, E., Bohlen, P., Dewerchin, M., Herbert, J-M., Fava, R., Matthys, P., Carmeliet, G., Collen, D., Dvorak, H.F., Hicklin, D.J. and Carmeliet, P. Revascularization of ischaemic tissues by PlGF treatment, and inhibition of tumor angiogenesis, arthritis and atherosclerosis by anti-Flt1. Nature Med. **8**, 831-840 (2002).
309. Barleon, B., Sozzani, S., Zhou, D., Weich, H.A., Mantovani, A. and Marmé, D. Migration of human monocytes in response to vascular endothelial growth factor (VEGF) is mediated via the VEGF receptor flt-1. Blood 87, 3336-3343 (1996).
310. Nakagawa, M., Kaneda, T., Arakawa, T., Morita, S., Sato, T., Yomada, T., Hanada, K., Kumegawa, M. and Hakeda, Y. Vascular endothelial growth

factor (VEGF) directly enhances osteoclastic bone resoprtion and survival of mature osteoclasts. FEBS letters, **473**, 161-164 (2000).

311. Hattori, K., Heissig, B., Wu, Y., Dias, S., Tejada, R., Ferris, B., Hicklin, D.J., Zhu, Z., Bohlen, P., Witte, L., Hendrikx, J., Hackett, N.R., Crystal, R.G., Moore, M.A.S., Werb, Z., Lyden, D. and Rafii, S. Placental growth factor reconstitutes hematopoiesis by recruiting $VEGFR1^+$ stem cells from bone-marrow microenvironment. Nature Med. **8**, 841-849 (2002).
312. Colotta, F., Dower, S.K., Sims, J.E. and Mantovani, A. The type II 'decoy' receptor: a novel regulatory pathway for interleukin 1. Immunol. Today **15**, 562-566 (1994).
313. Jang, J-H. Identification and characterization of soluble isoform of fibroblast growth factor receptor 3 in human SaOS-2 osteosarcoma cells. Biochem. Biophys. Res. Comm. **292**, 378-382 (2002).
314. Raines, M.A., Liu, L., Quan, S.G., Joe, V., DiPersio, J.F. and Golde, D.W. Identification and molecular cloning of a soluble human granulocyte-macrophage colony-stimulating factor receptor. Proc. Natl. Acad. Sci. USA **88**, 8203-8207 (1991).
315. Kendall, R.L. and Thomas, K.A. Inhibition of vascular endothelial cell growth factor activity by an endogenously encoded soluble receptor. Proc. Natl. Acad. Sci. USA **90**, 10705-10709 (1993).
316. Kendall, R.L., Wang, G. and Thomas, K.A. Identification of a natural soluble form of the vascular endothelial growth factor receptor, FLT-1, and its heterodimerization with KDR. Biochem. Biophys. Res. Comm. **226**, 324-328 (1996).
317. Goldman, C.K., Kendall, R.L., Cabrera, G., Soroceanu, L., Heike, Y., Gillespie, G.Y., Siegal, G.P., Mao, X., Bett, A.J., Huckle, W.R., Thomas, K.A. and Curiel, D.T. Paracrine expression of a native soluble vascular endothelial growth factor receptor inhibits tumor growth, metastasis, and mortality rate. Proc. Natl. Acad. Sci. USA **95**, 8795-8800 (1998).
318. Miotla, J., Maciewicz, R., Kendrew, J., Feldmann, M. and Paleolog, E. Treatment with soluble VEGF receptor reduces disease severity in murine collagen-induces arthritis. Lab. Invest. **80**, 1195-1205 (2000).
319. Ebos, J.M.L., Bocci, G., Man, S., Thorpe, P.E., Hicklin, D.J., Zhou, D., Jia, X. and Kerbel, R.S. A naturally occurring soluble form of vascular endothelial growth factor receptor 2 detected in mouse and human plasma. Mol. Cancer Res. **2**, 315-326 (2004).
320. Huang, X., Gottstein, C., Brekken, R.A. and Thorpe, P.E. Expression of soluble VEGF receptor 2 and characterization of its binding by surface plasmon resonance. Biochem. Biophys. Res. Comm. **252**, 643-648 (1998).
321. Pridie, K.H. A method of resurfacing osteoarthritic knee joints. J. Bone Joint Surg. **41-B**, 618-619 (1959).
322. Ochi, M., Uchio, Y., Tobita, M. and Kuriwaka, M. Current concepts in tissue engineering technique for repair of cartilage defect. Artificial Organs **25**, 172-179 (2001).
323. Hunziker, E.B. Articular cartilage repair: are the intrinsic biological constraints undermining this process insuperable? Osteoarthritis Cartilage **7**, 15-28 (1999).
324. Brittberg, M., Lindahl, A., Nilsson, A., Ohlsson, C., Isaksson, O. and Peterson, L. Treatment of deep cartilage defects in the knee with autologous chondrocyte transplantation. New Eng. J. Med. **331**, 889-895 (1994).

325. Ritsilä, V.A., Santavirta, S., Alhopuro, S., Poussa, M., Jaroma, H., Rubak, J.M., Eskola, A., Hoikka, V., Snellman, O. and Österman, K. Periosteal and perichondral grafting in reconstructive surgery. Clin. Orthop. Rel. Res. **302**, 259-265 (1994).
326. Kreder, H.J, Moran, M., Keeley, F.W. and Salter, R.B. Biologic resurfacing of a major joint defect with cryopreserved allogeneic periosteum under the influence of continuous passive motion in a rabbit model. Clin. Orthop. Rel. Res. **300**, 288-296 (1994).
327. Grande, D.A., Pitman, M.I., Peterson, L., Menche, D. and Klein, M. The repair of experimentally produced defects in rabbit articular cartilage by autologous chondrocyte transplantation. J. Orthop. Res. **7**, 208-218 (1989).
328. Aigner, J., Tegeler, J., Hutzler, P., Campoccia, D., Pavesio, A., Hammer, C., Kastenbauer, E. and Naumann, A. Cartilage tissue engineering with novel nonwoven structured biomaterial based on hyaluronic acid benzyl ester. J. Biomed. Mater. Res. **42**, 172-181 (1998).
329. Ochi, M., Uchio, Y., Kawasaki, K., Wakitani, S. and Iwasa, J. Transplantation of cartilage-like tissue made by tissue engineering in the treatment of cartilage defects of the knee. J. Bone Joint Surg. **84-B**, 571-578 (2002).
330. Nehrer, S., Breinan, H.A., Ramappa, A., Young, G., Shortroff, S., Louie, L.K., Sledge, C.B., Yannas, I.V. and Spector, M. Matrix collagen type and pore size influence behaviour of seeded canine chondrocytes. Biomaterials **18**, 769-778 (1997).
331. Grigolo, B., Lisignoli, G., Piacentini, A., Fiorini, M., Gobbi, P., Mazzotti, G., Duca, M., Pavesio, A. and Facchini, A. Evidence for redifferentiation of human chondrocytes grown on a hyaluronan-based biomaterial (HYAFF®11)\: molecular, immunohistochemical and ultrastructural analysis. Biomaterials **23**, 1187-1195 (2002).
332. Kisiday, J., Jin, M., Kurz, B., Hung, C., Semino, C., Zhang, S. and Grodzinsky, A.J. Self-assembling peptide hydrogel fosters chondrocyte extracellular matrix production and cell division: implications for cartilage tissue repair. Proc. Natl. Acad. Sci. USA **99**, 9996-10001 (2002).
333. Ibusuki, S., Fuji, Y., Iwamoto, Y. and Matsuda, T. Tissue-engineered cartilage using an injectable and *in situ* gelable thermoresponsive gelatin: fabrication and *in vitro* performance. Tissue Eng. **9**, 371-384 (2003).
334. Girotto, D., Urbani, S., Brun, P., Renier, D., Barbucci, R. and Abatangelo, G. Tissue-specific gene expression in chondrocytes grown on three-dimensional hyaluronic acid scaffolds. Biomaterials **24**, 3265-3275 (2003).
335. Allemann, F., Mizuno, S., Eid, K., Yates, K.E., Zaleske, D. and Glowacki, J. Effects of hyaluronan on engineered articular cartilage extracellular matrix gene expression in 3-dimensional collagen scaffolds. J. Biomed. Mater. Res. **55**, 13-19 (2001).
336. Mauck, R.L., Soltz, M.A., Wang, C.C.B., Wong, D.D., Chao, P-H.G., Valhmu, W.B., Hung, C.T. and Ateshian, G.A. Functional tissue engineering of articular cartilage through dynamic loading of chondrocyte-seeded agarose gels. J. Biomech. Eng. **122**, 252-260 (2000).
337. Barbucci, R., Lamponi, S., Borzacciello, A., Ambrosio, L., Fini, M., Torricelli, P. and Giardino, R. Hyaluronic acid hydrogel in the treatment of osteoarthritis. Biomaterials **23**, 4503-4513 (2002).

338. Solchaga, L.A., Yoo, J.U., Lundberg, M., Dennis, J.E., Huibregtse, B.A., Goldberg, V.M. and Caplan, A.I. Hyaluronan-based polymers in the treatment of osteochondral defects. J. Orthop. Res. **18**, 773-780 (2000).
339. Grigolo, B., Roseti, L., Fiorini, M., Fini, M., Giavaresi, G., Aldini, N.N., Giardino, R. and Facchini, A. Transplantation of chondrocytes seeded on a hyaluronan derivative (Hyaff®-11) into cartilage defects in rabbits. Biomaterials **22**, 2417-2424 (2001).
340. Hunziker, E.B. Growth-factor-induced healing of partial-thickness defects in adult articular cartilage. Osteoarthritis Cartilage **9**, 22-32 (2001).
341. Hunziker, E.B. and Rosenberg, L.C. Repair of partial-thickness defects in articular cartilage: cell recruitment from the synovial membrane. J. Bone Joint Surg. **78-A**, 721-733 (1996).
342. Hunziker, E.B. and Driesang, I.M.K. Functional barrier principle for growth-factor-based articular cartilage repair. Osteoarthritis Cartilage **11**, 320-327 (2003).
343. Kaps, C., Bramlage, C., Smolian, H., Haisch, A., Ungethüm, U., Burmester, G-R., Sittinger, M., Gross, G. and Häupl, T. Bone morphogenetic proteins promote cartilage differentiation and protect engineered artificial cartilage from fibroblast invasion and destruction. Arthritis Rheumatism **46**, 149-162 (2002).
344. Gelse, K., von der Mark, K., Aigner, T., Park, J. and Schneider, H. Articular cartilage repair by gene therapy using growth factor-producing mesenchymal cells. Arthritis Rheumatism **48**, 430-441 (2003).
345. de Bandt, M., Grossin, M., Weber, A-J., Chopin, M., Elbim, C., Pla, M., Gougerot-Pocidalo, M-A. and Gaudry, M. Suppression of arthritis and protection from bone destruction by treatment with TNP-470/AGM-1470 in a transgenic mouse model of rheumatoid arthritis. Arthritis Rheum. **43**, 2056-2063 (2000).
346. Koch, A.E., Szekanecz, Z., Friedman, J., Haines, G.K., Langman, C.B. and Bouck, N.P. Effects of thrombospondin-1 on disease course and angiogenesis in rat adjuvant-induced arthritis. Clin. Immun. Immunopath. **86**, 199-208 (1998).
347. Elzie, C.A. and Murphy-Ullrich, J.E. The N-terminus of thrombospondin: the domain stands apart. Int. J. Biochem. Cell Biol. **36**, 1090-1101 (2004).
348. Friedlander, M., Brooks, P.C., Shaffer, R.W., Kincaid, C.M., Varner, J.A. and Cheresh, D.A. Definition of two angiogenic pathways by distinct α_v integrins. Science **270**, 1500-1502 (1995).
349. Conway, J.G., Andrews, R.C., Beaudet, B., Bickett, D.M., Boncek, V., Brodie, T.A., Clark, R.L., Crumrine, R.C., Leenitzer, M.A., McDougald, D.L., Han, B., Hedeen, K., Lin, P., Milla, M., Moss, M., Pink, H., Rabinowitz, M.H., Tippin, T., Scates, P.W., Selph, J., Stimpson, S.A., Warner, J. and Becherer, J.D. Inhibition of tumor necrosis factor-α (TNF-α) production and arthritis in the rat by GW3333, a dual inhibitor of TNF-α-converting enzyme and matrix metalloproteinases. J. Pharm. Exp. Therap. **298**, 900-908 (2001).
350. Zhu, Z., Rockwell, P., Lu, D., Kotanides, H., Pytowski, B., Hicklin, D.J., Bohlen, P. and Witte, L. Inhibition of vascular endothelial growth factor-induced receptor activation with anti-kinase insert domain-containing receptor single-chain antibodies from a phage display library. Cancer Res., **58**, 3209-3214 (1998).

351. Cao, Y. Endogenous angiogenesis inhibitors and their therapeutic implications. Int. J. Biochem. Cell Biol. **33**, 357-369 (2001).
352. Dinarello, C.A. Interleukin-1 and interleukin01 antagonism. Blood, **77**, 1627-1652 (1991).
353. Jiang, Y., Jahagirdar, B.N., Reinhardt, R.L., Schwartz, R.E., Keene, C.D., Ortiz-Gonzalez, X.R., Reyes, M., Lenvik, T., Lund, T., Blackstad, M., Du, J., Aldrich, S., Lisberg, A., Low, W.C., Largaespaeda, D.A. and Verfaillie, C.M. Pluripotency of mesenchymal stem cells derived from adult marrow. Nature **418**, 41-49 (2002).
354. Nakahara, H., Goldberg, V.M. and Caplan, A.I. Culture-expanded human periosteal-derived cells exhibit osteochondral potential in vivo. J. Orthop. Res. **9**, 465-476 (1991).
355. De Bari, C., Sell'Accio, F., Tylzanowski, P. and Luyten, F.P. Multipotent mesenchymal stem cells from adult human synovial membrane. Arthritis Rheum. **44**, 1928-1942 (2001).
356. Barry, F.P. and Murphy, J.M. Mesenchymal stem cells: clinical applications and biological characterization. Int. J. Biochem. Cell Biophys. **36**, 568-584 (2004).
357. Alsalameh, S., Amin, R., Gemba, T. and Lotz, M. Identification of mesenchymal progenitor cells in normal and osteoarthritic human articular cartilage. Arthritis Rheumatism **50**, 1522-1532 (2004).
358. Butnariu-Ephrat, M., Robinson, D., Mendes, D.G., Halperin, N. and Nevo, Z. Resurfacing of goat articular cartilage by chondrocytes derived from bone marrow. Clin. Orthop. Rel. Res. **330**, 234-243 (1996).
359. Majumdar, M.K., Banks, V., Peluso, D.P. and Morris, E.A. Isolation, characterization, and chondrogenic potential of human bone marrow-derived multipotential stromal cells. J. Cell. Physiol. **185**, 98-106 (2000).
360. Tsuchiya, H., Kitoh, H., Sugiura, F. and Ishiguro, N. Chondrogenesis enhanced by overexpression of sox9 gene in mouse bone marrow-derived mesenchymal stem cells. Biochem. Biophys. Res. Comm. **301**, 338-343 (2003).
361. Indrawattana, N., Chen, G., Tadokoro, M., Shann, L.H., Ohgushi, H., Tateishi, T., Tanaka, J. and Bunyaratvej, A. Growth factor combination for chondrogenic induction from human mesenchymal stem cell. Biochem. Biophys. Res. Comm. **320**, 914-919 (2004).
362. De Bari, C., Dell'Accio, F. and Luyten, F.P. Failure of in vitro-differentiated mesenchymal stem cells from the synovial membrane to form ectopic stable cartilage in vivo. Arthritic Rheumatism **50**, 142-150 (2004).
363. Grande, D.A., Mason, J., Light, E. and Dines, D. Stem cells as platforms for delivery of genes to enhance cartilage repair. J. Bone Joint Surg. **85-A**, 111-116 (2003).
364. Quarto, R., Thomas, D. and Liang, C.T. Bone progenitor cell deficits and the age-associated decline in bone repair capacity. Calcif. Tissue Int. 56, 123-129 (1995).
365. Murphy, J.M., Dixon, K., Beck, S., Fabian, D., Feldman, A. and Barry, F. Reduced chondrogenic and adipogenic activity of mesenchymal stem cells from patients with advances osteoarthritis. Arthrits Rheum. **49**, 704-713 (2002).
366. de la Fuente, R., Abad, J.L., García-Castro, J., Fernández-Miguel, G., Petriz, J., Rubio, D., Vicaro-Abejón, C., Guillén, P., González, M.A. and Bernad, A.

Dedifferentiated adult articular chondrocytes: a population of human multipotent primitive cells. Exp. Cell Res. **297**, 313-328 (2004).

367. Reddi, A.H. Symbiosis of biotechnology and biomaterials: applications in tissue engineering of bone and cartilage. J. Cell. Biochem. **56**, 192-195 (1994).
368. Li, J.K., Wang, N. and Wu, X.S. Poly(vinyl alcohol) nanoparticles prepared by freezing–thawing process for protein / peptide drug delivery. J. Controlled Rel. **56**, 117-126 (1998).
369. Stammen, J.A., Williams, S., Ku, D.N. and Guldberg, R.E. Mechanical properties of a novel PVA hydrogel in shear and unconfined compression. Biomaterials **22**, 799-806 (2001).
370. Sawtell, R.M., Downes, S. and Kayser, M.V. An *in vitro* investigation of the PEMA/THFMA system using chondrocyte culture. J. Mater. Sci.:Mater. Med. 6, 676-679 (1995).
371. Reissis, N., Downes, S., Kayser, M. and Bentley, G. A simple method of cartilage regeneration using a new polymerising system: ultrastructural characteristics of the repair tissue. J. Mater. Sci.: Mater. Med. **5**, 793-797 (1994).
372. Hutcheon, G.A., Messiou, C., Wyre, R.M., Davies, M.C. and Downes, S. Water absorption and surface properties of novel poly(ethylmethacrylate) polymer systems for use in bone and cartilage repair. Biomaterials **22**, 667-676 (2001).
373. Lohmann, C.H., Schwartz, Z., Niederauer, G.G., Carnes Jr., D.L., Dean, D.D. and Boyan, B.D. Pretreatment with platelet derived growth factor-BB modulates the ability of costochondral resting zone chondrocytes incorporated into PLA/PGA scaffolds to form new cartilage in vivo. Biomaterials **21**, 49-61 (2000).
374. Chu, C.R., Monosov, A.Z. and Amiel, D. *In situ* assessment of cell viability within biodegradable polylactic acid polymer matrices. Biomat. **16**, 1361-1384 (1995).
375. Eerola, I., Salminen, H., Lammi, P., Lammi, M., von der Mark, K., Vuorio, E. and Säämänen, A-M. Type X collagen, a natural component of mouse articular cartilage. Association with growth, ageing and osteoarthritis. Arthritis Rheumatism **41**, 1287-1295 (1998).
376. Buma, P., Pieper, J.S., van Tienen, T., van Susante, J.L.C., van der Kraan, P.M., Veerkamp, J.H., van den Berg, W.B., Veth, R.P.H. and van Kuppevelt, T.H. Cross-linked type I and type II collagenous matrices for the repair of full-thickness articular cartilage defects – a study in rabbits. Biomaterials **24**, 3255-3263 (2003).
377. van Susante, J.L.C., Pieper, J., Buma, P., van Kuppevelt, T.H., van Beuningen, H., van der Kraan, P.M., Veerkamp, J.H., van den Berg, W.B. and Veth, R.P.H. Linkage of chondroitin-sulfate to type I collagen scaffolds stimulates the bioactivity of seeded chondrocytes in vitro. Biomat. **22**, 2359-2369 (2001).
378. Sakiyama-Elbert, S.E. and Hubbell, J.A. Development of fibrin derivatives for controlled release of heparin-binding growth factors. J. Control. Rel. **65**, 389-402 (2000).
379. Homandberg, G.A. Cartilage damage by matrix degradation products: fibronectin fragments. Clin. Orthop. Rel. Res. **391S**, 100-107 (2001).

380. Suh, J-K. F. and Matthew, H.W.T. Application of chitosan-based polysaccharide biomaterials in cartilage tissue engineering: a review. Biomaterials **21**, 2589-2598 (2000).
381. Zhang, S., Holmes, T., Lockshin, C. and Rich, A. Spontaneous assembly of a self-complementary oligopeptide to form a stable macroscopic membrane. Proc. Natl. Acad. Sci. USA **90**, 3334-3338 (1993).
382. Holmes, T.C., de Lacalle, S., Su, X., Liu,G., Rich, A. and Zhang, S. Extensive neurite outgrowth and active synapse formation on self-assembling peptide scaffolds. Proc. Natl. Acad. Sci. USA **97**, 6728-6733 (2000).
383. Schneiderman, R., Keret, D. and Maroudas, A. Effects of mechanical and osmotic pressure on the rate of glycosaminoglycan synthesis in the human adult femoral head cartilage: an in vitro study. J. Orthop. Res. **4**, 393-408 (1986).
384. Inoue, H., Kondo, J., Koike, T., Shukunami, C. and Hiraki, Y. Identification of an autocrine chondrocyte colony-stimulating factor: chondromodulin-1 stimulates the colony formation of growth plate chondrocytes in agarose culture. Biochem. Biophys. Res. Comm. **241**, 395-400 (1997).
385. Rahfoth, B., Weisser, J., Sternkopf, F., Aigner, T., von der Mark, K. and Bräuer, R. Transplantation of allograft chondrocytes embedded in agarose gel into cartilage defects of rabbits. Osteoarthritis Cartilage **6**, 50-65 (1998).
386. Guo, J.F., Jourdian, G.W. and MacCallum, D.K. Culture and growth characteristics of chondrocytes encapsulated in alginate beads. Conn. Tissue Res. **19**, 277-297 (1989).
387. Paige, K.T., Cima, L.G., Yaremchuk, M.J., Schloo, B.L., Vacanti, J.P. and Vacanti, C.A. De novo cartilage generation using calcium alginate-chondrocyte constructs. Plast. Reconstr. Surg. **97**, 168-178 (1996).
388. Van Susante, J.L.C., Buma, P., van Osch, G.J.V.M, Versleyen, D., van der Kraan, P.M., van der Berg, W.B. and Homminga, G.N. Culture of chondrocytes in alginate and collagen carrier gels. Acta Orthop. Scand. **66**, 549-556 (1995).
389. Ghosh, P., Holbert, C., Read, R. and Armstrong, S. Hyaluronic acid (hyaluronan) in experimental osteoarthritis. J. Rheumatol. **22** (suppl. 43), 155-157 (1995).
390. Larsen, N.E. and Balazs, E.A. Drug delivery systems using hyaluronan and its derivatives. Adv. Drug Deliv. Rev. **7**, 279-293 (1991).
391. Larsen, N.E., Pollak, C.T., Reiner, K., Leshchiner, E. and Balazs, E.A. Hylan gel biomaterial: dermal and immunologic compatibility. J. Biomed. Mater. Res. **27**, 1129-1134 (1993).
392. Larsen, N.E., Lombard, K.M., Parent, E.G. and Balazs, E.A. Effect of hylan on cartilage and chondrocyte cultures. J. Orthop. Res. **10**, 23-32 (1992).
393. Martens, P.B. Bilateral symmetric inflammatory reaction to hylan G-F 20 injection. Arthritis Rheum. **44**, 978-983 (2001).
394. Rastrelli, A., Beccaro, M., Biviano, F., Calderini, G. and Pastorello, A. Hyaluronic acid esters, a new class of semisynthetic biopolymers: chemical and physico-chemical properties. Clin. Implant Mat. **9**, 199-205 (1990).
395. Cortivo, R., Brun, P., Rastrelli, A. and Abatangelo, G. *In vitro* studies on biocompatibility of hyaluronic acid esters. Biomaterials **12**, 727-730 (1991).
396. Campoccia, D., Hunt, J.A., Doherty, P.J., Zhong, S.P., O'Regan, M., Benedetti, L. and Williams, D.F. Quantitative assessment of the tissue

response to films of hyaluronan derivatives. Biomaterials **17**, 963-975 (1996).

397. Catapano, G., De Bartolo, L., Vico, V. and Ambrosio, L. Morphology and metabolism of hepatocytes cultured in petri dishes on films and in non-woven fabrics of hyaluronic acid esters. Biomaterials **22**, 659-665 (2001).
398. Brun, P., Cortivo, R., Radice, M. and Abatangelo, G. Hyaluronan-based biomaterials in tissue engineering. In: Abatangelo, G. and Weigel, P.H., editors. New frontiers in medical sciences: refining hyaluronan. Elsevier Science B.V., 269-278 (2000).
399. Solchaga, L.A., Dennis, J.E., Goldberg, V.M. and Caplan, A.I. Hyaluronic acid-based polymers as cell carriers for tissue-engineered repair of bone and cartilage. J. Orthop. Res. **17**, 205-213 (1999).
400. Barbucci, R., Rappuoli, R., Borzacchiello, A. and Ambrosio, L. Synthesis, chemical and rheological characterization of new hyaluronic acid-based hydrogels. J. Biomater. Sci. Polymer Edn. **11**, 383-399 (2000).
401. Shu, X.Z., Liu, Y., Palumbo, F.S., Luo, Y. and Prestwich, G.D. In situ crosslinkable hyaluronan hydrogels for tissue engineering. Biomaterials **25**, 1339-1348 (2004).
402. Park, Y.D., Tirelli, N. and Hubbell, J.A. Photopolymerized hyaluronic acid-based hydrogels and interpenetrating networks. Biomaterials **24**, 893-900 (2003).
403. Doillon, C.J., Silver, F.H. and Berg, R.A. Fibroblast growth on a porous collagen sponge containing hyaluronic acid and fibronectin. Biomaterials **8**, 195-200 (1987).
404. Liu, L-S., Thompson, A.Y., Heidaran, M.A., Poser, J.W. and Spiro, R.C. An osteoconductive collagen/hyaluronate matrix for bone regeneration. Biomaterials 20, 1097-1108 (1999).
405. Bulpitt, P. and Aeschlimann, D.P. New strategy for chemical modification of hyaluronic acid: preparation of functionalized derivatives and their use in the formation of novel biocompatible hydrogels. J. Biomed. Mater. Res. **47**, 152-169 (1999).
406. Thompson, W.D. and Reid, A. Quantitative assays for the chick chorioallantoic membrane. In: Ed: Maragoudakis. Angiogenesis: from the molecular to integrative pharmacology. Kluwer, New York, 225-236 (2000).
407. West, D.C., Thompson, W.D., Sells, P.G. and Burbridge, M.F. Angiogenesis assays using chick chorioallantoic membrane. In: Ed: Murray, J.C. Methods in molecular medecine, vol. 46: angiogenesis protocols. Humana Press Ltd., Totowa, 107-129 (2001).
408. Hazel, S.J. A novel early chorioallantoic membrane assay demonstrates quantitative and qualitative changes caused by antiangiogenic substances. J. Lab. Clin. Med. **141**, 217-228 (2003).
409. Berghuis, H.M., Dieudonné, S.C., Goei, W. and Veldhuijzen, J.P. Effects of TGF-β2 on mineral resorption in cultured embryonic mouse long bones; ^{45}Ca release and osteoclast differentiation and migration. Eur. J. Orthodont. **16**, 130-137 (1994).
410. Drobnik, J. Hyaluronan in drug delivery. Adv. Drug Deliv. Rev. **7**, 295-308 (1991).
411. Mensitieri, M., Ambrosio, L., Nicolais, L., Bellini, D. and O'Regan, M. Viscoelastic properties modulation of a novel autocrosslinked hyaluronic acid polymer. J. Mater. Sci. Mater. Med. **7**, 695-698 (1996).

412. Trudel, J. and Massia, S.P. Assessment of the cytotoxicity of photocrosslinked dextran and hyaluronan-based hydrogels to vascular smooth muscle cells. Biomaterials **23**, 3299-3307 (2002).
413. Segura, T., Anderson, B.C., Chung, P.H., Webber, R.E., Shull, K.R. and Shea, L.D. Crosslinked hyaluronic acid hydrogels: a strategy to functionalize and pattern. Biomaterials **26**, 359-371 (2005).
414. Bothner, H. and Wik, O. Rheology of hyaluronate. Acta Otolaryngol. suppl. **442**, 25-30 (1987).
415. Laurencin, C., Domb, A., Morris, C., Brown, V., Chasin, M., McConnell, R., Lange, N. and Langer, R. Poly(anhydride) administration in high doses in vivo: studies of biocompatibility and toxicology. J. Biomed. Mater. Res. **24**, 1463-1481 (1990).
416. Snyder, S.L. and Sobocinski, P.Z. An improved 2,4,6-trinitrobenzenesulfonic acid method for the determination of amines. Analyt. Biochem. **64**, 284-288 (1975).
417. Bitter, T. and Muir, H.M. A modified uronic acid carbazole reaction. Anat. Biochem. **4**, 330-334 (1962).
418. Farrar, D.F. and Rose, J. Rheological properties of PMMA bone cements during curing. Biomaterials **22**, 3005-3013 (2001).
419. Chiang, E.H., Laing, T.J., Meyer, C.R., Boes, J.L., Rubin, J.M. and Adler, R.S. Ultrasonic characterization of *in vitro* osteoarthritic articular cartilage with validation by confocal microscopy. Ultrasound in Med. & Biol. **23**, 205-213 (1997).
420. Cho, K.Y., Chung, T.W., Kim, B.C., Kim, M.K., Lee, J.H., Wee, W.R. and Cho, C.S. Release of ciprofloxacin from poloxamer-graft-hyaluronic acid hydrogels in vitro. Int. J. Pharmaceutics **260**, 83-91 (2003).
421. Winter, H.H. Can the gel point of a cross-linking polymer be detected by the G′ - G″ crossover? Polymer Eng. Sci. **27**, 1698-1702 (1987).
422. Winter, H.H. Polymer gels, materials that combine liquid and solid properties. MRS Bulletin **16**, 44-48 (1991).
423. Chambon, F., Petrovic, Z.S., MacKnight, W.J. and Winter, H.H. Rheology of model polyurethanes at the gel point. Macromolecules **19**, 2146-2149 (1986).
424. Elisseeff, J., Anseth, K., Sims, D., McIntosh, W., Randolph, M. and Langer, R. Transdermal photopolymerization for minimally invasive implantation. Proc. Natl. Acad. Sci. USA **96**, 3104-3107 (1999).
425. Schumacher, H.R. Synovial inflammation, crystals, and osteoarthritis. J. Rheumatol. **22**, suppl. 43, 101-103 (1995).
426. Piossek, C., Schneider-Mergener, J., Schirner, M., Vakalopoulou, E., Germeroth, L. and Thierauch, K-H. Vascular endothelial growth factor (VEGF) receptor II-derived peptides inhibit VEGF. J. Biol. Chem., **274**, 5612-5619 (1999).
427. Fairbrother, W.J., Christinger, H.W., Cochran, A.G., Fuh, G., Keenan, C.J., Quan, C., Shriver, S.K., Tom, J.Y.K., Wells, J.A. and Cunningham, B.C. Novel peptides selected to bind vascular endothelial growth factor target the receptor-binding site. Biochemistry, **37**, 17754-17764 (1998).
428. Pan, B., Li, B., Russell, S.J., Tom, J.Y.K., Cochran, A.G. and Fairbrother, W.J. Solution structure of a phage-derived peptide antagonist in complex with vascular endothelial growth factor. J. Mol. Biol. **316**, 769-787 (2002).

429. Binétruy-Tournaire, R., Demangel, C., Malavaud, B., Vassy, R., Rouyre, S., Kraemer, M., Pluoët, J., Derbin, C., Perret, G. and Mazié, J.C. Identification of a peptide blocking vascular endothelial growth factor (VEGF)-mediated angiogenesis. EMBO J. **19**, 1525-1533 (2000).
430. Siemeister, G., Schirner, M., Reusch, P., Barleon, B., Marmé, D. and Martiny-Baron, G. An antagonistic vascular endothelial growth factor (VEGF) variant inhibits VEGF-stimulated receptor autophosphorylation and proliferation of human endothelial cells. Proc. Natl. Acad. Sci. USA **95**, 4625-4629 (1998).
431. Ferrara, N. Role of vascular endothelial growth factor in regulation of physiological angiogenesis. Am. J. Physiol. Cell Physiol. **280**, C1358-C1366 (2001).
432. Herley, M.T., Yu, Y., Whitney, R.G. and Sato, J.D. Characterization of the VEGF binding site on the Flt-1 receptor. Biochem. Biophys. Res. Comm., **262**, 731-738 (1999).
433. Shibuya, M., Yamaguchi, S., Yamane, A., Ikeda, T., Tojo, A., Matsushime, H. and Sato, M. Nucleotide sequence and expression of a novel human receptor-type tyrosine kinase gene (*flt*) closely related to the *fms* family. Oncogene, **5**, 519-524 (1990).
434. Wiesmann, C., Christinger, H.W., Cochran, A.G., Cunningham, B.C., Fairbrother, W.J., Keenan, C.J., Meng, G. and de Vos, A.M. Crystal structure of the complex between VEGF and a receptor-blocking peptide. Biochemistry **37**, 17765-17772 (1998).
435. Smyth, N., Odenthal, U., Merkl, B. and Paulsson, M. Eukaryotic expression and purification of recombinant extracellular matrix proteins carrying the strep II tag. In: Ed: Streuli, C. and Grant, M. Methods in molecular biology, vol. 139: extracellular matrix protocols. Humana Press, Towata, ch. 5, 1-9 (1999).
436. Kohfeldt, E., Maurer, P., Vannahme, C. and Timpl, R. Properties of the extracellular calcium binding module of the proteoglycan testican. FEBS lett. **414**, 557-561 (1997).
437. Van Craenenbroeck, K., Vanhoenacker, P. and Haegeman, G. Episomal vectors for gene expression in mammalian cells. Eur. J. Biochem. **267**, 5665-5678 (2000).
438. Starovasnik, M.A., Christinger, H.W., Wiesmann, C., Champe, M.A., de Vos, A.M. and Skelton, N.J. Solution structure of the VEGF-binding domain of flt-1: comparison of its free and bound states. J. Mol. Biol. **293**, 531-544 (1999).
439. Fairbrother, W.J., Champe, MA., Christinger, H.W., Keyt, B.A. and Starovasnik, M.A. ^{1}H, ^{13}C and ^{15}N backbone assignment and secondary structure of the receptor-binding domain of vascular endothelial growth factor. Protein Sci. **6**, 2250-2260 (1997).
440. Längle-Rouault, F., Patzel, V., Benavente, A., Taillez, M., Silvestre, N., Bompard, A., Sczakiel, G., Jacobs, E. and Rittner, K. Up to 100-fold increase of apparent gene expression in the presence of Epstein-barr virus oriP sequences and EBNA1: implications of the nuclear import of plasmids. J. Virol. **72**, 6181-6185 (1998).
441. He, Y., Smith, S.K, Day, K.A., Clark, D.E., Licence, D.R. and Charnock-Jones, D.S. Alternative splicing of vascular endothelial growth factor

(VEGF)-R1 (FLT-1) pre-mRNA is important for the regulation of VEGF activity. Mol. Endocrin. **13**, 537-545 (1999).

442. Ma, L., Wang, X., Zhang, Z., Zhou, X., Chen, A. and Yao, L. Identification of the ligand-binding domain of human vascular-endothelial-growth-factor receptor Flt-1. Biotechnol. Appl. Biochem. **34**, 199-204 (2001).
443. Takita, H., Kikuchi, M., Sato, Y. and Kuboki, Y. Inhibition of BMP-induced ectopic bone formation by an antiangiogenic agent (epigallocatechin 3-gallate). Connect. Tiss. Res. **43**, 520-523 (2002).
444. La Rocca, R.V., Meer, J., Gilliatt, R.W., Stein, C.A., Cassidy, J., Myers, C.E. and Dalakas, M.C. Suramin-induced polyneuropathy. Neurology **40**, 954-960 (1990).
445. Montesano, R., Orci, L. and Vassalli, P. In vitro rapid organization of endothelial cells into capillary-like networks is promoted by collagen matrices. J. Cell Biol. **97**, 1648-1652 (1983).
446. Hernández, G.L., Volpert, O.V., Íñiguez, M.A., Lorenzo, E., Martínez-Martínez, S., Grau, R., Fresno, M. and Redondo, J.M. Selective inhibition of vascular endothelial growth factor-mediated angiogenesis by cyclosporin A: roles of the nuclear factor of activated T cells and cyclooxygenase 2. J. Exp. Med., **193**, 607-620 (2001).
447. Pertovaara, L., Kaipsainen, A., Mustonen, T., Orpana, A., Ferrara, N., Saksela, O. and Alitalo, K. Vascular endothelial growth factor is induced in response to transforming growth factor-β in fibroblastic and epithelial cells. J. Biol. Chem. **269**, 6271-6274 (1994).
448. Nicosia, R.F. and Ottinetti, A. Growth of microvessels in serum-free matrix culture of rat aorta. A quantitative assay of angiogenesis *in vitro*. Lab. Invest. **63**, 115-122 (1990).
449. Kragh, M., Hjarnaa, P-J.V., Bramm, E., Kristjansen, P.E.G., Rygaard, J. and Binderup, L. *In vivo* chamber angiogenesis assay: an optimised matrigel plug assay for fast assessment of anti-angiogenic activity. Int. J. Oncol. **22**, 305-311 (2003).
450. De Luca, F., Uyeda, J.A., Mericq, V., Mancilla, E.E., Yanovski, J.A., Barnes, K.M., Zile, M.H. and Baron, J. Retinoic acid is a potent regulator of growth plate chondrogenesis. Endocrin. **141**, 346-353 (2000).
451. Leenders, W., Lubsen, N., van Altena, M., Clauss, M., Deckers, M., Löwik, C., Breier, G., Ruiter, D. and de Waal, R. Design of a variant of vascular endothelial growth factor-A (VEGF-A) antagonizing KDR/flk-1 and flt-1. Lab. Invest. **82**, 473-481 (2002).
452. Weinrich, S.L., Pruzan, R., Ma, L., Ouellette, M., Tesmer, V.M., Holt, S.E., Bodnar, A.G., Lichsteiner, S., Kim, N.W., Trager, J.B., Taylor, R.D., Carlos, R., Andrews, W.H., Wright, W.E., Shay, J.W., Harley, C.B. and Morin, G.B. Reconstruction of human telomerase with the template RNA component hTR and the catalytic protein subunit hTRT. Nature Gen. **17**, 498-502 (1997).
453. Gagliardi, A., Hadd, H. and Collins, D.C. Inhibition of angiogenesis by suramin. Cancer Res. **52**, 5073-5075 (1992).
454. Ruppert, R., Hoffmann, E. and Sebald, W. Human bone morphogenetic protein 2 contains a heparin-binding site which modifies its biological activity. Eur. J. Biochem. **237**, 295-302 (1996).
455. Wu, S. and De Luca, F. Role of cholesterol in the regulation of growth plate chondrogenesis and longitudinal bone growth. J. Biol. Chem. **279**, 4642-4647 (2004).

456. Scheufler, C., Sebald, W. and Hülsmeyer, M. Crystal structure of human bone morphogenetic protein-2 at 2.7Å resolution. J. Mol. Biol. **287**, 103-115 (1999).
457. Roghani, M., Mansukhani, A., Dell'Era, P., Bellosta, P., Basilico, C., Rifkin, D.B. and Moscatelli, D. Heparin increases the affinity of basic fibroblast growth factor for its receptor but is not required for binding. J. Biol. Chem. **269**, 3976-3984 (1994).
458. García-Olivas, R., Hoebeke, J., Castel, S., Reina, M., Fager, G., Lustig, F. and Vilaró, S. Differential binding of platelet-derived growth factor isoforms to glycosaminoglycans. Histochem. Cell Biol. **120**, 371-382 (2003).
459. Devi, G.R., Yang, D-H., Rosenfeld, R.G. and Oh, Y. Differential effects of insulin-like growth factor (IGF)-binding protein-3 and its proteolytic fragments on ligand binding, cell surface association, and IGF-I receptor signalling. Endocrin. **141**, 4171-4179 (2000).
460. Hosang, M. Suramin binds to platelet-derived growth factor and inhibits its biological activity. J. Cell. Biochem. **29**, 265-273 (1985).
461. Coffey Jr., R.J., Leof, E.B., Shipley, G.D. and Moses, H.L. Suramin inhibition of growth factor receptor binding and mitogenicity in AKR-2B cells. J. Cell. Physiol. **132**, 143-148 (1987).
462. Trieb, K. and Blahovec, H. Suramin suppresses growth, alkaline-phosphatase and telomerase activity of human osteosarcoma cells in vitro. Int. J. Biochem. Cell Biol. **35**, 1066-1070 (2003).
463. Zhang, Z-J., Huckle, J., Francomano, C.A. and Spencer, R.G.S. The effects of pulsed low-intensity ultrasound on chondrocyte viability, proliferation, gene expression and matrix production. Ultrasound Med. Biol. **29**, 1645-1651 (2003).
464. Homandberg, G.A., Ummadi, M. and Kang, H. High molecular weight hyaluronan promotes repair of IL-1β-damaged cartilage explants from both young and old bovines. Osteoarthritis Cartilage **11**, 177-186 (2003).
465. Peattie, R.A., Nayate, A.P., Firpo, M.A., Shelby, J., Fisher, R.J. and Prestwich, G.D. Stimulation of in vivo angiogenesis by cytokine-loaded hyaluronic acid hydrogel implants. Biomaterials **25**, 2789-2798 (2004).
466. Bendele, A.M. and Hulman, J.F. Spontaneous cartilage degeneration in guinea pigs. Arthritis Rheum. **31**, 561-565 (1988).
467. Kim, H.D. and Valentini, R.F. Retention and activity of BMP-2 in hyaluronic acid-based scaffolds *in vitro*. J. Biomed. Mater. Res. 59, 573-584 (2002).
468. Loeser, R.F., Pacione, C.A. and Chubinskaya, S. The combination of insulin-like growth factor 1 and osteogenic protein 1 promotes increased survival of and matrix synthesis by normal and osteoarthritic human articular chondrocytes. Athritis Rheumatism **48**, 2188-2196 (2003).
469. Kieswetter, K., Schwartz, Z., Alderete, M., Dean, D.D. and Boyan, B.D. Platelet derived growth factor stimulates chondrocyte proliferation but prevents endochondral maturation. Endocrine **6**, 257-264 (1997).
470. Iwata, H., Ono, S., Sato, K., Sato, T. and Kawamura, M. Bone morphogenetic protein-induced muscle- and synovium-derived cartilage differentiation *in vitro*. Clin. Orthop. **296**, 295-300 (1993).
471. Gafni, Y., Turgeman, G., Liebergal, M., Pelled, G., Gazit, Z. and Gazit, D. Stem cells as vehicles for orthopedic gene therapy. Gene Therapy **11**, 417-426 (2004).

472. Moutsatsos, I.K., Turgeman, G., Zhou, S., Kurkalli, B.G., Pelled, G., Tzur, L., Kelley, P., Stumm, N., Mi, S., Müller, R., Zilberman, Y. and Gazit, D. Exogenously regulated stem cell-mediated gene therapy for bone regeneration. Mol. Therapy **3**, 449-461 (2001).
473. Nesterenko, M.V., Tilley, M. and Upton, S.J. A simple modification of Blum's silver stain method allows for 30 minute detection of proteins in polyacrylamide gels. J. Biochem. Biophys. Meth. **28**, 239-242 (1994).
474. Martin, R.B., Burr, D.B. and Sharkey, N.A. Ch. 2: Skeletal Biology. In: Skeletal Tissue Mechanics. New York: Springer-Verlag (1998).
475. Quintavalla, J., Uziel-Fusi, S., Yin, J., Boehnlein, E., Pastor, G., Blancuzzi, V., Singh, H.N., Kraus, K.H., O'Byrne, E. and Pellas, T.C. Fluorescently labelled mesenchymal stem cells (MSCs) maintain multilineage potential and can be detected following implantation into articular cartilage defects. Biomat. **23**, 109-119 (2002).
476. Ayad, S., Boot-Handford, R., Humphries, M.J., Kadler, K.E. and Shuttleworth, A. The extracellular matrix FactsBook. San Diego: Harcourt Brace and co., 2nd edition (1998).
477. Newman, P.J. The biology of PECAM-1. J. Clin. Invest. **99** (1), 3-8 (1997).

APPENDIX 1: Recipes

A1.1 Hydrogel Characterisation

Hyaluronidase buffer: 30mM citric acid, 150mM Na_2HPO_4, 150mM NaCl

A1.2 Expression and purification of flt-1(1-3)

LB broth: 10g/l tryptone, 5g/l yeast extract, 340 mM sodium chloride, 2mM sodium hydroxide.

LB agar: 10g/l tryptone, 5g/l yeast extract, 15g/l agar, 85mM sodium chloride, 1mM sodium hydroxide.

TBE buffer: 0.089M Tris, 0.089 M Borate, 0.002M EDTA.

TAE buffer: 27mM Tris, 2mM EDTA, 0.11% (v/v) acetic acid. pH 8.5.

Glycoprotein denaturing buffer (10X): 5% sodium dodecyl sulphate, 10% β-mercaptoethanol.

Cell extraction buffer: 0.25M sucrose, 1% Triton X-10.

PBS: 1 mM potassium dihydogen orthophosphate, 3mM disodium hydrogen orthophosphate, 155 mM sodium chloride.

Immunoblotting

Sample buffer (2X): 200mM Tris/HCl, pH 6.8, 4% SDS, 10mM EDTA, 30% glycerol, 0.3% bromophenol blue, 2% mercaptoethanol.

SDS-PAGE running buffer: 25mM Tris, 192mM Glycine, 3.5mM SDS.

Transfer buffer: 25mM Tris/HCl, 192mM glycine, 20% (v/v) methanol.

Ponceau S: 0.1% (w/v) ponceau S, 5% (v/v) acetic acid.

TBS: 50mM Tris/HCl, 200mM NaCl pH7.4.

Stripping buffer: 0.7% β-mercaptoethanol, 2% sodium dodecyl sulphate, 62.5mM Tris.

Purification

Strep-Tactin wash buffer:	100mM Tris (pH8.0), 150 mM NaCl, 1 mM EDTA.
Strep-Tactin elution buffer:	100mM Tris (pH8.0), 150mM NaCl, 1mM EDTA, 2.5mM desthiobiotin.
Heparin Sepharose washing buffer:	0.45mM sodium dihydrogen orthophosphate, 0.5mM disodium hydrogen orthophosphate, 120mM sodium chloride, pH 7.4.
Heparin Sepharose elution buffer:	0.45mM sodium dihydrogen orthophosphate, 0.5mM disodium hydrogen orthophosphate, 2M sodium chloride, pH 7.4.
Cation exchange start buffer:	20mM MES (2-(N-morpholino) ethanesulfonic acid), 100mM sodium chloride, pH 6.0.
Cation exchange elution buffer:	20mM MES, 1M sodium chloride, pH 6.0.

A1.3 Flt-1(1-3)/VEGF binding assay

HBS-EP buffer:	0.01M HEPES, 0.15M NaCl, 3mM EDTA, 0.005% polysorbate 20 (v/v).

Appendix 2: HUVEC medium supplements

Endothelial cell growth supplement	0.4%
Foetal bovine serum	2%
Epidermal growth factor	0.1ng/ml
Hydrocortisone	1μg/ml
Basic fibroblast factor	1ng/ml
Amphotericin B	50μg/ml
Gentamicin	50μg/ml

Supplied by Promocell (Heidelberg, Germany)

Appendix 3: Vectors

A3.1. Vector map of pCEP-Pu

Derived from pCEP-4 vector (Invitrogen).

This vector contains a Strep-tag where indicated.

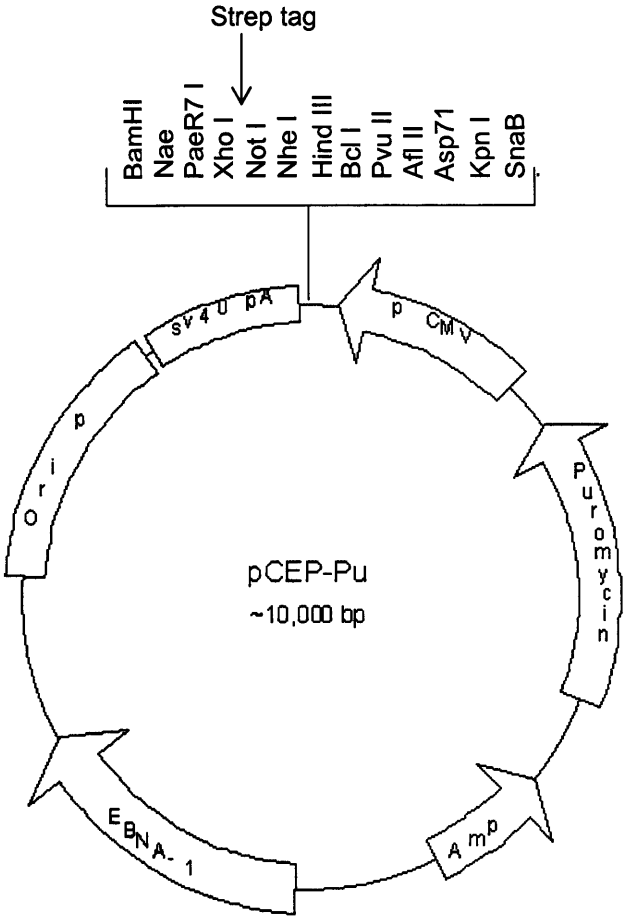

- CMV: Cytomegalovirus immediate early gene enhancer-promoter: drives expression of recombinant protein.
- Puromycin N-acetyltransferase gene for selection.
- Contains Epstein Barr virus (EBV) origin of replication. Sensitive to action of EBV nuclear antigen, which is expressed in 293 EBNA cells. This leads to maintenance of plasmid extrachromasomally, thus the plasmid replicates independent of host cell division. Episomal plasmid, with possibly higher protein production.

A3.2. Vector map of pCRII

Used in the TA cloning kit (Invitrogen)

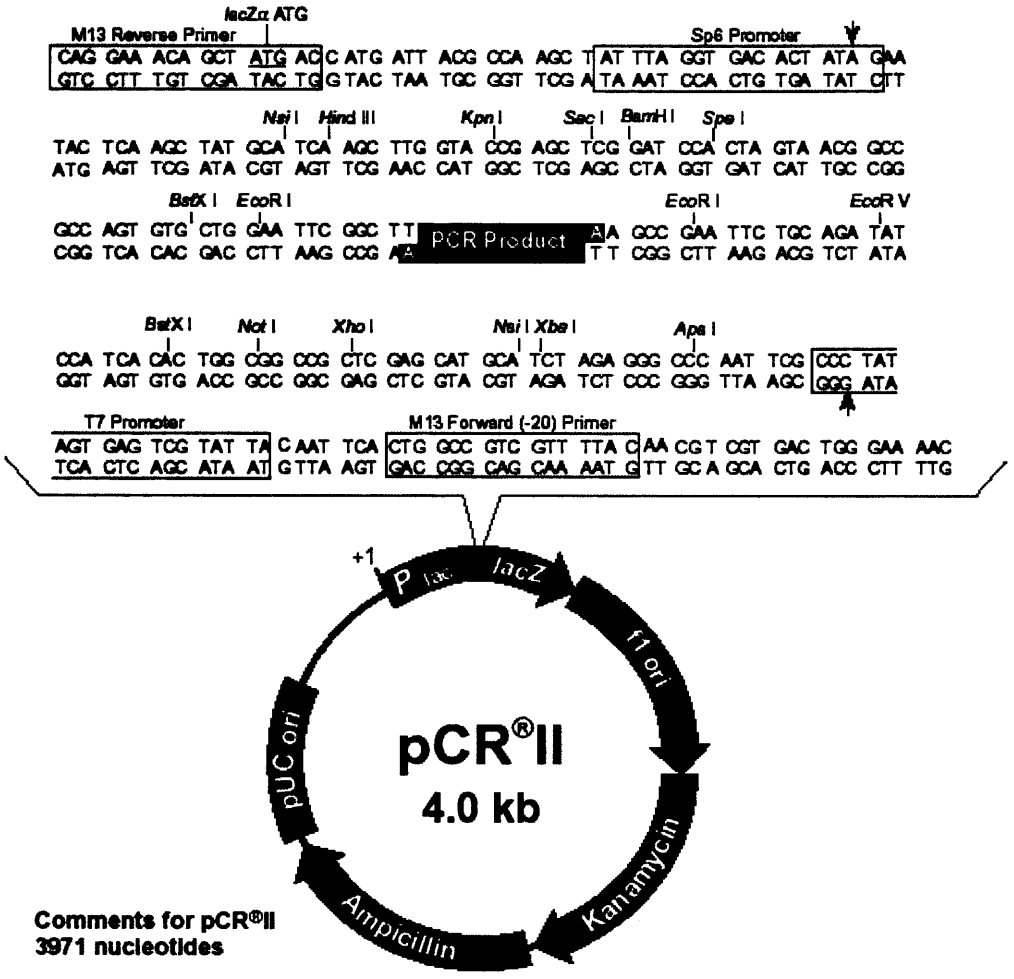

Comments for pCR®II
3971 nucleotides

LacZα gene: bases 1-587
M13 Reverse priming site: bases 205-221
Sp6 promoter: bases 239-256
T7 promoter: bases 404-423
M13 (-20) Forward priming site: bases 431-446
f1 origin: bases 588-1025
Kanamycin resistance ORF: bases 1359-2153
Ampicillin resistance ORF: bases 2171-3031
pUC origin: bases 3176-3849

Information courtesy of Invitrogen.

Appendix 4: Statistical analysis of flow cytometry data

All statistical analysis was undertaken using SPSS software, and a 5% significance level was used throughout.

Descriptive statistics for each variable in the study, values refer to the percentage of live cells, deduced from the flow cytometry data:

	N	Mean	Std. Deviation	Std. Error	95% Confidence Interval for Mean		Minimum	Maximum
					Lower Bound	Upper Bound		
0:1 XL	5	82.2600	3.69833	1.65394	77.6679	86.8521	78.17	86.67
0.1:1 XL	5	80.6860	2.56068	1.14517	77.5065	83.8655	76.38	83.08
0.5:1 XL	5	70.4160	11.17732	4.99865	56.5375	84.2945	55.90	81.58
1:1 XL	5	83.5640	3.21464	1.43763	79.5725	87.5555	80.80	88.88
1.5:1 XL	5	82.3900	2.61673	1.17024	79.1409	85.6391	78.30	85.58
2:1 XL	5	81.5660	8.07555	3.61150	71.5389	91.5931	72.79	90.12
6mg/ml HAED	5	78.9500	3.92435	1.75502	74.0773	83.8227	73.82	83.14
12mg/ml HAED	5	80.7260	5.58670	2.49845	73.7892	87.6628	71.94	86.67
SPA2 (3.4kD)	5	80.2280	5.53159	2.47380	73.3596	87.0964	71.24	84.58
SC4 (20kD)	5	80.1460	3.04087	1.35992	76.3703	83.9217	75.30	83.14
dead cells	5	41.5900	17.74203	7.93448	19.5604	63.6196	18.04	59.67
monolayer	5	92.0267	1.12358	.50248	90.6316	93.4218	90.79	93.84
Total	60	77.8791	13.62338	1.75877	74.3598	81.3983	18.04	93.84

A. Changes in cell death and survival compared to controls.

For the comparison of test samples against the positive (dead) and negative (monolayer) control, an independent samples t-test was conducted of the test samples against each control.

1. Ratio of 0:1 crosslinker : HAED

a. Comparison with the negative (live) control:

		Levene Test ...		t-test for Equality...						
		F	Significance	t	df	Sig(2-tailed)...	Mean Difference	Std. Error Diff...	95% Confidence Interval of the Difference	
									Lower	Upper
% of PI +ve cells	Equal variances ...	1.200	.305	-6.336	8	.00022	-10.4760	1.65337	-14.28867	-6.66333
	Not Equal variances ...			-6.336	6.765	.00045	-10.4760	1.65337	-14.41323	-6.53877

b. Comparison with the positive (dead) control:

b. Comparison with the positive (dead) control:

		Levene Test ...		t-test for Equality...						
		F	Significance	t	df	Sig(2-tailed)...	Mean Difference	Std. Error Diff...	95% Confidence Interval of the Difference	
									Lower	Upper
% of PI +ve cells	Equal variances ...	9.886	.014	-4.842	8	.00128	-45.3400	9.36370	-66.93272	-23.74728
	Not Equal variances ...			-4.842	4.983	.00475	-45.3400	9.36370	-69.43531	-21.24469

Conclusion: the significance is less that 0.05: the null hypothesis is rejected, there is a significant difference between cells cultured in 2:1 HAED hydrogels and both controls.

7. Hydrogels containing 6mg/ml HAED

a. Comparison with the negative (live) control:

		Levene Test ...		t-test for Equality...						
		F	Significance	t	df	Sig(2-tailed)...	Mean Difference	Std. Error Diff...	95% Confidence Interval of the Difference	
									Lower	Upper
% of PI +ve cells	Equal variances ...	1.990	.196	5.437	8	.00062	10.2100	1.87796	5.87942	14.54058
	Not Equal variances ...			5.437	6.111	.00151	10.2100	1.87796	5.63495	14.78505

b. Comparison with the positive (dead) control:

		Levene Test ...		t-test for Equality...						
		F	Significance	t	df	Sig(2-tailed)...	Mean Difference	Std. Error Diff...	95% Confidence Interval of the Difference	
									Lower	Upper
% of PI +ve cells	Equal variances ...	17.012	.003	-4.724	8	.00149	-42.4380	8.98320	-63.15330	-21.72270
	Not Equal variances ...			-4.724	4.281	.00773	-42.4380	8.98320	-66.74632	-18.12968

Conclusion: the significance is less that 0.05: the null hypothesis is rejected, there is a significant difference between cells cultured in hydrogels containing 6mg/ml and both controls.

8. Hydrogels containing 12mg/ml HAED

a. Comparison with the negative (live) control:

		Levene Test ...		t-test for Equality...						
		F	Significance	t	df	Sig(2-tailed)...	Mean Difference	Std. Error Diff...	95% Confidence Interval of the Difference	
									Lower	Upper
% of PI +ve cells	Equal variances ...	2.508	.152	3.270	8	.01136	8.7360	2.67185	2.57470	14.89730
	Not Equal variances ...			3.270	4.971	.02240	8.7360	2.67185	1.85561	15.61639

b. Comparison with the positive (dead) control:

		Levene Test ...		t-test for Equality...						
		F	Significance	t	df	Sig(2-tailed)...	Mean Difference	Std. Error Diff...	95% Confidence Interval of the Difference	
									Lower	Upper
% of PI +ve cells	Equal variances ...	12.385	.008	-4.782	8	.00139	-43.9120	9.18205	-65.08584	-22.73816
	Not Equal variances ...			-4.782	4.648	.00599	-43.9120	9.18205	-68.06318	-19.76082

Conclusion: the significance is less that 0.05: the null hypothesis is rejected, there is a significant difference between cells cultured in hydrogels containing 12mg/ml and both controls.

9. Hydrogels crosslinked with SPA_2-PEG (3.4kDa)

a. Comparison with the negative (live) control:

		Levene Test ...		t-test for Equality...						
		F	Significance	t	df	Sig(2-tailed)...	Mean Difference	Std. Error Diff...	95% Confidence Interval of the Difference	
									Lower	Upper
% of PI +ve cells	Equal variances ...	2.353	.164	3.226	8	.01213	7.9900	2.47662	2.27889	13.70111
	Not Equal variances ...			3.226	5.146	.02237	7.9900	2.47662	1.67760	14.30240

b. Comparison with the positive (dead) control:

		Levene Test ...		t-test for Equality...						
		F	Significance	t	df	Sig(2-tailed)...	Mean Difference	Std. Error Diff...	95% Confidence Interval of the Difference	
									Lower	Upper
% of PI +ve cells	Equal variances ...	13.448	.006	-4.893	8	.00120	-44.6580	9.12715	-65.70524	-23.61076
	Not Equal variances ...			-4.893	4.547	.00580	-44.6580	9.12715	-68.84169	-20.47431

Conclusion: the significance is less that 0.05: the null hypothesis is rejected, there is a significant difference between cells cultured in hydrogels crosslinked with SPA_2-PEG (3.4kDa) and both controls.

9. Hydrogels crosslinked with SC_4-PEG (20kDa)

a. Comparison with the negative (live) control:

		Levene Test ...		t-test for Equality...						
		F	Significance	t	df	Sig(2-tailed)...	Mean Difference	Std. Error Diff...	95% Confidence Interval of the Difference	
									Lower	Upper
% of PI +ve cells	Equal variances ...	.417	.536	6.542	8	.00018	8.9560	1.36892	5.79926	12.11274
	Not Equal variances ...			6.542	7.789	.00020	8.9560	1.36892	5.78435	12.12765

b. Comparison with the positive (dead) control:

		Levene Test ...		t-test for Equality...						
		F	Significance	t	df	Sig(2-tailed)...	Mean Difference	Std. Error Diff...	95% Confidence Interval of the Difference	
									Lower	Upper
% of PI +ve cells	Equal variances ...	20.508	.002	-4.914	8	.00117	-43.6920	8.89073	-64.19407	-23.18993
	Not Equal variances ...			-4.914	4.112	.00742	-43.6920	8.89073	-68.11385	-19.27015

Conclusion: the significance is less that 0.05: the null hypothesis is rejected, there is a significant difference between cells cultured in hydrogels crosslinked with SC_4-PEG (3.4kDa) and both controls.

B. Comparison within variable groups to reveal effects of different hydrogels.

An unrelated one-way ANOVA test was performed to test between different variables within the variable groups.

1. Comparison of crosslinker ratios.

a. Levene statistic to determine if variances are equal:

Levene Statistic	df1	df2	Significance
4.758	5	24	.004

b. One way Anova:

	Sum of Squares	df	Mean Square	F	Significance
Between Groups	590.933	5	118.187	3.116	.026
Within Groups	910.252	24	37.927		
Total	1501.185	29			

c. Contrasts: 1 and -1 indicate the two variables being compared for differences for each contrast.

Contrast	Crosslinker ratio					
	0:1	0.1:1	0.5:1	1:1	1.5:1	2:1
1	0	-1	1	0	0	0
2	0	0	0	-1	1	0
3	0	0	0	0	-1	1

d. Compare of contrasts: as the Levene statistic had a significance level below 0.05, we do not assume equal variances in the below table.

		Contrast	Value of Contrast	Std. Error	t	df	Significance (2-tailed)
% live cells	Assume equal variances	1	-10.2700	3.89498	-2.637	24	.014
		2	-1.1740	3.89498	-.301	24	.766
		3	-.8240	3.89498	-.212	24	.834
	Does not assume equal variances	1	-10.2700	5.12815	-2.003	4.419	.109
		2	-1.1740	1.85371	-.633	7.684	.545
		3	-.8240	3.79636	-.217	4.831	.837

Conclusion: the significance level is above 0.05, therefore there are no significant differences between the variables compared above.

2. Comparison of concentrations of HAED in the hydrogels.

a. Levene statistic to determine if variances are equal:

Levene Statistic	df1	df2	Significance
.627	2	12	.551

b. One way Anova:

	Sum of Squares	df	Mean Square	F	Significance
Between Groups	54.162	2	27.081	1.427	.278
Within Groups	227.782	12	18.982		
Total	281.945	14			

c. Contrasts: 1 and -1 indicate the two variables being compared for differences for each contrast.

Contrast	HAED concentration		
	6 mg/ml HAED	9 mg/ml HAED	12 mg/ml HAED
1	-1	1	0
2	0	-1	1

d. Compare of contrasts: as the Levene statistic had a significance level above 0.05, we assume equal variances in the below table.

		Contrast	Value of Contrast	Std. Error	t	df	Significance (2-tailed)
% live cells	Assume equal variances	1	4.6140	2.75549	1.674	12	.120
		2	-2.8380	2.75549	-1.030	12	.323
	Does not assume equal variances	1	4.6140	2.26867	2.034	7.701	.078
		2	-2.8380	2.88254	-.985	6.387	.361

Conclusion: the significance level is above 0.05, therefore there are no significant differences between the variables compared above.

3. Comparison between crosslinker types.

a. Levene statistic to determine if variances are equal:

Levene Statistic	df1	df2	Significance
1.195	2	12	.336

b. One way Anova:

	Sum of Squares	df	Mean Square	F	Significance
Between Groups	38.042	2	19.021	1.137	.353
Within Groups	200.717	12	16.726		
Total	238.759	14			

c. Contrasts: 1 and -1 indicate the two variables being compared for differences for each contrast.

Contrast	Crosslinker type		
	SPA2 (3.4kD)	SPA4 (20kD)	SC4 (20kD)
1	-1	1	0
2	0	-1	1

d. Compare of contrasts: as the Levene statistic had a significance level above 0.05, we assume equal variances in the below table.

		Contrast	Value of Contrast	Std. Error	t	df	Significance (2-tailed)
% of cells with PI +ve	Assume equal variances	1	3.3360	2.58661	1.290	12	.221
		2	-3.4190	2.58661	-1.322	12	.211
	Does not assume equal variances	1	3.3360	2.86120	1.166	6.425	.285
		2	-3.4190	1.97893	-1.728	7.975	.122

Conclusion: the significance level is above 0.05, therefore there are no significant differences between the variables compared above.

Appendix 5: DNA sequencing of pCEP-Pu/flt-1(1-3) construct

Raw data from DNA sequencing of pCEP-Pu/flt-1(1-3) construct, showing the 3′ sequence of flt-1(1-3) at the top left, followed by the sequence for the primer P2a, with the Not I site indicated. The Strep-tag is shown in frame. The brackets correspond to the codons.

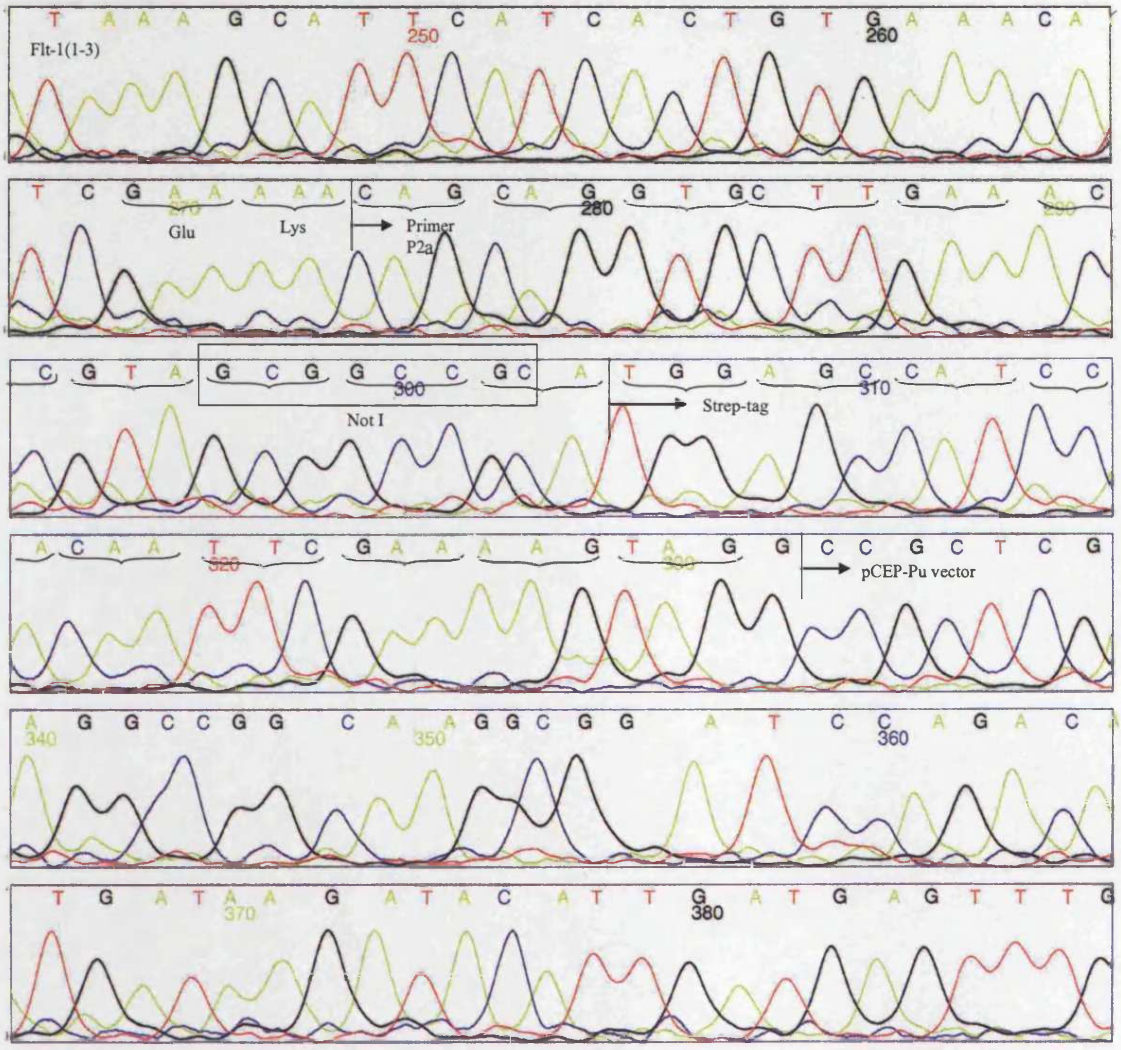

Appendix 6: Statistical analysis of foetal rat metatarsal assay

Statistical analysis was performed on the length of the calcified zone of foetal rat metatarsal to establish if there was a significant difference between (a) the length of calcified zone over 3 and 7 days and (b) the lengths following different treatments. All analyses were tested to a 5% significance level. The data was confirmed beforehand as having a normal distribution (not shown). Analysis was carried out using SPSS software.

A. Change in metatarsal length after 3 days of culture

The paired T-test was performed to determine this.

1. Descriptive statistics of each sample.

		Mean	N	Std. Deviation	Std. Error Mean
Pair 1	Hydrogel only day 0	.197411306	17	.0438076622	.0106249187
	Hydrogel only day 3	.203295935	17	.0532275630	.0129095803
Pair 2	Hydrogel + VEGF 100ng day 0	.182926454	13	.0462790711	.0128355049
	Hydrogel + VEGF 100ng day 3	.183385723	13	.0537286845	.0149016559
Pair 3	Hydrogel + flt-1(1-3) day 0	.166055192	12	.0429319997	.0123934008
	Hydrogel + flt-1(1-3) day 3	.147835433	12	.0408182807	.0117832227
Pair 4	Hydrogel + VEGF 28ng + flt-1(1-3) day 0	.175120273	15	.0465318124	.0120144623
	Hydrogel + VEGF 28ng + flt-1(1-3) day 3	.154204367	15	.0481646698	.0124360643
Pair 5	Hydrogel + suramin day 0	.169051225	16	.0584255569	.0146063892
	Hydrogel + suramin day 3	.159411531	16	.0626322638	.0156580659
Pair 6	Hydrogel + WT control day 0	.160934613	15	.0406327722	.0104913367
	Hydrogel + WT control day 3	.134372547	15	.0333689581	.0086158279
Pair 7	Hydrogel + VEGF 25ng + WT control day 0	.207633975	16	.0745371615	.0186342904
	Hydrogel + VEGF 25ng + WT control day 3	.208023263	16	.0896190372	.0224047593
Pair 8	Hydrogel + std sflt-1 day 0	.270921043	14	.0467828251	.0125032359
	Hydrogel + std sflt-1 day 3	.268255564	14	.0504317435	.0134784504
Pair 9	Hydrogel + VEGF 28ng day 0	.267801356	18	.0557154155	.0131322494
	Hydrogel+ VEGF 28ng day 3	.254407844	18	.0377744357	.0089035199

2. Paired samples test.

		Paired Differences					t	df	Sig. (2-tailed)
		Mean	Std. Deviation	Std. Error Mean	95% Confidence Interval of the Difference				
					Lower	Upper			
Pair 1	Hydrogel only day 0 - Hydrogel only day 3	-.005884629	.0335988851	.0081489266	-.023159582	.011390323	-.722	16	.481
Pair 2	Hydrogel + VEGF 100ng day 0 - Hydrogel + VEGF 100ng day 3	-.000459269	.0256929500	.0071259422	-.015985363	.015066825	-.064	12	.950
Pair 3	Hydrogel + flt-1(1-3) day 0 - Hydrogel + flt-1(1-3) day 3	.018219758	.0237054815	.0068431831	.003158014	.033281503	2.662	11	.022

Pair 4	Hydrogel + VEGF 28ng + flt-1(1-3) day 0 - Hydrogel + VEGF 28ng + flt-1(1-3) day 3	.020915907	.0327248109	.0084495099	.002793510	.039038303	2.475	14	.027
Pair 5	Hydrogel + suramin day 0 - Hydrogel + suramin day 3	.009639694	.0263351726	.0065837932	-.004393329	.023672717	1.464	15	.164
Pair 6	Hydrogel + WT control day 0 - Hydrogel + WT control day 3	.026562067	.0167154375	.0043159074	.017305366	.035818767	6.154	14	.000
Pair 7	Hydrogel + VEGF 25ng + WT control day 0 - Hydrogel + VEGF 25ng + WT control day 3	-.000389287	.0389613918	.0097403480	-.021150348	.020371773	-.040	15	.969
Pair 8	Hydrogel + std sflt-1 day 0 - Hydrogel + std sflt-1 day 3	.002665479	.0645993554	.0172649040	-.034633079	.039964036	.154	13	.880
Pair 9	Hydrogel + VEGF 28ng day 0 - Hydrogel+ VEGF 28ng day 3	.013393511	.0391400840	.0092254063	-.006070395	.032857417	1.452	17	.165

Conclusion: only three metatarsals exhibited a significance levels of less than 0.05, indicating a significant change in metatarsal length. These were:

- Pair 3: Hydrogel + flt-1(1-3)
- Pair 4: Hydrogel + flt-1(1-3) and VEGF
- Pair 6: Hydrogel + WT

B. Change in metatarsal length after 7 days of culture

The paired T-test was performed to determine this.

1. Descriptive statistics of each sample.

		Mean	N	Std. Deviation	Std. Error Mean
Pair 1	Hydrogel only day 0	.197411306	17	.0438076622	.0106249187
	Hydrogel only day 7	.209429547	17	.0385100987	.0093400709
Pair 2	Hydrogel + VEGF 100ng day 0	.182838036	14	.0444647240	.0118836974
	Hydrogel + VEGF 100ng day 7	.185281721	14	.0450264068	.0120338134
Pair 3	Hydrogel + flt-1(1-3) day 0	.171455708	13	.0405465963	.0112456025
	Hydrogel + flt-1(1-3) day 7	.184361323	13	.0470980244	.0130626417
Pair 4	Hydrogel + VEGF 28ng + flt-1(1-3) day 0	.175120273	15	.0465318124	.0120144623
	Hydrogel + VEGF 28ng + flt-1(1-3) day 7	.177613260	15	.0468630298	.0120999823
Pair 5	Hydrogel + suramin day 0	.165762175	16	.0583545614	.0145886404
	Hydrogel + suramin day 7	.128824313	16	.0275124332	.0068781083
Pair 6	Hydrogel + WT control day 0	.160934613	15	.0406327722	.0104913367
	Hydrogel + WT control day 7	.140661780	15	.0355975424	.0091912459
Pair 7	Hydrogel + VEGF 25ng + WT control day 0	.207633975	16	.0745371615	.0186342904
	Hydrogel + VEGF 25ng + WT control day 7	.230341375	16	.0992467273	.0248116818
Pair 8	Hydrogel + std sflt-1 day 0	.270921043	14	.0467828251	.0125032359
	Hydrogel + std sflt-1 day 7	.280478550	14	.0526520584	.0140718545
Pair 9	Hydrogel + VEGF 28ng day 0	.267801356	18	.0557154155	.0131322494

Hydrogel+ VEGF 28ng day 7	.284998072	18	.0429732615	.0101288949

2. Paired samples test.

		Paired Differences					t	df	Sig(2-tailed)...
		Mean	Std. Deviation	Std. Error Mean	95% Confidence Interval of the Difference				
					Lower	Upper			
Pair 1	Hydrogel only day 0 - Hydrogel only day 7	-.012018241	.0323580648	.0078479835	-.028655223	.004618741	-1.531	16	.145
Pair 2	Hydrogel + VEGF 100ng day 0 - Hydrogel + VEGF 100ng day 7	-.002443686	.0469274839	.0125418976	-.029538808	.024651437	-.195	13	.849
Pair 3	Hydrogel + flt-1(1-3) day 0 - Hydrogel + flt-1(1-3) day 7	-.012905615	.0419890958	.0116456798	-.038279372	.012468141	-1.108	12	.289
Pair 4	Hydrogel + VEGF 28ng + flt-1(1-3) day 0 - Hydrogel + VEGF 28ng + flt-1(1-3) day 7	-.002492987	.0248182978	.0064080569	-.016236902	.011250929	-.389	14	.703
Pair 5	Hydrogel + suramin day 0 - Hydrogel + suramin day 7	.036937862	.0563242720	.0140810680	.006924777	.066950948	2.623	15	.019
Pair 6	Hydrogel + WT control day 0 - Hydrogel + WT control day 7	.020272833	.0266958965	.0068928508	.005489139	.035056528	2.941	14	.011
Pair 7	Hydrogel + VEGF 25ng + WT control day 0 - Hydrogel + VEGF 25ng + WT control day 7	-.022707400	.0419991142	.0104997785	-.045087148	-.000327652	-2.163	15	.047
Pair 8	Hydrogel + std sflt-1 day 0 - Hydrogel + std sflt-1 day 7	-.009557507	.0611688196	.0163480547	-.044875332	.025760318	-.585	13	.569
Pair 9	Hydrogel + VEGF 28ng day 0 - Hydrogel+ VEGF 28ng day 7	-.017196717	.0499601731	.0117757257	-.042041326	.007647893	-1.460	17	.162

Conclusion: only three metatarsals exhibited a significance levels of less than 0.05, indicating a significant change in metatarsal length. These were:

- Pair 5: Hydrogel + suramin
- Pair 6: Hydrogel + WT
- Pair 7: Hydrogel + WT + VEGF (27.8ng)

C. Comparison of the % changes in length over 3 days of metatarsals cultured on hydrogels containing different agents.

The percentage change over 3 days of the calcified zone of each metatarsal was calculated, 100% being the starting length, <100 indicates shrinkage and >100 indicates expansion. Each treatment group of metatarsals was compared to metatarsals that had been cultured on hydrogels containing no additional substances. To determine statistical significance, the non-paired T-test was performed.

1. Hydrogels with VEGF (100ng)

a. Descriptive statistics:

	Sample	N	Mean	Std. Deviation	Std. Error Mean

% of start length	Hydrogel only	17	103.0713	16.93477	4.10728
	Hydrogel + VEGF 100ng	13	100.1020	17.67076	4.90099

b. Non-paired T-test:

		Levene's Test for Equality of Variances		t-test for Equality of Means						
		F	Sig.	t	df	Sig. (2-tailed)	Mean Difference	Std. Error Difference	95% Confidence Interval of the Difference	
									Lower	Upper
% of start length	Equal variances assumed	.114	.739	.467	28	.644	2.9694	6.35704	-10.05246	15.99117
	Equal variances not assumed			.464	25.384	.646	2.9694	6.39449	-10.19024	16.12894

Conclusion: as Levene significance level is above 0.05, we assume that variances are equal. The significance level is above 0.05, indicating that there is no significant change in metatarsal calcified zone following treatment with 100ng VEGF compared to the hydrogel only.

2. *Hydrogel with flt-1(1-3)*

a. Descriptive statistics:

	Sample	N	Mean	Std. Deviation	Std. Error Mean
% of start length	Hydrogel only	17	103.0713	16.93477	4.10728
	Hydrogel + flt-1(1-3)	15	89.3063	13.51558	3.48971

b. Non-paired T-test:

		Levene's Test for Equality of Variances		t-test for Equality of Means						
		F	Sig.	t	df	Sig. (2-tailed)	Mean Difference	Std. Error Difference	95% Confidence Interval of the Difference	
									Lower	Upper
% of start length	Equal variances assumed	.063	.803	2.518	30	.017	13.7650	5.46733	2.59924	24.93078
	Equal variances not assumed			2.554	29.731	.016	13.7650	5.38961	2.75380	24.77623

Conclusion: as Levene significance level is above 0.05, we assume that variances are equal. The significance level is below 0.05, indicating that there is a significant change in metatarsal calcified zone following treatment with flt-(1-3) compared to the hydrogel only.

3. Hydrogel with flt-(1-3) and 27.8ng VEGF

a. Descriptive statistics:

	Sample	N	Mean	Std. Deviation	Std. Error Mean
% of start length	Hydrogel only	17	103.0713	16.93477	4.10728
	Hydrogel + flt-1(1-3) + VEGF 27.84ng	15	89.4295	18.54503	4.78831

b. Non-paired T-test:

		Levene's Test for Equality of Variances		t-test for Equality of Means						
		F	Sig.	t	df	Sig. (2-tailed)	Mean Difference	Std. Error Difference	95% Confidence Interval of the Difference	
									Lower	Upper
% of start length	Equal variances assumed	.818	.373	2.175	30	.038	13.6418	6.27173	.83318	26.45036
	Equal variances not assumed			2.162	28.623	.039	13.6418	6.30854	.73196	26.55158

Conclusion: as Levene significance level is above 0.05, we assume that variances are equal. The significance level is below 0.05, indicating that there is a significant change in metatarsal calcified zone following treatment with flt-(1-3) and VEGF compared to the hydrogel only.

4. Hydrogel with suramin

a. Descriptive statistics:

	Sample	N	Mean	Std. Deviation	Std. Error Mean
% of start length	Hydrogel only	17	103.0713	16.93477	4.10728
	Hydrogel + suramin	16	94.2544	14.17038	3.54259

b. Non-paired T-test:

		Levene's Test for Equality of Variances		t-test for Equality of Means						
		F	Sig.	t	df	Sig. (2-tailed)	Mean Difference	Std. Error Difference	95% Confidence Interval of the Difference	
									Lower	Upper
% of start length	Equal variances assumed	.238	.629	1.617	31	.116	8.8169	5.45400	-2.30661	19.94039
	Equal variances not assumed			1.626	30.598	.114	8.8169	5.42400	-2.25133	19.88510

Conclusion: as Levene significance level is above 0.05, we assume that variances are equal. The significance level is above 0.05, indicating that there is no significant change in metatarsal calcified zone following treatment with suramin compared to the hydrogel only.

5. Hydrogel with the WT control

a. Descriptive statistics:

	Sample	N	Mean	Std. Deviation	Std. Error Mean
% of start length	Hydrogel only	17	103.0713	16.93477	4.10728
	Hydrogel + WT control	15	84.3597	10.19602	2.63260

b. Non-paired T-test:

		Levene's Test for Equality of Variances		t-test for Equality of Means						
		F	Sig.	t	df	Sig. (2-tailed)	Mean Difference	Std. Error Difference	95% Confidence Interval of the Difference	
									Lower	Upper
% of start length	Equal variances assumed	1.175	.287	3.721	30	.001	18.7116	5.02813	8.44280	28.98043

	Equal variances not assumed			3.835	26.697	.001	18.7116	4.87856	8.69632	28.72691

Conclusion: as Levene significance level is above 0.05, we assume that variances are equal. The significance level is below 0.05, indicating that there is a significant change in metatarsal calcified zone following treatment with the WT control compared to the hydrogel only.

6. Hydrogel with the WT control and VEGF

a. Descriptive statistics:

	Sample	N	Mean	Std. Deviation	Std. Error Mean
% of start length	Hydrogel only	17	103.0713	16.93477	4.10728
	Hydrogel + WT + VEGF 25ng	16	98.5868	20.34487	5.08622

b. Non-paired T-test:

		Levene's Test for Equality of Variances		t-test for Equality of Means						
		F	Sig.	t	df	Sig. (2-tailed)	Mean Difference	Std. Error Difference	95% Confidence Interval of the Difference	
									Lower	Upper
% of start length	Equal variances assumed	.935	.341	.690	31	.495	4.4846	6.50053	-8.77338	17.74248
	Equal variances not assumed			.686	29.272	.498	4.4846	6.53754	-8.88082	17.84992

Conclusion: as Levene significance level is above 0.05, we assume that variances are equal. The significance level is above 0.05, indicating that there is no significant change in metatarsal calcified zone following treatment with the WT control and VEGF compared to the hydrogel only.

7. Hydrogel with the soluble flt-1 standard

a. Descriptive statistics:

	Sample	N	Mean	Std. Deviation	Std. Error Mean
% of start length	Hydrogel only	17	103.0713	16.93477	4.10728
	Hydrogel + std flt-1	14	102.1203	30.06286	8.03464

b. Non-paired T-test:

		Levene's Test for Equality of Variances		t-test for Equality of Means						
		F	Sig.	t	df	Sig. (2-tailed)	Mean Difference	Std. Error Difference	95% Confidence Interval of the Difference	
									Lower	Upper
% of start length	Equal variances assumed	1.662	.208	.111	29	.912	.9510	8.56620	-16.56885	18.47085

	Equal variances not assumed			.105	19.595	.917	.9510	9.02359	-17.89686	19.79885

Conclusion: as Levene significance level is above 0.05, we assume that variances are equal. The significance level is above 0.05, indicating that there is no significant change in metatarsal calcified zone following treatment with the WT control and VEGF compared to the hydrogel only.

8. Hydrogel with 27.8ng VEGF

a. Descriptive statistics:

	Sample	N	Mean	Std. Deviation	Std. Error Mean
% of start length	Hydrogel only	17	103.0713	16.93477	4.10728
	Hydrogel + VEGF 27.84ng	18	98.1000	20.52360	4.83746

b. Non-paired T-test:

		Levene's Test for Equality of Variances		t-test for Equality of Means						
		F	Sig.	t	df	Sig. (2-tailed)	Mean Difference	Std. Error Difference	95% Confidence Interval of the Difference	
									Lower	Upper
% of start length	Equal variances assumed	.224	.639	.779	33	.442	4.9713	6.38149	-8.01197	17.95451
	Equal variances not assumed			.783	32.435	.439	4.9713	6.34593	-7.94816	17.89070

Conclusion: as Levene significance level is above 0.05, we assume that variances are equal. The significance level is above 0.05, indicating that there is no significant change in metatarsal calcified zone following treatment with VEGF compared to the hydrogel only.

D. Comparison of the % changes in length over 7 days of metatarsals cultured on hydrogels containing different agents.

1. Hydrogels with VEGF (100ng)

a. Descriptive statistics:

	Sample	N	Mean	Std. Deviation	Std. Error Mean
% of start length	Hdrogel only	17	108.1220	17.92914	4.34846
	Hydrogel + VEGF 100ng	14	104.8972	30.41370	8.12840

b. Non-paired T-test:

		Levene Test ...		t-test for Equality...						
		F	Significance	t	df	Sig(2-tailed)	Mean Difference	Std. Error	95% Confidence Interval of the Difference	
									Lower	Upper
% of start length	Equal variances ...	.522	.476	.367	29	.716	3.2248	8.78123	-14.73486	21.18441
	Not Equal variances ...			.350	20.164	.730	3.2248	9.21846	-15.99457	22.44413

Conclusion: as Levene significance level is above 0.05, we assume that variances are equal. The significance level is above 0.05, indicating that there is no significant change in metatarsal calcified zone following treatment with 100ng VEGF compared to the hydrogel only.

2. Hydrogel with flt-1(1-3)

a. Descriptive statistics:

	Sample	N	Mean	Std. Deviation	Std. Error Mean
% of start length	Hdrogel only	17	108.1220	17.92914	4.34846
	Hydrogel + flt-1(1-3)	13	109.5053	24.03401	6.66584

b. Non-paired T-test:

		Levene Test ...		t-test for Equality...						
		F	Significance	t	df	Sig(2-tailed)...	Mean Difference	Std. Error	95% Confidence Interval of the Difference	
									Lower	Upper
% of start length	Equal variances ...	2.841	.103	-.181	28	.858	-1.3833	7.65115	-17.05597	14.28938
	Not Equal variances ...			-.174	21.470	.864	-1.3833	7.95880	-17.91247	15.14587

Conclusion: as Levene significance level is above 0.05, we assume that variances are equal. The significance level is above 0.05, indicating that there is no significant change in metatarsal calcified zone following treatment with flt-1(1-3) compared to the hydrogel only.

3. Hydrogel with flt-1(1-3) and VEGF (27.8ng)

a. Descriptive statistics:

	Sample	N	Mean	Std. Deviation	Std. Error Mean
% of start length	Hdrogel only	17	108.1220	17.92914	4.34846
	Hydrogel + flt-1(1-3) + VEGF 27.84ng	15	103.0265	15.77300	4.07257

b. Non-paired T-test:

		Levene Test ...		t-test for Equality...						
		F	Significance	t	df	Sig(2-tailed)...	Mean Difference	Std. Error	95% Confidence Interval of the Difference	
									Lower	Upper
% of start length	Equal variances ...	.116	.736	.848	30	.403	5.0955	6.00698	-7.17238	17.36341
	Not Equal variances ...			.855	30.000	.399	5.0955	5.95776	-7.07186	17.26288

Conclusion: as Levene significance level is above 0.05, we assume that variances are equal. The significance level is above 0.05, indicating that there is no significant change in metatarsal calcified zone following treatment with flt-1(1-3) and VEGF compared to the hydrogel only.

4. Hydrogel with suramin

a. Descriptive statistics:

	Sample	N	Mean	Std. Deviation	Std. Error Mean
% of start length	Hdrogel only	17	108.1220	17.92914	4.34846
	Hydrogel + suramin	16	84.3446	25.72775	6.43194

b. Non-paired T-test:

		Levene Test ...		t-test for Equality...						
		F	Significance	t	df	Sig(2-tailed)	Mean Difference	Std. Error	95% Interval Difference	Confidence of the
									Lower	Upper
% of start length	Equal variances ...	2.026	.165	3.096	31	.004	23.7774	7.68029	8.11336	39.44146
	Not Equal variances ...			3.063	26.630	.005	23.7774	7.76395	7.83675	39.71807

Conclusion: as Levene significance level is above 0.05, we assume that variances are equal. The significance level is below 0.05, indicating that there is a significant change in metatarsal calcified zone following treatment with suramin compared to the hydrogel only.

5. Hydrogel with Wild-Type (WT) control

a. Descriptive statistics:

	Sample	N	Mean	Std. Deviation	Std. Error Mean
% of start length	Hdrogel only	17	108.1220	17.92914	4.34846
	Hydrogel + WT control	15	88.5502	13.64393	3.52285

b. Non-paired T-test:

		Levene Test ...		t-test for Equality...						
		F	Significance	t	df	Sig(2-tailed)...	Mean Difference	Std. Error	95% Confidence Interval of the Difference	
									Lower	Upper
% of start length	Equal variances ...	.819	.373	3.438	30	.002	19.5718	5.69351	7.94414	31.19954
	Not Equal variances ...			3.497	29.414	.002	19.5718	5.59639	8.13294	31.01074

Conclusion: as Levene significance level is above 0.05, we assume that variances are equal. The significance level is below 0.05, indicating that there is a significant change in metatarsal calcified zone following treatment with the WT control compared to the hydrogel only.

6. Hydrogel with WT control and VEGF (27.8ng)

a. Descriptive statistics:

	Sample	N	Mean	Std. Deviation	Std. Error Mean
% of start length	Hdrogel only	17	108.1220	17.92914	4.34846

	Hydrogel + WT + VEGF 25ng	16	108.3813	20.23031	5.05758

b. Non-paired T-test:

		Levene Test ...		t-test for Equality...						
		F	Significance	t	df	Sig(2-tailed)...	Mean Difference	Std. Error	95% Confidence Interval of the Difference	
									Lower	Upper
% of start length	Equal variances ...	.650	.426	-.039	31	.969	-.2593	6.64492	-13.81169	13.29310
	Not Equal variances ...			-.039	30.003	.969	-.2593	6.66995	-13.88108	13.36249

Conclusion: as Levene significance level is above 0.05, we assume that variances are equal. The significance level is above 0.05, indicating that there is no significant change in metatarsal calcified zone following treatment with the WT control and VEGF compared to the hydrogel only.

7. Hydrogel with the soluble flt-1 standard

a. Descriptive statistics:

	Sample	N	Mean	Std. Deviation	Std. Error Mean
% of start length	Hdrogel only	17	108.1220	17.92914	4.34846
	Hydrogel + std flt-1	14	106.3771	30.33852	8.10831

b. Non-paired T-test:

		Levene Test ...		t-test for Equality...						
		F	Significance	t	df	Sig(2-tailed)...	Mean Difference	Std. Error	95% Confidence Interval of the Difference	
									Lower	Upper
% of start length	Equal variances ...	1.368	.252	.199	29	.844	1.7449	8.76604	-16.18363	19.67348
	Not Equal variances ...			.190	20.196	.851	1.7449	9.20075	-17.43557	20.92542

Conclusion: as Levene significance level is above 0.05, we assume that variances are equal. The significance level is above 0.05, indicating that there is no significant change in metatarsal calcified zone following treatment with the soluble flt-1 standard compared to the hydrogel only.

8. Hydrogel with VEGF (27.8ng)

a. Descriptive statistics:

	Sample	N	Mean	Std. Deviation	Std. Error Mean
% of start length	Hdrogel only	17	108.1220	17.92914	4.34846
	Hydrogel + VEGF 27.84ng	18	110.6811	27.89957	6.57599

b. Non-paired T-test:

	Levene Test ...		t-test for Equality...					
	F	Significance	t	df	Sig(2-tailed)...	Mean Difference	Std. Error	95% Confidence Interval of the Difference

									Lower	Upper
% of start length	Equal variances ...	2.680	.111	-.321	33	.750	-2.5591	7.98068	-18.79593	13.67769
	Not Equal variances ...			-.325	29.188	.748	-2.5591	7.88370	-18.67859	13.56035

Conclusion: as Levene significance level is above 0.05, we assume that variances are equal. The significance level is above 0.05, indicating that there is no significant change in metatarsal calcified zone following treatment with VEGF compared to the hydrogel only.

A periosteum or perichondrium autograft sutured over the site of injury has also induced growth of a cartilaginous material, the periosteum exhibiting greater chondrogenesis than the perichondrium[325]. However, the environment into which the graft is inserted influences the type of repair. For instance, a low oxygen tension results in cartilage production, whereas a high oxygen tension produces bone[2,325]. The quality of the repair is dependent on the age of the patient, in terms of the chondrogenic potential of the autograft[326].

1.5.3 Chondrocyte transplantation

In 1989, a method was described whereby chondrocytes were extracted from cartilage in a non-weight bearing region in rabbits, expanded in culture and implanted into cartilage defects in the same animal, demonstrating growth of new cartilage[327] (Figure 1.9C). Five years later, Brittberg *et al.*[324] reported the use of this technique in the treatment of chondral defects in human subjects. Although the group did not biochemically assess the repaired tissue, some regrowth of a hyaline-type cartilage was observed with attachment to the subchondral bone.

However, there are a number of shortcomings with this method. Firstly, a non-weight bearing site of cartilage is damaged to obtain the cells. Secondly, chondrocytes grown in culture have a tendency to dedifferentiate after a few passages of monolayer growth and cease synthesising the components required for cartilage matrix formation[322]. Thirdly, the chondrocytes introduced into the lesion may leak , despite sutured periosteal flaps over the site. Fourthly, the cells are not evenly distributed throughout the void of the lesion and thus, newly formed cartilage would not completely fill the void[322]. Finally, the change of conditions could potentially upset the delicate balance between catabolic and anabolic activity of chondrocytes. Fluctuations in oxygen levels can lead to increased production of ROS[165]. Although the use of autologous chondrocytes is promising, a number of changes to the procedure have been performed to address the above issues.

Aigner *et al.*[328] described a culture method using chondrocytes obtained by biopsy of hyaline nasoseptal cartilage, which would alleviate the problem of a donor site. However, although the chondrocytes produced type II collagen, the workers did not

use a chondral defect model to test the ability of these chondrocytes to produce articular cartilage.

During endochondral ossification, the periosteum is the site blood vessel invasion and mineralization (Section 1.1.8). Evidence of hypertrophy of introduced chondrocytes in the presence of the periosteal flap has raised doubts about the use of this material[329]. Alternatively, non-viable periosteum or a biodegradable introduced membrane could be used in its place[329].

Chondrocytes cultured in biodegradable three-dimensional scaffolds can maintain their phenotype[328,330-5]. Transplantation of this cartilaginous material into defects has demonstrated good integration with the subchondral bone and formation of smooth hyaline-like cartilage[329]. As chondrocytes respond to dynamic loading *in vivo* by increasing matrix synthesis, the application of a dynamic load onto a chondrocyte-containing matrix *in vitro* has been found to increase matrix synthesis[336]. The incorporation of cells into a scaffold immediately prior to implantation into a defect, has led to increased growth of a more hyaline-like cartilage compared to chondrocytes implanted on their own[337,338,339]. Scaffolds can also anchor chondrocytes into the site of injury, removing the need for a periosteal flap[337,338,339] (Figure 1.9A and B).

Chondroitinase has been used to facilitate integration of implanted material, to remove GAGs in the surrounding tissue that would otherwise inhibit adhesion [340,341]. However, OA cartilage has already suffered proteoglycan depletion and exposed collagen fibrils may be sufficient for binding[134].

1.5.3 Growth factor approaches

Several growth factors have been shown to be involved in chondrogenesis and the maintenance of the cartilage phenotype, summarised in Tables 1.1 and 1.5. The administration of growth factors avoids the drawbacks associated with chondrocyte transplantation[342]. Using a biomaterial as a delivery system and as a scaffold, a chemotactic growth factor, such as BMP-2, can attract mesenchymal stem cells from the periosteum, synovial membrane or subchondral bone into the biomaterial, stimulate differentiation to a chondrocyte phenotype and induce formation of replacement cartilage matrix[64,81,343]. Addition of TGF-β, IGF-1 or bFGF into a

previously determined by the oscillation method. The "creep" method provided a tan δ at the same time point of 0.031, which concurs with that obtained by the oscillation method. As the oscillation method also provided information on the storage (G′) and loss (G″) moduli, this was the more suitable method for quantifying these parameters.

In summary, the findings of these experiments were:

- The ideal concentrations of crosslinker and HAED correlated with those found with earlier observations (Section 3.2.2).
- Addition of pepsinised collagen led to more elastic hydrogels, whereas fibrillised telocollagen resulted in less elastic hydrogels than in its absence.
- Hydrogels formed in aqueous conditions were not as elastic as those formed under air.
- The crosslinking reaction reached completion within 30 minutes, using the SPA_4-PEG (20kDa) crosslinker.

3.2.4. Fourier-transform infrared spectroscopy

To examine the extent of crosslinking of hydrogels, fourier-transform infrared spectroscopy (FT-IR) was applied. This technique examines the vibrational energy of covalent bonds and can reveal the type of bonds present in a sample. HA preparations were derivatised to HAED from 2% to 20% modification to the carboxyl groups, to provide a series of amine concentrations on the polymer. This was achieved by altering the concentration of the carbodiimide catalyst during the derivatisation reaction from a 0-fold to a 10-fold Molar excess (Table 3.2). The HAED was lyophilised, as water peaks would have interfered with the results and reduced to fine particles either, by snap-freezing with crushing or by cutting with scissors. The latter produced the most homogenous particles.

It was hypothesised that the increase in amine groups would result in increased spectrum peaks at the wavenumbers shown in Table 3.3, in accordance with the form of vibrational energy emitted by the bond. Likewise, peaks caused by carboxyl groups would be diminished, compared to non-derivatised HA. Upon crosslinking, newly created amide groups would be identified in the same manner, by an increase in

peaks already present due to the amide on the N-acetyl-D-glucosamine monomer of HA.

The HAED FT-IR spectra shown in Figure 3.9 are a mixture of HAED preparations overlaid (n=7), the red representing higher levels of derivatisation, thus increased numbers of amine groups. The black spectra represent samples with virtually no derivatisation, so contain little or no amine groups. Although fluctuations between each sample were observed, there was no discernable difference in the pattern of fluctuations between the red and black lines at any peak, indicating that proposed changes in amine groups were not detected. N-acetyl-D-glucosamine, D-glucuronic acid and ethylenediamine controls were analysed for comparative purposes. These confirmed the positions of the spectrum peaks of interest in HAED samples.

The carboxyl (COOH) and amide (CONH) peaks labelled are apparent in the HAED spectra, albeit with some overlapping. The peaks between 1500 and 1000 cm^{-1} are primarily caused by bonds within the ring structures and hydroxyl groups of D-glucuronic acid and N-acetyl-D-glucosamine, as indicated in Figure 3.9. However, the amine (NH) peak observed in the ethylenediamine sample cannot be identified clearly in the HAED samples, where an increase would be expected following derivatisation.

It appears that any change in this peak was masked by signals from the carboxyl and amide groups. The shoulder of the carboxyl peak could be attributed to amine groups, but as there is no obvious change from the un-derivatised samples, the amide group may be responsible.

In summary, this technique was unsuitable for determining the extent of derivatisation or crosslinking of HAED, as changes in functional groups could not be detected. Possible explanations for this are discussed in Section 3.3.3.

recovery of protein. However, Western blotting revealed that this approach did not increase flt-1(1-3) recovery from the medium and furthermore flt-1(1-3) was not retained in the matrix (Figure 4.13). A further three attempts adjusting the incubations produced the same result. These results, plus the lack of specific recognition by the anti-strep tag antibody, suggested that there were problems with the strep tag. It was hypothesised that the strep-tag was being internalised into the flt-1(1-3) structure or cleaved. Western blotting under reducing conditions indicated that the strep tag was being cleaved off, as the reducing conditions under which the Western blotting was conducted would have exposed any internalised tag. As previous work in our laboratory demonstrated recognition of the strep tag on unrelated proteins by antibodies, it appears that proteolytic processing led to the removal of the peptide.

4.2.3.2. Heparin affinity chromatography

As truncated flt-1 had previously been purified by heparin sepharose[290,315], this method was also attempted. Conditioned medium (200ml) was removed from transfected cells, centrifuged to remove particular matter and loaded onto a heparin sepharose column. Protease inhibitors were added, as these slightly increased the yield, as assessed by Western blot (data not shown). Fractions from heparin affinity chromatography were assessed by slot blotting using anti-flt-1 antibodies, a technique which enabled a more rapid analysis of a large number of samples, compared to Western blotting. The large protein peak (fractions 1-15) of unbound protein did not contain significant amounts of flt-1. Flt-1(1-3) exhibited some interaction with the column since little flt-1(1-3) was detected in the wash fractions. Flt-1(1-3) eluted off the column over a range from 277mM to 571mM sodium chloride, indicated as region B in Figures 4.14 and 4.15. Elution over a broad range of ionic strength is consistent with the observed differential glycosylation discussed previously. No flt-1(1-3) was detected in the high salt cleaning and re-equilibration steps.

The flt-1(1-3)-positive fractions were pooled and concentrated from fractions around 32 to around 70 to approximately 1ml, using a Centriprep ultrafiltration cartridge, as outlined in Section 2.2.9. The total protein concentration was determined by absorbance at 280nm and was typically between 50μg/ml and 500μg/ml. Purity was assessed by running the concentrate on an SDS/PAGE gel followed by silver staining (Figure 4.16, lane 4). The presence of multiple bands indicated that this technique did

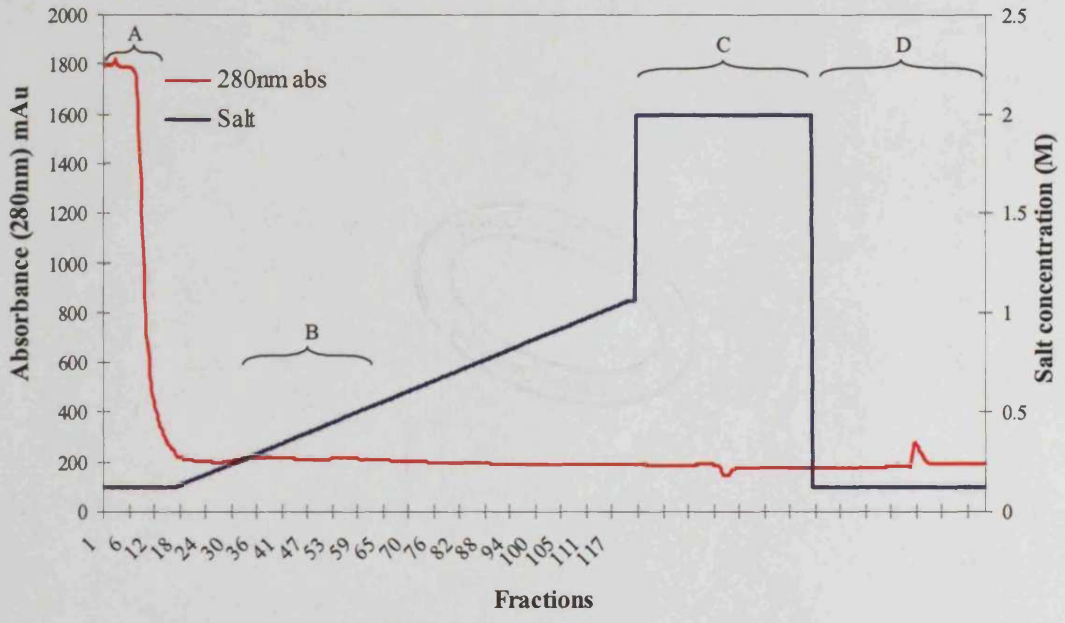

Figure 4.14: Chromatogram of heparin affinity purification of 200ml conditioned medium run over a heparin sepharose column (20ml bed volume), showing the absorbance of proteins at 280nm and the salt gradient. A: initial wash step. B: the region flt-1(1-3) was detected in. C: the cleaning step (2M salt). D: the re-equilibration of the column.

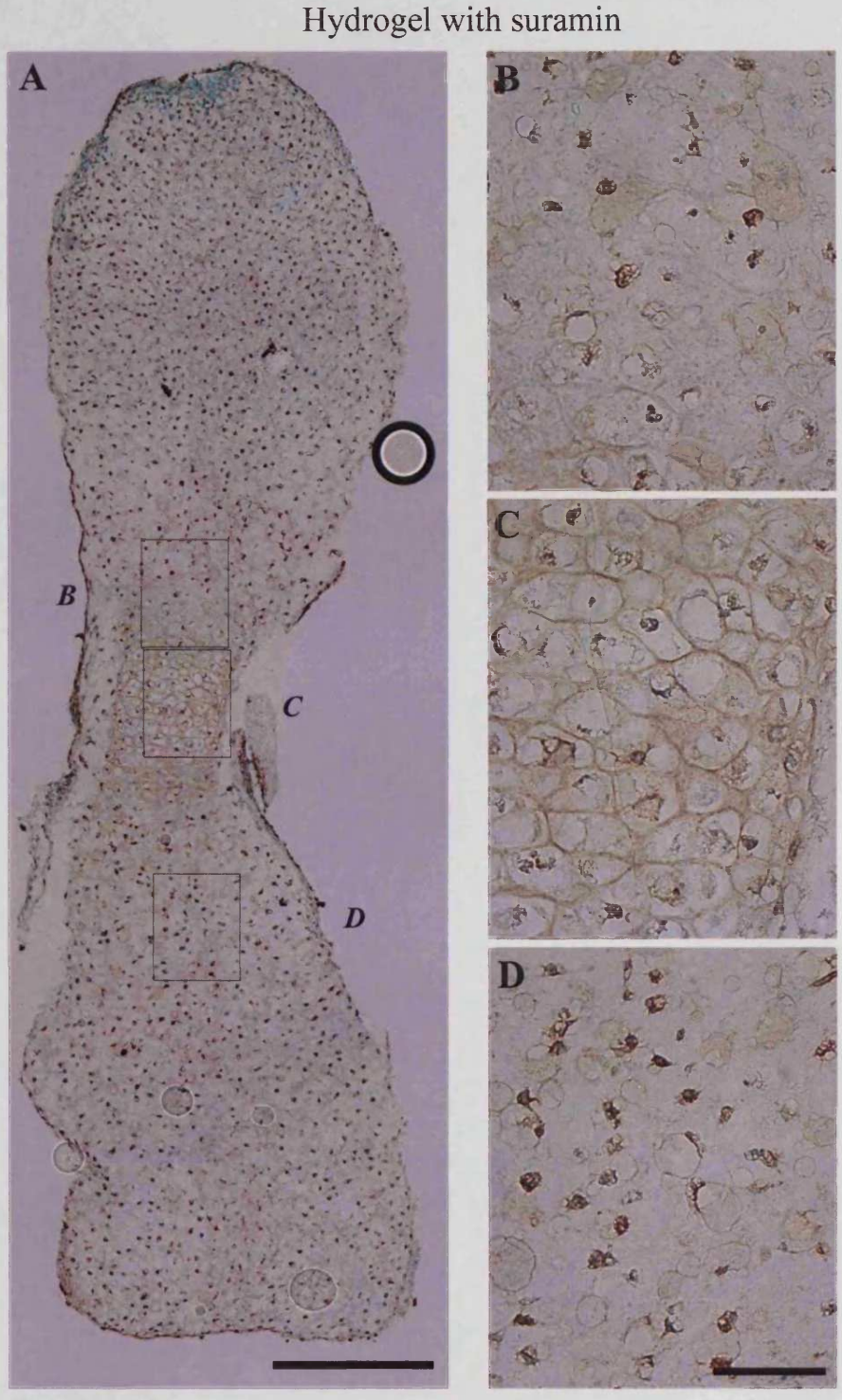

Figure 5.14: Immunostaining of a foetal rat metatarsal with anti-von Willebrand Factor (brown), counterstained with methyl green. The metatarsal was cultured for 7 days on a hydrogel containing the soluble flt-1 standard (0.2ng). Selected areas of the proliferating zone (B), hypertrophic zone (C) and epiphyseal region (D) are shown at a higher magnification. The zones formed during endochondral ossification are illustrated in the corresponding image in Figure 5.5I. Scale bars = 300μm (A) and 50μm (B-D).

5.3. Biological Assays Discussion

As cartilage has a limited capacity for spontaneous repair, several strategies have been employed to induce repair. One such approach has been to introduce chondrogenic growth factors, in order to promote repair or regeneration. However, the sudden addition of a highly concentrated growth factor into a lesion does not mirror the endogenous signalling mechanism *in vivo* and the growth factor can easily diffuse and act in other areas, leading to inappropriate tissue remodelling[344].

Chapter 3 describes the evaluation of a HA-based hydrogel for the delivery of bioactive agents. Chapter 4 describes the production of an inhibitory decoy receptor for VEGF, based on the first 3 extracellular domains of its receptor, flt-1 (flt-1(1-3). The present chapter combined the hydrogel delivery system with flt-1(1-3), to investigate any anti-angiogenic effects of the material. It also assessed the material for inhibition of chondrocyte differentiation and ossification.

5.3.1. Chick chorioallantoic membrane assay

The CAM assay was employed to assess angiogenesis inhibition by flt-1(1-3). Pro- and anti-angiogenesis controls included 100ng VEGF and 500μg suramin, respectively. Suramin inhibited angiogenesis, as observed by a lack of small vessel growth around the hydrogel, correlating with previous reports of inhibition of angiogenesis by suramin, using this assay[453]. Previously published work has reported a 'spoke wheel' pattern of blood vessel formation around the implant containing VEGF[407]. This was not observed in the present study. It was possible that the larger VEGF did not diffuse as readily out of the hydrogel to stimulate angiogenesis over 3 days. Suramin is a relatively small molecule (1.4kDa) (supplier literature), whereas $VEGF_{165}$ used herein exists as a homodimer of 46kDa[230], of a similar size to flt-1(1-3). This may have resulted in slower diffusion of VEGF out of the hydrogel. During the foetal rat metatarsal assay, hydrogels were maintained in culture medium over 7 days, which may have resulted in increased diffusion of bioactive factors from the hydrogel. However, further work is required to

		Levene Test ...		t-test for Equality...						
		F	Significance	t	df	Sig(2-tailed)...	Mean Difference	Std. Error Diff...	95% Confidence Interval of the Difference	
									Lower	Upper
% of PI +ve cells	Equal variances ...	18.507	.003	-4.718	8	.00151	-42.1720	8.93895	-62.78525	-21.55875
	Not Equal variances ...			-4.718	4.200	.00815	-42.1720	8.93895	-66.53115	-17.81285

Conclusion: the significance is less that 0.05: the null hypothesis is rejected, there is a significant difference between cells cultured in HAED and both controls.

2. Ratio of 0.1:1 crosslinker : HAED

a. Comparison with the negative (live) control:

		Levene Test ...		t-test for Equality...						
		F	Significance	t	df	Sig(2-tailed)...	Mean Difference	Std. Error Diff...	95% Confidence Interval of the Difference	
									Lower	Upper
% of PI +ve cells	Equal variances ...	.128	.730	6.825	8	.00013	9.5540	1.39982	6.32601	12.78199
	Not Equal variances ...			6.825	7.690	.00016	9.5540	1.39982	6.30320	12.80480

b. Comparison with the positive (dead) control:

		Levene Test ...		t-test for Equality...						
		F	Significance	t	df	Sig(2-tailed)...	Mean Difference	Std. Error Diff...	95% Confidence Interval of the Difference	
									Lower	Upper
% of PI +ve cells	Equal variances ...	20.529	.002	-4.844	8	.00128	-43.0940	8.89554	-63.60716	-22.58084
	Not Equal variances ...			-4.844	4.121	.00777	-43.0940	8.89554	-67.50924	-18.67876

Conclusion: the significance is less that 0.05: the null hypothesis is rejected, there is a significant difference between cells cultured in 0.1:1 HAED hydrogels and both controls.

3. Ratio of 0.5:1 crosslinker : HAED

a. Comparison with the negative (live) control:

		Levene Test ...		t-test for Equality...						
		F	Significance	t	df	Sig(2-tailed)...	Mean Difference	Std. Error Diff...	95% Confidence Interval of the Difference	
									Lower	Upper
% of PI +ve cells	Equal variances ...	7.233	.028	4.018	8	.00385	17.6400	4.39072	7.5149 8	27.76502
	Not Equal variances ...			4.018	4.338	.01352	17.6400	4.39072	5.8150 6	29.46494

b. Comparison with the positive (dead) control:

		Levene Test ...		t-test for Equality...						
		F	Significance	t	df	Sig(2-tailed)...	Mean Difference	Std. Error Diff...	95% Confidence Interval of the Difference	
									Lower	Upper
% of PI +ve cells	Equal variances ...	5.481	.047	-3.565	8	.00735	-35.0080	9.82088	-57.65498	-12.36102
	Not Equal variances ...			-3.565	5.797	.01257	-35.0080	9.82088	-59.24435	-10.77165

Conclusion: the significance is less that 0.05: the null hypothesis is rejected, there is a significant difference between cells cultured in 0.5:1 HAED hydrogels and both controls.

4. Ratio of 1:1 crosslinker : HAED

a. Comparison with the negative (live) control:

		Levene Test ...		t-test for Equality...						
		F	Significance	t	df	Sig(2-tailed)...	Mean Difference	Std. Error Diff...	95% Confidence Interval of the Difference	
									Lower	Upper
% of PI +ve cells	Equal variances ...	.735	.416	3.353	8	.01004	5.8900	1.75689	1.83861	9.94139
	Not Equal variances ...			3.353	6.437	.01383	5.8900	1.75689	1.66087	10.11913

b. Comparison with the positive (dead) control:

		Levene Test ...		t-test for Equality...						
		F	Significance	t	df	Sig(2-tailed)...	Mean Difference	Std. Error Diff...	95% Confidence Interval of the Difference	
									Lower	Upper
% of PI +ve cells	Equal variances ...	17.953	.003	-5.219	8	.00080	-46.7580	8.95867	-67.41674	-26.09926
	Not Equal variances ...			-5.219	4.236	.00548	-46.7580	8.95867	-71.09372	-22.42228

Conclusion: the significance is less that 0.05: the null hypothesis is rejected, there is a significant difference between cells cultured in 1:1 HAED hydrogels and both controls.

5. Ratio of 1.5:1 crosslinker : HAED

a. Comparison with the negative (live) control:

		Levene Test ...		t-test for Equality...						
		F	Significance	t	df	Sig(2-tailed)...	Mean Difference	Std. Error Diff...	95% Confidence Interval of the Difference	
									Lower	Upper
% of PI +ve cells	Equal variances ...	.080	.785	5.242	8	.00078	7.2440	1.38201	4.05708	10.43092
	Not Equal variances ...			5.242	7.749	.00087	7.2440	1.38201	4.03899	10.44901

b. Comparison with the positive (dead) control:

		Levene Test ...		t-test for Equality...						
		F	Significance	t	df	Sig(2-tailed)...	Mean Difference	Std. Error Diff...	95% Confidence Interval of the Difference	
									Lower	Upper
% of PI +ve cells	Equal variances ...	20.707	.002	-5.106	8	.00092	-45.4040	8.89276	-65.91073	-24.89727
	Not Equal variances ...			-5.106	4.116	.00644	-45.4040	8.89276	-69.82306	-20.98494

Conclusion: the significance is less that 0.05: the null hypothesis is rejected, there is a significant difference between cells cultured in 1.5:1 HAED hydrogels and both controls.

6. Ratio of 2:1 crosslinker : HAED

a. Comparison with the negative (live) control:

		Levene Test ...		t-test for Equality...						
		F	Significance	t	df	Sig(2-tailed)...	Mean Difference	Std. Error Diff...	95% Confidence Interval of the Difference	
									Lower	Upper
% of PI +ve cells	Equal variances ...	12.068	.008	2.254	8	.05419	7.3080	3.24155	-.16702	14.78302
	Not Equal variances ...			2.254	4.640	.07799	7.3080	3.24155	-1.22295	15.83895